NASA
Reference
Publication
1080

November 1981

ATS-6 Final Engineering Performance Report

Volume II - Orbit and Attitude Controls

NASA

NASA Reference Publication 1080

1981

ATS-6 Final Engineering Performance Report

Volume II - Orbit and Attitude Controls

Robert O. Wales, *Editor*
Goddard Space Flight Center
Greenbelt, Maryland

NASA
National Aeronautics and Space Administration

Scientific and Technical Information Branch

An Engineering Evaluation

in

Six Volumes

This document makes use of international metric units according to the Systeme International d'Unites (SI). In certain cases, utility requires the retention of other systems of units in addition to the SI units. The conventional units stated in parentheses following the computed SI equivalents are the basis of the measurements and calculations reported.

For sale by the National Technical Information Service
Springfield, Virginia 22161
Price

VOLUME II
CONTENTS

VOLUME II
CONTENTS (continued)

VOLUME II
CONTENTS (continued)

VOLUME II
CONTENTS (continued)

VOLUME II
CONTENTS (continued)

VOLUME II
CONTENTS (continued)

VOLUME II
CONTENTS (continued)

VOLUME II
CONTENTS (continued)

VOLUME II
CONTENTS (continued)

LIST OF ILLUSTRATIONS

VOLUME II
CONTENTS (continued)

VOLUME II
CONTENTS (continued)

VOLUME II
CONTENTS (continued)

VOLUME II
CONTENTS (continued)

LIST OF TABLES

VOLUME II
CONTENTS (continued)

FOREWORD

ATS-6 has been referred to as Arthur C. Clarke's "Star," because Mr. Clarke originated the idea for synchronous communications satellites in an article that he wrote in 1945. In 1975, Mr. Clarke was actively engaged in monitoring the Indian Satellite Instructional Television Experiment on ATS-6 and giving feedback to the Indian Space Research Organization. We, therefore, felt that it would be appropriate for him to contribute the foreword for this report.

An excerpt from his response to our request and selected paragraphs from his contribution, "Schoolmaster Satellite," follow.

ශ්‍රී ලංකා මොරටුව විශ්වවිද්‍යාලයේ
කුලපති කාර්යාලයෙනි

FROM THE DESK OF THE CHANCELLOR
UNIVERSITY OF MORATUWA, SRI LANKA

ආතර් සී. ක්ලාර්ක්
බී.ඇස්.සී., ඇෆ්.ආර්.ඒ.ඇස්., ඇෆ්.බී.අයි.ඇස්.
ලන්ඩනයේ කිංග්ස් විද්‍යාලයේ අයි සාමාජික
Arthur C. Clarke
B.Sc., F.R.A.S., F.B.I.S.
Fellow of King's College, London.

වැලිපෝන්: 94255
කේබල්: අන්ඩර්සී
කොළඹ
Tel: 94255
Cable: Undersea
Colombo

"ලෙස්ලිගෙ නිවස"
25, බාන්ස් පෙදෙස,
කොළඹ 7.
"Leslie's House"
25, Barnes Place,
Colombo 7.

24th September 1980

The extracts that follow are from an essay that was written in 1971, almost five years before the SITE program became fully operational, and originally appeared in the *Daily Telegraph Colour Magazine* for 17 December 1971. It was later read into the *Congressional Record* (27 January 1972) by Representative William Anderson, first commander of the nuclear submarine *Nautilus*, and now forms Chapter 12 of *The View From Serendip* (Random House, 1977; Ballantine, 1978).

To me, it brings back vivid recollections of my meetings with Dr. Sarabhai, the chief instigator of the program. I would like to dedicate it to his memory – and to that of another good friend, also closely associated with the project – Dr. Wernher von Braun.

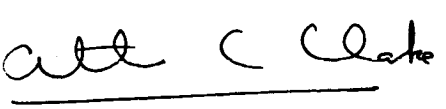

Arthur C. Clarke
Vikram Sarabhai Professor, Physical Research
Laboratory, Ahmedabad
India

Chancellor
University of Moratuwa
Sri Lanka

"For thousands of years, men have sought their future in the starry sky. Now this old superstition has at last come true, for our destinies do indeed depend upon celestial bodies—those that we have created ourselves . . .

"In 1974 there will be a new Star of India; though it will not be visible to the naked eye, its influence will be greater than that of any zodiacal signs. It will be the satellite ATS-F (Applications Technology Satellite F), the latest in a very successful series launched by America's National Aeronautics and Space Administration. For one year, under an agreement signed on September 18, 1969, ATS-F will be loaned to the Indian Government by the United States, and will be "parked" 22,000 miles above the Equator, immediately to the south of the sub-continent. At this altitude it will complete one orbit every 24 hours and will therefore remain poised over the same spot on the turning Earth; in effect, therefore, India will have a TV tower 22,000 miles high, from which programmes can be received with almost equal strength over the entire country . . .

"ATS-F, now being built by the Fairchild-Hiller Corporation, represents the next step in the evolution of communications satellites. Its signals will be powerful enough to be picked up, not merely by multi-million dollar Earth stations, but by simple receivers, costing two or three hundred dollars, which all but the poorest communities can afford. This level of cost would open up the entire developing world to every type of electronic communication—not only TV; the emerging societies of Africa, Asia and South America could thus by-pass much of today's ground-based technology, and leap straight in to the space age. Many of them have already done something similar in the field of transportation, going from ox-cart to aeroplane with only a passing nod to roads and railways.

"It can be difficult for those from nations which have taken a century and a half to slog from semaphore to satellite to appreciate that a few hundred pounds in orbit can now replace the continent-wide networks of microwave towers, coaxial cables and ground transmitters that have been constructed during the last generation. And it is perhaps even more difficult, to those who think of television exclusively in terms of old Hollywood movies, giveaway contests and soap commercials to see any sense in spreading these boons to places which do not yet enjoy them. Almost any other use of the money, it might be argued, would be more beneficial . . .

"Those who actually live in the East, and know its problems, are in the best position to appreciate what cheap and high-quality communications could do to improve standards of living and reduce social inequalities. Illiteracy, ignorance and superstitution are not merely the results of poverty—they are part of its cause, forming a self-perpetuating system which has lasted for centuries, and which cannot be changed without fundamental advances in education. India is now beginning a Satellite Instructional Television Experiment (SITE) as a bold attempt to harness the technology of space for this task; if it succeeds, the implications for all developing nations will be enormous.

"Near Ahmedabad is the big 50-foot diameter parabolic dish of the Experimental Satellite Communication Ground Station through which the programmes will be beamed up to the hovering satellite. Also in this area is AMUL, the largest dairy co-operative in the world, to which more than a quarter of a million farmers belong. After we had finished filming at the big dish, our camera team drove out to the AMUL headquarters, and we accompanied the Chief Veterinary Officer on his rounds.

"At our first stop, we ran into a moving little drama that we could never have contrived deliberately, and which summed up half the problems of India in a single episode. A buffalo calf was dying, watched over by a tearful old lady who now saw most of her worldly wealth about to disappear. If she had called the vet a few days before—there was a telephone in the village for this very purpose—he could easily have saved the calf. But she had tried charms and magic first; they are not always ineffective, but antibiotics are rather more reliable . . .

"I will not quickly forget the haggard, tear-streaked face of that old lady in Gujerat; yet her example could be multiplied a million times. The loss of real wealth throughout India because of ignorance or superstition must be staggering. If it saved only a few calves per year, or increased productivity only a few per cent, the TV set in the village square would quickly pay for itself. The very capable men who run AMUL realise this; they are so impressed by the possibilities of TV education that they plan to build their own station to broadcast to their quarter of a million farmers. They have the money, and they cannot wait for the satellite—though it will reach an audience two thousand times larger, for over 500 million people will lie within range of ATS-F . . .

"And those who are unimpressed by mere dollars should also consider the human aspect—as demonstrated by the great East Pakistan cyclone of 1971. That was tracked by the weather satellites—but the warning network that might have saved several hundred thousand lives did not exist. Such tragedies will be impossible in a world of efficient space communications.

"Yet it is the quality, not the quantity, of life that really matters. Men need information, news, mental stimulus, entertainment. For the first time in 5,000 years, a technology now exists which can halt and perhaps even reverse the flow from the country to the city. The social implications of this are profound; already, the Canadian Government has discovered that it has to launch a satellite so that it can develop the Arctic. Men accustomed to the amenities of civilisation simply will not live in places where they cannot phone their families, or watch their favourite TV show. The communications satellite can put an end to cultural deprivation caused by geography. It is strange to think that, in the long run, the cure for Calcutta (not to mention London, New York, Tokyo), may lie 22,000 miles out in space . . .

"The SITE project will run for 1 year, and will broadcast to about 5,000 TV sets in carefully selected areas. This figure may not seem impressive when one considers the size of India, but it requires only one receiver to a village to start a social, economic and educational revolution. If the experiment is as great a success as Dr. Sarabhai and his colleagues hope (and deserves), then the next step would be for India to have a full-time communications satellite of her own. This is, in any case, essential for the country's internal radio, telegraph, telephone and telex services . . .

"Kipling, who wrote a story about "wireless" and a poem to the deep-sea cables, would have been delighted by the electronic dawn that is about to break upon the sub-continent. Gandhi, on the other hand, would probably have been less enthusiastic; for much of the India that he knew will not survive the changes that are now coming.

"One of the most magical moments of Satyajit Ray's exquisite Pather Panchali is when the little boy Apu hears for the first time the Aeolean music of the telegraph wires on the windy plain. Soon those singing wires will have gone forever; but a new generation of Apus will be watching, wide-eyed, when the science of a later age draws down pictures from the sky—and opens up for all the children of India a window on the world."

A. C. Clarke

INTRODUCTION

ATS-6 was the final satellite in a series of six of the Applications Technology Satellite Program of the National Aeronautics and Space Administration. It was designed and built by Fairchild Space and Electronics Company, Germantown, Maryland, under NASA Contract NAS5-21100 from NASA Goddard Space Flight Center.

At the time of its launch, it was the largest and most powerful communications satellite to go into orbit.

The mission of ATS-6 was to demonstrate and evaluate the application of new technologies for future satellite systems. This it accomplished by demonstrating the first direct-broadcast television from geosynchronous orbit; by demonstrating many new communications technologies; by relaying data from, and tracking, low-orbiting satellites; by relaying communications and positions of ships and aircraft; and by supporting a variety of other experiments involving communications, meteorology, particle and radiation measurements, and spacecraft technology.

The purpose of this report is to document the lessons learned from the 5-year ATS-6 mission that might be applicable to spacecraft programs of the future. To satisfy this purpose, the six volumes of this report provide an engineering evaluation of the design, operation, and performance of the system and subsystems of ATS-6 and the effect of their design parameters on the various scientific and technological experiments conducted.

The overall evaluation covers the following:

- A summary of the ATS-6 mission objectives, operations, and results
- A summary description of the spacecraft system and subsystem requirements, the designs evolved to meet these requirements, and special analyses and ground testing performed to validate these designs and to confirm the flight integrity of the spacecraft
- A comparative evaluation of the 5-year performance and operations in orbit relative to those specified and demonstrated during ground tests prior to launch
- A summary of anomalies that occurred in the hardware, probable causes, and recommendations for future spacecraft systems
- A summary evaluation of the various technological and scientific experiments conducted
- A summary of conclusions and recommendations at the spacecraft system and subsystems levels that address considerations that might be relevant to future spacecraft programs or similar experiments.

ACKNOWLEDGMENTS

Many scientists, engineers, and technicians, too numerous to mention by name, have contributed to these volumes. Engineers at Fairchild Space and Electronics Company and Westinghouse Defense and Electronic Systems Center composed the chapters from material supplied by subsystems designers of the various systems and experiments, and have worked closely with the editors to complete this report. They have the editor's gratitude.

In particular, thanks go to Mr. Ralph Hall at Fairchild Space and Electronics Company and Mr. James Meenen of Westinghouse Defense and Electronic Systems Center for their patient cooperation, thorough review, and constructive comments and suggestions.

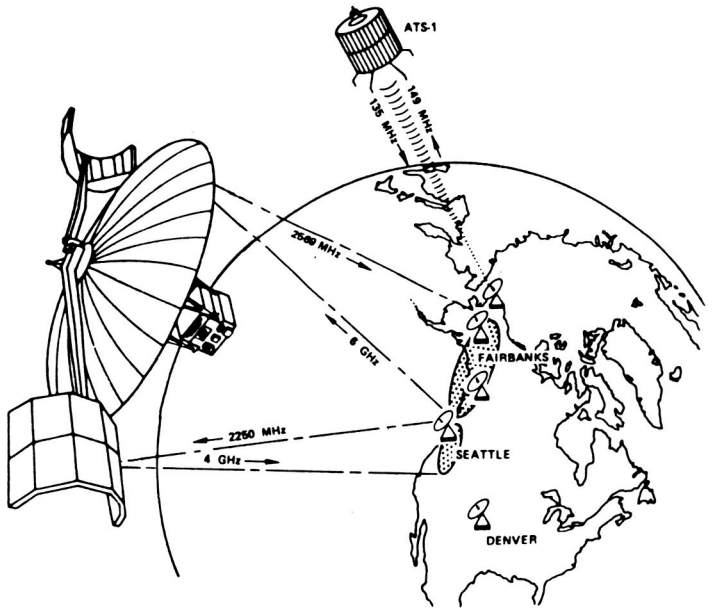

Alaska/Northwest

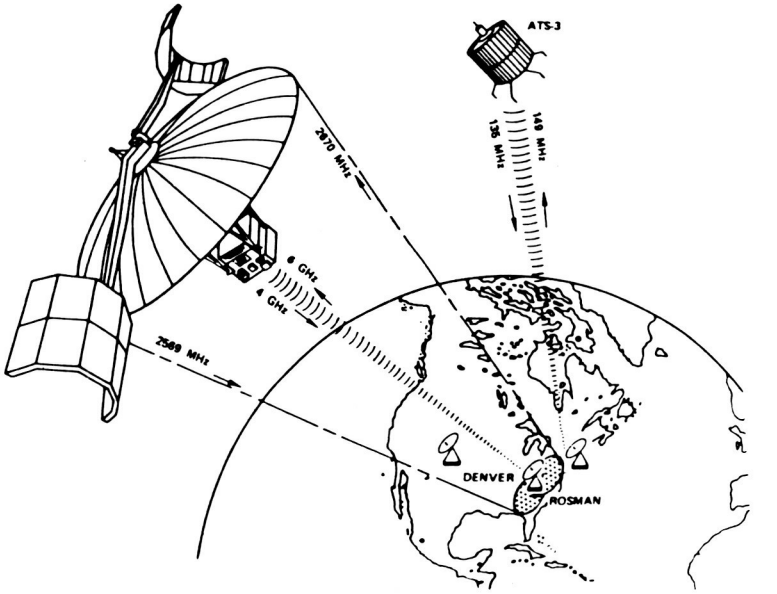

Appalachian Regional Commission

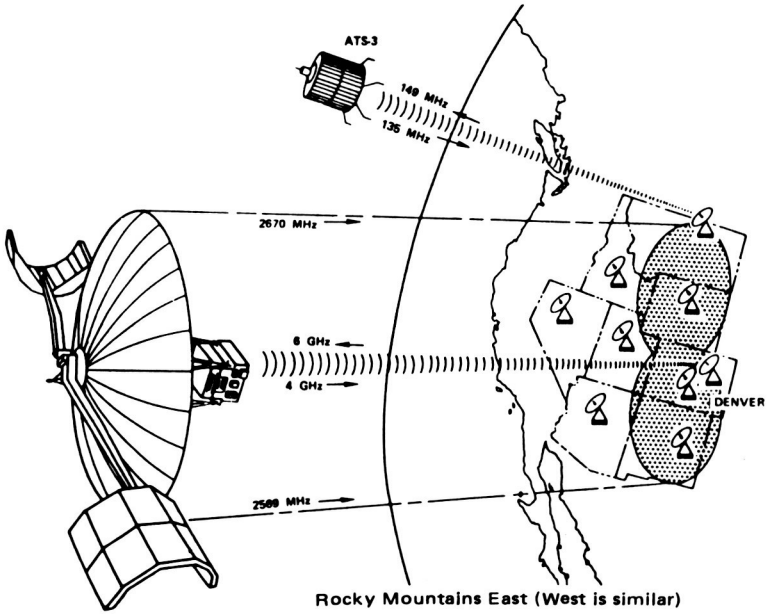

Rocky Mountains East (West is similar)

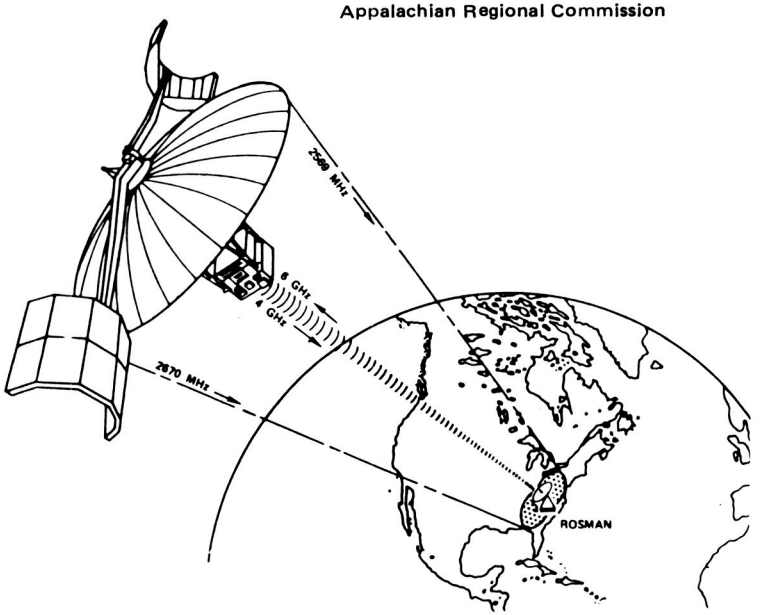

Veterans Administration

Spacecraft Pointing Accuracy of 0.1 Degree Was Required to Cover the User Terminals

Part A
Attitude Control

CHAPTER 1

ATTITUDE CONTROL SUBSYSTEM

FUNCTIONAL REQUIREMENTS

The attitude control subsystem (ACS) was required to stabilize and orient the spacecraft in response to ground commands. Upon receipt of the appropriate command sequence, including sensor, controller and actuator selection, and ground coordinate and/or satellite ephemeris data required, the spacecraft under ACS control was required to:

- Achieve local vertical orientation from an arbitrary initial orientation and rate
- Achieve attitudes and rates necessary to track fixed or moving targets by closed-loop tracking
- Achieve attitude and rates necessary to produce prescribed point-axis (Z-axis) motions by closed-loop following of ground commands.

In addition, the spacecraft ACS served as a test bed for the Spacecraft Attitude Precision Pointing and Slewing Adaptive Control experiment wherein telemetered ACS sensor data was processed on the ground; the results of that processing were commands issued to the ACS torquers.

Initial acquisition modes included rate damp, Sun acquisition, Earth acquisition, and Polaris acquisition. Closed-loop tracking modes included station-point and satellite-track modes. Closed-loop command following modes were local vertical, offset point, reference orientation, slew maneuver, satellite track, antenna pattern, and low jitter modes. The most important operational modes, the spacecraft reference axes/angles, and the design goals are defined in Figure 1-1.

Low jitter was an operational mode that for limited time periods maintained extremely low spacecraft tracking error angles and tracking error rates. In the antenna-pattern mode, the spacecraft Z-axis traversed a cloverleaf pattern by following a self-contained preprogrammed sequence of slew maneuvers.

DESIGN DESCRIPTION

Introduction

Honeywell Inc. designed and manufactured the attitude control subsystem under the direction of the prime contractor, Fairchild Space and Electronics Company.

The attitude control subsystem was divided into three main categories: sensors, controllers, and torquers as shown in Figure 1-2.

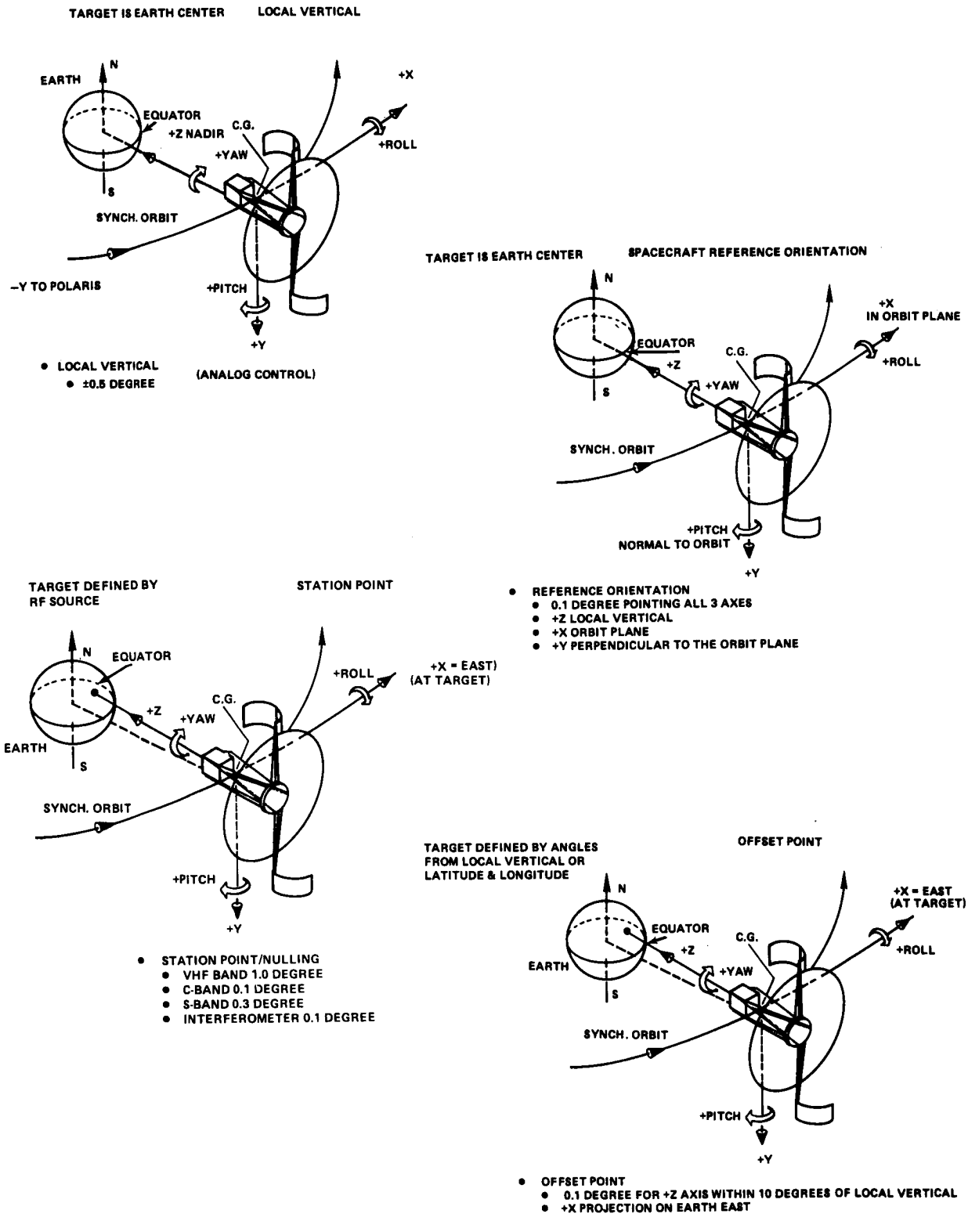

Figure 1-1. Principal Operational Modes (Sheet 1 of 2)

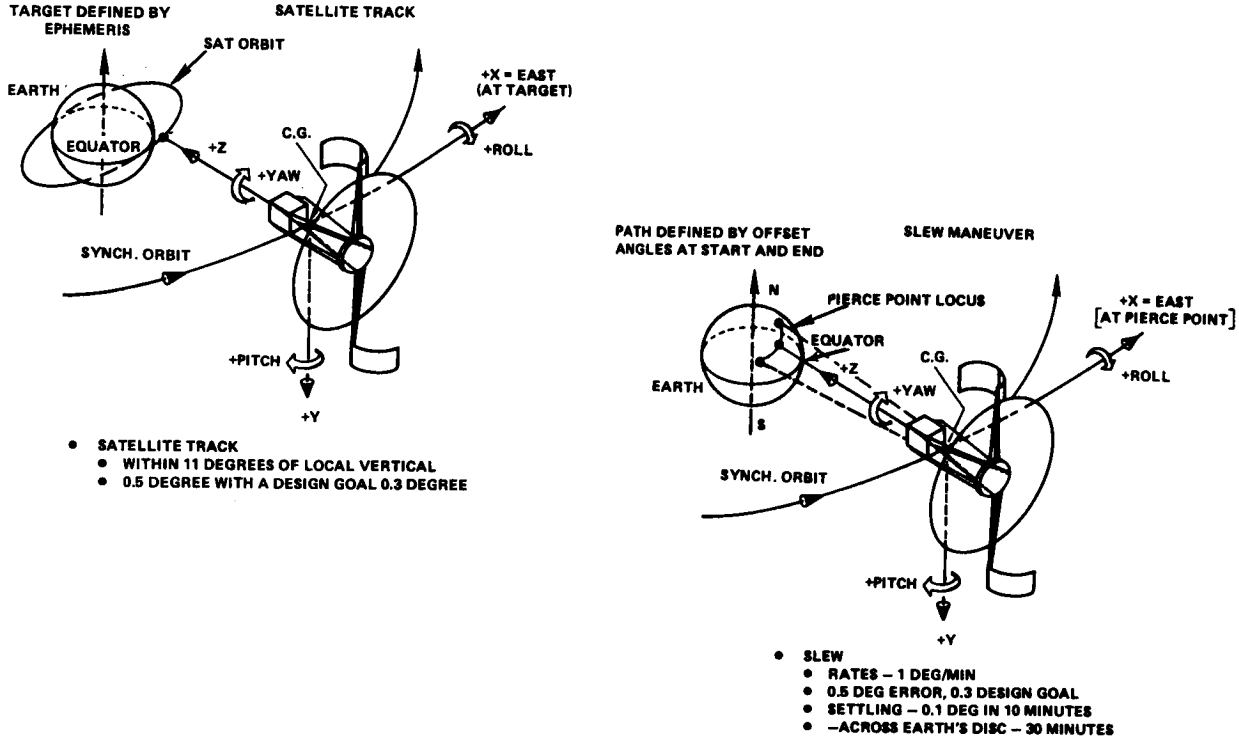

Figure 1-1. Principal Operational Modes (Sheet 2 of 2)

Suitable sets of components were used to achieve the various ACS modes.

A block diagram of the acquisition control modes is shown in Figure 1-3. The sensors used are shown in their order of use. The rate gyro assembly (RGA) provided rate damping signals. The coarse and fine Sun-sensor signals were used to acquire the Sun. The Earth sensor was used for Earth acquisition and provided the desired local vertical reference (roll/pitch) for subsequent operational control modes. The digital Sun sensor (DSS) was used to position the spacecraft pitch axis near the orbit normal until final referencing by the Polaris sensor assembly (PSA) was possible. Subsequently, the Polaris sensor was used to provide a reference for the control of the yaw axis. The very high frequency (vhf) monopulse provided a backup capability for roll and pitch acquisition of the Earth. A standby yaw inertial reference unit (YIRU) provided yaw hold capability. The acquisition modes used the propulsion system for torquing the spacecraft and the inertia wheels for subsequent attitude holding after each of the acquisitions. Backup control modes at reduced power levels included an analog backup controller (ABC) and ground command of the spacecraft propulsion subsystem (SPS) jets based on telemetered sensor data.

The block diagram of Figure 1-4 shows the primary operational control modes and the mode in which each of the sensors could be used. Only one of two digital operational controllers is shown; however, a duplicate set of interfaces was provided so that either controller could perform the functions. The inertia wheels were the prime means for torquing the spacecraft with the propulsion subsystem providing torques for unloading the wheels. The SPS was also capable of supporting all modes, except for low jitter, without the wheels. For orbit control, the SPS was the prime means of producing torque.

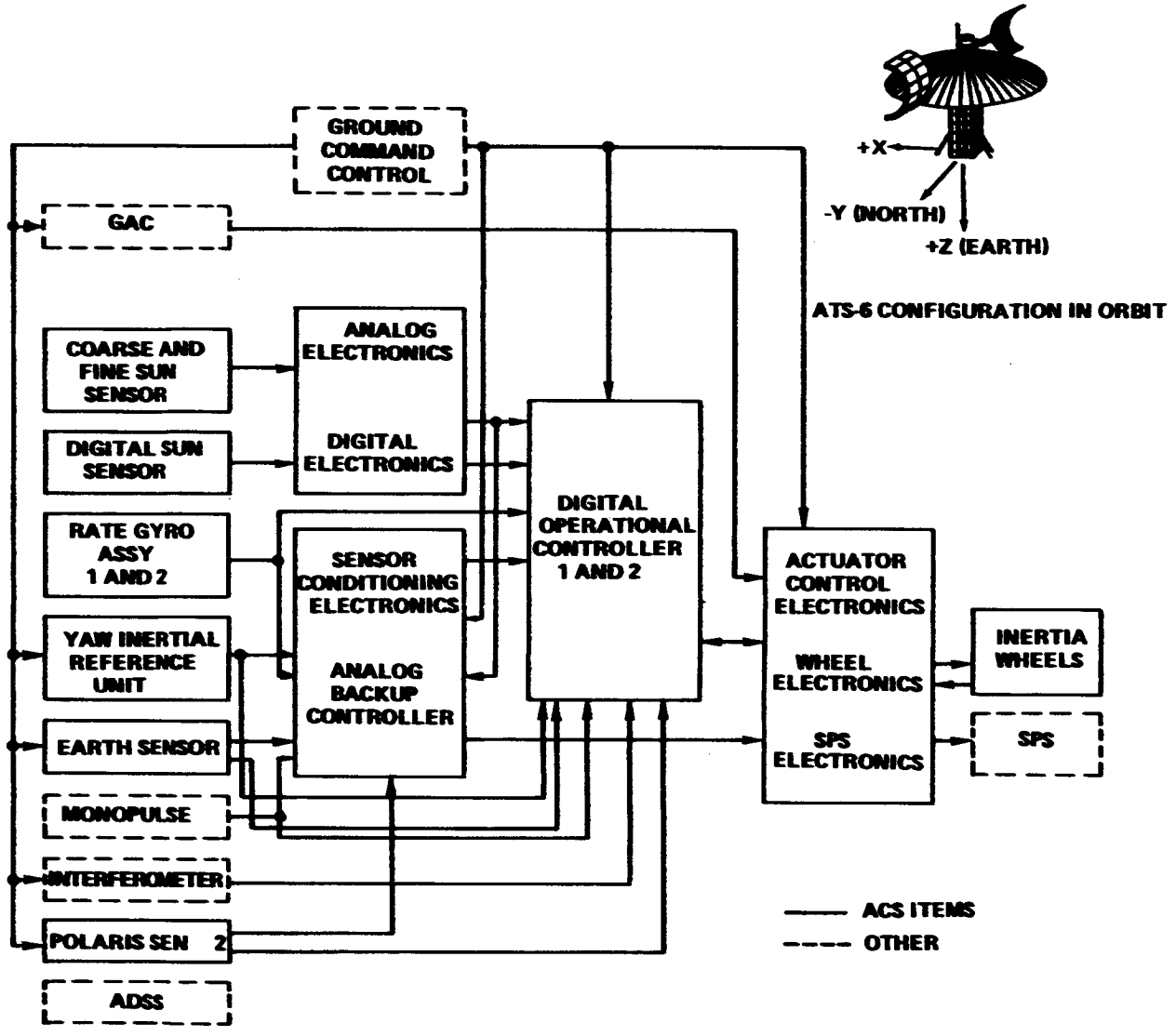

Figure 1-2. Simplified Block Diagram of Attitude Control Subsystem

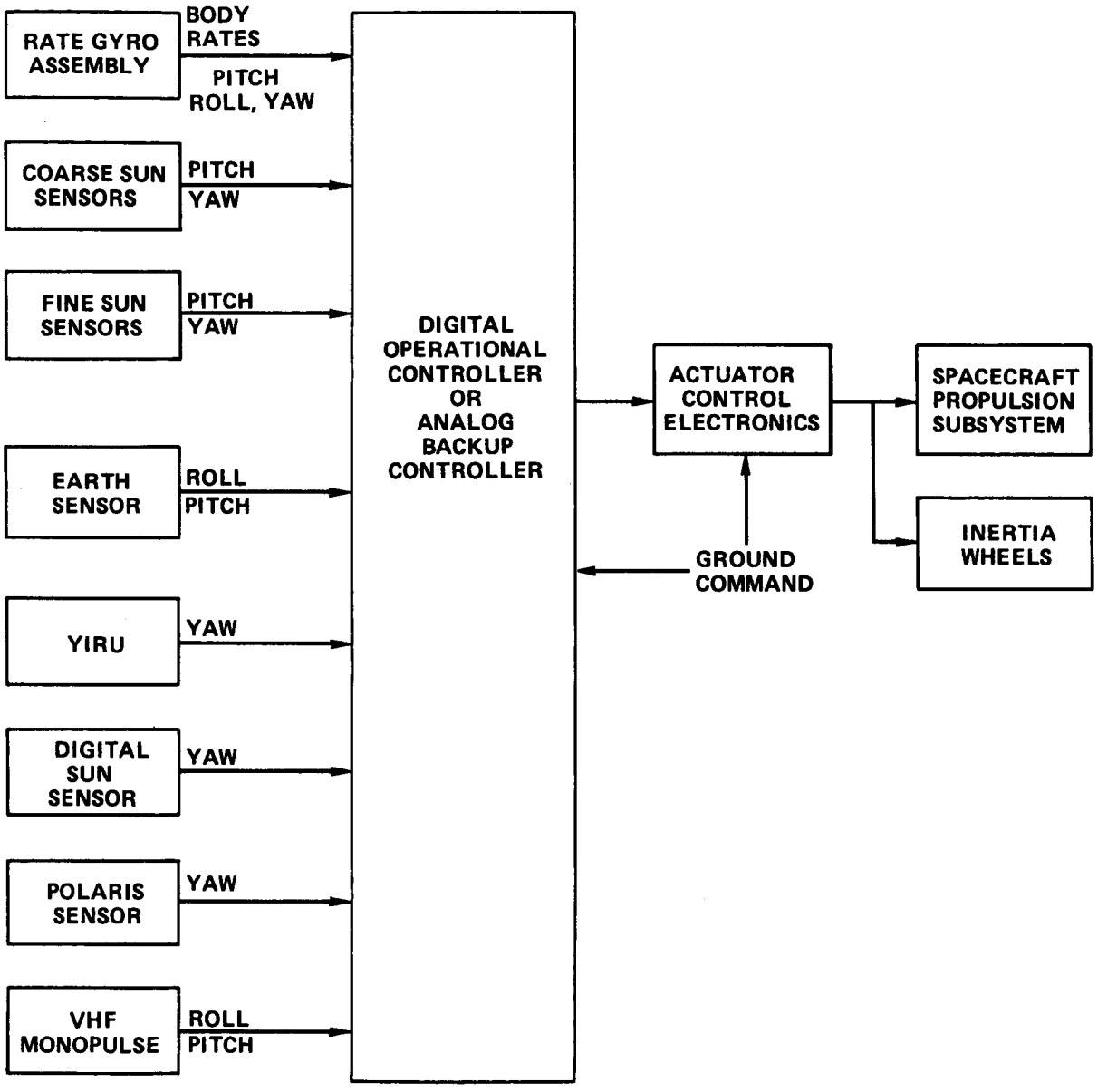

Figure 1-3. Acquisition Control Modes Block Diagram

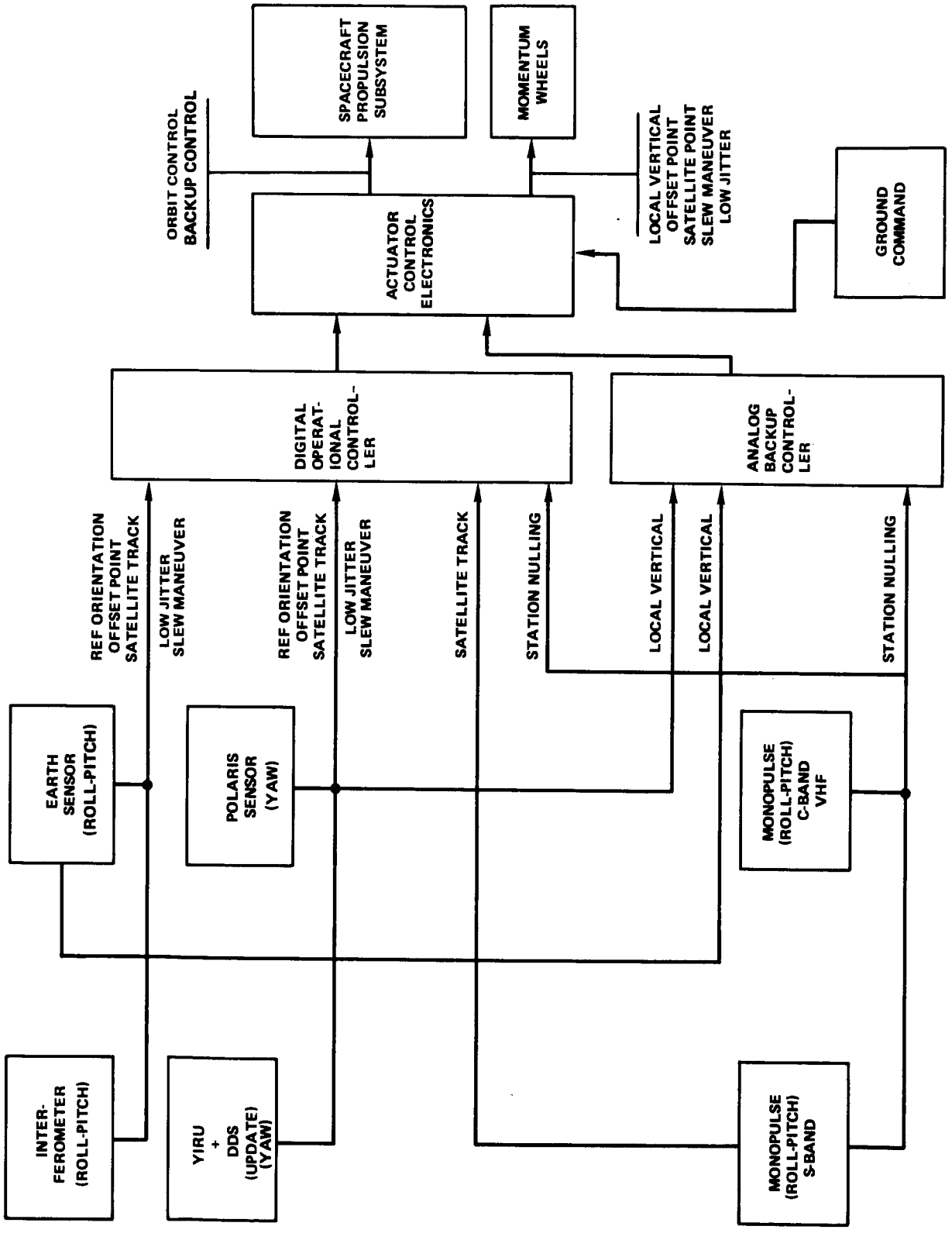

Figure 1-4. Operational Control Modes Block Diagram

Components

Sensors

Rate Gyro Assembly—The two assemblies of three single-axis gyros were referred to as RGA 1 and 2. They were used during the acquisition modes for rate damping and rate compensation. Each RGA consisted of three spring-restrained rate gyros mounted in an orthogonal frame to sense pitch, roll, and yaw spacecraft rates. Each RGA also contained power monitoring and conversion electronics, and signal conditioning electronics to provide the necessary interface between itself and the ABC, digital operational controller (DOC), data acquisition and control units, and command/decoder distributor (CDD).

The RGA provided roll, pitch, and yaw analog rate signals to the DOC's and ABC, which were proportional to the angular rates about each of the three mutually perpendicular axes. Outputs from each gyro had a linear range of -2.0 to +2.0 degrees per second with a scale factor of 2.5 volts per degree per second. Nominal zero uncertainty of each gyro was 0.05 degree per second maximum with a threshold and resolution not to exceed 0.01 degree per second.

Output signals were also conditioned and provided for telemetry, and each direct current (d.c.) analog rate signal was level shifted and scaled for the 0 to 5 Vdc telemetry. The telemetry scale factor was 1.5 volts per degree over -1.0 to +1.0 degree per second and 0.25 volt per degree out to ±5 degrees per second. A single spin motor sync detector was developed for all three gyros and the discrete signal provided as long as all three were synchronous. Mechanical stops limited the sensing gimbal movement to less than 5 degrees deflection, corresponding to a rate of 40 degrees per second.

If the two RGA's were both on, the output of the two were averaged, because the output of both RGA's were cross-strapped, and the gain was approximately 15 percent greater than for a single gyro.

Coarse/Fine Sun Sensors—Coarse Sun sensors (CSS) were used in initial acquisition to provide all attitude information with respect to the Sun line to allow the attitude control subsystem to roughly position the +X or -X axis of the spacecraft in the direction of the Sun line.

Fine Sun sensors (FSS) took over from the CSS when the spacecraft +X (or -X) axis was within ±8 degrees of the Sun line. The FSS provided pitch and yaw error signals prior to the acquisition of Polaris in the analog backup controller mode.

- Coarse Sun Sensor Assembly—The coarse Sun sensor assembly was a two-axis device that measured the angular displacement of the Sun line from the spacecraft in the X-Y and X-Z planes. The CSS's were used to control the X-axis of the spacecraft to within approximately eight degrees of the Sun line during acquisition of the Sun. Four CSS assemblies were used in the attitude control subsystem (ACS). Two of the four assemblies were mounted on the Earth viewing module (EVM), one on the +X and the other on the -X side, and the other two assemblies were mounted on the hub as shown in Figure 1-5. The two EVM assemblies consisted of three sensing elements, and the two hub assemblies consisted of

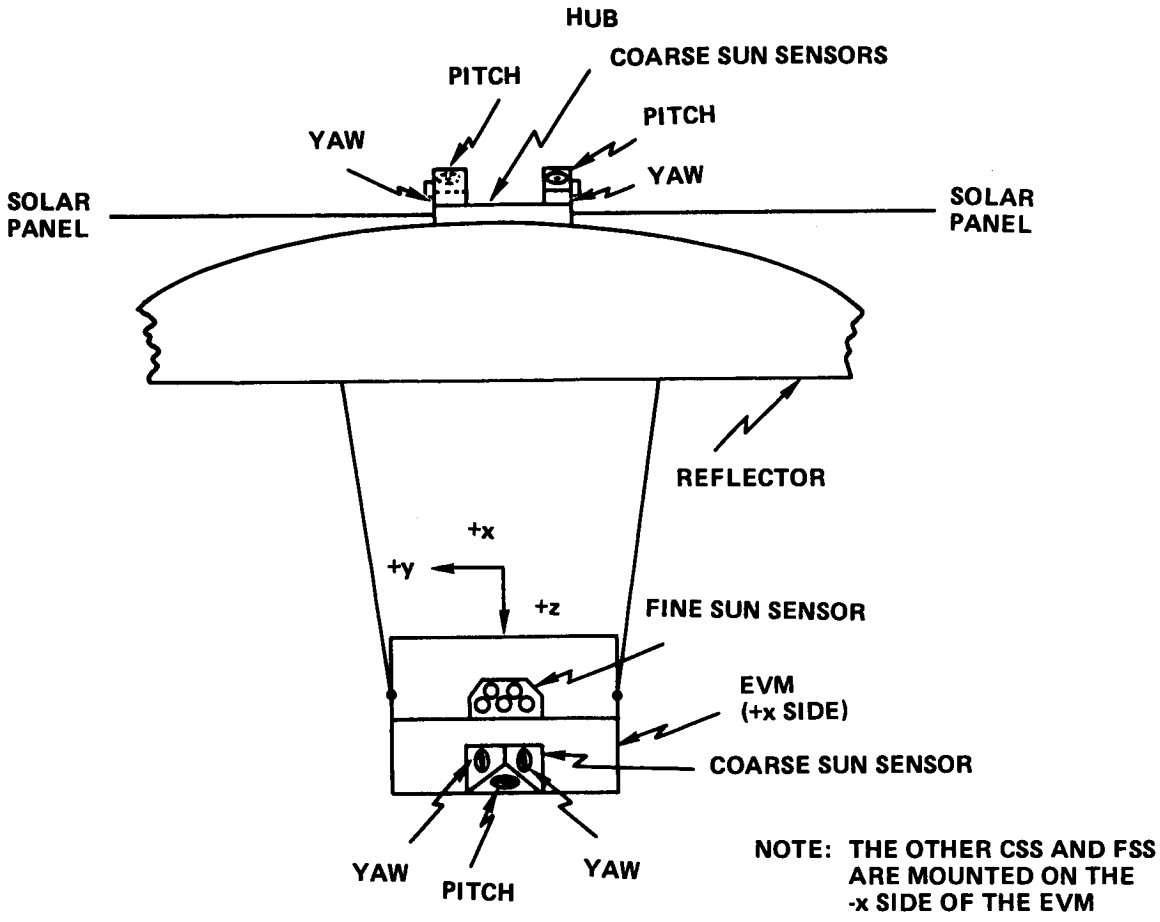

Figure 1-5. Sun Sensor Configuration

two sensing elements each. Silicon photovoltaic diode eyes were used for sensing elements in each of the CSS assemblies. The field of view of each eye was normally a hemisphere; however, masking was used to restrict the field of view, so that reflections would not be seen from the reflector or solar arrays. Each eye provided an analog output signal to the Sun sensor electronics assembly that was related to the angle between the Sun line and a vector normal to the sensor. When used in conjunction with the electronics, the output from two differentially connected eyes provided a null when the Sun was at equal angles relative to each of them. The total field of view provided by all the coarse eyes was 4π steradians.

- Fine Sun Sensor Assembly—Two fine Sun sensor assemblies were used by the ACS. One was aligned along the spacecraft +X axis and the other was aligned along the spacecraft -X axis. These assemblies also measured the angular displacement of the Sun line from the spacecraft X-Y and X-Z planes but to a greater accuracy than the CSS. Each FSS assembly consisted of silicon photovoltaic diode eyes and one target eye as shown in Figure 1-5. Two eyes were summed differentially to provide yaw attitude information and

two to provide pitch attitude information. The fifth eye was a target eye that detected the presence of the Sun and switched control from the CSS to FSS when the Sun was within a ±9-degree field of view. The field of view of both the pitch and yaw eyes was ±15 degrees; however, the signal to the controller was limited to ±6.7 degrees in pitch and ±12.3 degrees in yaw.

- Sun Sensor Electronics Assembly—The Sun sensor electronics assembly was used to process the pitch and yaw signals for the coarse/fine Sun sensors. The electronics interfaced with the CSS and FSS assemblies to provide analog output signals that represented the angular deviations from null in the pitch and yaw axes. The unlimited outputs, which were fed to the data acquisition and control unit for telemetry, had a range of ±50 degrees in the nonsensitive axis. Limited outputs of ±12.7 degrees in yaw and 6.7 degrees in pitch, were fed to the digital operational controller and the analog backup controller. The FSS target eye Sun-presence indication was used by the Sun sensor electronics assembly to switch outputs to the controllers from the CSS to the FSS.

Digital/Auxiliary Digital Sun Sensor—The digital Sun sensor (DSS) provided discrete information that defined the Sun vector relative to the spacecraft. The digital Sun sensors and their associated electronics were used by the digital operational controller to provide the proper Sun-bias error signal during Polaris acquisition and also for yaw backup control.

The auxiliary digital Sun sensors (ADSS) provided telemetry information only and defined the Sun vector information primarily in the areas not covered by the DSS.

- Digital Sun Sensor Assembly—The DSS used on ATS-6 measured two angles in orthogonal planes that described the vector from the DSS to the Sun. Each sensor had two quartz reticle blocks oriented orthogonally that produced a coded light pattern on the photocells located behind the reticles. The DSS is shown in Figure 1-6. The DSS quantized the field of view into 256 elements that covered a field of view of ±64 degrees about each slit, giving a resolution of approximately 0.5 degree over the entire field of view. However, the transition accuracy of each bit was approximately ±0.10 degree out to ±30 degrees. Since the material used in the sensor between the slit and the coded pattern had an index of refraction other than one, a cross-coupling effect was produced. The cross-coupling effect was the greatest toward the limit of the field of view of the sensor where the two angles were equal.

  The digital Sun sensors were mounted on the +X and -X sides of the service module. Because of the requirements for masking the DSS, the operational field of view was limited to 40 degrees up (-Z direction) and 64 degrees down in the pitch axis.

  The output of the DSS came from the photocells via amplifiers into buffer storage. The output of the buffer was a Gray code pattern that permitted only one bit to change for each unit angle change.

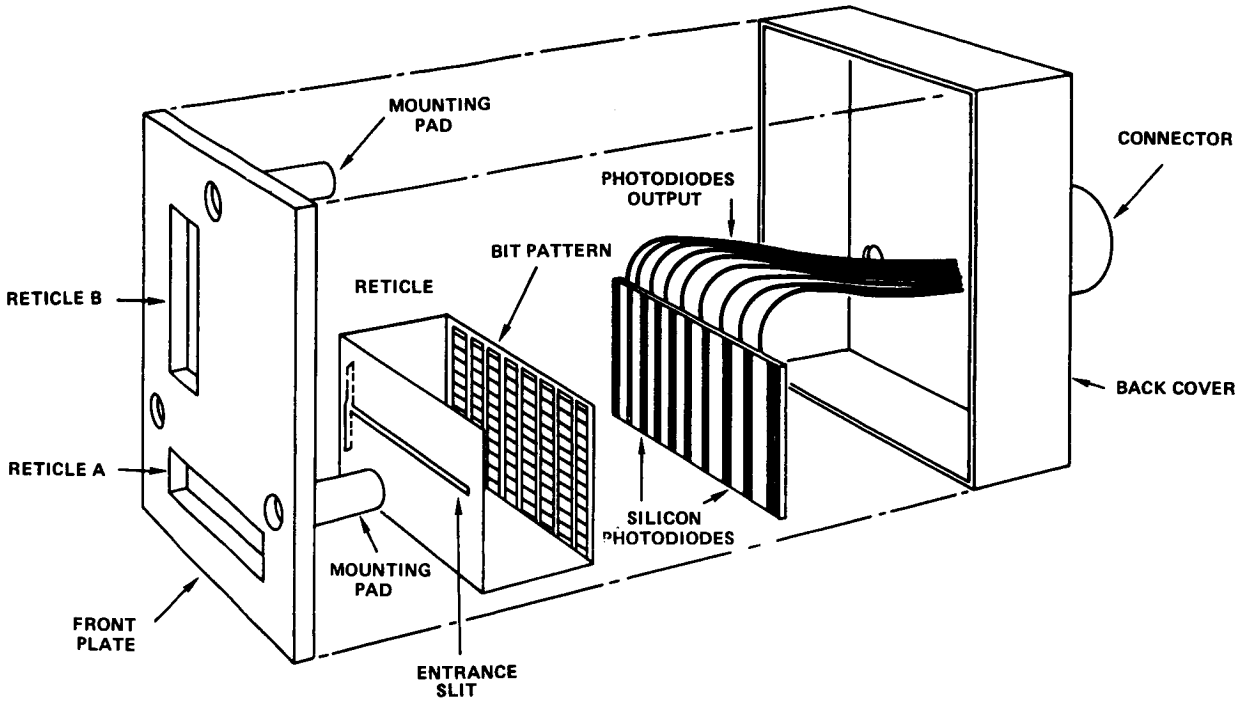

Figure 1-6. Digital Sun Sensor Head

The DSS electronics provided for parallel transfer of attitude data to the data acquisition and control units (DACU) and nondestructive serial data transfer to the DOC's. The electronics selected which DSS data was to be transferred to the DACU's and DOC's depending on the sensor being illuminated.

- Auxiliary Digital Sun Sensors—The auxiliary digital Sun sensors (ADSS) system consisted of three sensor heads mounted in conjunction with the DSS to provide 4 π steradian coverage. One of the ADSS was mounted on the north solar array boom and was aligned along the -yaw (-Z) axis. The other two sensors were mounted on +Y and -Y sides of the service module; however, they were inclined 31 degrees toward the +Z axis of the spacecraft. The ADSS was used primarily for determining attitude; i.e., to find the direction of the Sun line with respect to ATS. The ADSS quantized the field of view into 128 elements that covered a field of view of ±64 degrees about each axis for a resolution of 1.0 degree.

Earth Sensor Assembly—The Earth sensor assembly (ESA) was used to provide Earth reference data to the ACS. The ESA provided the primary pitch and roll inputs for all operational modes of the attitude control subsystem. The ESA consisted of a pitch sensing head, a roll sensing head, and associated electronics. Each sensing head consisted of an Earth sensing bolometer-telescope, a Sun sensor, a scan mirror, an offset mirror and an electronic package that provided the drive circuits for the mirror torquers and the output quantities. The Earth sensor was mounted on the Earth-facing end of the spacecraft and looked along the +Z-axis.

The sensor heads scanned the Earth disc in two dimensions to obtain measurements of pitch and roll attitudes of the spacecraft (Figure 1-7). From synchronous orbit, the Earth subtended an angle of 17.4 degrees. The two head scans were 26 degrees and provided excess coverage in each axis.

The Earth sensing bolometer-telescopes had an instantaneous field of view of approximately 0.6 X 0.1 degree. The scan mirrors were motor driven back and forth at 4 Hz to provide a scanned field of view of ±13 degrees. The scan mirrors could also bias the ±13-degree scan during offset pointing so that the scan remained centered on the Earth in the sensitive axis. The maximum amplitude of this scan bias was ±11.25 degrees. In addition to the scan bias in the scan plane, an offset mirror was provided that caused the scan to be offset in a direction perpendicular to the scan plane. The scan-plane offset was required during offset pointing operations so that the scan plane was along the maximum chord of the Earth. Thus, for pitch-offset point (off the local vertical) the pitch-scan mirror was biased by the desired amount, and the roll-offset mirror was also biased or offset by the same amount.

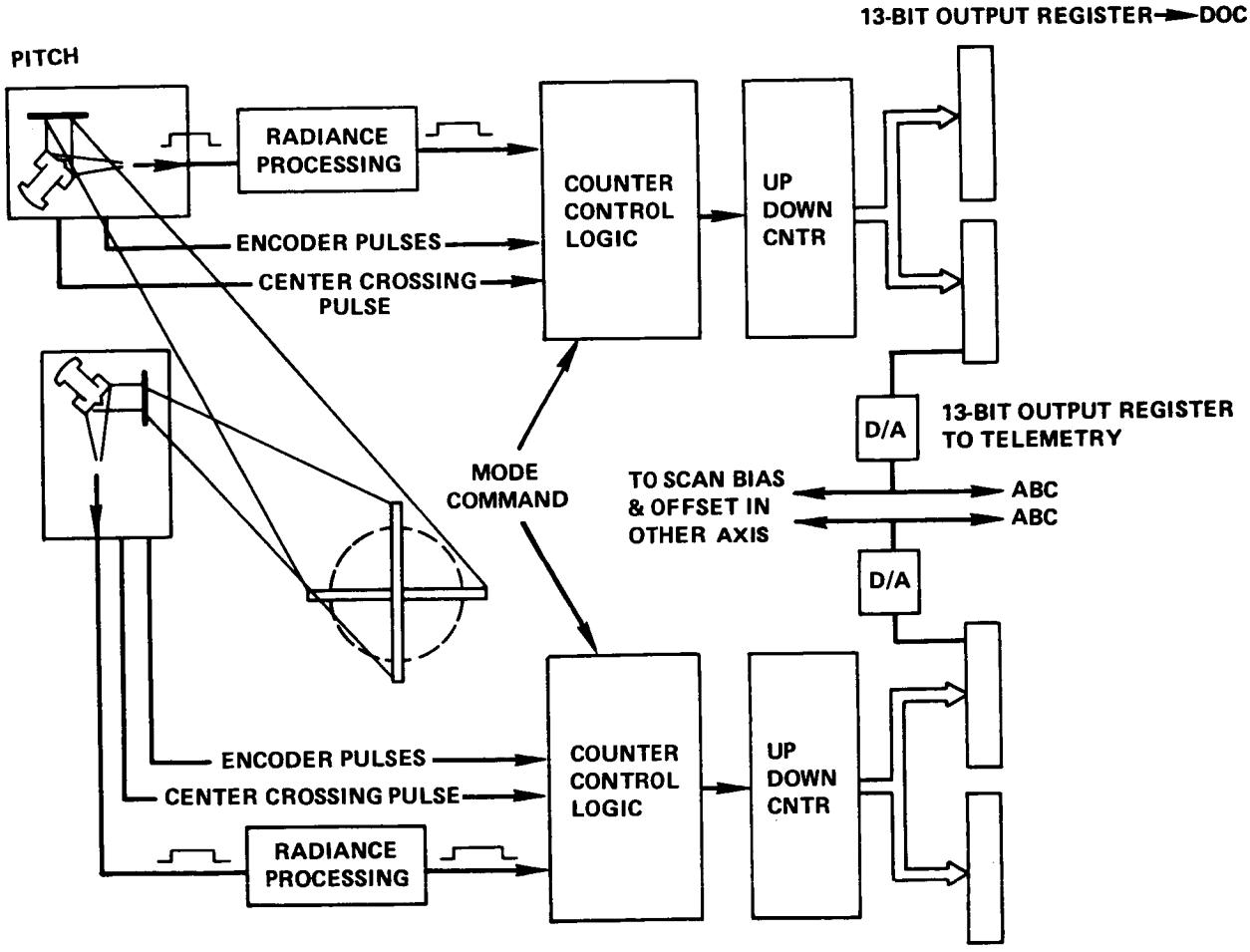

Figure 1-7. Earth Sensor Assembly

The scanning and offset mirrors were positioned by dc bias voltages that were developed by a digital-to-analog (D/A) converter in the Earth sensor assembly electronics to keep the ±13-degree scan centered on the Earth disc. These dc bias voltages were also provided to the analog backup controller where they were used to control the roll and pitch axes in analog backup controller (ABC) control modes. Since the ABC did not provide an offset pointing capability, the bias would always be operating near null for these control modes.

The digital error, which was a representation of the Earth sensor attitude angle, was derived in the following manner. During the scan of the instantaneous field of view, pulses out of an encoder mounted on the scan mirror were gated into an up/down counter based on:

- Space-to-Earth crossing
- Center crossing on the encoder (Z-axis null plane)
- Earth-to-space crossing.

For the off-local-vertical case, counting started from the space-to-Earth crossing, reversed sign at the center crossing, and stopped at the Earth-to-space crossing. If r is the Earth radius in counts, x is the number of counts between center crossing and the Earth-to-space crossing, and e_1 is the attitude angle in counts, then the counter contents up to center crossing were r+ (r-x). As indicated, the counter logic from center to Earth-to-space crossing subtracted x; therefore, at the end of a scan across the counter held:

$$r + (r-x) - x = 2r-2x = 2e_1$$

The scan back added $2e_1$; therefore, at approximately 0.25-second intervals, an attitude angle of $4e_1$ was available from the counter.

The avoidance of Sun interference in the Earth sensor was automatically achieved by offsetting the scan plane away from the Sun disc while still scanning through a sizeable portion of the Earth chord. To accomplish this, each Earth sensing element was equipped with a dual-cell Sun sensor that was aligned with the bolometer and had a sensing field radius of 3 degrees, which was concentric with the bolometer field of view. When Sun presence was detected, the split detector provided logic to offset the scan plane (by biasing the offset mirror) to minimize Sun interference. The maximum offset was 3.5 degrees of bias, at which point, if Sun presence was still detected, the scan automatically switched to an opposite polarity offset to get behind the Sun.

Yaw Inertial Reference Unit—The yaw inertial reference unit (YIRU) provided a functional backup to the Polaris star tracker. Late in the design of the attitude control subsystem, it was decided to substitute the YIRU for the Polaris sensor assembly 1 (PSA 1) to provide functional redundancy instead of standby redundancy for yaw sensing. The YIRU measured yaw angles to the following accuracies over a 1-hour period:

Goal:	±0.25°
Spec:	±0.5°
Worst Case:	±1.0°

The YIRU was capable of providing yaw sensing during acquisition or operational modes with either the digital operational controller or the analog backup controller.

The YIRU assembly consisted of a single-degree-of-freedom gas-bearing gyro with a fluid supported and damped float and an interface electronics box that was designed and built at Goddard Space Flight Center. The float was magnetically suspended in its bearings. The gyro package contained the rate integrating gyro and associated electronics packaged in one sealed container that was filled with helium for thermal reasons. The interface electronics box contained the electronics that provided the interfaces between the attitude control subsystem and the gyro package. Figure 1-8 is a functional block diagram of the YIRU. The three operational modes of the YIRU were: uncage, cage, and torque.

In the uncage mode, the gyro was uncaged and would measure the inertial position deviation (position error) from a reference point about the yaw axis. The gyro could be placed in this mode by command without putting it in control of the spacecraft. The gyro could maintain spacecraft reference over ±1.2 degrees minimum deviation from null. The ±1.2 degrees was determined by the gyro stops and by float damping, hence gyro temperature. The maximum spacecraft stop angle was ±3.9 degrees. The uncompensated drift in this mode could not exceed 0.3 degree per hour.

In the cage mode, the gyro torquer was driven by the gyro signal generator and effectively reset the gyro to a null position. This mode (followed by uncaging) was used to establish a new reference position (e.g., just prior to the Sun moving out of the digital Sun sensor's field of view with the digital Sun sensor providing yaw attitude control). It was used as a standby mode when the gyro was not controlling.

There were two torquing modes of the YIRU. Upon receipt of a high-torque command from the ground, the YIRU could be torqued at a rate of 0.33 degree per second. The direction of gyro torquing was established by a high torque plus or minus polarity command. This torque rate was stopped by the high-torque-off commands. When the high-torque-off command was sent from the ground, it not only stopped the high torquing of the gyros, but it incremented the gyro reference by approximately 0.035 degree. The high-torque-off command generated a 100-millisecond pulse to the torquer and moved the float 0.035 degree each time it was issued. By issuing high-torque-off commands, the YIRU could be referenced in ±0.035 degree increments. The polarity of the rereferencing pulses was determined by the high torque plus or minus commands.

Drift compensation torquing provided a means for trimming the gyro drift in orbit. The gyro drift was sent to the spacecraft in a five-bit command word that was stored by relays in the interface electronics box. The digital word was then converted to an analog current within the gyro and fed to the gyro torquer. The total drift compensation capability was ±1.5 degrees per hour with a resolution of 0.1 degree per hour. This drift-compensation command was set and stored in the interface electronics box, and the YIRU was torqued at this rate whenever it was in the uncaged, or attitude mode.

The YIRU normally was used as a backup to the Polaris tracker (PSA 2) except after initial Sun and Earth acquisition when the YIRU maintained the yaw attitude reference until subsequent Polaris acquisition was commanded. When used as a backup in the reference-orientation mode (using the

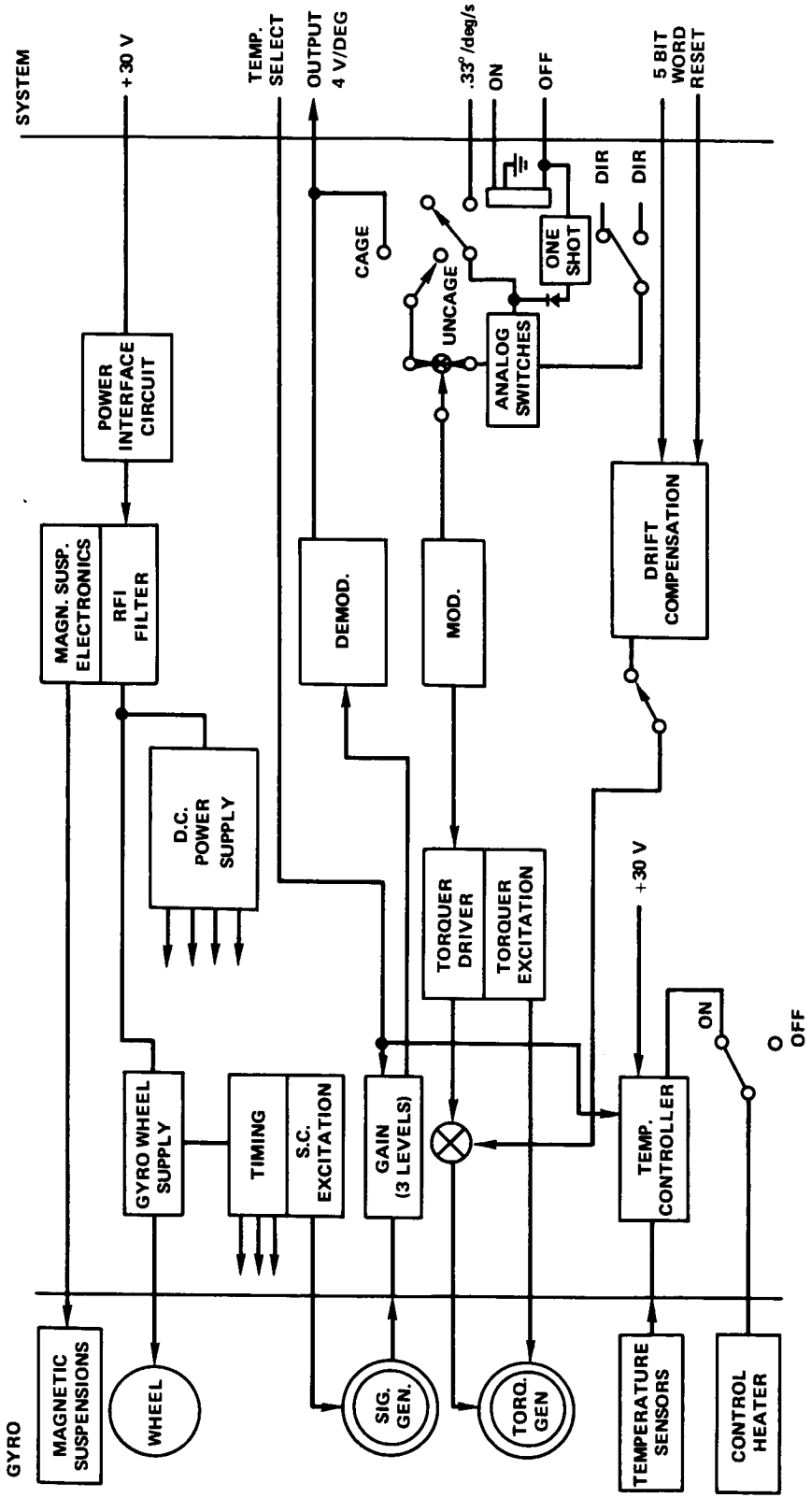

Figure 1-8. YIRU Functional Block Diagram

digital operational controller), the YIRU presented no special operational problems except to update the yaw reference once or twice per day with the DSS and to recompensate the gyro when the drift exceeded ±0.15 degree per hour. However, when the spacecraft was performing an offset pointing so that the yaw axis was no longer in the orbit plane, the YIRU would sense a component of the Earth's rate that was a function of the angle between the Z-axis and the orbit plane. The YIRU could be compensated for this effect with the drift bias compensation term (±1.5 degrees per hour) up to an angle of approximately 5 degrees. Beyond this the YIRU re-reference command (0.035 degree per pulse) had to be used to compensate the YIRU.

Polaris Sensor Assembly—The Polaris tracker and associated electronics were used by the attitude control subsystem. The Polaris sensor assembly (PSA) was used during Polaris acquisition modes and served as the primary yaw sensor for all operational and most experimental modes. The PSA was mounted with its optical axis parallel to the -Y axis of the spacecraft. The total field of view of the Polaris tracker was approximately 9 degrees in yaw by 28 degrees in roll. The sensor provided an analog output signal that was linear over a range of about ±3.5 degrees and was in a saturated condition range to about ±4.5 degrees. The analog output voltage was proportional to the angle between the line of sight to Polaris and the plane containing the Y-Z axes of the sensor.

The images of any objects within the field-of-view limits were formed by the objective lens on the image dissector tube photocathode. The emitted photoelectrons were accelerated and imaged by the focus potentials into, or through, a conducting, grounded aperture plate that separated the focusing section from the dynode multiplier section. The electron image of the field-of-view was scanned by the aperture plate by the application of a saw-tooth voltage to the electron yaw-angle deflection plates in the tube image section. Demodulation of this signal, after further amplification, provided a signal whose time-averaged amplitude and polarity was related to the mean star position offset from the center of the electron aperture. This current signal was summed in an intergrator, amplified, and fed back to the yaw-angle deflection plates. This completed a control loop that nulled the mean star position on the electron aperture plates. The star yaw-angle offset was then directly proportional to the offset (tracking) voltage that maintained the null position. This voltage was provided to the attitude control electronics as a yaw-angle signal to be used for yaw stabilization of the spacecraft.

Prior to star acquisition, the field of view (FOV), which is the image of the electron aperture projected forward through the objective lens, was biased to the limiting yaw angle (+4.0 degrees, ±0.5 degree) or acquisition bias position. If a star entered the FOV and exceeded the threshold of the intensity magnitude gate, the bias signal was then removed from the deflection plates and the FOV was allowed to track the star. In the event of loss of acquisition, a flyback and sweep search of the entire yaw angle FOV (±4.5 degrees maximum) was made automatically in an attempt to reacquire. If the search was not successful, the FOV would return to the acquisition bias position.

Identification of Polaris was made on the basis of the modulated and amplified signal that was remodulated and summed to provide a signal, with a narrow noise bandwidth, related to the intensity of the star illumination. This signal provided the reference for the voltage supply that fed the dynode multiplier structure. This completed an automatic gain-control loop that provided a constant

tube modulated output over a wide range of star intensities. Star intensity information was obtained from the dynode voltage supply and was compared against low-brightness limits (gates) for an identification decision. If the decision was affirmative, an acquisition signal was provided to the attitude control electronics and the FOV would track as previously described. If no star met the brightness criteria, the FOV would remain in the search position. Signals might be sent to the PSA that stepped the low gate to a lower value. Subsequent signals would set the low gate to a still lower value, then reset it to the original level and recycle. The acquisition of a star satisfying the brightness gates initiated logic that maintained track until such time as the FOV became dark enough to fall below the drop-out level of the effective low gate.

The roll-angle deflection plates in the image dissector tube were used to provide five discretely-stepped, roll-angle offsets in the FOV to follow the variation in roll angle of Polaris due to spacecraft roll maneuvers. Pulse commands sent to predetermined Polaris sensor assembly input pins stepped the FOV.

A Sun detector mounted to the baffle assembly activated the Sun shutter when the spacecraft became oriented in such a way as to allow sunlight to enter the tracker optics.

Interferometer Sensor—The interferometer was a precision, wide field-of-view attitude sensor for the spacecraft attitude control subsystem. It used six antennas on board the spacecraft, placed in the Earth-viewing surface of the EVM with three each arranged in lines parallel to the pitch and roll axes. The three pitch-sensitive horns and three roll-sensitive horns, which received C-band signals from continuously transmitting ground stations, were spaced to give phase information from a closely spaced pair and from a widely spaced pair in each axis. After measuring the phase differences received at paired antenna elements, the interferometer converted this information into digital data related to spacecraft attitude angle.

The basic equation used to convert the measured phase difference, γ, between the received signals with wavelength, λ, at two antennas separated by distance, D, into the incidence angle, θ, was:

$$\theta = \cos^{-1} \frac{\lambda\gamma}{2\pi D}$$

Thus, the transfer characteristic was a fixed relationship between the digitized electrical phase angle and the spatial spacecraft attitude angle. It should be noted that the relationship was trigonometric rather than linear. The coarse and vernier baseline distances, D, in terms of signal frequency were 1.66 λ and 19.95 λ, respectively. It can be seen that the coarse characteristic was unambiguous (single-valued) over a field of view of $\pm$17.5 degrees; twelve times larger than the vernier's unambiguous field of view. It was this feature that allowed the use of the high resolution vernier outputs, without ambiguity, over the full coarse unambiguous field of view (when the coarse field of view itself was known). An angular resolution 0.017 degree was provided for the coarse mode and 0.0014 degree for the vernier mode.

There were four commandable modes of operation:

- Vernier or coarse or both outputs
- Roll or pitch or both axes outputs
- Operating frequency f_1 or f_2 or both
- Baseline phase reversal (for calibration).

A single ground station provided two-axis sensing (pitch and roll) while for three-axis sensing with computed yaw, two ground stations were required. In the single-frequency mode, the interferometer could be directly connected to the attitude control subsystem. In the baseline calibration mode, phase readings (phase and phase reversal) were taken over two diagonal baselines, thus providing in-flight calibration. Nominally, the ground sources were the same NASA stations provided for the communications experiments.

The rf interferometer consisted of four functional assemblies:

- Antenna Array—The antenna array, mounted on the Earth-viewing surface of the Earth-viewing module, consisted of two orthogonal baselines, each baseline being orthogonal to the yaw angle of the spacecraft.
- Receiver—A two-channel receiver was provided, with one channel for the reference signal and one for the comparison signal. A coupler/switch module provided for time division multiplexing between the signals from the coarse and vernier antennas. The first local oscillator converted the signals down to 150 MHz. The signals were then applied to the second mixer where a 2-kHz frequency difference was introduced by the dual local oscillator. Two signal paths, offset by 5 MHz, provided for simultaneous two-frequency operation. The outputs of the receiver system were low-frequency signals (2 kHz) which had preserved the phase relationship of the microwave signals received at the antennas.
- Spacecraft Data Converter—The interferometer data converter measured the phase relationship of the receiver output signals with respect to a coherent reference signal and converted these measurements to digital form that could be telemetered to the ground or connected to the attitude control subsystem. A complete measurement could be made every 230 milliseconds and telemetered once every three seconds.
- Interferometer High Speed Data Link (IHSDL)—The IHSDL was the resultant output of the digital converter phase-count gate and a 4-MHz oscillator. These were combined to yield clock pulses proportional to the detected phase of the interferometer responses to angular offsets (255 clock pulses equal 360 degrees). The waveform was a pulse-width modulated signal burst at a 1-kHz sample rate. The spacecraft IHSDL output was contained in a 300-kHz to 1-MHz base bandwidth that was diplexed on a dedicated 1-MHz

bandwidth channel with the very high resolution radiometer (VHRR) (Figure 1-9) converted up to 4 GHz (C-band) and transmitted on the downlink. The IHSDL could respond to a maximum 500-Hz jitter frequency that could be read on the ground in real time or recorded on tape and processed at a later time.

A summary of interferometer characteristics follows:

Type of Receiver	Dual conversion, dual channel Switched antenna elements
Input Frequency	6.150 and 6.155 GHz
Noise Figure	15 dB
Vernier Baseline	97.262 cm (38.292 in.) (19.95 λ)
Coarse Baseline	8.105 cm (3.191 in.) (1.66 λ)
Configuration	Crossed baselines
Antenna Gain	+12 dB
Angle Accuracy (pitch, roll)	0.018° (3σ) over ±12.5° angle range 0.025° (3σ) over ±30° angle range
Antenna Element	Compensated horn
First I.F./I.F. Bandwidth (BW)	150 MHz/15 MHz
Second I.F./I.F. BW	(Dual) 32.5 MHz and 27.5 MHz/1 MHz
Output Frequency/BW	2 kHz/600 Hz
First Local Oscillator (LO) Frequency	6.000 GHz
Second LO Frequency	122.5 and 122.502 MHz
Post-Filter SNR	+41 dB at +73 dBW ground e.i.r.p.
Vernier Clock Frequency	1024 kHz
Coarse Clock Frequency	1024 kHz
Counter Input Rate	2 kHz
Vernier Averaging	64 samples
Telemetry Output	Digital 72 bits/3 sec (1 or 2 sta modes)
Weight	53.8 kg (18.5 lb)
Power	15.5 watts

Monopulse—The communication subsystem's C-band, S-band, or vhf monopulse provided error signals to the attitude control subsystem (ACS) that were proportional to the tracking error in the pitch and roll planes of the prime focus feed antenna. The basic characteristics of these error signals are listed in Table 1-1.

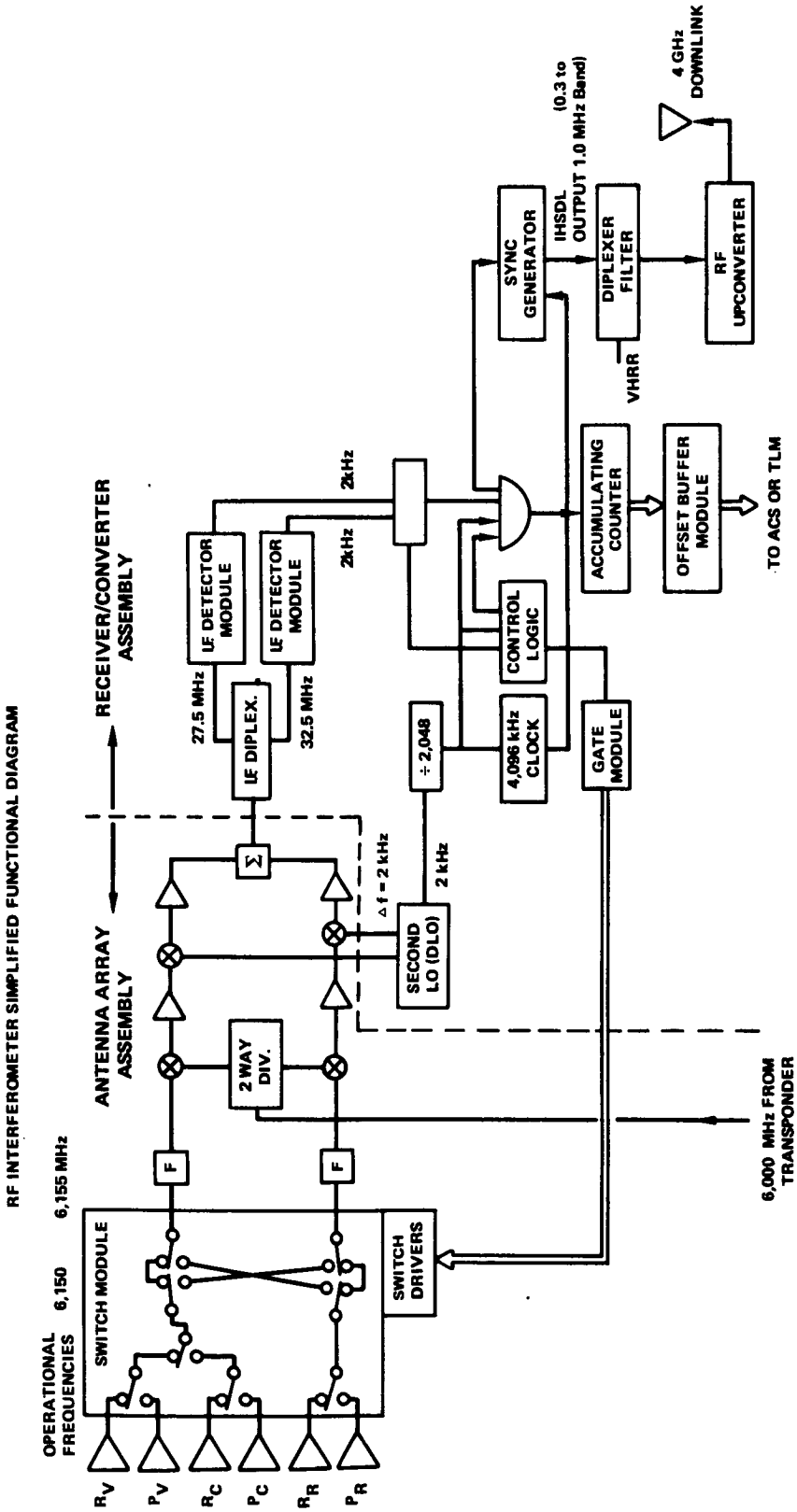

Figure 1-9. Block Diagram of Interferometer Subsystem

Table 1-1
Monopulse Error Characteristics
(Design Requirements)

Freq.	Scale Factor (V/deg)	Rms Noise at Null (mV)	Off-Boresight Linearity Angle (deg)	Off-Boresight Saturation Angle (deg)	Off-Boresight Roll-Off Angle (deg)
Vhf	1.0	±10	±3	±7.5, ±0.5	±11.0
S-band	8.0	±10	±0.25	±0.67, ±0.1	±1.0
C-band	24.0	±10	±0.1	±0.23, ±0.05	±0.35

The error signals were linear with the given scale factor to within ±5.0 percent out to the indicated off-boresight linearity angle as a minimum. The rms noise level at null related to the same scale factor. A smooth, continuous error signal versus the angle off boresight was provided from this linearity angle point to the off-boresight saturation angle point within the given tolerances. The error signal from this angle point to the roll-off off-boresight angle point as a minimum was flat or monotonically increasing at 6.5 volts ±0.5 volt level. The signal characteristics in orbit for the vhf monopulse differed significantly from the design values given in Table 1-1; however, a viable attitude control subsystem station pointing mode was demonstrated with the vhf monopulse.

Controllers

The onboard controllers were the two digital operational controllers and the analog backup controller. A control mode was also provided using telemetered sensor data and ground control of the momentum wheels or jet torquers by command.

Digital Operational Controller—Two digital operational controllers (DOC) were provided in the attitude control subsystem (one primary and one backup). They were each 26.9 cm (10.6 in.) wide by 30.5 cm (12 in.) long by 15.2 cm (6 in.) high with a 5 cm (2 in.) connector plate and weighed 10.6 kg (23.4 lb) nominal. Each DOC required 27.2 watts nominal at 30.5 Vdc and were protected for overvoltage, undervoltage and overcurrent.

The operations personnel at ATSOCC chose the controller to be used. The digital operational controller served as the prime controller for all modes of operation (Figure 1-10). In addition to performing control loop computations for stabilizing the spacecraft, the DOC provided the following functions:

- Accepted a wide variety of sensor inputs, computed the control commands, and commanded torquers for all modes

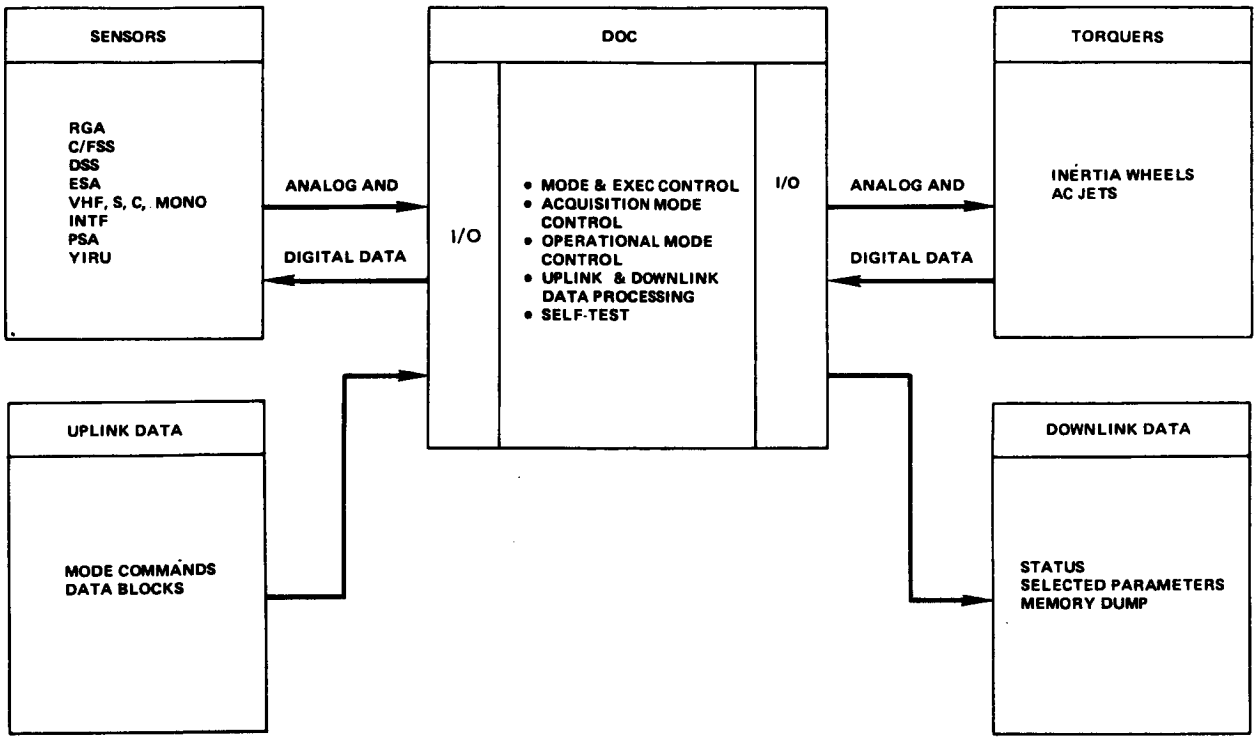

Figure 1-10. DOC Modes of Operation

- Executed acquisition logic to acquire the Sun, Earth, and Polaris
- Accepted commands for offset pointing (angle and ground coordinate commands)
- Computed compensations required for pointing commands to account for orbit eccentricity, orbit inclination, and Polaris diurnal motion
- Computed commands for performing Z-axis tracking of a low altitude satellite based on transmitted ATS and satellite ephemeris data
- Computed commands for performing slew maneuvers for antenna pattern measurements
- Provided a self-test routine within the DOC.

The basic DOC was a digital computer and consisted of a power supply, central processor, a memory, and an input/output section (Figure 1-11). The DOC provided for transfer of blocks of data to the telemetry data acquisition and control unit or complete data transfer from memory on command from the ground station. In addition, the DOC could be reprogrammed in orbit (a vital capability used a number of times during the ATS-6 mission) by changing instructions stored within its memory on commands from the ground controllers.

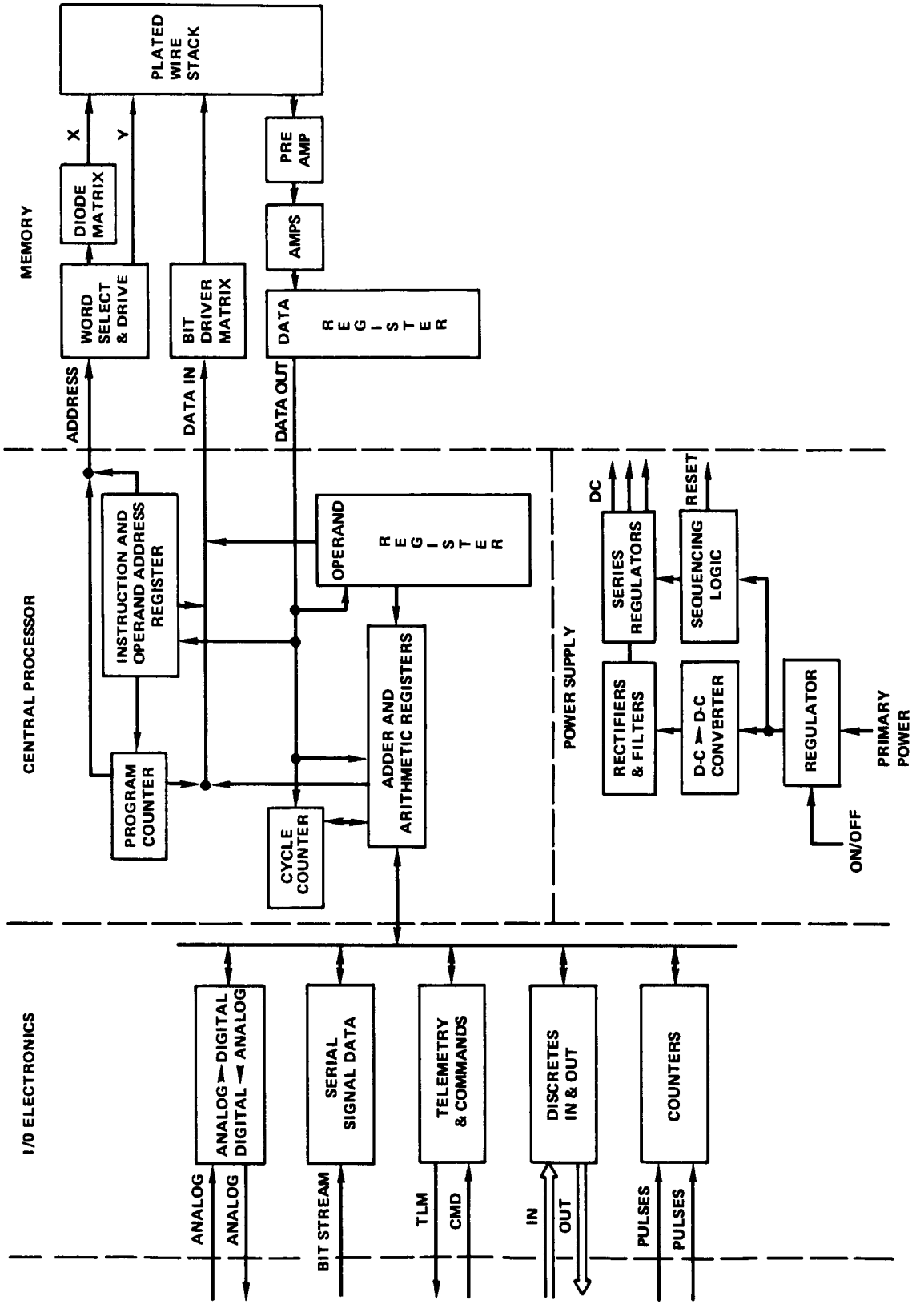

Figure 1-11. Digital Operational Controller

The heart of the DOC was the central processor that performed programs stored within the memory. The input/output electronics accepted both analog and digital signals and could supply monitoring signals to telemetry, and control signals to sensors and to the actuator control electronics (ACE) for controlling the momentum wheels and torquing jets. The features of the central processor and memory are as follows:

Central Processor

- Four-bit byte serial machine organization
- Sixteen-bit word, two's complement arithmetic
- Two full-word arithmetic registers
- Provided memory with only 5-microsecond cycle time and 1.0-microsecond access time
- Memory addressing to 32 sectors (16,384 words)
- 512-word memory sectors
- Multilevel indirect addressing and indexing
- 40 instructions
- Most instructions executed in 10 microseconds
- Hardware multiply, 90 microseconds
- Hardware divide, 160 microseconds
- Crystal oscillator frequency reference, 2 MHz

Memory Description

- Plated wire (5 mil)
- Word organized, random access, nonvolatile, nondestructive readout
- Data output register—data input and address register not required
- Access time less than 1.0 microsecond
- Storage capacity 4096 words (16 bits) with growth capability to 8192 words with no increase in size
- Sector 00 alterable; sectors 01 through 07 normally read only sectors; however, 00, 02 to 07 could be altered in flight

A DOC contained a 4096-word by 16-bit memory. The programmable central processing unit served as a key element in the attitude control subsystem (ACS). The flight computer program (FCP) handled all the ACS control modes (Figure 1-12). In addition, the FCP could test the DOC and memory.

A subset of the FCP was the telemetry service program. This program could be commanded from the ground station to telemeter various DOC status words and core contents, including a full memory dump.

The DOC could also be reprogrammed or reloaded from the ground station by an input data block. Input data blocks were groups of commands received by the command service program from the command/decoder distributor, and decoded as data words. Thus, DOC data could be updated by the normal ATS-6 command system. Besides rewriting memory, data words representing ephemeris data, rate biases, interferometer counts, or sensor misalignments could be updated.

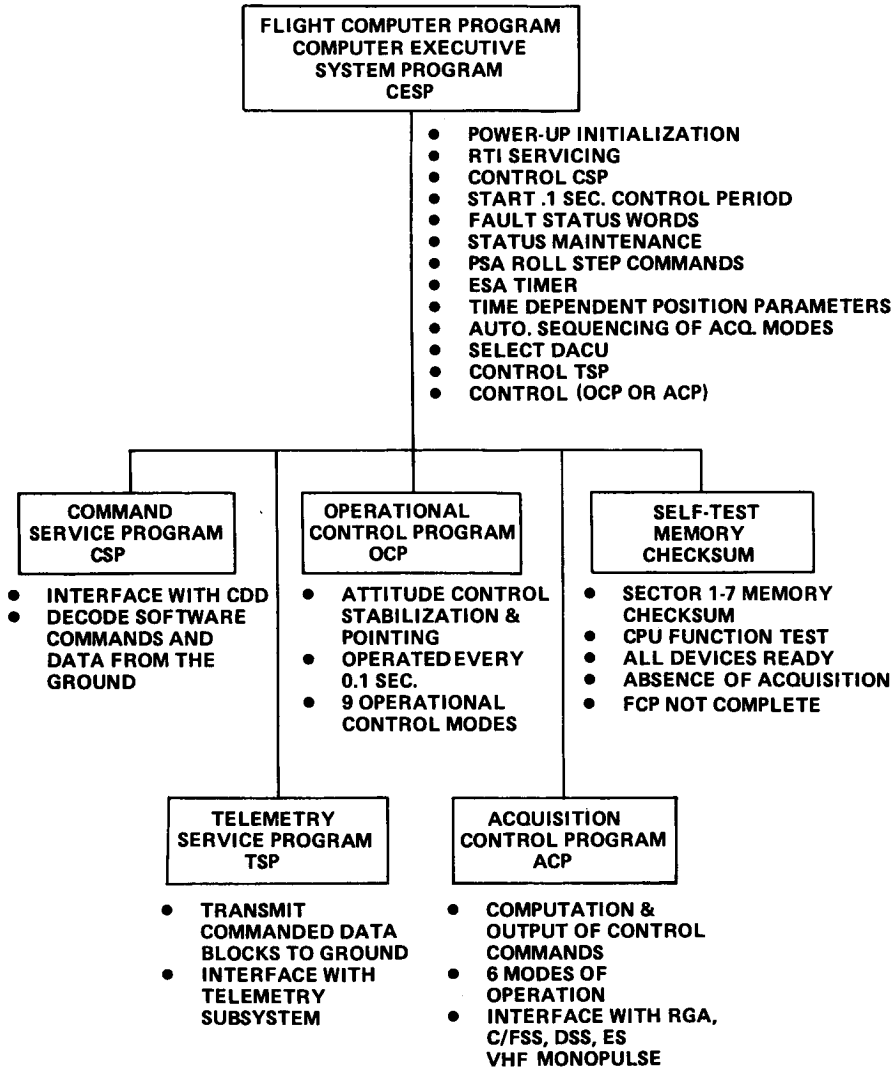

Figure 1-12. Flight Computer Program Organization

For each DOC, there were 12 input and 5 output data block types. Telemetry for DOC 1 appeared on channel 33 and for DOC 2 on channel 34. The DOC's could effectively subcommutate their own channel, using software.

The DOC was a commandable element of ATS-6. By the use of commands, instructions and parameters were fed to the DOC. The type of information the DOC was to telemeter back was also selectable. The mode and sensor select commands are shown in the following listing:

Mode	Commands
16 Prime Mode	Rate damp, normal
	Rate damp, yaw inhibit
	Positive X Sun acquisition
	Negative X Sun acquisition
	Earth acquisition
	Polaris acquisition
	Local vertical, orbit plane east
	Offset point, ground coordinate
	Offset point, angle point
	Station null point
	Antenna pattern, 5 degrees
	Antenna pattern, 3 degrees
	Satellite track
	Low jitter mode
	Offset point, control slew
	Local vertical, orbit plane, east/west
12 Secondary Mode	Select DACU 1
	Select DACU 2
	Select wheels
	Select jets
	Select fine deadband
	Select coarse deadband
	Auto acquisition sequence disable
	Auto acquisition sequence enable
	Fault override disable
	Fault override enable
	Unlatch faults
	Latch faults
13 Sensor Select Commands	Earth sensor, acquisition required
	Earth sensor, acquisition not required
	Interferometer
	Vhf monopulse

Mode	Commands
13 Sensor Select Commands (continued)	S-band monopulse
	C-band monopulse
	YIRU, control required
	YIRU, control not required
	PSA 2, acquisition required
	PSA 2, acquisition not required
	DSS, yaw backup
	DSS for Sun acquisition
	Analog Sun sensor

DOC commands consisted of the following:

Function Commands	Data Commands
On/off	12 input data blocks
Primary modes (16)	(specifies such data as
Secondary modes (12)	ephemeris, misalignments,
Sensor select (13)	biases, ground coordinates, etc.)
Output data block select (5)	

All commands going to the DOC were routed by the command decoder and distributor. Telemetry data leaving the DOC was formatted into the telemetry stream by the data acquisition and control unit. The DOC flight computer program had a command service program to assemble data going to telemetry via the data acquisition and control unit.

1. DOC Capabilities–The DOC was the primary controller for all normal modes of operation for the attitude control subsystem. The DOC had the following capabilities:

- Iteration Rate–The iteration rate for the DOC was 0.100 second.
- Input/Output–
  - Priority interrupt
  - Five input/output instructions
  - Parallel word transfers (16 bits)
  - Maskable real-time interrupt, 20 milliseconds
  - Input/output signals were mostly either digital differential or high level for high noise immunity
  - Dedicated registers: command; telemetry; ADA; output discretes
  - Eleven output discretes (expandable to 16)
  - Four input discretes (expandable to 14)
  - Four serial inputs (expandable to 8) any word length

- Fifteen analog inputs; all were differential. Input attenuators and low pass filters or over-voltage input protection circuits were available. Converted words were 12 bits, 2's complement.
- Three analog outputs (expandable to 7); all were single ended. Developed from 12 bit, 2's complement words.
- Telemetry discretes: control mode; write mode; and primary power on
- Command discretes: write enable/disable; control/monitor; on/off

- Input Data Blocks—The DOC would accept the following operational input data:

Data Block

1	ATS ephemeris
2	Tracked satellite or Sun ephemeris
3	Ground and interferometer station coordinates
4	Angle commands/slew maneuver data
5	Open
6	Interferometer null data
7	Rate gyro assembly bias rates
8	Sensor misalignment data
9	ATS time dependent angles
10	Track satellite or Sun time dependent angles
11	Sun and Polaris bias angles
12	Memory rewrite data.

- Output Data Blocks—The DOC provided 1 of 5 output data blocks on command. The data blocks were structured to provide:

Command verification
Operational parameters – most significant bits
Operational parameters – least significant bits
Variable memory
Memory dump.

- Mode Commands--The DOC accepted all mode commands from either command/decoder distributor. Receipt of a new command would automatically cause the DOC to switch to the new mode of operation.

- Back-Up Modes—The DOC accepted inputs from the +X and -X axis digital Sun sensors to provide yaw-axis backup control for the reference orientation, station point, and offset point modes.

- Sensor Alignment Computation—The DOC provided a capability to compute corrections to be summed with the sensor outputs for known sensor misalignments. The roll, pitch, and yaw sensor angular misalignments, each for all three axes, could be transmitted to the

DOC as part of input data block 8. Only one set of sensor misalignment data could be stored in the computer at any one time. If the sensors were changed, new alignment data was sent.

- Interferometer Computation—Whenever use of the interferometer was indicated, the DOC would compute the roll and pitch error signals from interferometer data by nulling them against bias-counts computed by the DOC.

- Attitude Error Filtering—The DOC provided appropriate filtering for all attitude sensors as a function of individual noise characteristics and specific loop bandwidth requirements.

- Rate Derivation—Whenever the inertia wheels had been selected to act as a torquer, the DOC monitored the attitude sensor outputs and made a computation that provided the rate stabilization signal. Whenever the reaction jets were selected to act as the torquer, the DOC provided a pseudo-rate computation for the rate stabilization signal for the control loop, except during those acquisition modes where the RGA was used for rate stabilization purposes. During those acquisition modes, the DOC provided a computation based on the rate gyro assembly outputs for rate stabilization of the control loop.

- Roll Angle Step Commands—The DOC monitored the roll angle during all operational modes (not including acquisition). Depending upon the magnitude and polarity of the roll angle, the DOC issued separate discrete commands for the Polaris sensor assembly for roll-angle magnitudes of ±2.35 degrees and ±7.85 degrees nominally. These discretes were changed when the roll angle as determined by the DOC was less than the values indicated. When the Earth sensor was the selected sensor, the roll output of the Earth sensor would be used by the DOC to determine the step commands. When the Earth sensor was not selected, the DOC used the interferometer counts or station latitude/longitude as transmitted by the ground.

- Yaw Pointing Bias Computation—Using the ATS ephemeris data, the ATS time-dependent orbital parameters, and either the offset data or the ground-site data, the DOC computed the yaw pointing command to keep the X-axis of the vehicle in the orbit plane or projection of the X-axis on the Earth pointed east as required. The yaw pointing command remained at zero following any power-on to the DOC until all required time-dependent orbital parameters had been transmitted to the DOC. When new orbital parameters were sent to the DOC via the command/decoder distributor, the DOC used the previously transmitted parameters until all new parameters had been transmitted, verified, and the proper copy command received.

- Roll/Pitch Bias Computation—Using the ATS ephemeris data, the ATS time-dependent orbital parameters, the offset angle data or the ground site data, and if appropriate, the ephemeris data for a tracked satellite, the DOC computed the roll/pitch attitude and rate commands to keep the Z-axis of the vehicle properly pointed.

- Controller Accuracy—The controller error due to the computation of the control law would not exceed 0.01 degree. The angle command and orbit bias compensation computations would not cause an error of greater than 0.01 degree for static conditions or of greater than 0.03 degree for maneuvering modes.

- Jet Deadband Control—During all but the acquisition modes of operation, when the select-jets command was received by the DOC and the coarse-deadband command had not been received, the DOC would select a deadband equivalent to 0.044 degree (fine deadband). If the coarse-deadband command had been received, the DOC selected a deadband equivalent to 0.44 degree and would return to the fine deadband upon receipt of the fine-deadband command. Acquisition deadbands were as specified for the acquisition modes.

- Control-Monitor—The DOC used was selected by external commands. Each DOC was separately powered from the spacecraft bus. Power could be applied to and removed from the DOC by a command from either command/decoder distributor. The DOC would be in monitor status upon the application of power. A discrete was required to command the DOC into control.

- Wheel Commands—The DOC provided an analog output (proportional to the error signal) to the wheel drive electronics in the actuator control electronics. The maximum output was capable of driving the pulse modulator in the wheel drive electronics at 100 percent duty cycle.

- Jet Commands—The DOC issued a three level (-1, 0, +1) digital output to the actuator control electronics for driving jets about each of the three control axes.

- In-Line Fault Detection—The Flight Computer Program (FCP) provided detection of faults in an in-line manner, i.e., while the FCP was performing its normal control computations, it was also monitoring for various faults and indicating/storing the fact that a fault had occurred.

  The in-line faults were classified as one of the following:

  I. Noncritical nonlatchable faults
  II. Noncritical latchable faults with no effect on yaw axis control
  III. Noncritical latchable faults with potential effect on positive yaw axis control
  IV. Critical nonlatchable faults (there were none in this category)
  V. Critical latchable faults.

  Category I and II faults reported conditions that did not affect the control functions of the DOC/FCP. Category III faults resulted in an uncontrolled yaw axis (i.e., no torquer commands were issued and the yaw inertia wheel was allowed to run down) if "fault override" was disabled. Category IV and V faults indicated presumed DOC hardware failure or lack of a valid roll/pitch sensor in the loop. DOC response resulted in a pseudo-monitor condition, if "fault override" was disabled, wherein the DOC appeared as if it was in a monitor

status (jet-off commands, zero-inertia-wheel commands, and an active wheelhold discrete). However, the DOC telemetry would indicate fault 222_8 and the DOC/FCP would continue to compute and issue Polaris sensor assembly (PSA) roll-step commands.

In addition to the critical versus noncritical distinction, faults were also classified as latchable or nonlatchable. The latch-unlatch faults secondary mode commands governed whether or not a latchable fault would be held, both from a telemetry and a response standpoint, if it occurred and was detected even once. Otherwise, the nonlatchable faults, and the latchable faults under the "unlatch faults" condition, were cleared in synchronism with the sensor read rate (0.3 second for the Earth sensor assembly (ESA), 0.16 second average for the interferometer and 0.1 second for all others) no more often than once every 0.3 second.

- Sensor Data—Sensor data available to the DOC was either analog (RGA, wheel tachometer, CSS/FSS, C-band/S-band/vhf monopulse, PSA, or YIRU) or digital (DSS with 18-bit Gray code word of combined pitch/yaw data, ESA with 13-bit pitch and 13-bit roll, and interferometer with 24 bits of combined roll/pitch data). All analog data and DSS Gray inputs were converted to binary every 0.1 second, whereas the ESA and interferometer inputs were strobed in every 0.3 second and 0.160 second (on average), respectively.

2. DOC Modes—When the DOC was commanded into a primary mode, it used a preselected configuration of sensors and actuators for operation with the appropriate control law. The actual online configurations might be changed from the initial configuration by ground selection of alternatives. The DOC, in addition to commanding the vehicle to the specific mode attitude/rate requirement, also sequenced those requirements as required by the specific goal of the individual attitude control mode. Elaborations are given below for each DOC mode.

- Rate Damping—Upon receipt of a rate-damp command from either command/decoder distributor, the DOC selected the attitude control jets for the torquers and the outputs of the three axis rate gyro assembly (RGA).

  The DOC compared the three-axis angular rates from the RGA with a set value of 0.05 degree per second. If the computed value was positive and was greater than 0.05 degree per second, the DOC would provide a negative jet command, or on a similar basis, a positive jet command. When all three axes indicated that the rates were less than 0.065 degree per second, this was indicated in the status word.

  Upon receipt of the rate-damp-yaw-inhibit command, the DOC provided rate damping control for only roll and pitch.

- Automatic Acquisition—An automatic sequence for the acquisition of Sun, Earth, and Polaris was provided upon receipt of the automatic-acquisition command after receipt of either Sun-acquire (+X or -X) command. Transition to the next phase of the acquisition was accomplished when the attitude errors were less than 3.5 degrees and the rates were less than 0.065 degree per second for 5 minutes. In the event attitude and rates were not less than the indicated values, transition to the next phase was possible upon receipt of an Earth-acquire or Polaris-acquire command.

- Sun Acquisition—Upon receipt of either a Sun-acquire (+X) command or a Sun-acquire (-X) command, the DOC would select:

  - The attitude control jets as the torquers
  - The outputs of the three-axis RGA for angular rate information
  - The outputs of the Sun sensor electronics.

  When the pitch and yaw angle errors were less than ±3.5 degrees and the roll, pitch, and yaw body rates were less than 0.065 degree per second for 5 minutes, the DOC would provide an indication in the status word.

- Earth Acquisition—Upon receipt of Earth-acquire command from the command/decoder distributor (CDD) or from an internally generated source indicating that Sun acquisition was complete, the DOC selected:

  - The attitude control jets as torquers
  - The outputs of the three-axis RGA for rate data
  - The outputs of the Sun sensor electronics for attitude information in pitch and yaw.

  If acquisition of the Earth was not indicated, the DOC issued a negative roll-rate command of 0.250 degree per second. The rate was maintained within ±0.075 degree per second of the commanded value.

- The DOC monitored for a discrete signal indicating acquisition of the Earth from the Earth sensor. If Earth acquisition was indicated, the DOC selected the roll and pitch outputs of the Earth sensor for attitude information and the roll-rate command was removed.

  The DOC continued to use the RGA for rate data and the analog output of the fine Sun sensor (FSS) electronics for the yaw axis. When roll, pitch, and yaw attitudes and rates were less than ±3.5 degrees and 0.065 degree per second for 5 minutes, the DOC issued a discrete. If the Earth acquisition signal was interrupted, the DOC provided a positive roll-rate command of 0.1 ±0.05 degree per second exclusive of gyro null error and reverted to pitch control based on the coarse Sun sensor (CSS)/FSS output.

- Polaris Acquisition—Upon receipt of a Polaris-acquire command from the CDD or from an internally generated source indicating that Earth acquisition was complete, the DOC selected:

  - The attitude control jets as torquers
  - The outputs of the three-axis RGA for rate data
  - The Earth sensor outputs for roll and pitch attitude with the control law as used for completion of Earth acquisition, and
  - The +X or -X axis digital Sun sensors (DSS) for yaw attitude computation.

  The yaw angle bias to acquire Polaris was transmitted as part of input data block 11.

The DOC monitored the yaw attitude error from the Polaris sensor. If a Polaris acquisition signal was present and the yaw attitude error, as determined from the DSS attitude computation, was less than 3.0 degrees, the DOC used the yaw attitude error signal from the Polaris sensor for the control law computations. Both the yaw angle bias command and the DSS attitude computation was removed.

When the roll and pitch attitude error from the Earth sensor and the yaw attitude error from the Polaris sensor were less than ±3.5 degrees and the body rates were less than 0.065 degree per second, the DOC provided an indication in the status word.

- Reference Orientation—Upon receipt of a reference-orientation command from either CDD, the DOC selected:
  - The inertia wheels as the torquers unless the select-jets command had been received. If the select-jets command had been received, the fine deadband and the pseudo-rate computation were selected.
  - Polaris sensor for yaw attitude unless a select-DSS or select-YIRU command had been received.
  - The yaw pointing bias computation unless select-DSS/YIRU command had been received.
  - The Earth sensor for the roll and pitch attitude unless the select-interferometer command had been received.

- Offset Point—Upon receipt of an offset-point-angle command or an offset-point-ground-coordinates command, the DOC selected:
  - The inertia wheels as torquers unless the select-jets command had been received. If the select-jets command had been received, the fine deadband and pseudo-rate computation were selected.
  - Polaris sensor for yaw attitude unless a select-DSS or select-YIRU command had been received.
  - The normal Polaris yaw point bias computation unless a select-DSS/YIRU command had been received and the roll and pitch bias computation unless the select-interferometer command had been received.
  - The Earth sensor for roll and pitch attitude unless the select-interferometer command had been received. If offset-point angle command was received, the computation for the angle command was used. If offset-point-ground-coordinates command was received, the computation for latitude-longitude data was used to maintain a fixed ground aim point for the Z-axis.

- Antenna Pattern Maneuvers—The DOC generated the commands to perform slew maneuvers (cloverleaf) for antenna pattern measurements. Upon receipt of an antenna-pattern command, the DOC selected the following:
  - The wheels as the torquers unless the select-jets command had been received. If the select-jets command had been received, the DOC selected the fine deadband unless the coarse deadband had been selected.

- The Earth sensor for the roll and pitch attitude.
- The Polaris sensor for yaw attitude.
- The roll, pitch, and yaw pointing bias commands applied to the central offset point (boresight angle relative to reference orientation).

Also upon receipt of the command, the DOC stored the roll and pitch angle as measured by the sensor in use for the boresight reference. The DOC selected the proper sequence of commands depending upon the sign of the boresight angle. Eight sequential commands were required to complete each pattern.

- Station Point Nulling–Upon receipt of a station-point command the DOC selected:

  - The inertia wheels as torquers unless the select-jets command had been received. If the select-jets command had been received, the fine deadband and the pseudo-rate computation were selected.
  - Polaris sensor for yaw attitude unless a select-DSS or select-YIRU command had been received.
  - The normal Polaris yaw pointing bias computation unless the select-DSS/YIRU command had been received.
  - The computation for the vhf monopulse signals unless any of the following commands had been received by the DOC:

    Select S-band monopulse
    Select C-band monopulse
    Select interferometer.

  Upon receipt of any of the select commands, the DOC replaced the previous attitude error source with that commanded.

- Satellite Tracking–Upon the receipt of a satellite-track command from either CDD, the DOC selected:

  - The inertia wheels as the torquers with tachometer rate computation unless the select-jets command had been received. If the select-jets command had been received, the fine deadband and pseudo-rate computation were selected.
  - The Polaris sensor for yaw attitude unless a select-YIRU command had been received.
  - The Earth sensor for roll and pitch attitude with associated computation of the tracking commands by the DOC, unless the select S-band monopulse command had been received. The Earth sensor remained in an operational status to supply roll information for determining roll offset commands to the Polaris sensor.
  - The computation of the tracking commands unless the select S-band monopulse command had been received.

- Low Jitter–Upon receipt of a low-jitter command, the DOC selected:

  - The inertia wheel as the torquers with tachometer rate computation

- Polaris sensor for yaw attitude
- The Earth sensor for roll and pitch attitude unless the interferometer had been selected
- The normal Polaris yaw point bias computation.

Analog Backup Controller—The low-power analog backup controller (ABC), which used only analog inputs from the sensors, was used as a backup to the DOC's (with reduced operational and performance capabilities) or for a low-power mode of operation.

Upon receipt of power, the ABC was in a monitor status and the Sun acquisition mode. The monitor status was defined as the condition in which the ABC would accept sensor and command inputs, would not issue jet/wheel commands, and would provide error signals to the DACU's. Upon receipt of an ABC-control command, the ABC issued to the actuator control electronics (ACE) either an error signal to the wheel modulator or jet firing commands according to the specified mode. The ABC would return to a monitor status upon receipt of an ABC-monitor command. The ABC would output a discrete signal to the ACE whenever it was in the control status. As with the DOC, upon entrance into a mode, the ABC used a preset set of sensors and actuators and sequenced these sets as appropriate for the specific mode's goal.

The operational and performance capabilities of the ABC for the indicated modes were:

- Rate Damping—Upon receipt of the rate-damp command, the ABC would null the analog outputs of the rate gyro assembly (RGA) using commands via the ACE to the appropriate jets.

- Sun Acquisition and Hold—Upon receipt of the Sun-acquisition command, the ABC used the outputs of the Sun sensor electronics for pitch and yaw. The maximum value of the Sun sensor electronics output resulted in a nominal slew rate of 0.25 degree per second in pitch and yaw toward the Sun.

- Earth Acquisition and Hold—When the spacecraft was in the correct orbital position (orthogonal orientation of Earth and Sun sight vectors) and Earth acquisition was commanded by ground personnel, a negative roll rate of 0.25 degree per second was initiated by the ABC. When the Earth sensor indicated that acquisition of the Earth had taken place, the ABC removed the roll-rate command and the roll and pitch axes were controlled for Earth pointing by analog error signals from the Earth sensor.

- Pseudo-rate—Pseudo-rate was commanded only after the Sun or Earth was acquired. Upon receipt of the select-pseudo-rate command by the ABC, the RGA signal was inhibited and the pseudo-rate enabled in each axis. It was then possible to use either wheels or jets as actuators. However, pseudo-rate should have been selected by ground command prior to the selection of wheels to avoid the high duty cycle of a wheel/rate-gyro combination or to avoid the high fuel expenditure of the RGA/jet combination.

- Polaris Acquisition—The acquisition of Polaris with the ABC as the controller was aided by the ground. Upon receipt of a Polaris-acquire-winter command, the ABC commanded a

negative yaw rate of 0.10 degree per second, ±5 percent. Upon receipt of a Polaris-acquire-summer command, the ABC commanded a positive yaw rate of 0.10 degree per second, ±5 percent. The ABC removed the Sun sensor from the yaw control loop upon receipt of either command. When the Polaris sensor indicated that it had acquired a star by the presence of the acquisition signal, the ABC removed the yaw rate command and the Polaris sensor output was summed with the analog rate output of the RGA.

- Local Vertical—Upon receipt of a local-vertical command, the ABC used the analog outputs of the Earth sensor for roll and pitch attitude inputs and the analog output of either the Polaris sensor or YIRU for yaw attitude inputs. The roll, pitch, and yaw control acted to null the Earth sensor outputs and the Polaris sensor outputs to align the +Z spacecraft axis to local vertical and cause the YZ plane of the sensor to contain the line-of-sight to Polaris to within 0.5 degree.

  The normal mode of control was considered as using the wheels for torquers. Upon receipt of the wheel-control command, the ABC would output the wheel drive signals and inhibit the jet drive signals. Upon receipt of the jet-control command, the wheel drive signals were inhibited and the jet drive signals would be output to the ACE.

- Monopulse—Upon receipt of vhf-mono, S-mono, or C-mono commands, the ABC used the roll output and the pitch output of the monopulse, and the yaw output of the yaw inertial reference unit or Polaris sensor and acted to null these signals. Commands to select the inertia wheels or jets were the same as specified in the above paragraph.

Actuators/Control Electronics

A set of three reaction wheels and two sets of reaction jets were available for applying torques and forces on the spacecraft. The electronics to control and activate these elements were included in the actuator control electronics (ACE) box.

The primary functions of the actuator control electronics were as follows:

- Provided power interface control for the inertia wheels
- Controlled valve and catalyst bed primary and backup heaters (ground command)
- Provided latch valve control for thruster and tank selection (ground command)
- Activated orbital and attitude control jets
- Controlled pitch, roll, and yaw momentum (inertia) wheels
- Provided wheel unloading by firing attitude control jets.

Figure 1-13 is a functional block diagram of the ACE. Under normal operations, the ACE accepted actuator commands from either the digital operational controller (DOC) or analog backup controller (ABC) and provided the three inertia wheel drives, latch valve actuations, thruster valve actuations, heater power, transducer power, and signal conditioning required by the control actuators.

Upon receipt of an enable-ground-control-wheels command, the DOC/ABC control signals to the wheel drive electronics, to the spacecraft propulsion subsystem (SPS) 1 electronics, and to the SPS 2 electronics, were disabled. The wheel drive electronics then accepted wheel commands in all three axes from either the normal command encoder (NCE) and/or the ground attitude control (GAC) encoder via the command/decoder distributor (CDD).

Upon receipt of a wheel/jet-ground-control-disable command, the ground command capability for the wheel drive electronics and both the SPS 1 and SPS 2 electronics were disabled, and the DOC/ABC control signals were enabled.

Upon receipt of an enable-ground-control-jet command, the DOC/ABC control signals to the wheel-drive electronics, SPS 1 electronics, and SPS 2 electronics were disabled, except that the wheel-drive electronics inputs would not be disabled if either the DOC or the ABC were actively controlling with the wheels. Both the SPS 1 electronics and the SPS 2 electronics were enabled to accept jet commands in all three axes from either the NCE or GAC encoder via the CDD.

The NCE commands to the ACE were single-axis commands of 250 milliseconds duration. The GAC commands controlled one or more spacecraft axes through six dedicated lines corresponding to ±roll, ±pitch, and ±yaw; the minimum command duration was 11 milliseconds.

Inertia Wheels and Electronics—The inertia wheels and the inertia wheel electronics provided: (1) small torques to counteract the disturbance torques during all modes except acquisition, orbit control, and jet-only control; (2) large reaction torques (up to 6.0 in.-oz) during controlled spacecraft maneuvers; and (3) a wheel-hold mode and logic for unloading the stored momentum in each wheel.

- Inertia Wheels—Three inertia wheels were used by the attitude control subsystem (ACS) to provide the primary means for torquing the spacecraft during all ACS modes of operation, except acquisition, orbit control, and jet-only control.

Each inertia wheel consisted of a 13-inch diameter flywheel with a moment of inertia of 0.0637 slug-ft^2 that could be driven from zero to approximately 1800 revolutions per minute (rpm) by a two-phase squirrel cage induction motor. A two-phase 20.0 (±4.0) volt-400 (±4.0) Hz excitation signal was applied to each motor that would develop an angular momentum of approximately 8.2 ft-lb-sec at 1200 rpm. Each inertia wheel developed at least 6.0 in.-oz over the speed range of -1200 to +1200 rpm (Figure 1-14).

A pulse type tachometer, mounted on each inertia wheel, was used to accurately measure the flywheel speed. The tachometer provided a 32-pulse-per-revolution output pulse train to the actuator control electronics. The output voltage amplitude and pulse repetition rate was proportional to the

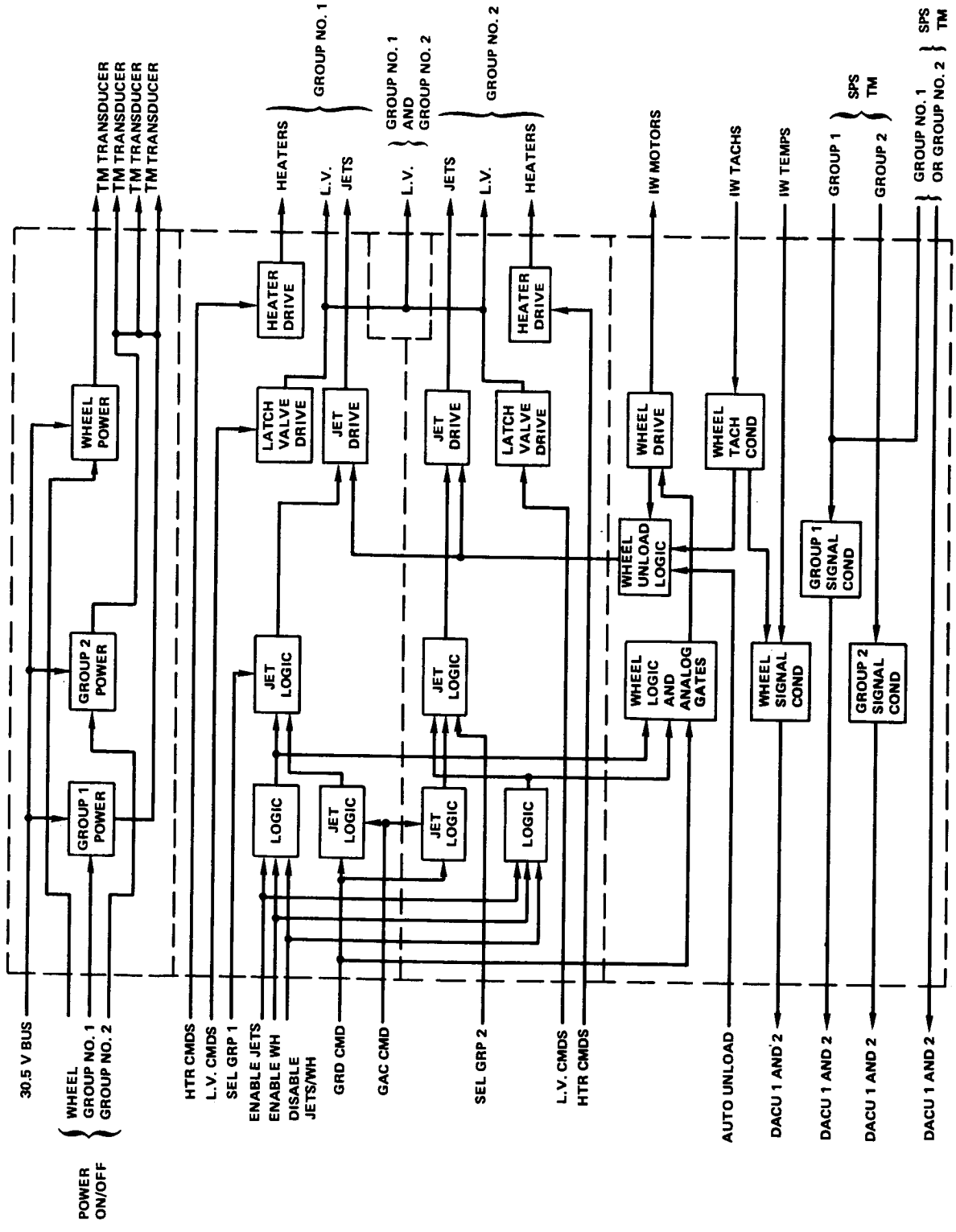

Figure 1-13. ACE Functional Diagram

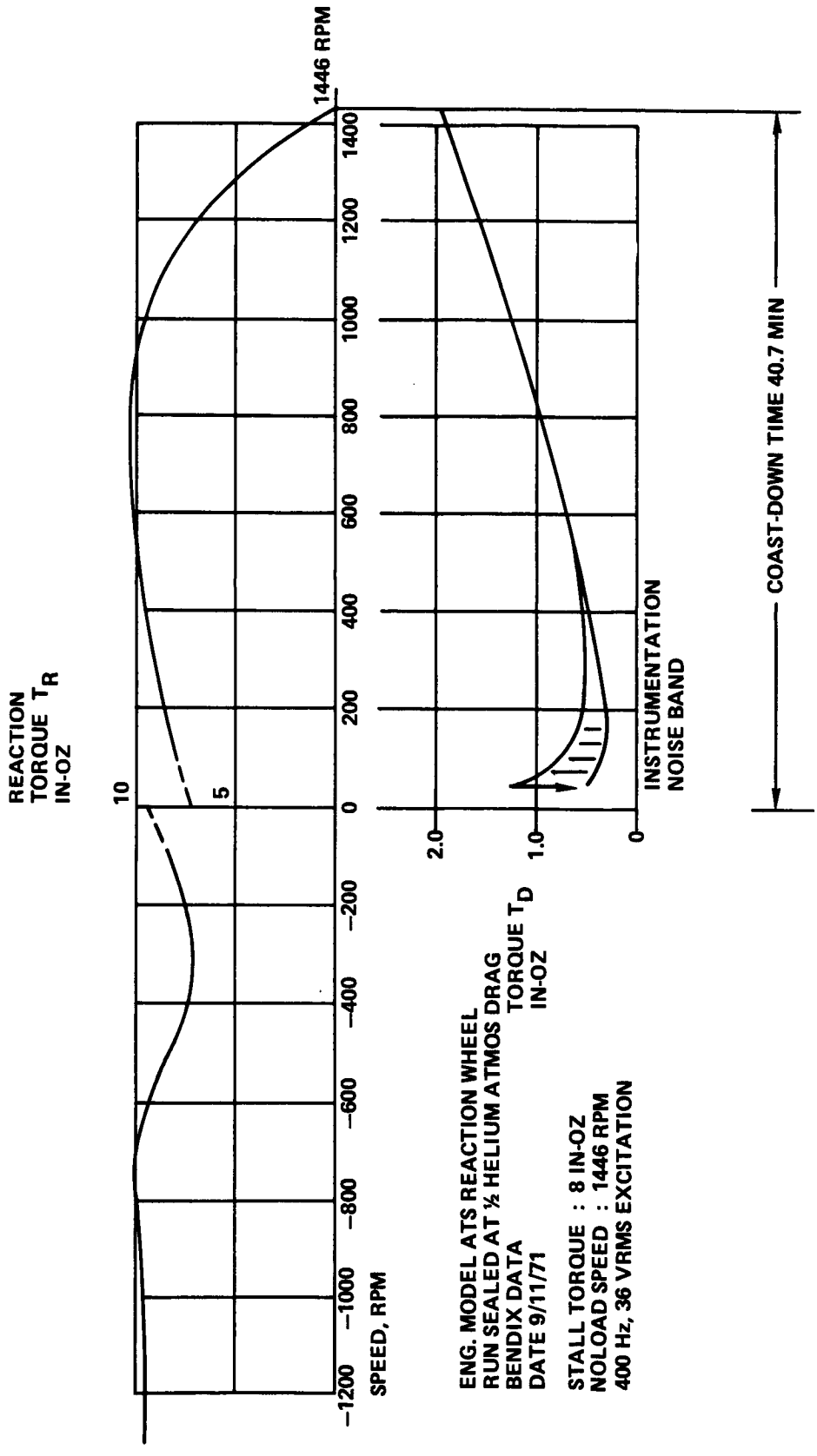

Figure 1-14. Inertia Wheel Torque/Speed and Drag Data

flywheel speed, and the polarity of the pulses indicated the direction of rotation (positive–clockwise, negative–counterclockwise).

- ACE Inertia Wheel Electronics–The inertia wheel electronics consisted of three identical channels, one for each inertia wheel. Each channel contained wheel drive electronics, tachometer electronics, and inertia wheel unload electronics.

Each inertia wheel channel accepted inertia wheel drive input signals from either DOC, NCE or GAC command (via the CDD), or the ABC. In response to the input supplied, each channel provided the 2-phase, 20 (±4) volt–400 (±4) Hz square wave excitation signal to the inertia wheel. The inertia wheel excitation signals were gated to each inertia wheel by a pulse train that had a duty cycle that was a function of the pitch, roll, and yaw attitude error signal from the DOC or ABC. No inertia wheel excitation pulses were generated for attitude error signals less than 0.667 volt (V), ±0.014 V inputs from the ABC or 1.345 V, ±0.027 V inputs from the DOC. Continuous gating of the excitation signals occurred for pitch, roll, and yaw attitude error signals that exceeded 2.00 V, ±0.10 V inputs from the ABC and 4.02 V, ±0.2 V inputs from the DOC. The minimum time during which the excitation signal was gated to the inertia wheels was 0.11 second, ±0.02 second.

Each inertia wheel channel also provided the capability of controlling the inertia wheel speed with commands from the NCE and GAC encoders via the CDD (Figure 1-15). The amount of change in the speed of the inertia wheel was determined by the duration of the command. An 11-millisecond (ms) GAC command produced a change of 0.5 rpm, ±0.05 rpm in the inertia wheel speed. A 250-ms normal NCE command produced a change of 11 rpm, ±1.1 rpm in the speed of the inertia wheel. In the hold speed mode, the drift rate of the inertia wheel should not have exceeded 4 rpm. A plus or minus 4.5-Vdc (±0.5 Vdc) drive direction signal was provided as an indication of the pulse ratio modulator output from each channel during periods that the inertia wheel was excited.

Each inertia wheel electronic channel contained a tachometer circuit, the function of which was to produce an analog output signal that was proportional to the speed of the flywheel and to produce a direction signal that indicated the direction of rotation of the flywheel. The output speed and direction data were fed to the data acquisition and control unit in the telemetry and command subsystem, inertia wheel unload circuits, and the DOC's.

Each inertia wheel electronic channel also contained an unload logic circuit. This circuit monitored the inertia wheel velocity and direction data supplied by the tachometer electronics and supplied a discrete pulse train to the appropriate attitude control jet electronics when a predetermined wheel velocity was exceeded. This pulse train generated a 200 millisecond (ms), ±40 ms command every 10 seconds (s), ±2 s, to turn jets on until the flywheel velocity, as measured by a tachometer circuit, had been reduced to a predetermined level. The flywheel velocities and tachometer frequencies at which the unload signals started and stopped are provided in Table 1-2.

The wheel drive electronics also provided signal conditioning of the wheel temperature for telemetry. The temperature transducer was of the thermistor type and operated over a temperature range of 0°F (-18°C) to 180°F (82.3°C). The signal conditioning circuitry provided this temperature indication to within ±20°F (±11.5°C) over the temperature range.

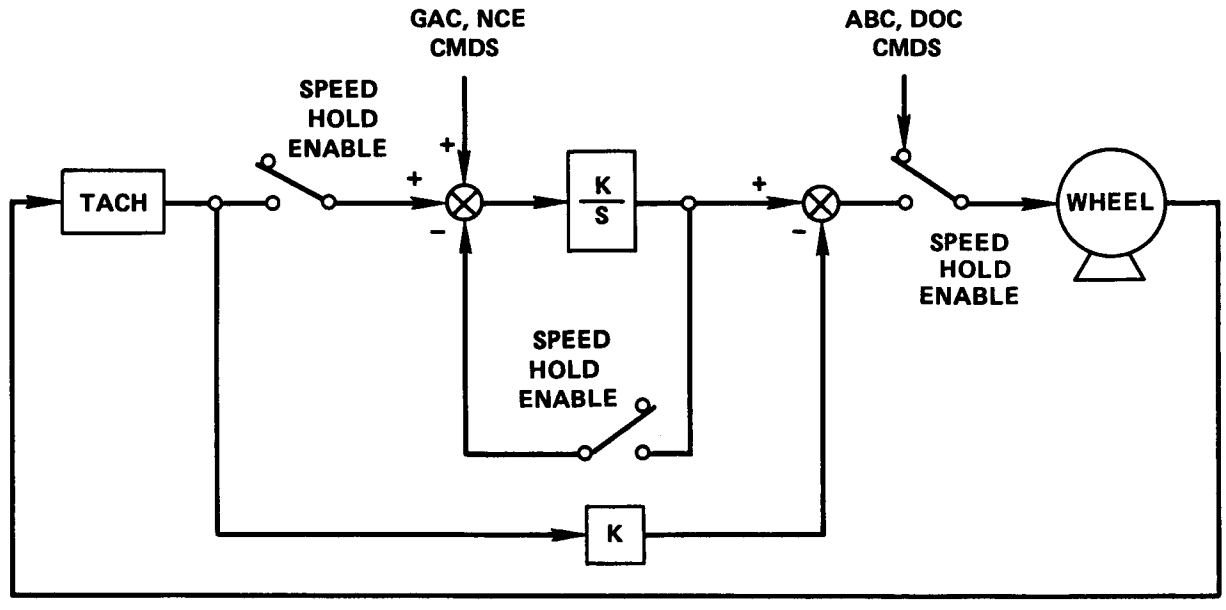

Figure 1-15. Wheel Speed Hold Loop

Table 1-2
Inertia Wheel Velocity and Tachometer Frequency

Signal	Pitch Axis	Roll Axis	Yaw Axis
Start unload wheel velocity	865 to 995 rpm	445 to 515 rpm	605 to 705 rpm
Tachometer input frequency	461 to 530 Hz	236 to 274 Hz	322 to 375 Hz
Stop unload wheel velocity	690 to 755 rpm	352 to 410 rpm	490 to 565 rpm
Tachometer input frequency	368 to 402 Hz	188 to 218 Hz	261 to 301 Hz

Spacecraft Propulsion Subsystem—The spacecraft propulsion subsystem (SPS) controlled the thrust required for attitude control, inertia wheel unloading, orbit control, and stationkeeping. It provided the primary means of torquing the spacecraft during rate damping, acquisition, and jet-only modes. The major components of the subsystem were the propellant tanks, latching valves, attitude and orbit control thruster assemblies, filters, fill/drain valves, various heaters, and SPS electronics.

The SPS consisted of two functionally redundant (SPS 1 and SPS 2) subsystems mounted primarily at the bottom of the Earth-viewing module. Eight attitude control thrusters for roll and pitch control were mounted on the EVM assembly. In addition, the four attitude control thrusters for yaw control and the four orbit control thrusters were mounted on truss bars on the east and west sides of the spacecraft. The moment arm of each EVM thruster was approximately 6.5 feet. The moment arm of the yaw thrusters was approximately 2.5 feet (Figure 1-16). The average thrust from each jet was approximately 0.36 Newton (N) over the system pressure blowdown range.

Control Loops

The ACS control loop function and performance depended upon the specific implementations. All loops were basically standard design using filtered sensor inputs; fixed (ABC) or calculated (DOC) commands; compensation with measured, calculated, or pseudo-rate; pulse-ratio modulated torquing of the wheels, and pulsed actuation of the jets.

Analog Backup Controller Laws

The modes of the analog backup controller were restricted to rate damping, Sun acquisition, Earth acquisition, Polaris acquisition, local vertical and monopulse modes. In these modes, selected sensor outputs were used together with spacecraft rate (measured by the rate gyros) or pseudo-rate to drive the actuators.

Digital Operational Controller Laws

Five laws for the digital operational controller were developed to support spacecraft operations. These control laws and their relation to the spacecraft operational modes were: (1) Standard wheel control law related to reference orientation, offset pointing (either in angle or ground coordinates), slew maneuvers, antenna pattern maneuvers, station point nulling, and satellite track; (2) low jitter control law related to low jitter and offset pointing to ground coordinates; (3) jet hold control law related to reference orientation, offset pointing (both angle and to ground), and station point nulling; (4) jet maneuvering control law related to slew maneuvers, antenna pattern maneuvers, and satellite track; and (5) yaw backup control law (wheels and jets) related to reference orientation, offset pointing (both angle and to ground), and station point nulling.

The standard wheel loops used smoothed input attitude error signals and computed attitude (or error) rate to pulse-torque the wheels. The jet maneuvering mode was similar but pulse-actuated the jets, whereas the jet hold mode used pseudo-rate for loop stabilization. The low-jitter control law used attitude error and its integral as input to a wheel-speed hold loop.

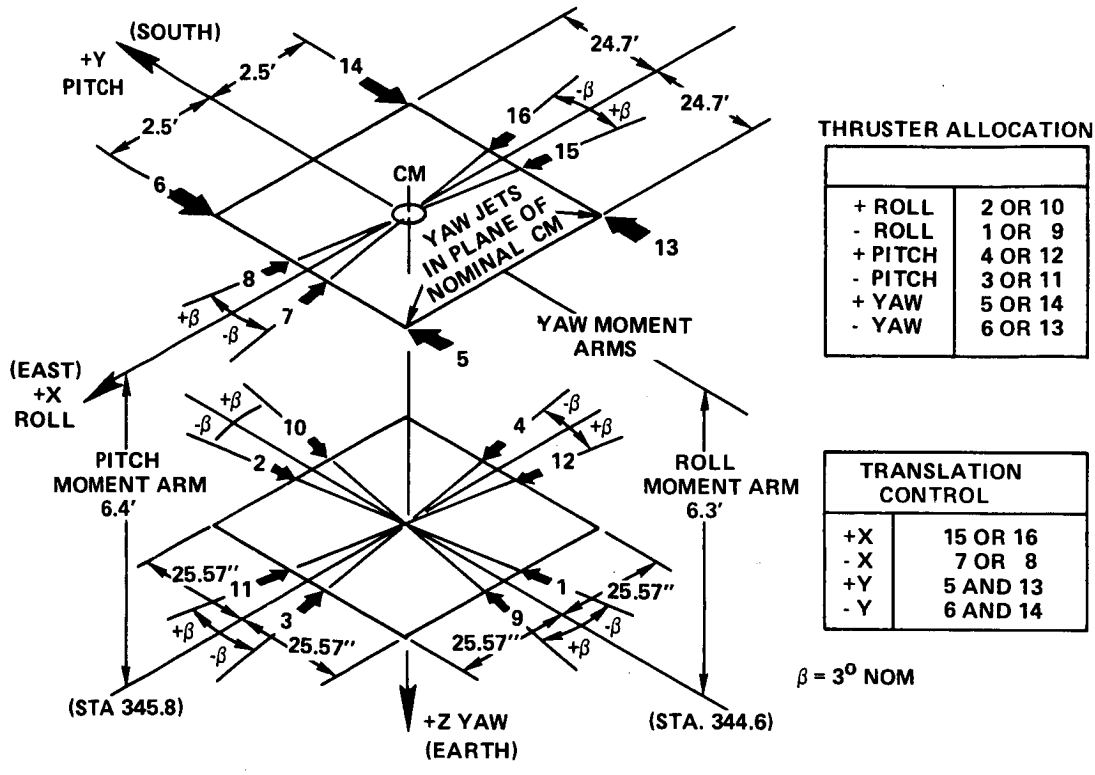

Figure 1-16. Spacecraft Propulsion Subsystem Geometry

Yaw backup modes, using pseudo-rate for stabilization, provided yaw axis control capability through the limited range of attitudes in which either of the two DSS's saw the Sun.

Control By Ground Operations Personnel

By command from the ground, either reaction jets or wheels could be actuated. The normal command encoder or the ground attitude control encoder could be used to activate the spacecraft torquers. Each wheel, when commanded, was in a wheel-speed hold loop that had as its command input an integrator whose level was incremented with each command from the ground. Each jet, when commanded, responded by opening for a fixed time.

Normal Ground Commanding—

- Addressed one axis at a time
- Commanded wheels or jets
- Commanded length multiples of 0.25 second (±11 rpm per 0.25-second wheel command)

Ground Attitude Control–

- Addressed one, two, or three axes at a time
- Had instantaneous response to transmission
- Commanded wheels or jets
- Commanded length multiples of 11 milliseconds (jets 100 milliseconds minimum)

Group Attitude Control commanding was done by the spacecraft attitude precision pointing and slewing adaptive control (SAPPSAC) experiment that used a computer on the ground for real-time, on-line spacecraft attitude determination and control. See Chapter 2 for a description of this experiment.

DESIGN VERIFICATION

In readying for launch, the adequacy of the attitude control subsystem was verified by a sequence of procedures including:

- Computer simulation testing of an ACS model
- Single axes testing with computer support
- Subsystem testing before, during, and after spacecraft integration
- Testing on the launch pad.

Simulation Testing

During the course of the ATS design, a computer simulation program, called 3XATS, was developed to permit the rapid synthesis and verification of the control system elements required to stabilize and control the spacecraft in its various operating modes. Through a continuous iterative refining of this software package, a highly representative model of ATS was developed.

The 3XATS program was a three degree-of-freedom simulation of ATS in rigid or flexible body form. The program simulated the dynamic operation of a digital operational controller, analog back-up controller, six attitude control jets, three inertia wheels, a dozen sensors, and the vehicle dynamics of the spacecraft. The Sun, Earth, and the Polaris star, represented in inertial space, served as reference targets for the ATS attitude sensors, with optional selection of local vertical, ground coordinates, angle offsets, or a low-altitude satellite as the operational targets of the ATS +Z axis. Gravity gradient and solar torques were modeled in 3XATS to produce a representative environmental model of ATS during actual operation.

Table 1-3 compares performance data obtained by using 3XATS and the ACS performance requirements.

Table 1-3
Key Requirements Verification Summary

Requirement	Method	Results
Rate Damp–DOC From 0.5°/s to 0.1°/s in 10 min.	Simulate and Test	$\dot{\theta}$ to <0.1°/s in 3 min. $\dot{\phi}$ to <0.1°/s in 5 min. $\dot{\psi}$ to <0.1°/s in 6 min.
Sun Acquisition–DOC ±X from 30° to 4.5° and 0.1°/s within 10 min.	Simulate and Test	+29° to 4° and <0.1°/s in 6 min. -29° to 4° and <0.1°/s in 4 min.
Sun Acquisition to 30° within 20 min.	Simulate	180° to 30° in 6 min. with normal thrust
Earth Acquisition–DOC Acquisition from ±15° to <4° in <80 min.	Simulate and Test	ϕ from 45° in 5 min. ϕ from 20° in 2 min. θ from 11° in 1.5 min.
Polaris Acquisition–DOC Point to within 3° using DSS and prestored data	Simulate and Test	ψ from -23° to <3° in 11 min.
Complete acquisition in 10 min. after transfer from DSS to PSA	Simulate	Acquisition in 7 min.
Reference Orientation ±0.1° static accuracy using ESA or interferometer, either PSA, wheels or jets	Simulate and Test	Control to deadband 0.044° (J) and 0.040 (W) supported system error analysis. R&P = 0.1, Y >0.1
Antenna Pattern Initiate from 6° roll and pitch from station point using monopulse. ±3° pattern complete in <90 min, with 0.2° accuracy	Test	3° pattern completed in 80 min. and max. error 0.035°
±5° pattern in <3 hr. with 0.2° accuracy	Simulate	Error <0.1°
Orbit Control Peak error ±0.5° (thrusting) Static error <±0.1° with 10 minute settling time	Simulate and Test	Pitch <0.4°, roll <0.32°, yaw <0.32° during disturbance

Table 1-3
Key Requirements Verification Summary (continued)

Requirement	Method	Results
Low Jitter Jitter amplitude $<\pm 0.01°$ Rate $<\pm 0.001°/s$ Error $<\pm 0.5°$	Simulate	ϕ and θ $<0.005°$ ψ $<0.009°$ $\dot{\phi}$ and $\dot{\theta}$ $<0.0005°/s$ $\dot{\psi}$ $<0.0008°/s$
	Test	θ, ψ = $\pm 0.009°$ $\dot{\theta}$, $\dot{\psi}$ = $\pm 0.0001°/s$ Roll not tested
Rate Damp–ABC From $0.5°/s$ to $<\pm 0.15°/s$ in 10 minutes	Simulate and Test	$\dot{\phi}$ to $<0.15°/s$ in 5 minutes $\dot{\theta}$ to $<0.15°/s$ in 3 minutes $\dot{\psi}$ to $<0.15°/s$ in 6 minutes
Sun Acquisition–ABC +X Axis Acquisition to $<30°$ in <20 minutes. $30°$ to $4.5°$ in <10 minutes	Simulate Test	$180°$ to $30°$ in 6 minutes $20°$ to $<4°$ in 2 minutes in pitch and yaw
Earth Acquisition–ABC $-0.25°/s$ search rate until Earth acquisition	Simulate and Test	$-0.23°/s$ search rate $20°$ to $<4°$ in 3 minutes in roll axis
Polaris Acquisition–ABC $-0.1°/s$ for winter acquisition $+0.1°/s$ for summer acquisition	Simulate and Test	$\pm 23°$ to $<2°$ in 7 minutes Polaris acquired in 4 minutes
Local Vertical $<0.5°$ error using ESA and PSA, pseudo-rate, wheels and/or tests	Simulate and Test	$<0.5°$ requirement met with normal disturbance torques included
Coarse Sun Sensor 4π Steradian FOV (Inferred from acquisition requirements)	Test and Analysis	Verified
Fine Sun Sensor Discrete $>\pm 9°$ target eye		$\approx 12°$
Sun Sensor Electronics Assembly CSS to FSS switchover $\pm 9°$	Test	Verified
Digital Sun Sensor Yaw FOV $>\pm 60°$ Pitch FOV $>+39°, -60°$	Test	$\pm 64°$ $+40°, -64°$

Table 1-3
Key Requirements Verification Summary (continued)

Requirement	Method	Results
Polaris Sensor Assembly Yaw FOV >9° Roll FOV >28°	Test	Yaw >10.6° Roll >32.69°
Max. null error ±0.05°	Test	±0.0489° (Acceptance Test) ±0.0588° (Qual) (S/N003)
Earth Sensor Assembly Roll, pitch FOV >23.25° Digital static error <+0.05°	Test	Roll >24.2° Pitch >24.4° 0.04° in roll and pitch
Analog null accuracy ±0.1°		Roll 0.045°, pitch 0.040°
Three Axis Rate Gyro Assembly Gyro zero uncertainty 0.05°/s	Test	0.002°/s (Typical at room temperature) (0.05 over temperature range)
Digital Operational Controller Implement all control laws	Test	Verified
Analog Backup Controller Implement backup control laws	Test	Verified
Inertia Wheels >6 oz-in. over ±1200 rpm	Test	Verified
Actuator Control Electronics		
Wheel Drive Electronics Provide PRM to wheels for DOC, ABC, NCE, GAC,	Test	Verified
NCE and GAC scale factor	Test	Verified
SPS Control Electronics Drive all thruster and latch valves	Test	Control verified
Power Control Overvoltage 38 V 100 msec	Test	All components met requirements
Undervoltage 1 msec	Test	All components met requirements
Supply voltage range 28 to 33 V	Test	All components met requirements

As component performance characteristics became available, they were incorporated in 3XATS. In particular, Earth sensor and Polaris sensor noise was incorporated to verify an acceptable effect on attitude control performance, fuel consumption, and wheel duty cycle.

Single-Axis Testing

During the single-axis testing, appropriate combinations of ACS elements were linked by an analog computer, a servoed single-axis table, appropriate sensor targets, and test input/output devices (Figure 1-17). The whole was then operated in closed-loop fashion over the full range of primary ACS modes and components. The goal was to gain confidence that the ACS would perform as predicted by 3XATS.

Sensors on the servoed table included the rate gyros, coarse and fine Sun sensors, digital Sun sensors, Earth sensor, and Polaris sensor. When, as appropriate, target acquisition was required by specific sensors in accordance with logic for operation of specific modes, those sensors were not on the table but were excited by hoods (Earth sensor and Polaris sensor) or target simulators (Sun sensors).

Inertia wheel response was monitored by an inertia wheel torque measuring fixture and the result was passed to the analog computer (a PACE machine).

Functions simulated on the PACE included the following:

- Single-axis vehicle dynamics with body bending contributions from the reflector and solar panel flexures
- Vhf, S-band and C-band monopulse outputs
- Jet operations including the following characteristics:
  - "On" delay and "off" delay of a jet pulse.
  - The jet warm-up and cool-down effect on the thrust magnitude.

Results of the single-axis tests are included in Table 1-3.

ACS/Spacecraft Testing

Besides the ACS elements themselves, the attitude control subsystem operation involved the following spacecraft elements:

- Power subsystem
- Propulsion subsystem
- Interferometer

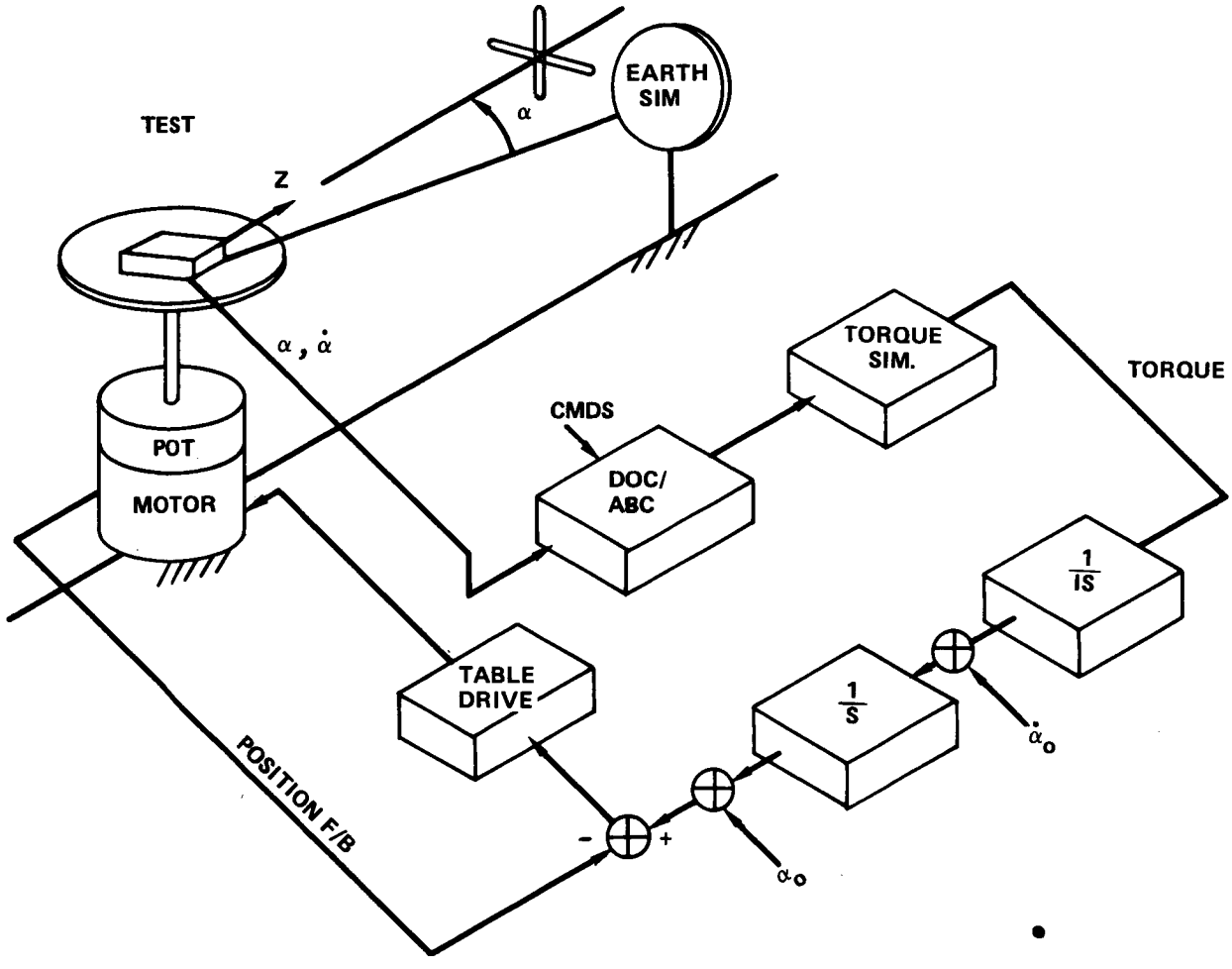

Figure 1-17. Typical Test/Simulation Setup

- Monopulse portion of the communications subsystem
- Telemetry and command subsystem
- Signal paths, interconnecting the above elements.

Reflecting the system interdependency of attitude control functions, the following objectives were identified for spacecraft testing of the ACS:

1. Verify that the ACS end-to-end loop performance in the integrated spacecraft corresponded to the baseline established during ACS acceptance testing as a complete subsystem after the single axis tests.
2. Verify that the ACS loops and components during mission mode operations did not interact adversely with other ATS elements.
3. Verify the correct operation of all possible signal paths within the integrated attitude control subsystem.
4. Verify that performance of ACS sensors and actuators corresponded to the baseline established during single-axis and complete subsystem acceptance tests.
5. Verify all command and telemetry functions related to the operation of the integrated attitude control subsystem.

It was evident that the first two objectives, which involved loop operations, dictated that the system be exercised through the entire sequence of mission modes specified for the ACS. The remaining three objectives were then fulfilled by a series of tests, conducted concurrently with the mode sequence that exercised in varying combinations, particular signal paths, components, and commands.

Most ACS tests were run using the same sensor stimulators and/or sensors output stimulators used during the ACS single-axis and complete subsystem tests. Special nonmagnetic stimulators were, however, devised for ESA and Polaris sensor excitation during electromagnetic interference testing.

A major portion of the tests verified operation and programming of the digital operational controllers. Items that were checked included:

- Control-loop configuration: (1) selection of proper components; (2) requesting, transmission, and acceptance of proper data; and (3) issuance of commands to proper torquers
- Control-loop calculations: attitude error and rate determination setting of proper gains, deadbands, filter characteristics, loop phasing

- Logical and fault mode switching: automatic selection of ACS control mode as a function of stored criteria

- Open-loop calculations: (1) vehicle ephemeris and attitude; (2) attitude and rate commands; (3) coordinate transformation

- Stored data: (1) ATS, tracked satellite, and Sun ephemeris constants and equations; (2) sensor misalignment and null data; (3) ground station coordinate data.

The ground support system for these tests included two PDP 11/20 computers that by a radio frequency link through coax cables, issued commands to and received telemetry from ATS-6. The software data base, later transferred intact to the ATS Operations Control Center (ATSOCC), included format of the telemetry frame, English language descriptors of the telemetry points and commands, and calibration information. This information was used to produce displays and hard copy outputs. The most valuable monitor for real-time test operations (also used at ATSOCC) was the CRT "page" format of ACS status and commands. Pages contained orderly presentations of individual telemetry items formatted for clarity and ready correlation. Two typical "half" pages are shown in Figure 1-18.

IN-ORBIT OPERATIONS/PERFORMANCE

ATS-6 was successfully launched into synchronous orbit at 13:00 GMT on Thursday, May 30, 1974. Injection occurred at 19:30:49 GMT into a near perfect orbit. The automatic separation and deployment sequence was successfully completed and the spacecraft was commanded through the Sun and Earth acquisition, and yaw reference sequences, with all operations being completed by 02:19 GMT the day after launch. During the next 2 weeks of flight, the spacecraft was commanded into its normal in-orbit configuration and all systems were evaluated. Following this spacecraft checkout phase, a series of tests was conducted to evaluate the performance of the onboard experiment systems and their respective ground system interfaces. At the end of the first month of flight, all systems had been successfully evaluated with very few anomalies encountered, and the spacecraft was declared operational.

The purpose of this section is to describe the major operational performance and characteristics after separation of the spacecraft from the launch vehicle.

Launch and Acquisition

Table 1-4 summarizes ACS performance during the acquisition modes. With the exception of the initial Earth acquisition, the nominal values were met. The exception, which was caused by an anomaly in the rate gyro assembly (RGA), is discussed later in this chapter. The only ACS components powered-on during launch were the RGA, digital Sun sensors (DSS), auxiliary digital Sun sensors (ADSS), coarse Sun sensor/fine Sun sensors (CSS/FSS), and the Polaris sensor assembly (PSA) Sun shutter. Spacecraft telemetry data indicated that all the sensors were operational during this period. However, the +X DSS identification bit was not illuminated until after separation because of optical blockage from an adapter leg. The RGA data was compared with the Titan rate

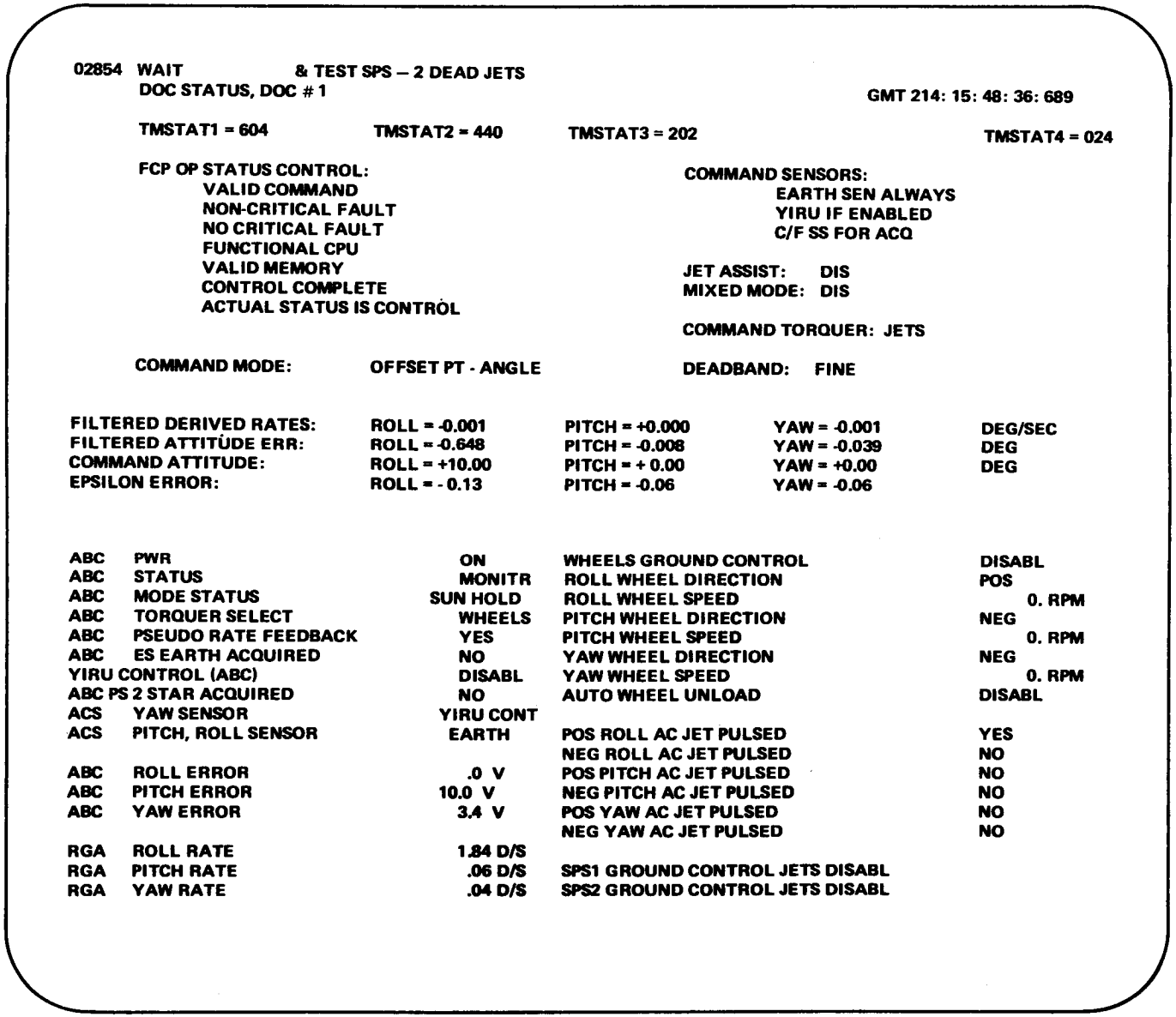

Figure 1-18. ACS CRT Half Pages

Table 1-4
ACS Acquisition Performance

Mode	Parameter	Spec		Actual	Comment
		Nominal	Max		
ABC Sun Acquisition	Time to Acquire	13 min	20 min	5.4 min	Any Offset to 30° of Sunline
		5 min	10 min	4.6 min	From 30° to 4.5° of Sunline
ABC Sun Acquisition	Pointing Accuracy	4.5°		2.2°	P = +0.89° Max. Y = -1.78° Max.
ABC Earth Acquisition	Time to Acquire	30 min	80 min	52 min	Within 4° of Local Vert.
ABC Earth Acquisition	Pointing Accuracy	±1°		R = -0.50° P = +0.47°	Torquer – Jets ΔR = 0.20°, ΔP = 0.30°
ABC Local Vertical	Pointing Accuracy	±1°		R = -0.33° P = +0.35°	Torquer – Wheels ΔR = 0.04°, ΔP = 0.04°
DOC Local Vertical	Pointing Accuracy	±0.1°		R = -0.04° P = +0.04°	

data and excellent correlation was observed. At separation, the tip-off rates were -0.22, +0.10 and -0.06 degree per second in roll, pitch and yaw. These were well within the specified 0.5 degree per second; therefore, the special-rate-damp mode was not required and the ACS remained inactive during the deployment phase. The spacecraft rates after deployment were -0.13, +0.06, and 0.08 degree per second in roll, pitch and yaw. Approximately 20 minutes after the deployment sequence was completed, RGA 2 was turned off. With both RGA's on, the rates were -0.15, +0.03 and +0.04 degree per second in roll, pitch and yaw. After turning RGA 2 off, the corresponding uncorrected readings were -0.22, +0.07 and +0.06 degree per second. The difference in roll rate (-0.07 degree per second) indicated a fairly large null shift in one or both of the roll gyros. After completion of deployment and RGA 2 turnoff, evacuation and bleed-in of SPS 1 was performed. Positive roll and positive pitch thruster valves were opened for approximately 7.9 minutes to evacuate the nitrogen gas contained in the lines. The west prime thruster was then commanded open for 5 minutes. Bleed-in was then accomplished, and SPS 1 was ready for operation.

Table 1-5 lists the sequence of events that occurred during the acquisition phases.

Sun Acquisition

After deployment, the spacecraft body rates were low enough to go directly to the Sun-acquisition mode without having to use rate damp.

Sun acquisition was accomplished using the coarse Sun sensor/fine Sun sensor (CSS/FSS) for pitch and yaw attitude control, the RGA for three-axis rate information, the ABC as the controller, and SPS 1 as the torquer. This was the planned ACS configuration for acquiring the Sun by aligning the +X axis to the Sun-line. The ADSS's and DSS's were operational and used by ground control (ATSOCC) to determine the attitude of the spacecraft during the Sun acquisition phase. At 150:21:10 (1 hour 37 minutes after separation) ABC Sun acquisition was commanded. At this time, the +X axis was approximately 122 degrees from the Sun-line.

The FSS outputs were saturated until the null phase was within 4.8 degrees of the Sun-line. When the CSS/FSS came out of saturation, it and the +X DSS tracked within 0.25 degree. The roll axis was controlled in rate only. Roll rate settled to an indicated value of +0.04 degree per second. The time required for the +X axis to settle out to its steady state value of approximately 2.0 degrees from the Sun-line, was 10 minutes. The time to go to, and remain within, the specification value of 4.5 degrees was 7.5 minutes. The offset from the Sun-line was due to RGA biases and the system deadband.

The SPS 1 jets were fired during the acquisition of the Sun, with pulse widths of 3 seconds to 121 seconds. (Telemetry resolution is 3 seconds.) Estimated propellant usage was 0.18 kilogram of hydrazine.

After steady-state attitude was obtained, the ABC pseudo-rate was commanded. The reaction wheels were then powered on and torquer control was switched from jets to wheels. Control on the wheels was maintained for 1.4 hours until acquisition of the Earth was commanded. During this time, wheel unloading was not required. DOC 1 and the YIRU were powered on and checked out prior to the acquisition of the Earth. No anomalies were found.

Table 1-5
ACS Acquisition Events

Event	Time	Comment
Liftoff	150:13:00:02	
Separation	19:33:21	Sep. rates R = -0.22, P = 0.10, Y = -0.06
Boom 1st Motion	19:39:23	Init. rates R = -0.22, P = 0.06, Y = -0.06
– Complete	19:40:34	
Solar Array Unfold	19:46:34	
– S Complete	19:50:03	Δt (+Y) = 3 min 29 sec
– N Complete	20:02:00	Δt (-Y) = 15 min 26 sec
Reflector Deploy.		
– Complete	20:08:12	
Boom Drop		
– Enable	20:14:14	
– Complete	20:14:32	Final rates R = 0.135, P = 0.05, Y = +0.08
Sun Acquisition		
– Command	21:10:02	ZAZ = -140.5°, ZCOEL = 52.5°
– Complete	21:20:18	ZAZ = -91.27°, ZCOEL = 90.25°, Total angle = 122 degrees
RGA 2 - Off		ΔR = -0.07, ΔP = +0.04, ΔY = +0.02°/sec
Pseudorate	21:23:09	
Select Wheels	21:35:53	
Cmd. Earth Acq.	23:10:36	
Complete Earth Acq.	151:00:00:00	Δt = 42 min
Yaw Ref. Cmd. (ABC Polaris Acq.)	151:01:46	
Yaw Ref. Complete YIRU Control	151:02:15	Δt = 29 min

Note: All rates in deg/sec

Earth Acquisition

The Earth was acquired during the first crossing of the terminator plane in the evening of May 30, 1974. The attitude control subsystem (ACS) was in its nominal configuration for Earth acquisition. The Earth sensor assembly (ESA) and CSS/FSS were used for attitude control, RGA 1 for rate, analog backup controller (ABC) as the controller, and spacecraft propulsion subsystem 1 (SPS 1) as the torquer. The ESA was powered on at 151:22:51 GMT so that it could be checked out before the start of the Earth acquisition window. The 3-minute warm-up transient occurred as expected. At 22:59, roll and pitch error signals appeared. Interferometer read-out also confirmed the presence

of the Earth at this time. At 150:23:10 (approximately 5:54 local satellite time), ABC Earth acquisition was commanded and at 23:18 the ESA acquired the Earth. At approximately 151:00:02 the ESA roll and pitch errors had been reduced to steady-state values of -0.04 and -0.05 degree, respectively. The total time for the ESA roll and pitch errors to reach steady state after ABC acquisition of the Earth had been commanded was approximately 52 minutes. The time to maneuver and remain within 4.0 degrees of local vertical was 50 minutes. The specification states that the time to maneuver the +Z axis to within 4.0 degrees of the local vertical shall not be greater than 80 minutes (30 minutes nominal).

The greater than nominal time required to complete acquisition of the Earth was caused by a large (-0.19 degree per second) gyro null shift in the RGA 1 roll gyro. The roll axis settled out in a 2-degree limit cycle with an offset of approximately 7 degrees. Pseudo-rate with wheels was commanded at approximately 150:23:42 GMT resulting in a roll overshoot in excess of 15 degrees (test data showed that acquisition of the Earth is normally lost at a roll angle of approximately 14.6 degrees). ABC acquisition of the Earth was commanded at 23:47 re-enabling jet control. RGA 2 was turned on and RGA 1 turned off, and the spacecraft settled out from an offset of 8.5 degrees in 6 minutes.

The time to settle in pitch from an initial error of 11.5 degrees was 3 minutes during the Earth acquisition mode. The yaw axis was controlled by the CSS/FSS, with yaw attitude error varying between +0.89 degree to -2.67 degrees during this period.

After the roll and pitch errors had reached a steady state, ABC pseudo-rate was commanded taking the RGA out of the control loops. Reaction wheels were then commanded to be the torquers and reduced the limit cycle from 0.2 to 0.3 degree to less than 0.1 degree. Estimated use of propellant while in the Earth acquisition mode was 0.44 kilogram of hydrazine.

Polaris Acquisition

Acquisition of Polaris was accomplished in two parts, the first being performed during the first day by rotating the spacecraft about its yaw axis to point the -Y axis toward Polaris. The actual acquisition of Polaris was performed several days later.

The acquisition of Polaris by the ABC (winter) was commanded at 151:01:21 GMT resulting in a negative rotation about the yaw axis while pitch and roll attitude were controlled by the Earth sensor assembly (ESA). This was done to avoid slewing the Sun across the north face of the Earth-viewing module. At a (-X) DSS yaw angle of approximately 19 degrees, the yaw rotation was stopped by ground command. This maneuver took 28.4 minutes for a rotation of 200 degrees, thus the yaw rate was -0.118 degree per second. Estimated use of propellant was 0.03 kilogram of hydrazine. After the yaw reference maneuver was completed, the ABC was commanded into local vertical using the yaw inertial reference unit as the yaw axis attitude sensor.

The Polaris sensor assembly (PSA) was turned on the fourth day and Polaris was acquired. During the Polaris checkout phase, frequent "glitches" were noticed in which a moving particle would appear to be tracked. In most cases, the PSA would reacquire Polaris after a small error buildup; in some cases, star acquisition was lost. The PSA was then turned off for 3 days to allow additional outgassing.

Initial 30-Day Checkout (Specification/Compliance)

Fairchild ATS-F Specification 862-0001 D established the attitude control subsystem performance requirements. These, together with actual achieved performance measured during the first 30 days of operation, are shown in Table 1-6. All performance specifications were met or bettered by a wide margin.

Comprehensive testing was confined to the first 30 days in orbit to focus subsequent operations on the support of ATS-6 communication experiments.

Absolute Accuracy Considerations

When considering the performance data of Table 1-6, it is important to note that evaluations of accuracy were made using the Earth sensor and Polaris sensor, the ACS control sensor themselves, to verify specification compliance. Changes in calibration of these prime elements are basically undetectable and, therefore, lead to uncertainty as to absolute accuracy. Illustrating this fact is Figure 1-19 that compares roll and pitch data available simultaneously from the Earth sensor and interferometer. A time-varying angular difference of up to 0.05 degree in roll and 0.05 degree in pitch is observed. Which is the more accurate? Why does the divergence exist? Attempts to answer these questions have been unsuccessful. Although the differences are not significant for ATS-6, they may well be in other spacecraft desiring to use these sensors.

Similarly, an uncertainty existed in the determination of the attitude of the spacecraft's -Y axis that nominally points due North. The PSA's "intensity" signal variation over a 1-week interval, shown in Figure 1-20, indicates the variation in light energy falling on the sensor's image dissector tube (IDT) photocathode. Correlations of the intensity variations with the star field near Polaris indicate the stellar source of the variations. Because the PSA tended to track the centroid of the light falling on the IDT, the introduction of extraneous stars into the PSA's field of view caused some errors in locating the prime source, Polaris.

Low Jitter Considerations

No accurate direct measurement of low jitter performance was available. Evaluation of performance using the onboard sensors (ESA interferometer and PSA 2) was difficult because of the noise inherent in the sensors, their readout rates, and their resolution. Resolutions of ESA, the interferometer, and PSA 2 are 0.0055 degree/bit, 0.0014 degree/bit, and 0.026 degree/bit. Minimum update intervals were 160 ms and 22.5 ms, respectively. Noisy interferometer and ESA sensors, typified by the outputs shown in Figure 1-21, indicated vehicle rates improperly. This analysis used the wheel excitation dwell data (i.e., readout every 22.5 ms) to determine the actual wheel torque-time history for the sample period. The alternate torquing due to wheel drive (10 in.-oz) and wheel rundown (0.74 in.-oz) resulted in a change in vehicle rate history. Rates calculated using this alternate torquing were believed to be representative of actual vehicle rates that would be measured by perfect sensors with bandwidth sufficient to include the control actions of the low-jitter control loops.

Table 1-6
ACS In-Orbit Performance Compliance

Mode	Parameter*	Spec (3-Sigma)	Actual
ABC Sun Acquisition	Time to acquire	⩽30 minutes	10 minutes
	Pointing accuracy	4.5°	2°
ABC Earth Acquisition	Time to acquire	⩽80 minutes	50 minutes
	Pointing accuracy	1.0°	0.35°
ABC Local Vertical	Pointing accuracy	1.0°	0.35°
DOC VHF Monopulse	Pointing stability	1.0°	0.5°
DOC S-Band Monopulse	Pointing stability	0.3°	0.01°
DOC C-Band Monopulse	Pointing stability	0.1°	0.002°
DOC Offset Point Ground**	Pointing accuracy	0.1°	0.049°
	Pointing stability	0.1°	0.01°
DOC Low Jitter**	Pointing accuracy	0.5°	<0.1°
	Pointing stability	0.01°	0.005°
	Rate stability (low freq.)	0.001°/sec	0.0003°/sec
DOC Satellite Track	Tracking Accuracy	0.5°	<0.2°
DOC Offset Point Slew	Rate	⩾0.5°/minute	1.2°/minute
	Settling time	⩽10 minutes	<3 minutes
DOC Operational Modes (Above)	Yaw accuracy using PSA	0.15°	<0.1°

*Indicated parameters pertain to roll and pitch except for the first mode which pertains to pitch and yaw and the last mode which pertains to yaw.

**Using either the Earth sensor or the interferometer.

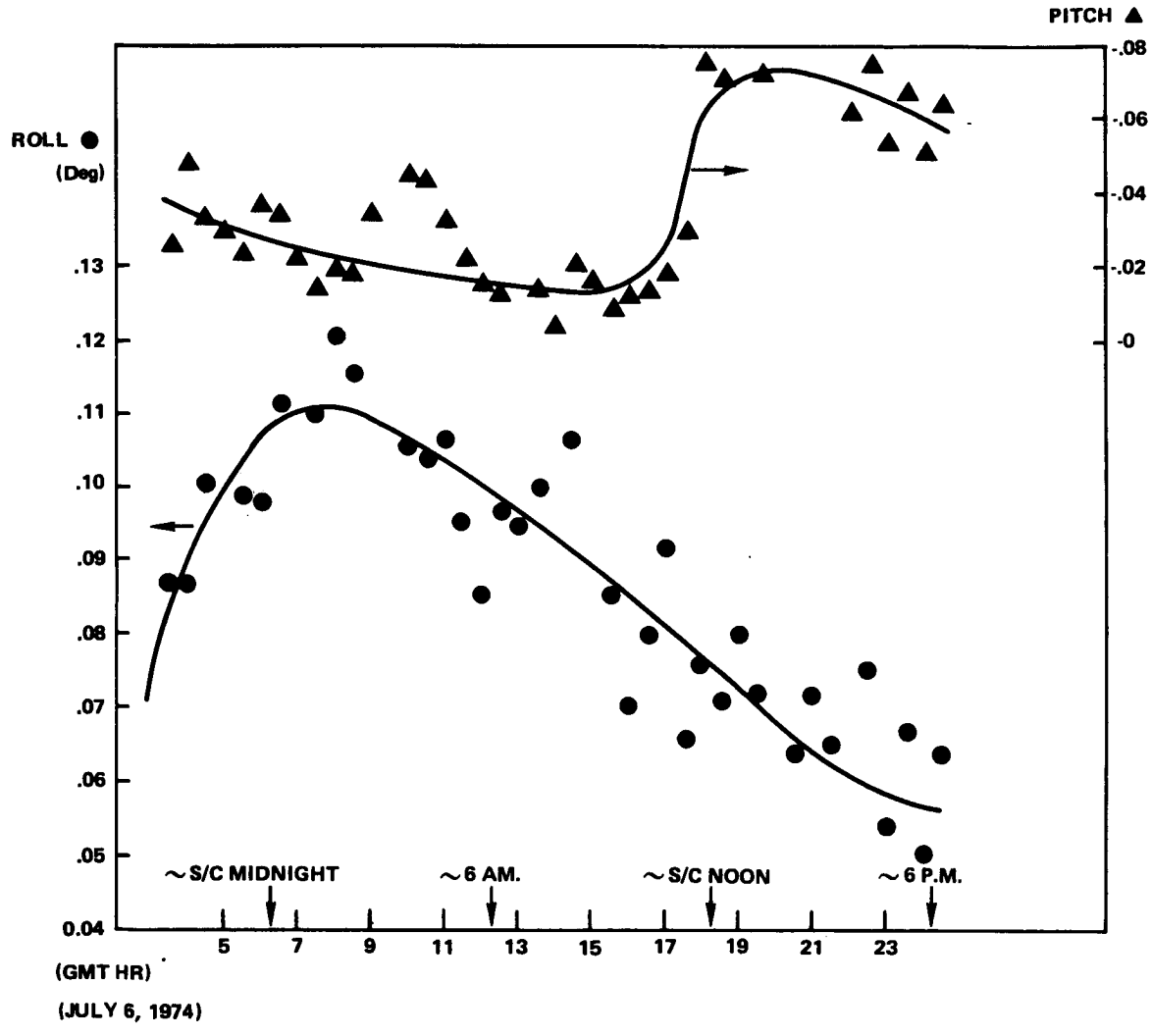

Figure 1-19. Difference Between ESA and Interferometer Outputs When Pointing at Rosman

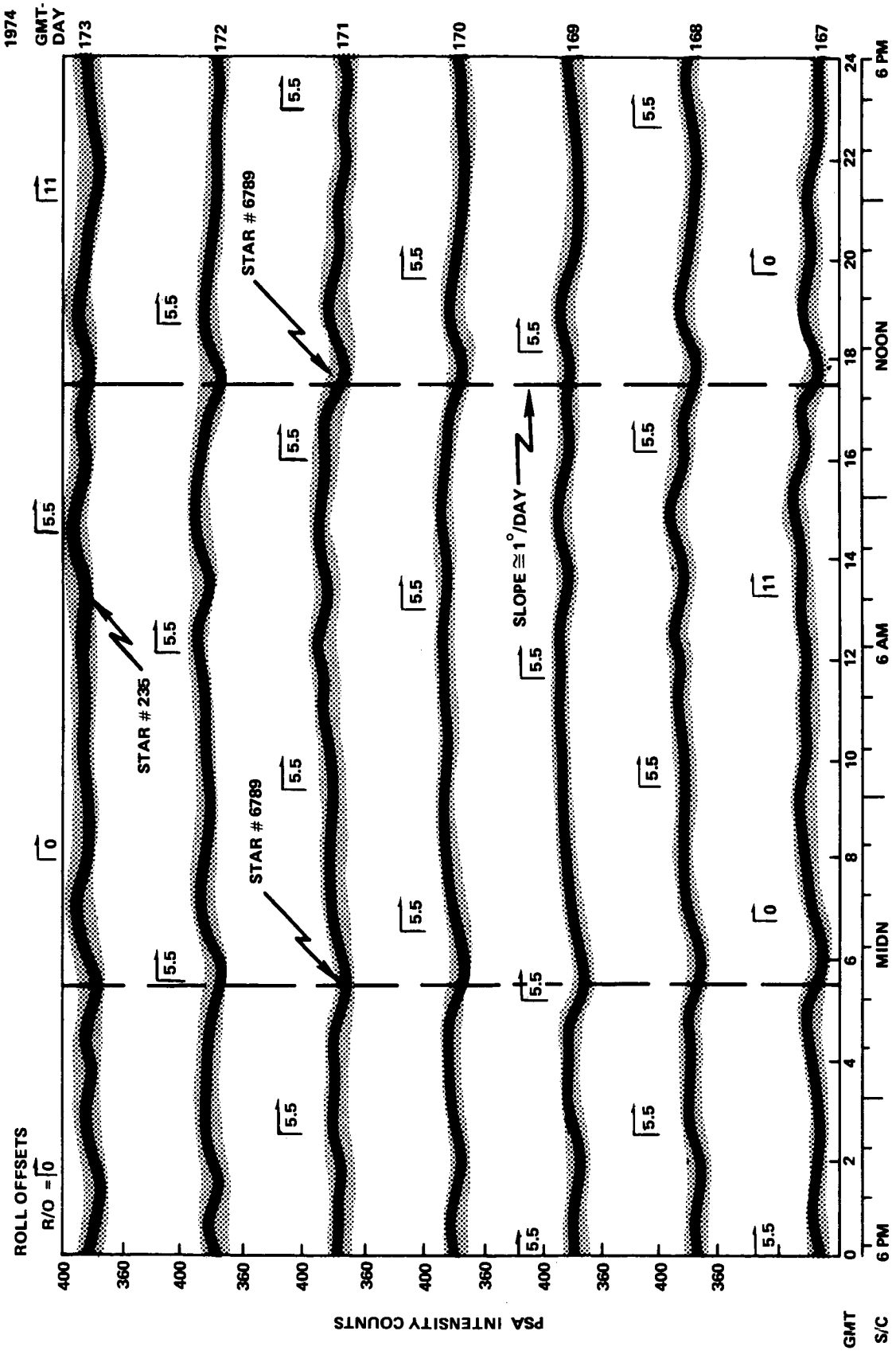

Figure 1-20. Variations in PSA Intensity Measurements

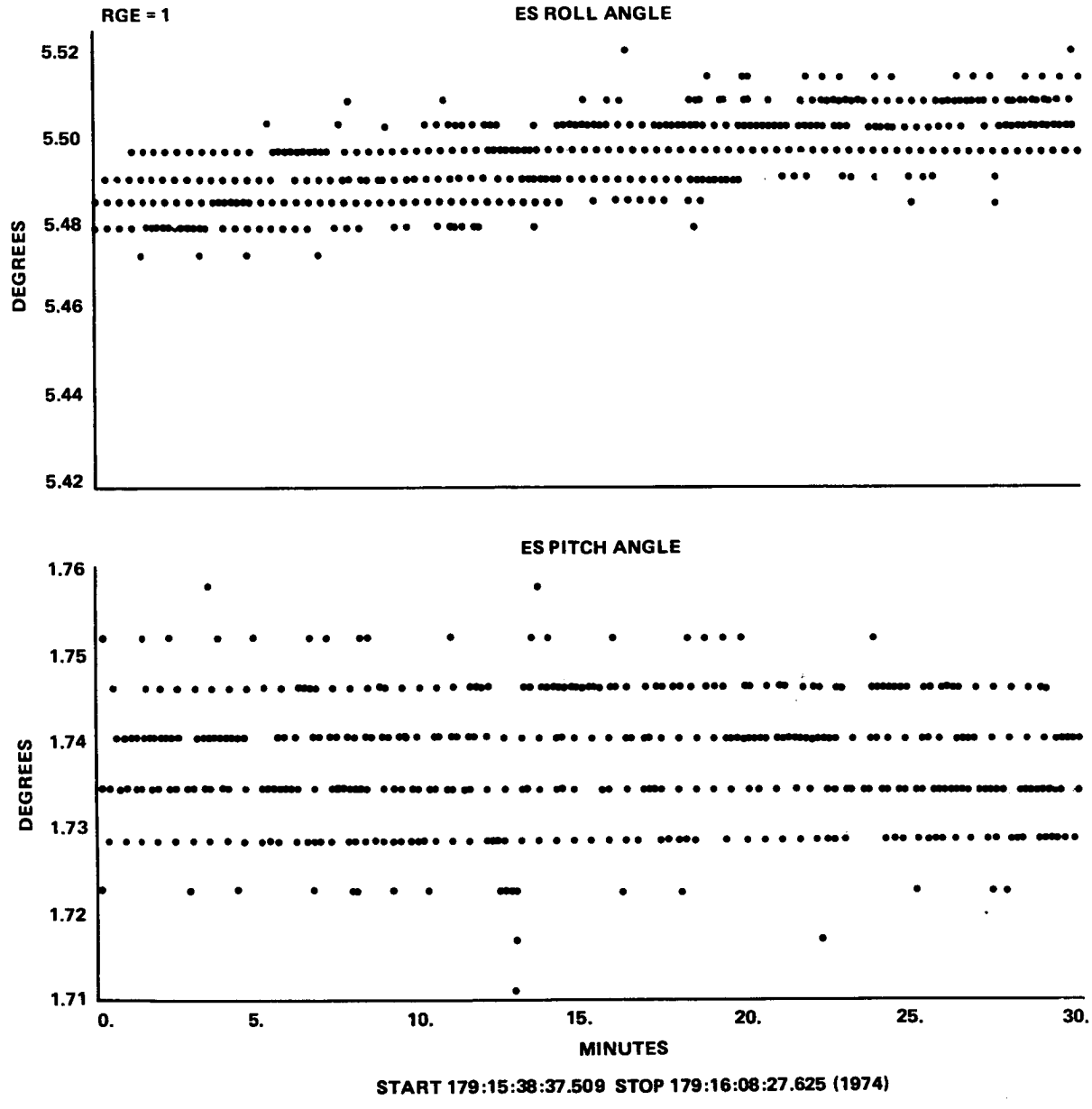

Figure 1-21. Typical ESA Outputs During Low-Jitter Mode

High-frequency disturbances outside the control-loop bandpass were applied to the system by oscillating components in the very high resolution radiometer and Environmental Measurements Experiments packages. These disturbances were about the pitch and roll axes only. If the satellite was rigid, the effects of those torques on attitude and rate would be negligible; however, the possibility existed of amplification due to structural resonance. Figure 1-22 contains the pitch and roll outputs of the interferometer with the ACS in low-jitter mode using both interferometer and ESA as pitch/roll sensors. No indication of resonance could be found at any frequency.

Normal Spacecraft Operations

After the initial performance verification period, the attitude control subsystem was used almost exclusively as a tool rather than as a subject for investigation. Consequently, actual relation of performance to specification was not investigated as long as the requirements of onboard experiments were satisified. To ensure this performance, continual monitoring of the operation and of the visual quality of the data transmission was made by the experimenters. At ATSOCC this monitoring was done by communications and attitude control engineers by using available displays.

Effects of Component Failures

Effects of Roll Wheel Drive Failure—From June 26, 1975, the time of the partial failure of the roll-wheel drive electronics, the wheel was not consistently capable of being electrically driven in the plus-wheel-speed direction (-ON times). (Wheel acceleration in this direction produces a negative torque on the spacecraft.) However, uncontrolled negative roll torquing, through wheel action, was available through the wheel windage and friction rundown torques when the wheel had negative speed. Negative roll torquing through jet thrusting was ordinarily used employing the jet-assist mode (JAM)* when the wheel's rundown torques were too small to maintain control, a situation that primarily occurred when wheel speed was essentially zero. This use of the minus-roll thruster via JAM effectively kept the roll wheel from attempting to drive into the plus rpm region.

Rundown torques ranged from about 0.2 to 1 in.-oz, depending upon wheel speed and temperature, compared with about 8 to 10 in.-oz normally available. Operations using these torques were satisfactory for attitude-hold modes when wheels torquing requirements were small. Occasionally, for maneuvering conditions, such as tracking of high inclination satellites (when required minus-roll torques might have exceeded 0.3 in.-oz), rundown torquing was not adequate so that jet assist was required. To ease these roll-torque requirements, an additional operational mode—satellite track electroscan mode—was added to the system. Here, the spacecraft roll-command angle to the control system was set to one-half the actual line-of-sight, roll-angle requirement. The remaining one-half nominal roll angle required to communicate with the tracked satellite was obtained by using the communication subsystem's offset beam capability.

*In JAM the negative-roll jet fired when the spacecraft, under wheel control, had hysteretic roll errors of +0.4/0.1 degree or +0.1/+0.04 degree in coarse or fine deadband, respectively.

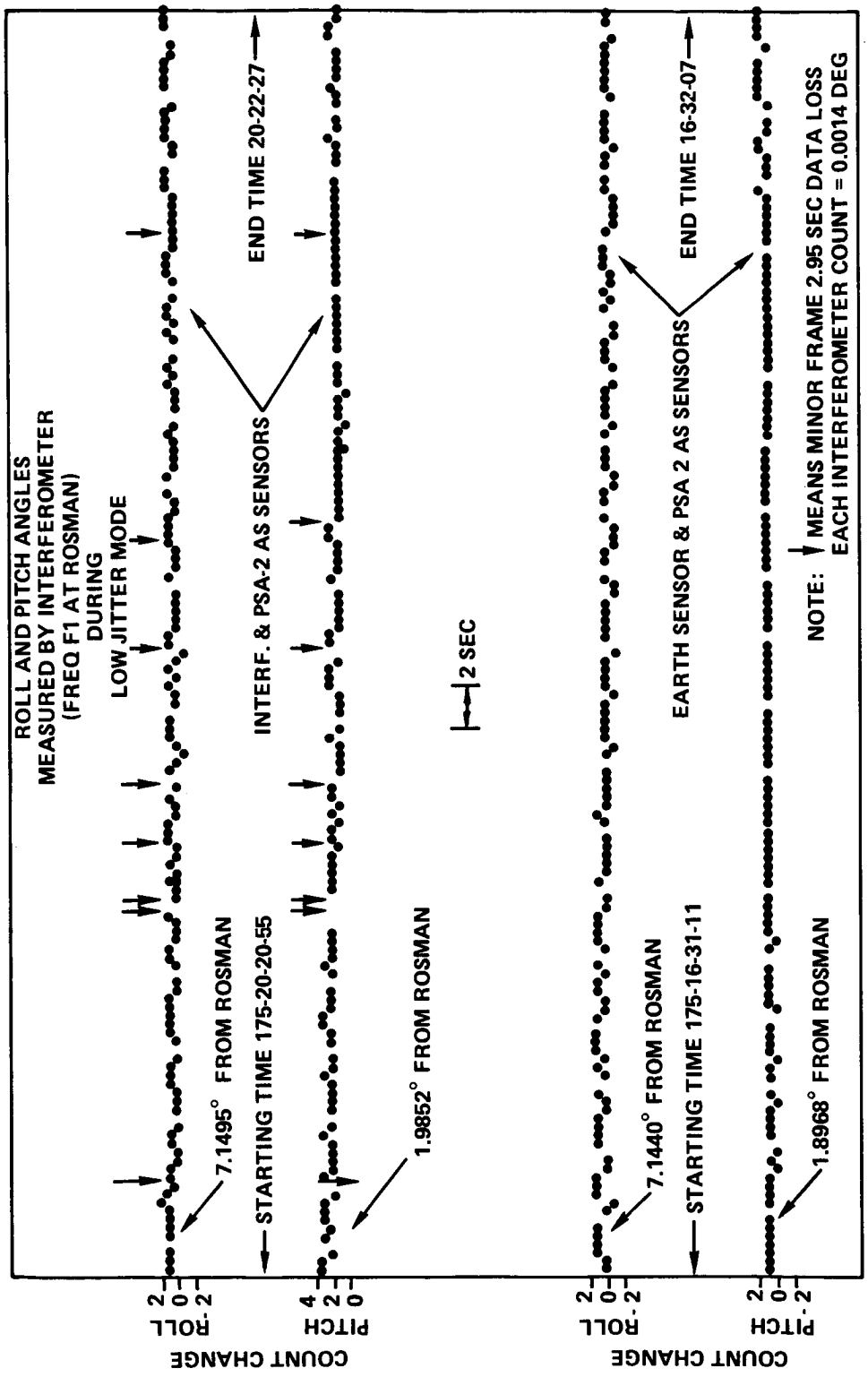

Figure 1-22. Best Resolution Measurements of Pitch and Roll During Low-Jitter Mode

Effect of Polaris Sensor Assembly Failure—On October 21, 1975, the Polaris sensor assembly failed and was turned off. From the time of that turnoff, there was a distinct change in knowledge of absolute attitude control performance. Thereafter, the yaw inertial reference unit (YIRU) was used as the primary yaw control sensor with the digital Sun sensors (DSS) used for periodic re-referencing. Thus, yaw attitude was determined using a dead-reckoning approach; i.e., based on the initial conditions and subsequent history of angle motions. The DSS contributed measurement inaccuracy (bit transition accuracy ±0.1 degree) and poor resolution bit size (0.5 degree). The YIRU contributed errors due to random drifts (0.1 degree per hour), orbital-rate coupling errors when the roll angle was nonzero, and Euler-rate coupling errors during vehicle motions. Together, these (without Euler-rate coupling compensation), yielded yaw attitude errors of about ±0.3 degree which was adequate for practically all ATS operational requirements. (When excessive pointing error occurred due to the yaw inaccuracy, as occasionally happened during the Satellite Instructional Television Experiment, attitude-rereference pulses were sent by ground command to achieve satisfactory Z-axis pointing.)

Operationally all control modes were supported by the DSS/YIRU combination with the possible exception of the low-jitter mode. The potential inability to support low jitter (hence the Very High Resolution Radiometer experiment) was of no significance due to the earlier failure of the Very High Resolution Radiometer experiment itself.

Use of Digital Operational Controller Reprogramming Capability

The versatility of the digital operational controller (DOC), through reprogramming, permitted simpler, more fuel-efficient, and a more component-failure-tolerant operation. Specific examples were:

Mixed Mode Added—Immediately after the roll-wheel drive failure occurred, the attitude control subsystem was used in the jet-control mode. To reduce the use of propellant, a new mode of operation—mixed mode—was introduced. In this mode, pitch and yaw axes were controlled by wheels with the roll axis controlled by jets. The projected life of ATS-6, based on fuel expenditure, increased with this mode from about 2 years (with restricted operations) to about 5 years (with restricted operations).

Jet-Assist Mode Added—Further reduction in fuel consumption from that used in the mixed mode was obtained in the jet-assist mode (JAM). Here, advantage was taken of the still operative negative-wheel drive capability of the roll-wheel electronics by using DOC to command negative-wheel accelerations (i.e., positive spacecraft torques). Negative spacecraft torques were obtained by the run-down friction and windage of the roll wheel and intermittently by negative-roll jet thrusting. The DOC issued no positive drive commands in this mode. The projected life of ATS-6, based on fuel expenditure, was thus raised from 5 years of restricted operations to nearly 7 years of unrestricted operations.

Fuel Use Counter Added—When roll-jet operations in the JAM mode became routine, some concern arose about fuel usage rate and the number of jet firings. To keep track of these data, a counter on DOC jet commands was added to the flight computer program.

ACS Parameters Modified—To reduce jet firings, ACS loop deadbands were altered.

Satellite Track Electroscan Mode Added—This mode was devised to reduce spacecraft motions incident to tracking a satellite target, and thereby reduce jet firings. In the electroscan mode, the nominal roll-track angle was halved with the remaining half-roll angle being supplied by the offset beam capability of the tracking antenna.

Satellite Track with Interferometer Added—To maintain near normal operation despite possible Earth sensor failure, or error due to the presence of the Moon in the Earth sensor's field of view, the interferometer was made a valid roll/pitch sensor for the satellite-track mode. To achieve this and add other DOC programs within the available memory, some DOC programs were deleted. Among these were the automatic-acquisition mode, which sequenced Sun, Earth, and Polaris acquisitions, and both antenna-pattern modes. Also deleted was all the DOC code relating to the use of a laser as a pitch/roll sensor, which had been considered early in the ATS history but never implemented. (To facilitate the code additions in neighboring memory locations, some code, relating to Polaris acquisition, was moved from its original location.)

Incremental Misalignment Data Blocks Added—The original flight computer program contained a 19-item data block for introduction of sensor misalignments into DOC computations. Incremental roll and pitch misalignment data was added in shorter, hence quicker to transmit, data blocks with two and four items. These additions facilitated reorientation of the spacecraft to accommodate the off-axis centerlines of the communication subsystem's antenna beams.

Simultaneous, Continuous Operation of Opposing Yaw Jets Added—After the failure of valve heaters on the spacecraft propulsion subsystem-1 truss valves, it was necessary to keep those valves warm to prevent failure. This warming was accomplished through the addition of a program to the DOC that continually commanded yaw pulsing of both positive and negative yaw jets. This program was used during occult periods after the truss-jet feed lines were emptied.

Effective Telemetry Reformatting Used—When assessing the low jitter performance of the spacecraft, it was desirable to obtain attitude information as frequently and accurately as possible. But, ordinarily, the interferometer and Earth sensor outputs were available to the ground, through standard telemetry, only once each minor frame (3 seconds). This limitation was due to the length of the sensor outputs (greater than 9 bits) and the ability of the telemetry system to dwell on only one telemetry channel at a time.

By dwelling on the DOC's telemetry channel and using output data block 4 to transmit the contents of the DOC's input-attitude sensor storage locations, it was possible to obtain updated pitch and roll attitude information from the interferometer every 0.4 second. The 0.4-second interval consisted of four successive 0.1-second intervals for obtaining the roll and pitch most significant and least significant bit sets.

Yaw 180-Degree Operation Added—After the failure of the Polaris sensor, there was no inherent advantage to operating the spacecraft with the negative-pitch axis pointing North rather than pointing South. Some thermal advantages by the battery with operation in the latter mode were realized.

To accommodate operation in this "flipped" orientation without changing the data content of the DOC input data blocks, the "flipped mode" was implemented.

This mode was used intermittently during the life of the spacecraft.

Use of Redundant Sensors

Pitch/Roll—Five pitch/roll signal sources—the Earth sensor assembly (ESA), the interferometer, and the three monopulse outputs—were available for use. With the exception of occasional use of an interferometer, the attitude control subsystem used the ESA almost full time.

The wide field of view (at least ±35 degrees) of the interferometer made it useful for restoration of Earth acquisition when the narrower field of view of the ESA was inadequate. This circumstance occurred several times during the mission when the ESA lost acquisition of the Earth.

Occasionally, on a predictable basis, the Moon passed through an ESA pitch or roll scan. Roll or pitch error outputs resulted, yielding transient spacecraft motions. By using the interferometer as sensor, rather than the ESA, these attitude perturbations could have been eliminated. Usually, this was not done because of the inconvenience associated with activating the ground transmitter required by the interferometer.

After the Polaris sensor assembly (PSA) failure, contingency plans were made to obtain yaw axis information from simultaneous outputs of the ESA and the interferometer. The necessary DOC reprogramming was done and the system operated. Noisy yaw information was obtained. Although never used operationally, this mode was retained as a backup to the yaw inertial reference unit (YIRU).

So successful was the operation of the attitude control subsystem that the analog backup controller modes using monopulse inputs were not used until those modes were tested in a set of final engineering tests before the decommissioning of ATS-6. Normal operations were obtained within specification limits.

Yaw—The PSA and the YIRU were provided for full-time control of the yaw axis. Part-time control capability existed by use of the digital Sun sensor (DSS). The DSS and auxiliary digital Sun sensors provided full yaw information albeit with high inaccuracy near orbit noon and midnight.

During the first 4 days in orbit, the YIRU was used as yaw reference. On the fourth day, the PSA was turned on and the star Polaris was acquired. During the Polaris checkout phase, it appeared that targets in the PSA's field of view were being tracked. In most instances the PSA would reacquire Polaris after a small error buildup; occasionally star acquisition was lost. On the assumption that the targets were particles being emitted by outgassing from the spacecraft, the PSA was turned off for 3 days. After being turned on again, the PSA was operated in the control loop with operation normal. Although there were periodic losses in Polaris tracking, the DOC operated in a mode that automatically switched the YIRU into the control loop when the PSA lost acquisition. Usually, automatic reacquisition of Polaris occurred resulting in the DOC reselecting the PSA as reference so that

intervention by ground control was not often required. At times, after a PSA anomaly, the vehicle had a yaw attitude so large that reacquisition of Polaris could not automatically be accomplished. At these times yaw backup control using DSS was commanded. In this mode the DSS, with one-half degree resolution, was used as yaw sensor and the DOC, using stored data, computed the required DSS output to maintain the same yaw attitude as would be achieved if the PSA was operating. Polaris acquisition was then obtained by ground commanded flyback and sweep, after stable DSS operation was achieved.

Use of Redundant Controllers

Two digital operational controllers (DOC) and an analog backup controller (ABC) comprised the onboard controller set.

With the exception of occasional use of the ABC during reacquisitions or during anomaly testing or for experiment response, the spacecraft was nearly continually under DOC control.

Before the launch of ATS-6, some uncertainty existed about the capability of the two DOC's to withstand launch without sustaining memory changes. To overcome this uncertainty, the ABC was charged with the task of initial acquisition and the task of providing limited operations control capability, i.e., local vertical and monopulse modes, in the event of failure of both DOC's. Implicit in this latter task allocation was the reasoning that simple analog systems would be more reliable than complex digital systems. ATS-6 history does not confirm nor deny this idea, since both the ABC and the DOC basically performed without flaw in all standard operations. Even the launch fears relating to DOC were unfounded; analysis of the memory dumps immediately after initial acquisition showed both onboard digital controller memories unaffected by the launch.

Because it appeared worthwhile to confirm the operability of the ABC after 5 years in orbit, years in which the ABC had been used only infrequently, some rechecking of ABC local vertical control was done during the final engineering tests. Control appeared similar to that obtained during the initial week in orbit.

After May 31, 1974, the second day in orbit, one of the two DOC's was used by the attitude control subsystem for control of the spacecraft. No functional failures of hardware were observed although software errors were found. Because, for an extended period of time, DOC 1 was in active control with DOC 2 in monitor, it appeared worthwhile to verify the control capability of DOC 2 during the final engineering tests. Normal ACS operation was observed.

Ordinarily, when spacecraft electrical power was not a problem, both DOC's were ON, one in control, the other in monitor. Turn-off of the DOC was only done during power-limited operation. Though both were on, their flight computer programs often were different to facilitate testing of new programs under conditions of minimum risk.

Use of Redundant Actuators

A set of 12 reaction jets, in redundant sets of 6, and a set of 3 reaction wheels comprised the attitude control subsystem actuator set. The function of the jets was to provide three-axis attitude control torquing and translation thrusting during orbit change or stationkeeping maneuvers, to provide three-axis control torquing as prime actuator in the event of the unavailability of reaction wheel control, and to provide reaction wheel momentum unload.

To conserve propellant, the reaction wheels were used whenever the torquing requirements permitted their use. The supplementing of wheel torquing by jets, made necessary by the roll wheel failure, has been described previously.

Selection of the active jets could be made by full sets or by specific choice of jets from each set. As the spacecraft mission progressed, the failure of various jets caused the use of both of these capabilities. Jet contingency plans were formulated to maintain control capability despite these progressive failures and the roll-wheel controllability limitation. Among the operational approaches devised and tested were to:

- Cause the spacecraft to achieve orientations for a short time in which the external torque effects were specifically desired rather than have the spacecraft merely follow arbitrary orientations (from the torque point of view).

- Cause the spacecraft to achieve orientations in which the total angular momentum stored in the spacecraft pitch-roll plane always had a component stored as a negative roll-wheel speed. A technique using repetitive 180-degree yaw turns was an example of this concept.

- Replace the capability of an inoperative jet by the capability of a still operating jet that was, temporarily, reoriented to achieve the desired angular momentum increment. An example of this was: positive roll jet capability is replaceable by negative pitch jet action at 90 degrees yaw.

- Periodically use the positive yaw jet to "reset" the yaw wheel speed so that the inherent yaw/roll wheel coupling forced the roll wheel to drive negatively after reset.

- Temporarily store the angular momentum in the spacecraft itself, which in a perfectly operating system would be stored in the roll wheel running with positive speed. This storage was visible as a spacecraft positive-roll rate.

A digital computer program with display was installed at ATSOCC for the purpose of familiarizing operating personnel with the effects of possible jet/orientation procedures (with prescribed roll/pitch trajectories) on wheel-speed trajectories. A copy of the display is given in Figure 1-23.

The first technique listed was used for about 6 months to maintain pitch-wheel control capability and the second technique listed was used for the final 2½ weeks of ATS operational life.

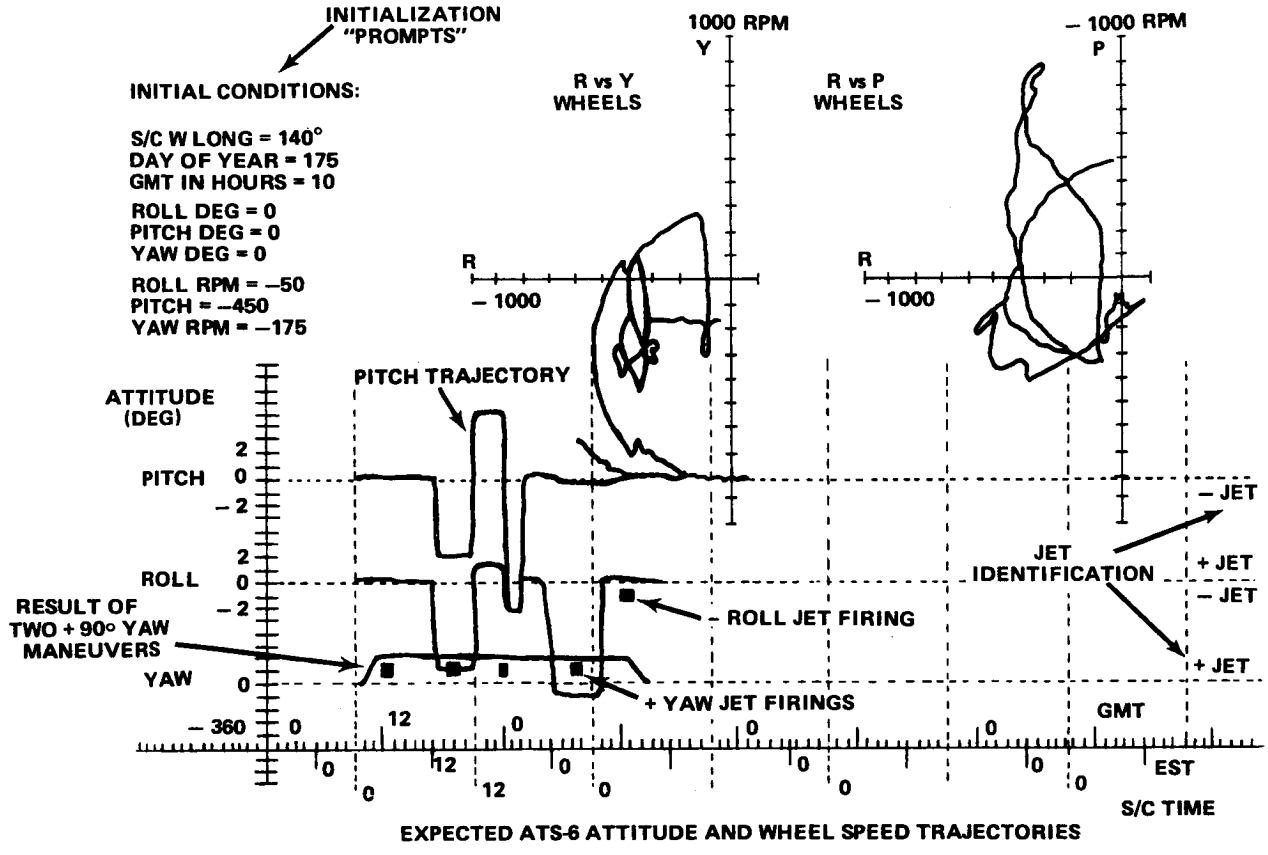

Figure 1-23. Momentum Management Planning Program Display

Final Engineering Tests

Just before the final ATS-6 orbit altitude reduction, a set of engineering tests were performed to:

- Verify the proper operation of system elements not used for an extended period of time (DOC 2 and ABC were tested)
- Verify the proper operation of system backup capabilities never used (ABC use of monopulse inputs was tested)
- Gather information, related to ACS components that failed, to determine the failure mechansim (PSA and RGA 1 were tested)
- Gather information related to component performance changes (tested were reaction wheels, YIRU, and related changes in ESA/interferometer performance)

Results of these tests are given under the heading "Design Verification," and in the following paragraphs.

IN-ORBIT ANOMALIES

Two classes of in-orbit anomalies may be considered. They may be denoted as either "true" or "pseudo" anomalies. The first results from an actual component anomaly, the second from normal component response to unexpected component stimulation or status. The following sections describe these anomalies in greater detail.

True Anomalies

Rate Gyro Assembly No. 1 Null Bias

During the initial phase of Earth acquisition, the attitude control subsystem (ACS) failed to drive the zero-attitude error in roll after the Earth was acquired by the Earth sensor assembly (ESA). The roll angles were held, with some oscillation, at about 8 to 9 degrees. Normal attitude control to zero-roll error was achieved when the rate gyro assembly (RGA) 2 was substituted for RGA 1 in the control loop.

A review and analysis of data led to the following observations:

- During and after boom deployment, the RGA 1 roll output had an offset -0.19 degree per second seen both on its telemetry and its ACS output signals. RGA 2 roll gyro had negligible offsets in both outputs.

- Because the RGA telemetry indicated no essential error before launch, it was concluded that the degradation in RGA 1 output occurred during launch and/or separation. The degradation was probably in the RGA electronics.

It is interesting to note that indications of the RGA 1 output offset were available nearly 3 hours before that flaw was made visible by the improper control during acquisition of the Earth. The following illustrates this.

Both RGA's were on before lift-off. Roll RGA telemetry indicated 0.02 degree per second. (A single signal indicates the combined sum of the RGA outputs.) The low indicated rate was well within expectation.

The boom drop was normal and took about 2 minutes to complete. RGA telemetry indicated roll rates of -0.28 degree per second before deployment and -0.19 degree per second after. The short time period for the total boom motion and the indicated low pitch and yaw rates (0 and 0.4 degree per second) suggest that the RGA roll readings were about a fixed inertial axis. The expected ratio of roll inertias from before to after deployment was 1:2.1. Actual vehicle rates can be inferred from this data by noting that the vehicle rates should vary inversely with the inertia ratio. The inferred final roll vehicle rate was -0.1 degree per second; i.e., the RGA 1 and 2 gyros indicated 0.1 degree per second less than the true rate.

About 50 minutes later, the roll RGA indicated the same rate (-0.19 degree per second) and RGA 2 was turned off. RGA telemetry then jumped to -0.27 degree per second. Assuming no change in vehicle roll rate, the RGA 1 telemetry bias is given by the difference between true and telemetry rates. If the inferred rate computed above is used as "true," then the RGA 1 roll telemetry bias was -0.18 degree per second (-0.27, +0.09). It should be noted that RGA circuitry tended to average RGA 1 and RGA 2 outputs when both were on. The approximate doubling in estimated telemetry bias from -0.1 degree per second with both RGA's on to -0.18 degree per second with RGA 1 only on was consistent with RGA 2 having zero bias and RGA 1 having -0.18 degree per second bias at that time.

After acquisition of the Sun at 150:21:10 Z, RGA roll telemetry indicated a near-zero rate (0.05 degree per second) and pseudo-rate wheels were commanded. Indicated roll RGA telemetry remained essentially constant. Two independent means were then available for measuring roll rate:

1. The angular momentum stored in the pitch and yaw wheels was interchanged as the vehicle rolled while holding on the Sun line. Using the characteristic period of the wheel-drive signals, the roll rate could be estimated at +0.25 degree per second.

2. The interferometer was turned on before acquisition of the Earth. Ground transmitters excited the interferometer at about 150:22:59. Indicated roll rate from interferometer count changes was +0.24 degree per second and the RGA 1 roll telemetry bias was therefore -0.19 degree per second (+0.05, -0.24) at that time.

Better on-line operations and analysis techniques would have revealed this anomaly before it became a source of difficulty. It should be noted that spacecraft integrity was never threatened; a threat only existed to the mental tranquillity of those monitoring the spacecraft operation.

Yaw Inertial Reference Unit Bias Compensation Dropout

During the initial in-orbit checkout of ATS-6, it was observed that the yaw inertial reference unit (YIRU) rate bias compensation function was not working properly. (The purpose of the compensation was to bias the torque on the gyro's float so that there would be no float motion due to inherent gyro drift torque and/or torques due to sensing components of spacecraft orbital rate.) The bias compensation, which has a ground-commanded value, was intermittently changing from its commanded value to zero, and not responding to subsequent compensation change commands until the rate-bias-reset/rate-bias-enable command was issued. The time durations for which the bias remained at the commanded value varied from less than a minute to several hours.

A review of the compensation circuitry resulted in a conclusion that the most probable cause of this behavior was a failure in a relay's circuitry that caused it to be sensitive to noise on the rate-bias-disable/YIRU-heater-enable command line. The source of that noise was found when it was noted that a dropping of the ATS-6 command carrier (at 154 MHz) correlated perfectly with the bias compensation dropout. Consequently, awareness of the situation eliminated the bias compensation problems. Usually, the carrier was maintained up.

Later it was found that transmission from the 154-MHz transmitter located at Brevard near Rosman, North Carolina, was interfering with the Greenville, North Carolina, fire department's mobile units that communicated at that frequency. ATS-6's alternate command frequency was then used; however, other spacecraft shared this command frequency, necessitating intermittent dropping of the ATS-6 command carrier with the concomitant bias compensation dropout.

It is worth noting that the integration testing, described earlier, was designed to uncover intersubsystem effects but did not reveal the bias compensation/telemetry and command system coupling, if indeed that coupling existed at that time.

The inconvenience and "workarounds" required to bypass the bias compensation anomaly emphasized the desirability of having the YIRU commandable by the digital operational controller (DOC). This linking was not done because the YIRU was installed as a functional backup to the Polaris sensor assembly (PSA) and as a substitute for a redundant PSA at a time too late for making the necessary input/output changes to the DOC.

Roll Wheel Anomaly

On June 26, 1975, (GMT Day 177), an instability developed in the attitude control subsystem (ACS) roll axis subsequent to an anticipated attitude perturbation induced by the Moon transiting the Earth-sensor roll scan. After the Moon exited the scan, the roll axis developed a divergent, double-sided limit cycle instead of stabilizing. Subsequent action by the ATSOCC personnel isolated the problem to the roll reaction wheel and/or its associated electronics. The spacecraft propulsion subsystem (SPS) was then selected for the system torquer and the roll axis stabilized.

ATS-6 engineers were directed to:

- Analyze the ACS telemetry recorded at the time of the instability, and define and conduct troubleshooting tests to further isolate the cause of the anomaly.
- Determine if the roll wheel could be used, under what operating conditions, and the impact on the mission.
- Generate the required changes to the DOC program to allow a mixture of the roll jets and pitch/yaw wheels to be used as the attitude torquers, and incorporate the changes into the DOC's. This mixture of jets and wheels has been designated as the ACS mixed mode.
- Determine the fuel consumption and impact on the mission if the mixed mode would be required for the remainder of the life of the spacecraft.

After the troubleshooting ACS test results were obtained, it was concluded that the problem was in the drive electronics, so a failure-mode-effects-criticality-analysis (FMECA) was conducted for the roll-wheel electronics. That analysis resulted in three candidate components that could malfunction and cause the type of roll wheel failure that was observed. These were: (1) an amplifier was breaking into a high frequency oscillation, (2) a 33-pf ceramic capacitor, used to stabilize that

amplifier, was leaking excessively or opening, or (3) one of the 1-μf ceramic capacitors around that amplifier was leaking during periods when it was being charged.

The wheel-drive circuit was breadboarded and tested to verify the FMECA results. An electronics card containing the circuitry was taken from the actuator control electronics (ACE) qualification unit and similarly tested. The results ruled out the failure of the 33-pf capacitor as causing the anomaly. The failure could not be duplicated with the capacitor open or shorted. An excessive leakage rate of one or more of the 1-μf capacitors could cause the anomaly. Also, if the amplifier broke into oscillation, the anomaly would result. However, since the amplifier was an integrated circuit, it could not be modified to cause it to break into oscillation.

Research conducted into histories of the failures of the amplifiers indicated that there had been a history of bonding-post separation failures on the amplifiers used on Honeywell's Centaur Program. These separations have commonly been associated with pins 1 and 8 that were the connections of the 33-pf compensation capacitor. The analysis of the Centaur failure, which was completed in early 1975, blamed the problem on faulty bonding processes. It is important to note that the Centaur bonding-post separation failures were discovered in piece part lots manufactured prior to those used in ATS-6 hardware. Presumably, therefore, the source of the prior difficulties would have been eliminated.

After the original failure, the roll wheel electronics worked properly on an intermittent basis.

The use of the DOC and the roll jets in overcoming the torquing limitations imposed by partially-failed roll wheel electronics was referred to previously. When the SPS-2 negative-roll jet proved inoperative in a test on February 19, 1977, the roll-attitude control situation became very serious; only one unfailed negative-roll torquing component (the SPS-1 negative-roll jet) remained for obtaining "normal" control. Contingency control plans, generated to maintain nearly normal operation despite even this last jet's failure, were previously presented under the heading "Use of Redundant Actuators." Fortunately, this jet worked very well until July 13, 1979. The 180-degree flip maneuver contingency technique was used from that time until the final spinup of ATS-6 on August 2, 1979.

Polaris Sensor and Earth Sensor Anomalies

On October 19, 1975, the Polaris sensor assembly (PSA) was turned off as a result of anomalous behavior extending over the preceding 9 days. The yaw inertial reference unit was then selected as the yaw attitude sensor. The PSA was turned off and remained so until a turn-on during an end-of-life test on August 2, 1979, just before the end of the active life of ATS-6.

The anomaly began on October 10, 1975, when the PSA's output became erratic, randomly varying over its full output range of ±3.5 degrees. Some Earth-sensor output disturbances were seen. The PSA's output then stabilized and the unit worked properly for 7 days after which erratic behavior recurred. After 2 days of intermittent periods of correct/incorrect operation, during which there appeared to be increasing effects on the Earth sensor, the PSA was turned off.

An engineering team was formed to determine the probable cause of the failure and if the PSA should be turned on again, in view of the potential damage to the Earth sensor assembly.

The probable cause of the failure of the PSA was corona/arcing in the intermediate voltage supply (-700 Vdc) to chassis ground. The suspected voltages were those to the image dissector tube cathode or focus. Either would explain the anomalous behavior of the tracker.

The possible causes were:

- A cracked printed circuit board ceramic stand-off terminal
- A void and/or contamination in a printed circuit board encapsulant
- A cold flow of teflon wire
- A partial pressure caused by outgassing.

An assessment of the PSA damage was:

- The cause of corona/arcing may be permanently established by carbonizing.
- The PSA logic circuits may be impaired, although this was not conclusive.

An assessment was made of the risks of turning on the tracker. If the arcing increased in severity, there was the possibility of damage to, or interference with, other spacecraft components, as demonstrated by the interference with the Earth sensor assembly. An investigation of the PSA circuitry showed that severe arcing of the cathode voltage could result in a capacitor discharge into the signal ground that could couple into other spacecraft components and possibly cause permanent damage. Arcing of the focus voltage would not be as severe, because the focus voltage was not capacitor protected.

The erroneous outputs of the Earth sensor assembly (ESA) were caused by its scan mirrors reacting to electronic noise on the signal ground lines. The noise was generated by PSA arcing. The history of the attitude control subsystem (ACS) test indicated that the ESA was sensitive to ground noise.

Based on the importance of the ESA to the mission and the ability of the yaw inertial reference unit to meet yaw attitude sensing requirements, it was decided to turn off the PSA until its turn-on could either aid in completing the mission or, without danger to the mission, provide engineering data for further failure analysis.

When the PSA was turned on, at the end of the mission, a failed response was again observed, for its output appeared pinned at one end of the sensor's field of view and random erroneous values appeared on the Earth sensor's output.

Earth Sensor Assembly Roll Output Anomaly

At 2108 GMT, December 27, 1975, spurious ESA roll outputs were noted. These occasionally resulted in small (0.15 degree) roll attitude perturbations by the vehicle. Equivalent perturbations were obtained through the remainder of the mission when ESA temperature was high.

A review of the ACS telemetry data for the period, plus additional data obtained during later periods, indicated that:

- The roll output behavior was temperature related. When it occurred, it always happened around spacecraft midnight, when the ESA temperature was peaking, particularly near eclipse seasons.

- High ESA temperature was not always accompanied by noise, indicating another input was required to create the problem. Efforts to determine the input were not successful. A correlation of ESA high temperature, non-ACS equipment being operated on board ATS-6, and ESA erratic behavior indicated the problem was independent of non-ACS equipment when being operated.

- The anomaly was not caused by sunlight reflecting into the roll head. During the umbra of the second night of the eclipse season that began on February 28, 1976, a roll spike was observed.

A short analysis of the ESA circuitry was made by its manufacturer to determine the source of the intermittent radiance bias noted during the occurrence of the anomalies. It was concluded that zener diodes and/or tantalum capacitors in the ESA's bolometer power supply could be the malfunctioning elements.

Vehicle performance and operations were impacted little or not at all. Configuration of the ACS into the jet-assist mode during periods of anticipated anomalies was restricted to prevent possible unnecessary expenditure of gas.

Interferometer 2 Failure

After a few days of proper operation, interferometer 2 failed to respond to a turn-on command until about 45 minutes had passed. This type of intermittent operation occurred several times before a final refusal to turn-on about 5 weeks after launch. When on, the unit performed perfectly.

Analysis and bench-testing revealed no clear cause of the problem although there is some belief, based on similarity to other failure symptoms, that the cause was a poor solder joint in the electronics.

Pseudo Anomalies

Polaris Sensor Assembly Tracking Anomalies

On May 31, 1974, the Polaris sensor assembly (PSA) was activated and successfully acquired and tracked Polaris. However, the unit appeared to be tracking particles assumed to be products of outgassing. The PSA was then powered down and reactivated on June 2, 1974. Polaris acquisition and track was again successful, but similar tracking anomalies were again observed. This tracking often spanned the full PSA output range of ±3.5 degrees and often resulted in loss of acquisition of the star Polaris by the PSA. When in the yaw-control loop, the resulting spacecraft yaw attitude errors were usually of such short duration (less than 1½ minutes) that they did not affect experiment performance. On those occasions when Polaris acquisition was lost, the DOC automatically selected the yaw inertial reference unit as yaw sensor. When Polaris was again acquired, either because of natural vehicle motion or ground-commanded reorientation, the PSA was automatically reselected as yaw attitude sensor.

Two causes were suggested: (1) Sun reflections into the PSA image dissecting tube from various reflecting surfaces, and (2) Sun reflections off particles resident in the field-of-view of the PSA. The sensitivity of the PSA to such stray light sources is illustrated by this example: if illuminated by the Sun, a 0.001-inch diameter particle, with 10 percent reflectivity, placed 20 feet from the PSA causes the PSA to see a brightness equivalent to that of Polaris.

A review of the data indicated the following:

- A sharp drop in anomaly rate with time observed as indicated by the following table:

Date	Mean anomalies/day
June 5 to June 25, 1974	19.1
August 21 to September 10, 1974	6.7
November 4 to November 24, 1974	1.1
January 30 to February 19, 1975	0.8
April 8 to April 28, 1975	1.07

- The direction of tracking during anomalies was mainly from east to west during spacecraft morning and from west to east during spacecraft afternoon.

- A daily variation in PSA intensity outputs (Figure 1-20) due to the star field and the temperature of the PSA is equivalent to an anomaly susceptibility curve because near the intensity peaks only small changes in incident light are needed to trigger flyback and sweeps (i.e., one form of anomaly).

- The prelaunch PSA calibration overestimated the output response to excitation by Polaris, so that the tracker's actual output, when tracking Polaris, was equal to that expected when tracking a star with intensity 0.45 times the intensity of Polaris.

Conclusions of the anomaly analysis were:

- Reflections from particles constituted the major cause of the initial PSA anomalies.
- Most of the continuing PSA anomalies were the result of solar reflections (after one "bounce" in the PSA baffle) due to ATS's north solar array and parabolic reflector.
- The flyback and sweep threshold voltage of 4.0 volts in the PSA was too low; a higher level would have eliminated large changes in PSA output in response to small incident light perturbations.
- The anomalies were not the result of abnormal PSA performance.

It is interesting to note that the observed anomalies were anticipated before launch—when the yaw inertial reference unit was considered as an alternative to a redundant PSA there were discussions about "erroneous tracking" due to "30-ft disk reflections or Velcro, Kromelar, dust, or ion engine particles."

Interferometer Loss-Of-Lock

On June 8, 1974, with the interferometer in control, the signal level from the ground transmitter at Rosman dropped. This resulted in the interferometer transmitting a constant value representing attitude to the DOC. In normal response to these attitude "outputs" the DOC generated "hard" drive signals to the wheels that eventually moved the spacecraft off the Earth, requiring its reacquisition.

To prevent a recurrence of this action, the DOC flight computer program was reprogrammed to recognize a 14-time repetition of fixed counts from the interferometer (and by inference, loss of good data) and to generate a critical fault. With a critical fault, the DOC stops issuing torquer commands, places the wheels into a hold mode, and sends telemetry indicating the critical fault. The resultant low spacecraft drift allows the ground operations personnel time to react and take appropriate action to prevent loss of Earth acquisition.

The particular characteristic of attitude perturbation due to an interferometer with lost-lock was recognized well before launch. Alarming the ground control center was proposed as a solution, but the necessary changes were not made. Monitoring reliance was placed on operating personnel. Earlier when the flight computer program was being generated, the solution eventually employed could have been used. But no action was taken, probably because this was a misinterpretation of the meaning of the "validity" bit in the interferometer's output to the DOC. The validity bit, equal to one in the interferometer's output data word, was meant to indicate that the interferometer's output register was in a stable rather than unstable state, not that the output data was good.

Earth Sensor Assembly Roll-Scan Anomaly

On May 1, 1975, Earth acquisition was temporarily lost when the Earth sensor assembly (ESA) roll output "hung up" and caused the DOC to drive the spacecraft off the edge of the Earth. At the same

time, the ESA temperature appeared to be higher than previously observed. As a result of detailed analysis by the analysis group, it was subsequently determined that the ESA hangup was caused by a unique set of flight conditions that was beyond the capability of the ESA Sun-avoidance function (i.e., not due to component failure or degradation), and that the ESA temperature was normal for the existing flight conditions and not due to failure or degradation. Furthermore, there was no relationship between the roll-scan anomaly and temperature.

The roll-scan anomaly began at 0610 GMT. The spacecraft was being slewed from +10 degrees in pitch to -10 degrees in pitch at a constant roll angle of approximately -5 degrees. Toward the end of the slew, the ESA roll output froze at -4.97 degrees. Offset-point-angle track was commanded at 061200, a new input data block 4 (angle track/slew data) was commanded at 061230. This resulted in a new ESA roll-command angle. The combining of the new command angle with the frozen ESA roll output resulted in a roll-torque command that drove the spacecraft off the Earth. ESA Earth acquisition was lost at 0627. Reacquisition was accomplished at 0722 using the Sun sensors and interferometer as reference sensors. The ESA then appeared to be operating properly and was commanded back into the control loop. It has operated properly since that time.

Subsequent investigation showed that the problem was caused by the inability of the ESA Sun-avoidance function to operate at the extreme pitch angles (i.e., nearly equal to -10°) that existed at the time the Sun came into view of the ESA roll-scan plane. Normally, the roll-scan plane would shift away from the approaching Sun until it reached +3.5 degrees, at which point it would automatically jump-shift back to -3.5 degrees (i.e., a delta of 7 degrees), thus avoiding the Sun. However, the roll-scan plane was already shifted approximately 10 degrees (due to the pointing angle) and it was limited to a total movement of approximately 11.25 degrees. Therefore, it was only able to initially move +1.25 degrees, which was insufficient to successfully avoid the Sun (the ESA Sun-avoidance Sun sensor field-of-view was 6 degrees). Since the presence of the Sun in the ESA Sun sensor field of view prevented the ESA output counter from updating, the counter essentially "hung up" and induced the sequence of events described above. The combinations of spacecraft attitude, Sun elevation (i.e., time of year), and Sun azimuth (i.e., time of day) that can cause this condition to occur are relatively rare and predictable and did not recur during the remainder of the ATS-6 mission.

Digital Operational Controller Command-Angle Anomaly

Shortly after the DOC was put into control, pitch attitude and yaw attitude command-angle anomalies were observed in both DOC's twice each day. The phenomenon was observed only during normal operations in the offset-point-ground-coordinates mode at approximately 13:20 GMT and 12 hours later at 01:10. At these times, the pitch-command attitudes would change polarity and the yaw-command attitudes would change in magnitude by ±0.75 degree. The command errors were transient in nature and were such that the incorrect commands were issued by the DOC's for approximately 3 3/4 minutes. After this interval, the correct command angles would be issued until the next occurrence 12 hours later.

The command-angle discrepancies were isolated to an overflow in the register for one of the elements of the inertial-to-local-vertical transformation matrix. On the assumption that the cause of the overflow was the result of a division, the DOC was reprogrammed to eliminate overflow due to that

cause. The reprogramming was successful in eliminating these anomalies for about a year and a half, when the pitch-command anomaly returned. A review established that the sign reversal of the command angle was due to an overflow, this time due to an addition calculation. Analysis showed the source of the difficulty to be finite word length in the DOC; i.e., all numbers could not be represented exactly, in particular the value 1.0 in DOC had the value 0.99996948. A routine in DOC normalized a vector magnitude to one, given three vector components. The normalization could lead to component lengths greater than one, which in the 2's complement representation of numbers in DOC would, with overflow, result in a sign reversal. By arbitrarily altering the vector components by the factor $1 - 2^{-15} - 2^{-14}$, the problem disappeared. This approach was employed and proved successful through the remainder of the ATS-6 mission.

Moon Interference in the Earth Sensor Assembly Field-Of-View

Prior to the launch of ATS-6, there was considerable discussion on possible effects of the Moon in the Earth sensor assembly (ESA) field-of-view, i.e., whether or not the angle subtended by the Moon as viewed from ATS-6 would be sufficiently large to have any detectable effect on ESA error processing. A brief description of the physical observations confirming the Moon's influence on normal ESA operation, the technical rationale for interferences, and some comments on impact to spacecraft operations follow.

The ESA was a two-axis (roll/pitch) scanning optical sensor capable of sensing infrared radiation from the Earth and its atmosphere. The ESA included two identical heads mounted on the Earth-viewing module. The heads were mounted at right angles to each other, so that the roll head scanned north/south in the YZ plane and the pitch head scanned east/west in the XZ plane. Each unit (or head) consisted of a lens-filter-bolometer detector, scanning mirror, and an offset mirror. The electronics package completed the ESA. In the normal operating mode, the ESA scanned through the major diameters of the Earth at a rate of 4 Hz. The scanned field-of-view was ±13 degrees and was automatically biased so that the Earth was always centered within the scans as long as both the roll and pitch errors were less than ±11.25 degrees.

ESA error computation was achieved by an encoder physically attached to each scan mirror. The encoder determined the angular scan position and reference null crossing. When the radiance threshold criterion was met, the electronics accumulated encoder pulses by an up/down count, with counter direction determined by the sequence of events.

Consider now what occurred when the Moon passed through the ESA field-of-view. The instantaneous bolometer field-of-view was approximately 0.6 degree and the lunar disc as viewed from the spacecraft was approximately 0.5 degree. When the Moon lay within the scan plane of either roll or pitch and its radiances exceeded the threshold, additional counting occurred, making the Earth appear as if it were wider than it actually was. In this case, the attitude error was derived from both bodies. With a full Moon entirely in the bolometer instantaneous field-of-view, the apparent delta-width was approximately 1.1 degrees. The ESA interpreted this delta as an attitude error in the affected axis and the spacecraft would attempt to null the error. The magnitude of the resulting error could vary depending on several factors such as the Moon's phase, the location within the scan, and the Earth/Moon radiance threshold sequence.

The frequency of lunar interferences was approximately 60 a year with duration time per interference ranging from 4 to 22 minutes. While periodic lunar interferences were annoying, they presented no real problem to online spacecraft operations. Computer-generated "predicts" were available at ATSOCC to alert personnel on the ACS console to pending interference times. The only effects on operations were minor perturbations in roll or pitch of spacecraft attitude lasting for the duration of the transit period.

As noted in the previous paragraph titled "Use of Redundant Sensors," avoidance of Moon interference effects by use of the interferometer was available to (but usually not used by) ground personnel, because the inconvenience associated with interferometer use was greater than the inconvenience of dealing with the effects of the Moon's interference.

C-Band Monopulse Anomaly

On July 4, 1974, a 24-hour test of C-band monopulse operation was performed with the goal of determining the monopulse misalignment with respect to the interferometer and to measure the diurnal variation in that misalignment. Test results indicated pitch misalignments of 0.03 to +0.05 degree and roll misalignments approximately sinusoidal over 24 hours.

Four losses of monopulse control at the nominal control attitude were experienced during the test: two were the result of ground station loss of signal; and without apparent cause, two occurred near spacecraft dawn and dusk. To determine the reason for these results, a test survey of monopulse/interferometer outputs was made of ±1 degree field about Rosman, North Carolina. Roll and pitch contour maps of monopulse outputs were generated; an overlay of roll and pitch zero-voltage outputs is presented in Figure 1-24. When the monopulse was used as the ACS pitch/roll attitude sensor, the ACS tended to converge to a point where the monopulse pitch/roll lines intersected was a potential convergence point. Also indicated on the overlay are arrowheads indicating the direction in which the ACS converged. Five locations were found to be convergence points. These points have been designated S_1–S_5 on the overlay. The locations are at coordinates:

Point	Roll	Pitch
S_1	-0.18	-0.03
S_2	-0.11	-0.38
S_3	-0.53	-0.48
S_4	-1.00	+0.52
S_5	+0.75	0.20

The most significant element demonstrated was the inherent coupling between monopulse roll and pitch outputs. Secondly, the sensitivity of the locations of the convergence points to small changes in pitch or roll patterns can be seen.

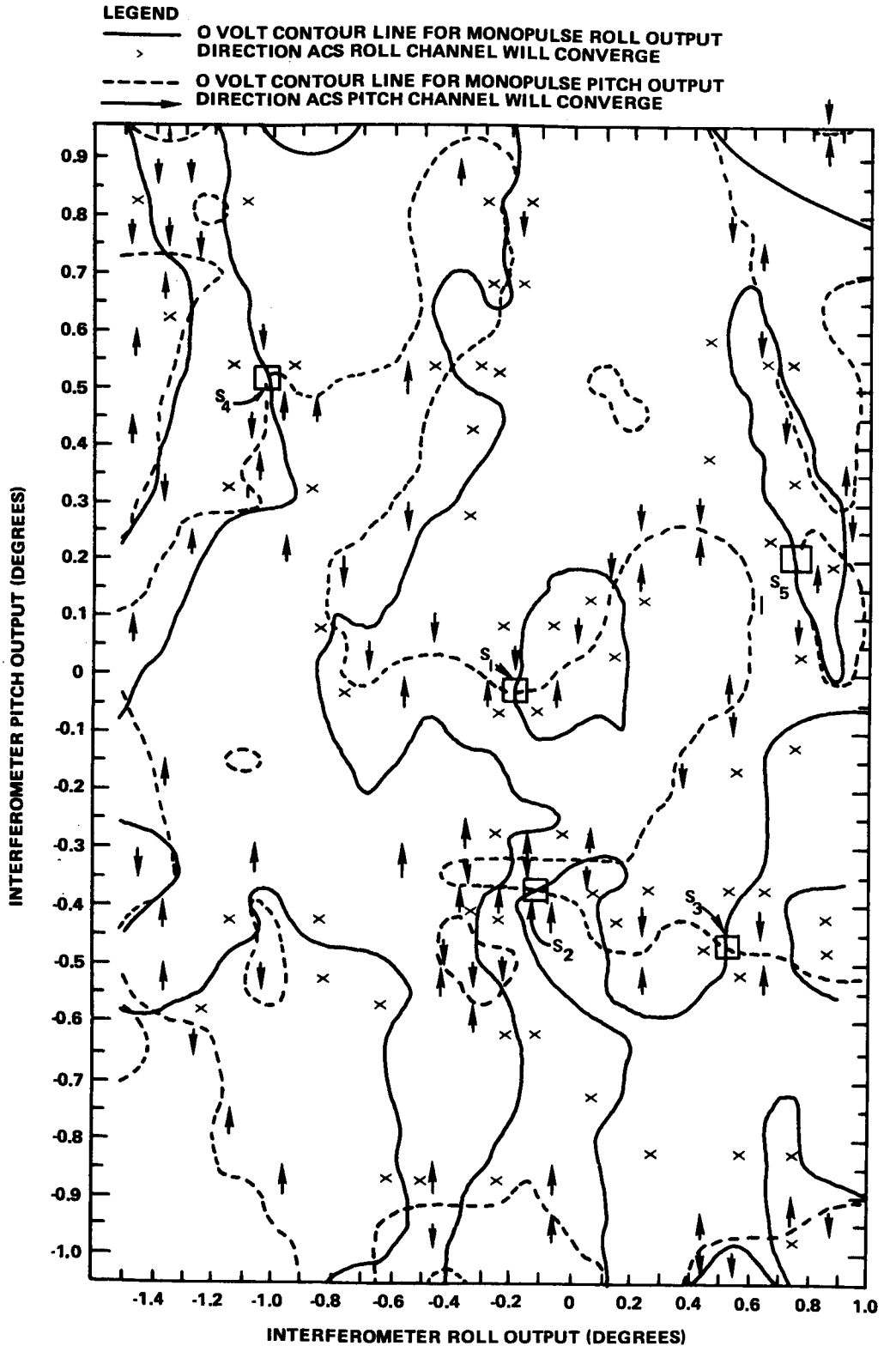

Figure 1-24. Pitch/Roll Zero-Volt Overlay

During the first control loss, the spacecraft moved from S_1 to S_3, at a loss in C-band uplink it moved from S_3 to S_5 (then at roll = 0.5 degree, pitch = 0.5 degree), and during the second control loss it moved from S_5 to S_1. The moves from S_1 to S_3 and S_5 to S_1 followed changes in roll wheel sense of rotation. Apparently, the change in roll attitude (required to supply the reversed wheel friction and windage torques) was enough to instigate the transfer towards the next stable control point.

While further operations with C-band monopulse were completely successful, it was concluded from this test that C-band monopulse as used in the control loops could only be used with caution. The source of the diurnal effects, whether temperature changes in the equipment or deformation of the 30-ft reflectors, was never satisfactorily resolved.

CONCLUSIONS AND RECOMMENDATIONS

Basic Design/Operations Considerations

The ability of the ACS to meet or better its specified mission performance requirements over extended periods of time and despite component anomalies was primarily the result of three characteristics:

- Complete functional and standby redundancy
- Capability of ground operations to reprogram the DOC in flight
- Easy and rapid interplay between ground operations and the operating spacecraft subsystems.

Specific examples of the benefits of these features are next described.

Functional and Standby Redundancy

- Rate gyro assembly (RGA) 2 was substituted for RGA 1 after anomalous performance.
- After the Polaris sensor assembly (PSA) was deactivated, yaw information was provided by the yaw inertial reference unit (YIRU) and digital Sun sensors (DSS).

DOC Command Reprogram Capability

After launch the digital operational controller (DOC) program changes included: (1) logic to verify the probable correctness of interferometer data tagged VALID, (2) a counter recording the total number of DOC-command jet pulses, (3) new control modes (mixed wheel/jet and jet assist), (4) calculations of yaw attitude from Earth sensor assembly (ESA) and interferometer data, and (5) revision of attitude control subsystem (ACS) deadbands as required.

Manual Interaction During Automatic Operations

- Wheel unloading and setting of wheel speeds at desired values was achieved through manually instigated jet firings.

- Re-referencing the YIRU was accomplished by ground commands.

- Jet actuated slews were implemented by ground commands when the roll reaction wheel torque capability was inadequate.

- Command changes in normal ground-point targets were made to compensate for transmitter antenna misalignment and yaw errors.

Clearly these system characteristics should be retained in any similar future spacecraft. Furthermore, based on the actual ACS flight experience, several proposed changes should be considered for possible future ACS designs of this type:

- The ESA could have been made self-redundant with some degradation in accuracy after failure. This could have been accomplished by using the two heads yielding pitch and roll separately but coupled as presently implemented. If one sensor head or its electronics failed, the operating head could be put into a scan-plane offset mode (similar to the existing roll scan-plane mode). The sensor outputs could then be processed to provide both pitch and roll information. The Earth sensors on the Communication Technology Satellite operated in this manner.

- When the roll inertia wheel electronics failed, it failed in such a manner that power could still be applied rather than in a shorted condition. If the latter had happened, or one of the inertia wheel coils had shorted, all of the wheels would have been disabled. The common power interface circuit (PIC) that supplied all these circuits should have been separated to eliminate such common failure modes.

- One mode of achieving additional sensor redundancy in all axes, was not implemented. This mode, in which the DOC would use the complete interferometer outputs based on two ground transmitters, would provide roll, pitch, and yaw outputs in a manner similar to that achieved by the combination of ESA and interferometer signals.

- The YIRU was torqued either impulsively (by angle reference pulses) or continually (by bias rate commands) by ground command only. No DOC-YIRU connection existed to allow torquing under DOC command. Had that connection existed, a sharp reduction in YIRU ground command operations could have been achieved.

Additional Design Considerations

Moving Element Reliability

Five attitude control subsystem elements used mechanically moving parts: the inertia wheels, the rate gyro assemblies (RGA), the yaw inertial reference unit (YIRU), the Polaris sensor assembly (in its Sun shutter), and the Earth sensor assembly. In these, three had continuously rotating elements and four had oscillating components. Ball bearings, air bearings, and flexible pivots (in the Earth sensor assembly) were used. No failure of a moving element or degraded performance was observed. Over the life span of ATS-6, there was a slight increase noticed in the reaction wheel friction and windage torque (0.05 to 0.15 in.-oz. depending upon speed), and a YIRU uncompensated drift rate change of less than 0.05 degree per hour (the maximum rate was 0.1 degree per hour). A possible failure exception was the rate gyro assembly 1 (roll gyro) whose output bias hang-off at initial Earth acquisition was ascribed to failure in the gyro's output electronics. All wheels, the YIRU, and the ESA were operating throughout the life of ATS-6. No turnoffs of the YIRU or ESA were permitted during useful ATS-6 life, but a number of successful YIRU on-off cycles were achieved during the end-of-life tests.

To permit some future life testing, the YIRU, ESA, and PSA shutter power was kept on at the conclusion of the end-of-mission tests with the spacecraft spinning about its roll axis at 1.6 rpm.

Comments on Monopulse

Of the three monopulse systems on ATS-6, only the S-band was completely successful—it provided successful pointing to fixed ground transmitters and airplane-borne and satellite-borne transmitters. After the PSA failure, closed-loop pointing to the signal source was particularly valuable because it eliminated dependence on tight yaw axis control accuracy ordinarily required during satellite tracking, that was achieved by following trajectory commands computed onboard.

The vhf monopulse output signals were somewhat disappointing because their slopes were about one-third to one-fifth of their nominal values, with even poorer slopes about zero. With the built-in control gains, the resultant steady attitude errors were acceptable, but the dynamic response was only marginally satisfactory. Reprogramming the DOC to improve control could have been done, but the analog backup controller loops were hardwired and, therefore, fixed. (Higher vhf gains were obtained with favorable results by using S-band and C-band gains when receiving a vhf signal.)

C-band control operation suffered from a very small initial acquisition range and the problem of potential shift in equilibrium control from one stable point to another due to the narrow beamwidth and coupling between pitch and roll outputs.

In using the monopulse-generated signals, there was completely normal action of the control system.

Usefulness of Interferometer

In all its applications, interferometer 1, the survivor of the original pair, performed flawlessly. Its high resolution (one vernier count = 0.0014 degree) and low noise characteristic made it particularly useful for evaluating the attitude control subsystem performance. Its wide field of view aided Earth reacquisitions as required throughout the mission.

The interferometer specification for 3-sigma performance in pitch and roll was ±0.018 degree or ±12 counts over the dynamic range of 40 dB (-55 dBm to -95 dBm). Test verification at -70 dBm into the receiver/converter yielded 3-sigma performance in pitch and roll of ±0.007 degree or ±4.8 counts. No significant change in performance with power input was noticed.

A particularly useful feature of the intererometer design was the ability to calibrate before-launch and in-orbit output changes (i.e., bias changes) without changes in input. During in-orbit calibration, after adjustments were made for receiver/converter temperature, the interferometer showed worst-case total receiver/converter bias changes of five counts in coarse mode and one count in vernier mode from those recorded prior to launch. As a result, the boresight bias counts loaded into DOC at launch required no change.

The interferometer and the Earth sensor assembly (ESA) were available as independent pitch/roll sensors. Attitude determinations by the ESA and the interferometer differed over ranges of +0.15 to +0.3 degree in roll and -0.10 to +0.21 degree in pitch compared to prelaunch misalignment measurements of -0.00 degree and +0.13 degree, respectively. The portion of these differences due to variation in interferometer output (temperature, attitude, etc.) that was calibrated is much less than the observed differences; thus, there remains a residual uncertainty as to the absolute accuracies of both the ESA and the interferometer.

Although not designed for use with modulated uplinks before launch, the question was raised whether or not the interferometer would also function properly using modulated uplink signals, with no resolution due to the difficulty in conducting a definitive analysis or ground test to determine the answer. On February 16, 1975, a series of flight tests were conducted on the interferometer, using carrier wave and various modulated uplink signals from the Rosman Ground Station, to resolve this question.

Test results showed that interferometer operation was significantly and adversely affected by the presence of the Satellite Instructional Television Experiment (10 MHz p-p deviation) and the Health, Education, Telecommunications experiment (20 MHz p-p deviation) modulation signals on the C-band uplink carrier. The use of the noisy interferometer signal in the control loop caused rapidly alternating wheel torquing, so that attitude control subsystem interferometer operation in the offset-point/ground-coordinates mode was unacceptable because prolonged operation could lead to failure of the actuator control electronics due to overheating. The low-pass filtering in the low-jitter mode control loop permitted functionally acceptable operation although pointing errors were in excess of specification requirements.

Interfaces With Digital Operational Computer

In concept the digital operational controller (DOC) was a digitized analog backup controller (ABC) with the advantages of superior computation capability, programmability, and digital-to-analog/analog-to-digital conversion. Like the ABC, it received analog signals and issued analog and on-off commands. Each controller's input sources and output receptors were fixed by hardware connection. These latter characteristics in the DOC prevented desirable system changes when the yaw inertial reference unit replaced a redudant Polaris sensor assembly late in the design cycle.

A next generation improvement to the DOC is represented by the control and data handling system developed for the multimission modular satellite program. This system employs a single general-purpose digital interface with its computer and links that interface with sensors and actuators by electrical busses. Adding new system components is achieved by coupling new interfaces to the bus, remotely, as required.

CHAPTER 2

SPACECRAFT ATTITUDE PRECISION POINTING AND SLEWING ADAPTIVE CONTROL EXPERIMENT

INTRODUCTION

The purpose of the Spacecraft Attitude Precision Pointing and Slewing Adaptive Control (SAPPSAC) experiment was to establish the feasibility and to evaluate the performance capabilities of attitude control in real time of ATS-6 using computer facilities located on the ground. Attitude control included maneuvers in precision pointing to fixed Earth targets, slewing between targets, and the generation of prescribed ground tracks.

There were felt to be several significant advantages in using a ground-based control system. The cost of implementation was much less than that for a comparable spacecraft system, the equipment was easily accessible for maintenance, and the equipment had the ability to be time shared or to be reassigned to other functions depending upon the mission requirements.

By using the rf command and telemetry links with ATS-6 in conjunction with the computer at the Earth station, a continuous closed-loop control function was achieved. This control feature also allowed the onboard spacecraft control equipment to be used as a backup system in the event of failure of the ground system.

The Earth station facilities for performing the SAPPSAC experiment was located at the Rosman, North Carolina, tracking station. This station had the capability of performing online, real-time processing of spacecraft sensor data and the generation of on/off commands for the spacecraft torquers. The SAPPSAC ground controller was continuously monitored and accepted commands for spacecraft control from either the ground station or from the remote terminal at the Applications Technology Satellite Operations Control Center (ATSOCC) located at the NASA Goddard Space Flight Center in Greenbelt, Maryland. With each of these terminals containing a computer and command/telemetry interface equipment, a redundancy of the terminal facilities was provided that increased the reliability of continuous SAPPSAC control. The remote ATSOCC terminal performed as a centrally located source for the selection of command modes and for monitoring the performance of the experiment.

SAPPSAC EXPERIMENT

The SAPPSAC experiment was developed to perform closed-loop attitude control of ATS-6. The experiment included provisions for online determination of spacecraft position and velocity using two interferometer beacons and the Earth sensor. The SAPPSAC ground controller was a PDP-11/20 minicomputer at the Rosman Ground Station performing online, real-time processing of spacecraft sensor measurements extracted from incoming telemetry and generation of on-off

commands for selected spacecraft torquers for transmission through the ground attitude control (GAC) uplink. There were provisions for continuous monitoring and commanding of the ground controller using a SAPPSAC remote terminal located in the ATS Operations Control Center (ATSOCC). The SAPPSAC remote terminal employed another PDP-11/20 computer in ATSOCC coupled to the ground controller by modems and bidirectional landlines.

SAPPSAC imposed no special spacecraft subsystem requirements other than the GAC decoder and interface to the actuator control electronics. The experiment was designed to use either onboard momentum wheels or the backup hydrazine reaction jets for attitude control. A unified algorithm was employed in the ground controller to determine both 3-axis attitude and spacecraft position, using combinations of onboard sensors (Polaris tracker, Earth sensor, and two-channel interferometer, with optional use of the yaw inertial reference unit). This information was extracted by the controller from the normal telemetry stream.

PROBLEM AREAS

The use of this concept brought about certain unique problems and design constraints:

- There were known one-way link transport delays ranging between 0.129 and 0.500 second. This limited feedback-control applications to frequency response of about 1 hertz or less without online state estimation and prediction models.

- Online ground control required a new consideration of link reliability over and above that applicable in the conventional sense.

- Rf linkages, operating over large bandwidth or high duty cycle, could introduce serious problems in the use of the rf spectrum and possible interference with other users.

- There were unique problems associated with the development and operation of ground terminals for dedicated online control. Many of these problems were quite similar to those encountered by electric utilities dealing with substation design, load distribution and sharing, and maintenance.

- There was the possibility of rf interference (or jamming) that could degrade the command uplink.

EXPERIMENT OBJECTIVES

The baseline objectives of the SAPPSAC experiment were as follows:

a. Extended term 3-axes attitude hold

b. Extended term reliability of command and telemetry links

c. Interchangeability of multiple sensor combinations

d. Point-to-point slew maneuver capability

e. Ability to follow a predetermined ground track

f. Tracking of flight vehicles

g. Ability to maintain attitude during orbit corrections

h. Ability to identify and track program parameters

i. Use as a diagnostic tool to evaluate spacecraft performance

j. Pointing vector alignment capability to a prescribed attitude reference

k. Real-time orbit determination using two interferometer stations and an Earth sensor

l. Ability to maintain attitude control during brief open loop operation.

All of these objectives were successfully demonstrated except (f) and (g) for which there were no tests scheduled. A limited amount of data was available for objective (k) due to the failure of the f_2 channel in the spacecraft interferometer hardware.

SYSTEM DESCRIPTION

Spacecraft

The only additional units required in the spacecraft for this system were a ground attitude control (GAC) deccder and an interface to the actuator control electronics. The GAC characteristics were as follows: (1) Addressed one, two, or three axes at a time; (2) responded to transmission instantaneously; (3) commanded wheels or jets; and (4) commanded length multiples of 11 milliseconds (ms) (jets 100 ms minimum). No modifications were permitted to the spacecraft onboard attitude control system except the interface between the GAC decoder and torquers. The constraint was acceptable for experiment verification, but the GAC/analog backup controller interfacing that would allow freezing attitude control in the event of a ground controller or link failure would provide a more complete operational backup system.

Ground System

Figure 2-1 represents an overview of the ground support equipment for the SAPPSAC Experiment. The inputs to the system were the regular telemetry transmissions from ATS-6. The outputs were the digital commands to the torquers in the spacecraft.

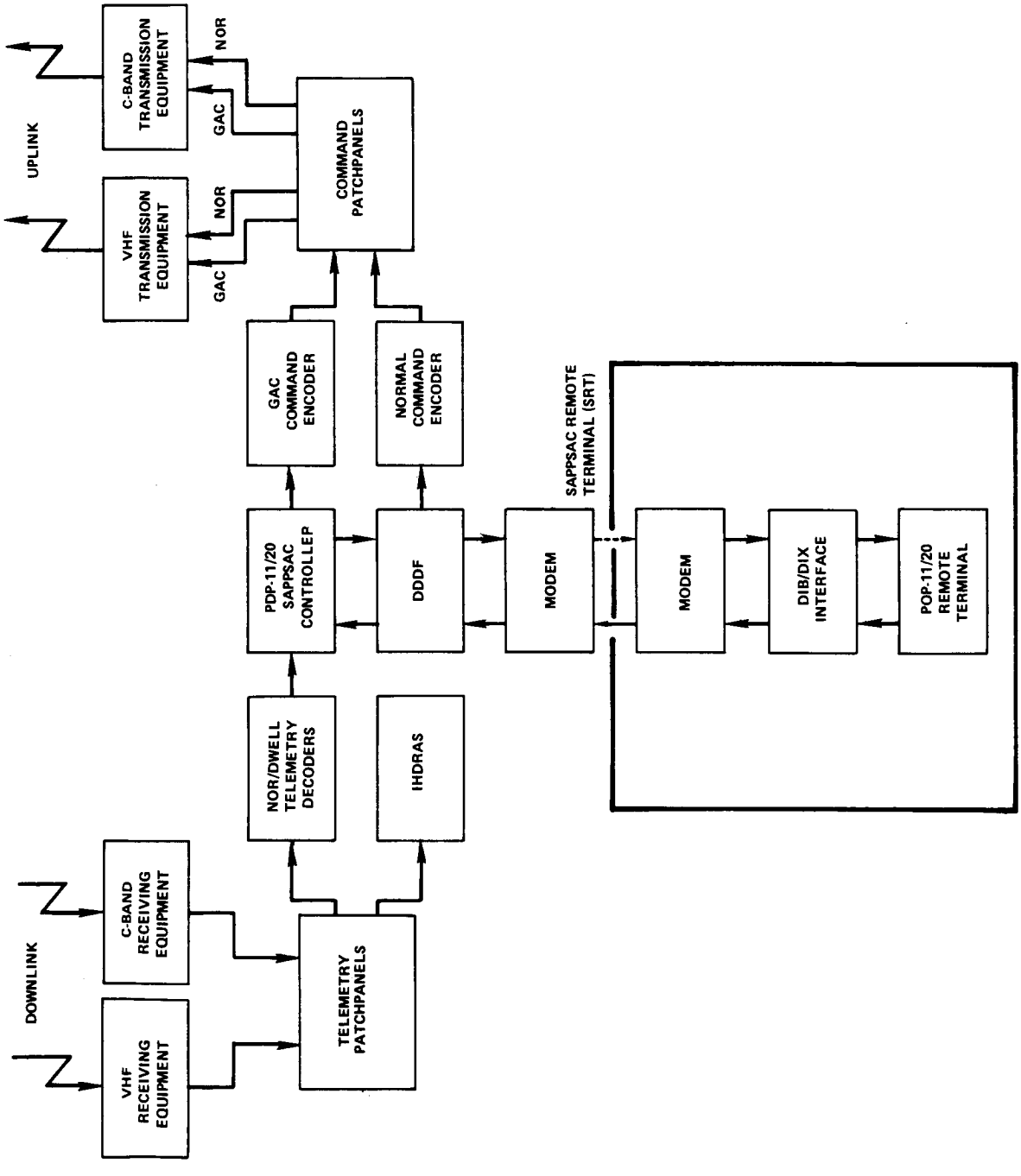

Figure 2-1. Overview of SAPPSAC Ground Support Equipment

The telemetry interfaces permitted simultaneous access to two data streams, normal and dwell. Normal telemetry contained all of the required sensor data needed by SAPPSAC for state measurements and was updated every 3 seconds. Dwell was used solely for GAC command validation. The GAC command encoder transformed torquer combination on/off digital words, obtained from the computer, into a pcm/fsk/am signal that could be patched either to vhf or C-band uplink modulation/transmission equipment. The GAC encoder read a 6-bit digital code from the computer every 10.8 ms, added a 7-bit address, and then transmitted the 13-bit command word to the spacecraft at the rate of 1200 bits per second (bps). The 6-bit digital code (five data bits plus parity) specified the on/off state for each of six different torque directions. The on-time duration was determined by use of the GAC read pulse to down-count one of the computer real-time clocks.

In the vhf configuration, commands used a 2.5-kW (kilowatt) transmitter coupled to the ATS small command antenna and were radiated as pcm/fsk/am/fm to the spacecraft. In the C-band configuration, commands used an 8-kW transmitter coupled to the Rosman II 26-m (meter) parabolic antenna and were radiated as pcm/fsk/am/fm to the spacecraft. The ground station computer used the duplex digital data formatter encoder/decoder equipment for communications with ATS Operations Control Center (ATSOCC). Normal commands were not processed by the SAPPSAC computer, but were either manually loaded at the ground station encoder or transmitted via the modem/duplex digital data formatter interface directly to the normal command encoder where they were checked and then transmitted to the spacecraft. SAPPSAC required normal commands for spacecraft subsystem configuration. The SAPPSAC remote terminal used one of the ATSOCC PDP-11/20 computers to monitor and control the ground station computer using the duplex modem ground lines. The ATSOCC interface between the modem and computer used a data input buffer for incoming transmissions and a data interface transmitter for outgoing transmissions.

SAPPSAC COMPUTER PROGRAM

The purpose of the SAPPSAC program was to issue spacecraft torque commands as computed by one of the available control laws, to monitor its input-output sequences, to guard the safety of the spacecraft, and to record sufficient information for postflight analysis. The program was a sequence of Fortran IV subroutines, collectively known as the main sequential program, (MASEP), invoked by a real-time executive (SAPSEX). SAPSEX therefore was the real-time interrupt linkage to MASEP, and all nonreal-time portions.

The following overall assumptions defined the program philosophy: (1) The SAPPSAC program would run synchronously; (2) SAPPSAC computations would be performed at the ground station within the interval of two telemetry minor frames decreased by uplink and downlink delays; (3) torquer pulses would be initiated on the spacecraft at the time of the spacecraft frame synchronization pulse. Pulses could be terminated at any time; (4) Kalman filter techniques would be used to compute state estimates; (5) all sensor information was taken at one time instant, TS seconds (Figure 2-2) from frame synchronization generation; (6) maximum use of Fortran IV was required for software development.

Timing of the program and synchronization with events on the spacecraft were the heart of the SAPPSAC concept. The basic sequence of events is shown in Figure 2-2. All timing was locked to

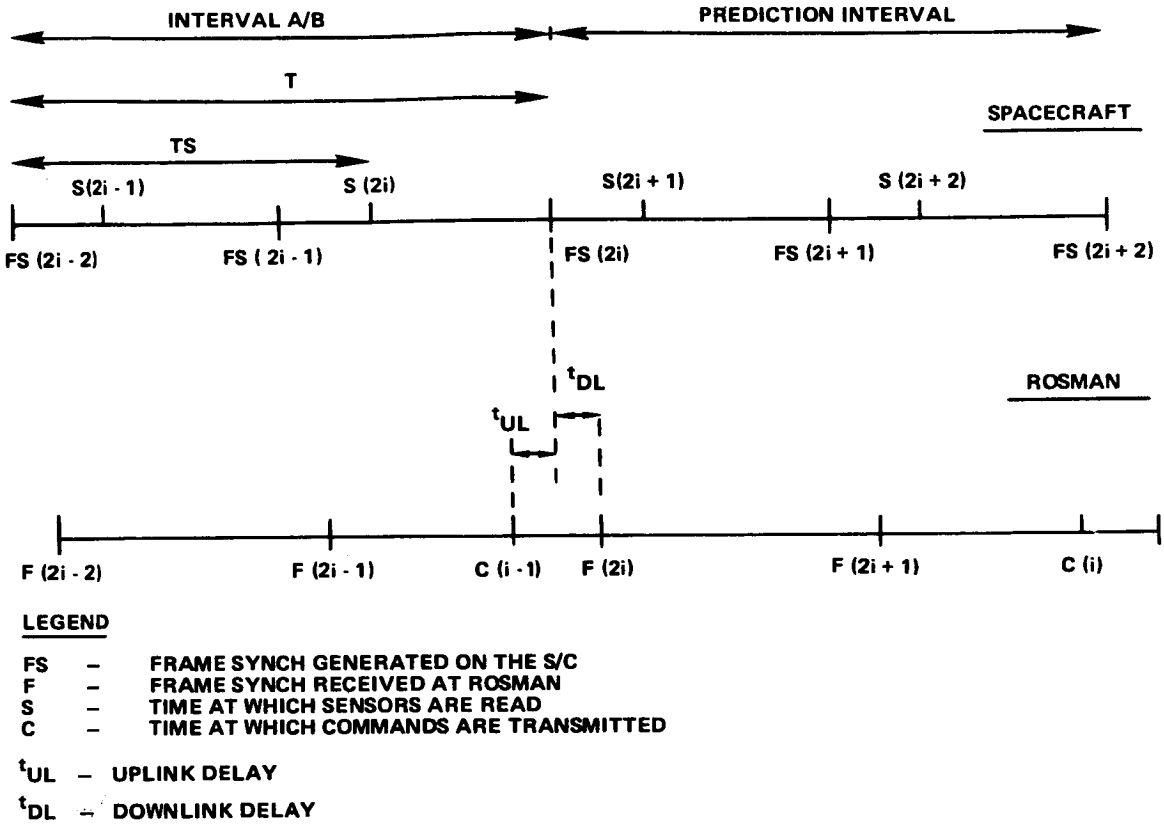

Figure 2-2. SAPPSAC Timing Diagram

the telemetry stream by means of an interrupt generated when the normal telemetry synch code was detected. Time-out was provided by the internal executive clock if an interrupt was not received within a period of seconds of its expected occurrence.

The program consisted of 17 specific operations starting with a quality check of the received telemetry signal. A mathematical model was used in the program to estimate the required action of the torquers for a 6-second update to produce the desired spacecraft state. The model included wheel speeds, a jet firing history for each jet, adaptive multipliers for the nine torquers (jets and wheels), and the spacecraft rotational dynamics.

TEST RESULTS

Introduction

Nine of the original 12 experiment objectives were successfully demonstrated during the test program. No testing was performed to assess the reaction jet attitude control capability of SAPPSAC because of constraints imposed in conserving onboard propellant.

The SAPPSAC experiment successfully completed support of the in-orbit operations for ATS-6 during the first 30 days following launch. The effort included online attitude determination at the Rosman Ground Station using the SAPPSAC PDP-11 computer during the first 5 days of checkout in orbit. This was followed by subsequent offline data analysis at Goddard Space Flight Center pertaining to preliminary attitude sensor evaluation and interferometer bias determination. The following onboard sensors were evaluated: Yaw inertial reference unit, Earth sensor, Polaris sensor, and interferometer. Online attitude determination using the Earth sensor and interferometer successfully tracked the yaw reference maneuver (roll, pitch, and yaw attitudes). Both single-station and two-station interferometer tests were performed with the Earth sensor and near-local vertical conditions. Using the Earth sensor/F1 interferometer, Earth sensor/F2 interferometer, and F1/F2 interferometer, it was found that the 3-axis attitude determination performed were in agreement to within 0.02 degree in roll, 0.06 degree in pitch, and 0.6 degree in yaw using zero bias corrections (preflight reference for SAPPSAC).

Extended Term Three-Axes Attitude Hold

SAPPSAC demonstrated the ability to hold yaw attitude to within 0.2 degree of reference throughout the tachometer dropout region (near-zero speed regime for the inertia wheels). Control used the F1 interferometer and Polaris sensors in a 30-second update. Disturbance acceleration gains were zeroed through the dropout interval and then reactivated once stable attitude was regained. This performance is significant because the yaw axis produced the largest excursions of attitude due to the tachometer dropout condition. Excursions of attitude for a given control update are inversely proportional to the moment of inertia in each axis. The smallest inertias (yaw axis), for example, will produce about twice the attitude excursion of the roll axis. Therefore, one could expect roll-attitude excursions of about 0.1 degree for the same control interval. It was found that stabilization performance for the 30-second control update was nearly the same as found during hold-mode performance using a 48-second update.

The longest single online attitude hold test lasted approximately 8 hours. With the exception of slight attitude excursions, when the wheel speeds went through zero, a high degree of attitude stabilization was demonstrated. The attitude excursions were held to 0.004 degree in pitch and roll, and 0.016 degree in yaw during a 43-minute segment of this 8 hours. For short durations of time (i.e., 5 minutes), very precise attitude stabilization was obtained; 0.002 degree in roll and pitch. This was limited primarily by available sensor characteristics (quantization and noise) and pulse modulator behavior and not by the command link response capability.

Extended Term Reliability of Command/Telemetry Links

During the test period, 50 hours of operation was logged using the ground attitude control command link at either vhf or C-band frequencies. In this period, the links exhibited excellent reliability because there were no detected dropouts or inhibit conditions, even during intervals of station microwave interference. More than 100 hours of telemetry data were logged by SAPPSAC where the data reliability was found to be excellent. There were only very occasional noise bursts that had no degrading effect upon operation of the ground controller.

Point-to-Point Slew Maneuver Capability

Several small angle slew tests were performed. Performance was 10 percent better than predictions. Overshoots in latitude and longitude were generally less than 3 percent of the slewing distance.

In initial tests, SAPPSAC successfully demonstrated slewing capability in the vicinity of the local vertical. Eight small angle maneuvers were conducted (1 degree in both pitch and roll angles), followed by individual larger slews of 2 degrees and then 4 degrees. Each maneuver had specified pierce-point coordinates (Z body axis/Earth intercept) and maximum body rate limits as commanded by the SAPPSAC computer input. A final slew to local vertical was followed by activation of an adaptive feature of the state estimator, which performs identification of unmodeled disturbance torques on each of the three body axes. The adaptive estimator functioned in an excellent manner, as evidenced by slight changes in spacecraft pointing that rapidly converged to within 0.02 degree latitude and longitude of subsatellite coordinates obtained from orbit ephemerides. All slewing maneuvers were performed using a 3.5-minute control update, and it was found in all cases that no more than three updates were needed to complete a slew. Maximum latitude overshoot was less than 0.3 degree, which was equivalent to approximately 0.05 degree in roll angle. Maximum longitude overshoot reached values as high as 0.8 degree that was equivalent to approximately 0.13 degree in pitch angle. It was observed that all easterly slews generated longitudinal undershoots, whereas all westerly slews generated longitudinal overshoots. This was attributed to the presence of unmodeled disturbance torques acting in the pitch axis, since the adaptive estimator had not yet been activated.

In later tests, ground control employed a vhf ground attitude control unplink at 154 MHz. The F1 interferometer channel was operational using the 25.9-m (85-foot) Rosman antenna to provide attitude sensing capability and as a backup at C-band in the event of vhf link problems. At the conclusion of an initial local vertical hold, the first slew maneuver started with repositioning of the +Z body axis to ground intercept points of +12 degrees (north) latitude and -82 degrees (west) longitude. Following a brief hold interval at these coordinates, the spacecraft was commanded through a slew to -12 degrees (south) latitude and -106 degrees (west) longitude. Following a third hold mode interval, a slew was performed back to +12 degrees latitude, -82 degrees longitude. After a fourth hold mode interval, a final slew was commanded back to local vertical, whereupon hold mode was maintained until the test was terminated.

The adaptive disturbances acceleration option was activated during these maneuvers to establish what effect, if any, this would have upon slew behavior. It was found that the addition of the derived disturbance torques had little influence upon the slew trajectories, other than to eliminate any undershoot offsets in final targets. Maximum overshoot occurred in the largest slew maneuver and produced 0.383 degree latitude and 1.22 degrees longitude values. The bearing angle was held at all times to better than 0.35 degree from north. It was determined that a longer settling time was required when disturbances were derived rather than fixed between slews. This was attributed to the significant lag in identification of disturbance levels during a slew maneuver. In one of the maneuvers, the maximum rate retention level was increased. As one would expect, this improved the behavior because the finite-settling time control algorithm was based upon zeroing of errors in two control updates. A comparison of sensed versus filter attitude indicated that the SAPPSAC state

estimator was tracking actual deterministic attitude to better than 0.01 degree. In the hold mode intervals, attitude errors were being driven close to zero as the disturbance levels settled out. Local-vertical piercepoint values agreed well with those taken from the ATS-6 ephemeris predicts. There was less than 0.02 degree error in both latitude and longitude.

Ability to Follow a Predetermined Ground Track and Large Angle Slew Capability

Two ground track maneuvers and a large angle slew maneuver were performed by SAPPSAC. The two prescribed ground tracks were from near-local vertical to the Rosman Ground Station and from Rosman to the Mojave Ground Station. The large slew occurred between Mojave and local vertical. Figure 2-3 shows the above tracks and slew maneuvers. A roll maneuver was required for a change in latitude and a pitch maneuver was required for a change in longitude.

The first ground track was performed using the Earth sensor/Polaris sensor combination. The maximum latitude or longitude deviation from the prescribed, time-tagged ground track (ignoring the initial and final 2-minute periods) was approximately 0.14 degree (0.024 degree roll or pitch). The reason for ignoring the initial and final 2-minute intervals is that the control interval (2-minute length) and the time-tagged target table are not synchronized and hence there can be an initial lag and another lag at the end. It should be noted that a time-tagged target table is essentially a satellite track. If the time tagging is ignored, the tracking errors are slightly less and there is no large error at the beginning and the end since these were due primarily to timing idiosyncrasies.

While pointing at Rosman, the sensor combination was changed to interferometer (F1)/Polaris sensor. For a 16-minute period, while holding at Rosman, the latitude (roll) excursions were within a deadband of 0.051 degree (0.008 degree) and longitude (pitch) within 0.163 degree (0.23 degree). During the track to Mojave, the maximum latitude or longitude errors from the prescribed, time-tagged ground track were 0.15 degree (0.22 degree in roll or pitch). While holding at Mojave, the latitude excursions were within a deadband of 0.013 degree (0.0019 degree) and longitude within 0.017 degree (0.0025 degree) for a period of approximately 8 minutes. The pointing error from Mojave for this period was (+0.007 degree minimum, +0.017 degree maximum) in latitude and (+0.111 degree minimum, +0.128 degree maximum) in longitude. The large angle slew back to local vertical was performed nominally with overshoots of 1.24 degrees in longitude and 0.45 degree in latitude. During the slew, the estimator tracked the sensor in roll with a maximum error of 0.055 degree.

The above-ground track tests demonstrated the capability of time synchronization of SAPPSAC as required for satellite tracking and ground track pattern generation at prescribed maneuver rates.

Interchangeability of Multiple Sensor Combinations

During online control operations, SAPPSAC used three sensors: the Earth sensor, the Polaris tracker, and the two-frequency interferometer. From these sensors there were six combinations that yielded pitch, roll, and yaw. All combinations were successfully employed by SAPPSAC. In one test, the excursions in pitch, roll, and yaw were held within 0.020 degree, 0.006 degree, and 0.15 degree, respectively, while changing between these sensors.

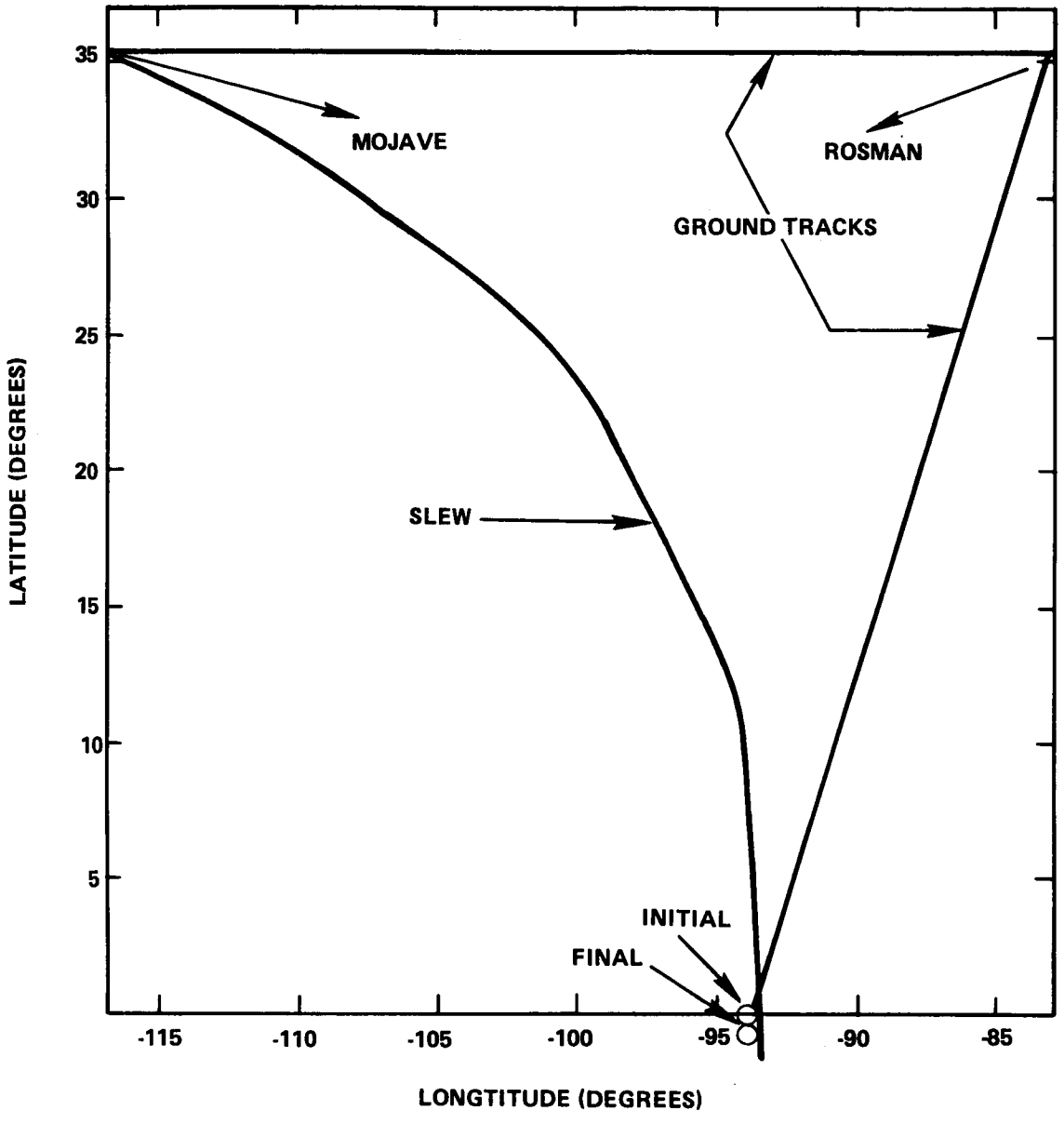

Figure 2-3. Latitude vs. Longitude for Slew and Ground Track Tests

A simulated disturbance was introduced into the system to determine the ability of the system to sense the disturbance and switch to an alternate sensor. While operating with the F1 interferometer and Polaris sensor control inputs, the SAPPSAC controller was commanded into the alternate sensor select mode. A brief power outage was deliberately introduced into the Rosman C-band interferometer uplink transmitter. The screening function immediately recognized unusable F1 data and switched control to the next level which was the Earth sensor/Polaris sensor combination. This was verified with the output displays. There was no noticeable perturbation in attitude control. The power was then reapplied to the transmitter and screening again recognized good interferometer data. This caused control to be switched back again to the F1 interferometer/Polaris sensor combination.

In the other tests using the Polaris sensor/interferometer combination, it was found that with a 10-frame control update, SAPPSAC could achieve stabilization to within 0.02 degree latitude and longitude of reference intercept coordinates 35.200 degrees latitude and -82.9 degrees longitude. This produced short-term pitch and roll angle stabilization better than 0.003 degree. When controlling with the Earth sensor/F1 interferometer, it was found that an initial yaw bias of approximately 0.1 degree was introduced. Further, greater noise was experienced in the yaw axis due to magnification of Earth sensor noise when used to compute yaw. Stabilization in pitch and roll was found to be similar to that obtained when using the Polaris sensor/F1 interferometer, wheras yaw errors reached 0.05 degree. Because the interferometer F2 channel was not operational during this test, SAPPSAC was unable to evaluate the remaining sensor combinations.

Spacecraft Performance Evaluation and Ability to Identify and Track Program Parameters

SAPPSAC demonstrated the ability to identify and track several disturbances acting upon ATS-6. Modeled parameters included torquer characteristics for the momentum wheels, intertial cross coupling of body rates, gyroscopic cross coupling, and the effect of gravity gradient torques. Unmodeled disturbance accelerations were tracked for continuous intervals as long as 7 hours and subsequent analysis isolated contributing effects from wheel rundown torques and solar radiation torques (inferred). During a 46-minute open-loop test, attitude error buildup indicated torque identification errors to be less than 2 percent.

The excellent ability of SAPPSAC to accurately track the state during open-loop tests is shown in Figure 2-4. The data shows the unmodeled disturbance accelerations identified by the filter during a SAPPSAC test. The approximate steady-state disturbance torques corresponded to 2.71×10^{-4}, -5.06×10^{-4}, and 0.04×10^{-4} N·m (2.00×10^{-4}, -3.73×10^{-4}, and 0.03×10^{-4} ft/lb) for roll, pitch and yaw, respectively. SAPPSAC was able to both identify and operate during various anomalies, including Polaris "hits" (tracking foreign objects), interferometer transients (ground transmitter power surges, erratic behavior of F2 before failure and when the beacon was on a sidelobe), telemetry dropouts, and excessive yaw-wheel rundown.

Pointing Vector Alignment Capability to a Prescribed Attitude Reference

The degree of stabilization of the pitch, yaw, and roll axes depends on the accuracy and stability of the control functions which are a function of time. In one test that lasted 4½ hours, stabilization of pitch and roll was maintained to better than 0.005 degree for more than 25 minutes with the F1

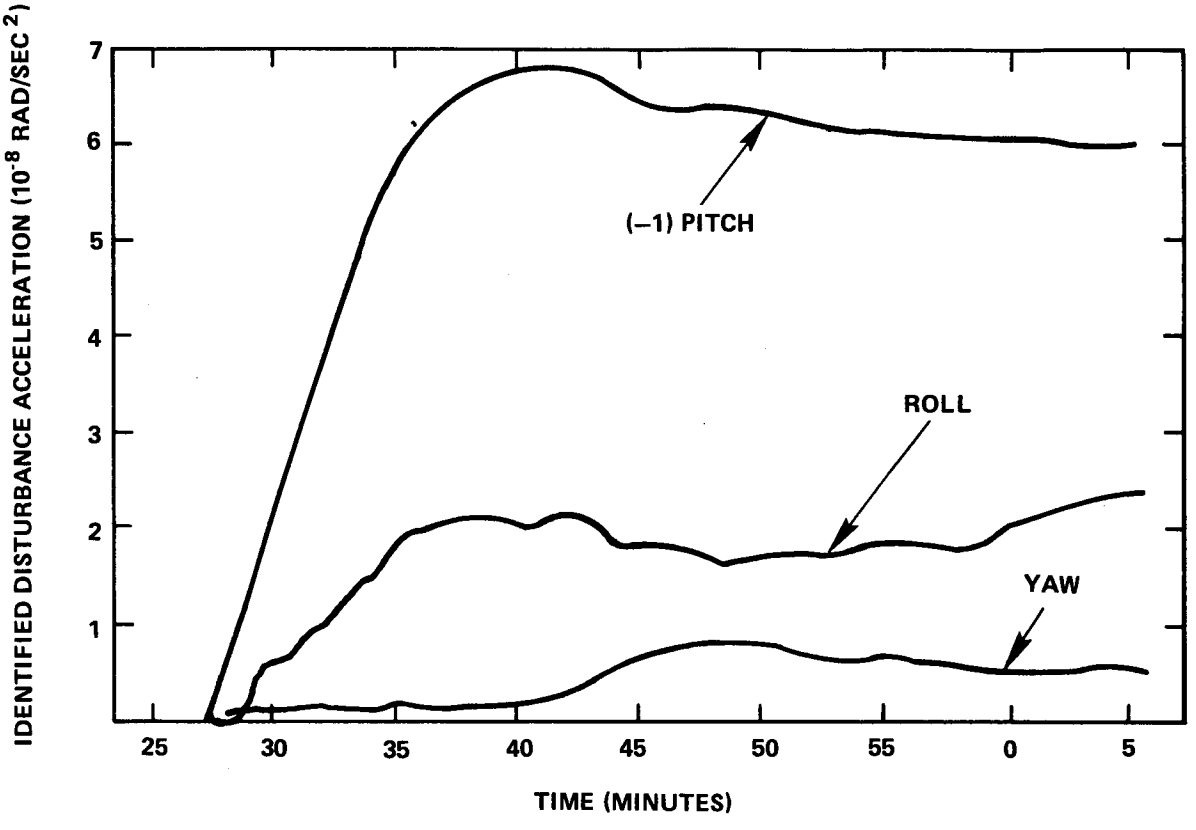

Figure 2-4. Disturbance Acceleration Identified by SAPPSAC Filter vs. Time

interferometer and the Polaris sensor in control. Pointing vector alignment with respect to Rosman intercept coordinates indicated a hold to within 0.01 degree throughout this interval. In another test, SAPPSAC stabilized the spacecraft Z-axis to within 0.007 degree pitch and roll for a period of 43 minutes.

In a particular test, it was determined that SAPPSAC could maintain a local vertical pointing mode for 2 hours. During this time, the following sensor combinations were briefly selected for control computations; Earth sensor/Polaris sensor, Earth sensor/Rosman interferometer (F1), Rosman interferometer (F1)/Mojave interferometer (F2), and Rosman interferometer (F1)/Polaris sensor. Attitude pointing behavior was found to be stable and nominal for all sensor combinations except Earth sensor/Rosman interferometer (F1), which exhibited a relative yaw bias. This behavior was found to be in agreement with previous SAPPSAC launch support data that indicated that one should expect a relative yaw bias of about 0.25 degree. It was demonstrated that SAPPSAC could hold the spacecraft Z-body axis to within 0.04 degree roll and 0.05 degree pitch of local vertical, while maintaining bearing within 0.25 degree of north. Attitude excursions peak-to-peak during the same intervals were 0.02 degree roll, 0.04 degree pitch, and 0.07 degree yaw. This performance was obtained with a control update interval of 1½ minutes which can be decreased to obtain tighter control. During this test SAPPSAC also demonstrated the ability to return to local vertical following a short drift period to introduce attitude errors.

Real-Time Orbit Determination Using Two Interferometer Stations and Earth Sensor

Very limited data was obtained for the orbit determination objective due to the failure of the F2 channel and the spacecraft interferometer hardware. The data that were available consisted of simultaneous telemetry from the Earth sensor and two-station interferometer that was used in a SAPPSAC algorithm to determine spacecraft orbital position as a function of time. These data were compared with a ranged orbit ephemeris near epoch for an interval of approximately 2 minutes. The following results were obtained:

Longitude position error	=	-2.4 km
Latitude position error	=	-0.8 km
Radial position error	=	0.4 km

The short span of data reduced gave a 70 percent confidence that the means were within 9 km in longitude and latitude and 2 km radially. Much more data would have been required to determine the stability of the interferometer biases and their effect on orbit determination.

Ability to Maintain Attitude Control During Brief Open-Loop Periods

During the course of the experimental test period, SAPPSAC operated without difficulty throughout several periods of sensor anomaly (Polaris hits and interferometer ground transmitter transients). In one reliability test, SAPPSAC operated in a mode that removed telemetry inputs from the control computation for a period of about 45 minutes. This simulated a condition where telemetry was lost and control was maintained with predictions from the state model. It was found that attitude errors grew to less than 0.5 degree in roll, 0.1 degree in pitch, and 0.4 degree in yaw. These changes posed no problem in loss of sensor acquisitions and therefore demonstrated that SAPPSAC can operate on its stored math model without telemetry for a duration of more than 1 hour. This should permit adequate time to reconfigure ground equipment to restore spacecraft telemetry. Previous tests had shown that without SAPPSAC ground attitude control commands, e.g., pure open-loop, control could not be maintained for more than 15 minutes without danger of losing the Polaris or Earth sensor acquisition.

CONCLUSIONS AND RECOMMENDATIONS

The overall objective of the SAPPSAC experiment was to evaluate the feasibility of a real-time, computer-controlled ground system for long term attitude control and orbit determination of a geosynchronous spacecraft through an rf command and telemetry link. The objective was fulfilled by a demonstration of the following capabilities:

- Feedback Control

  SAPPSAC demonstrated that link transport delays did not significantly affect control capability for ATS-6. This was a result of the ability to accurately model plant dynamics,

predict ahead in time to the point of application of control, and meter out a precise torque on-time using the ground attitude control command uplink.

- Reliability

  The command link was operated in both the vhf and C-band modes for approximately 50 hours with no errors detected.

  The vhf telemetry link was operated for approximately 100 hours. Occasional drop-outs were observed, but these had little effect on control.

  SAPPSAC accumulated a total of approximately 30 hours online control with no significant anomalies.

- Holding

  An extended term attitude hold of approximately 8 hours was performed successfully.

  Attitude excursions over a 43-minute interval were held to 0.004 degree in pitch and roll, and 0.016 degree in yaw.

  Attitude excursions over short durations of time; e.g., 5 minutes, were held to 0.002 degree in pitch and roll.

- Pointing

  Using the existing sensor calibration, SAPPSAC stabilized the spacecraft Z-axis for 43 minutes to within 0.007 degree in pitch and roll relative to prescribed Rosman coordinates.

- Slewing

  Several small angle slews and one large angle slew (from Mojave to local vertical) were successfully performed.

  Overshoots in longitude and latitude were generally less than 3 percent of the slew distance.

- Tracking

  Reference, time-tagged ground tracks were followed by SAPPSAC with errors less than 0.15 degree in latitude and longitude.

- Identification

  Excellent identification and tracking of solar and wheel rundown torques were demonstrated during a 46-minute open-loop test. Attitude error buildup indicated torque identification errors to be less than 2 percent.

- Diagnostic Tool

  SAPPSAC was able to identify telemetry dropouts, Polaris "hits" (tracking of foreign objects), interferometer transients (ground transmitter power surges, erratic behavior of f_2 prior to failure and when the beacon was on a sidelobe), and excessive yaw-wheel run-down.

- Interchangeability of Sensors

  Online switching between the six available sensor combinations was performed while maintaining precision control in pitch and roll.

- Orbit Determination

  In offline evaluation, the Earth sensor/two-beacon interferometer sensor combination was used to determine the ATS-6 orbit with a 70 percent confidence of about 9 km in the latitude and longitude components and 2 km radially.

CHAPTER 3

RF INTERFEROMETER EXPERIMENT

INTRODUCTION

The radio frequency (rf) interferometer experiment had the capability of providing a precision measurement of the three-axis attitude of ATS-6 with a wide field of view of 35 degrees. The basic function of the interferometer in the spacecraft was to measure the phase difference of either one or both of two C-band carriers transmitted from separated ground stations and received by two antenna arrays whose orthogonal baselines were parallel to the spacecraft pitch and roll axis.

The resulting analog-phase data were converted into a digital format that was transmitted by the interferometer high-speed data link to the Rosman ground station by downlink telemetry. These data were also supplied to the onboard digital operations controller that converted the data into spacecraft attitude information. For a known single uplink ground station signal, the antenna array provided phase measurements that were converted into spacecraft pitch and roll attitudes. Two known separated ground station carriers were necessary to provide phase information for determining the attitudes of all three axes of the spacecraft. Three-axis attitude could also be determined by employing a single ground station carrier for establishing the pitch and roll angles, and the Polaris tracker or Earth sensor for determining the yaw axis.

By employing two separated uplink ground station signals in conjunction with the Earth sensor data, the spacecraft orbit position and its three-axis attitude were determined. With three known separated uplink ground station signals, one of which was time multiplexed with either frequency channel, the orbit position and the three-axis attitude could also be established. An overall system functional block diagram of the spacecraft and ground stations is presented in Figure 3-1.

The primary objectives in performing the ATS-6 interferometer experiments were as follows:

- Evaluation of spacecraft link performance and its two-axis attitude determination when unmodulated carriers are employed
- Evaluation of phase measurement and attitude performance for narrowband and wideband carrier modulation
- Evaluation of performance for online spacecraft position determination, using a two-frequency interferometer and Earth sensor

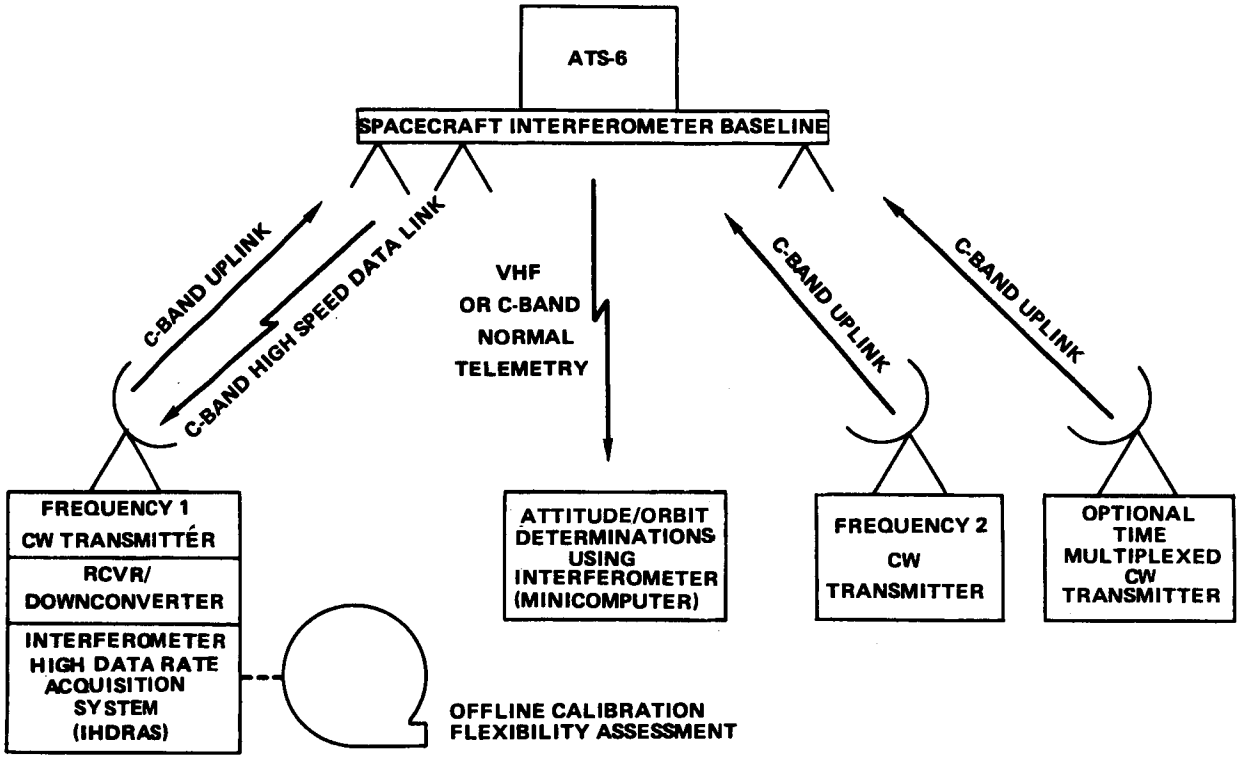

Figure 3-1. Interferometer Experiment Configuration

The two ground stations that provided the uplink transmission channels at frequencies of 6.150 gigahertz (GHz) and 6.155 GHz were Rosman (North Carolina) and Mojave (near Barstow, California) respectively. Unambiguous space angles of up to approximately +17.5 degrees relative to the boresight of either uplink station signal was measured with the interferometer. The tests used both modulated and unmodulated carriers for the measurement of the attitude of the spacecraft.

SYSTEM DESCRIPTION

Spacecraft Equipment

The phase difference measurement of the received carrier wave, that was performed by the onboard equipment of ATS-6, was accomplished with six horn antennas placed in the Earth-viewing module (EVM) with an arrangement of three antennas along each of two orthogonal baselines that were parallel to the spacecraft pitch and roll axis. A physical layout of the horn antenna configuration in the EVM is shown in Figure 3-2. One horn antenna provided the reference signal (P_r) while the remaining two antennas provided the coarse (P_c) and vernier (P_v) phase measurement.

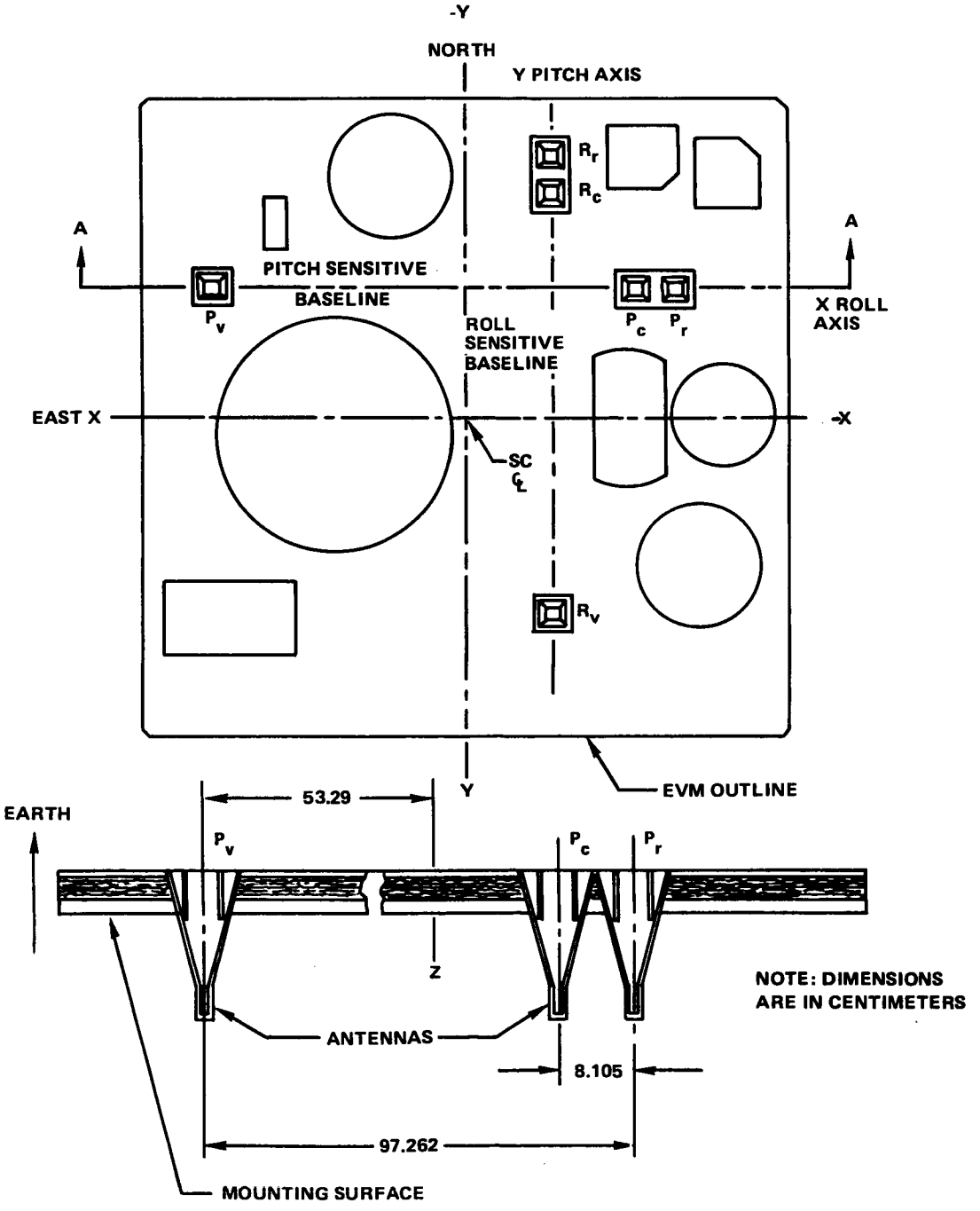

Figure 3-2. Horn Antenna Configuration in the EVM

The coarse baseline had a dimension of 8.105 cm or 1.66 λ (6.150 GHz) and could measure an unambiguous space angle of approximately ±17.5 degrees relative to the boresight of the uplink ground station signal. For the vernier baseline, the dimension was 97.26 centimeters or 19.95 λ (6.150 GHz) and provided a space angle resolution of approximately 0.0014 degree.

The phase measurement of a received signal from a ground station transmitter was accomplished by determining the phase difference or the number of wavelengths between the time of arrival of the incoming wavefront at the reference horn antenna with that at the coarse or vernier horn antenna. This basic method of phase measurement is illustrated in the diagram of Figure 3-3. The actual phase determination was much more complicated with the involvement of the three-axis coordinate system. The interferometer had the capability of simultaneous phase measurement on two frequencies at either baseline that was selected by a switch module with a command signal. A frequency channel could also be received at either antenna baseline by time sharing. A block diagram of the spacecraft interferometer system is presented in Figure 3-4. The switch module enabled the calibration of the receiver frequency dependent phase biases by reversing the two input signals when it was initiated by a calibrate command signal.

The spacecraft employed a dual-channel receiver where one channel was allocated for the reference signal and the other channel received either the coarse or vernier comparison signal. A coupler/switch module provided the time division multiplexing between the coarse and vernier input signals.

Double downconversion was employed by the dual-channel receiver where the first local oscillator of 6.00 GHz provided a nominal intermediate frequency (i.f.) of 150 megahertz (MHz). A dual local oscillator at a frequency of 120 MHz was used for the second mixer which had a nominal i.f. of 30 MHz. The two dual local oscillator outputs were offset 2 kilohertz (kHz) by a signal from the digital converter. The two i.f. output signals were combined and applied to a detector module where the 2-kHz difference frequency was extracted from the reference and comparison signals. A coherent relationship existed between the 2-kHz difference frequencies and the reference signal from the digital converter. For simultaneous reception of two rf signals, a diplexer separated the second i.f. signal into two center frequencies of 27.5 MHz and 32.5 MHz each of which was processed by its corresponding i.f. detector module.

The 2-kHz analog signal was digitized and phase compared in a digital phase comparator with the 2-kHz reference signal obtained from the 4-MHz clock frequency in the digital converter. From this phase information, a phase-count gate was generated that allowed the counting of a number of clock pulses that were proportional to the phase difference between the 2-kHz signals. These pulses constituted the electrical phase measurement and were then applied to an averaging counter.

These data formed a part of a 72-bit main word frame that was transmitted every 3 seconds by the interferometer high speed data link at C-band to the Rosman ground station for processing. The word frame consisted of 8 bits of interferometer status and 64 bits of phase data where each frequency channel included 32 bits of data. Phase-data format for each frequency channel included 5 bits of coarse phase and 11 bits of vernier phase for both the roll and pitch axis.

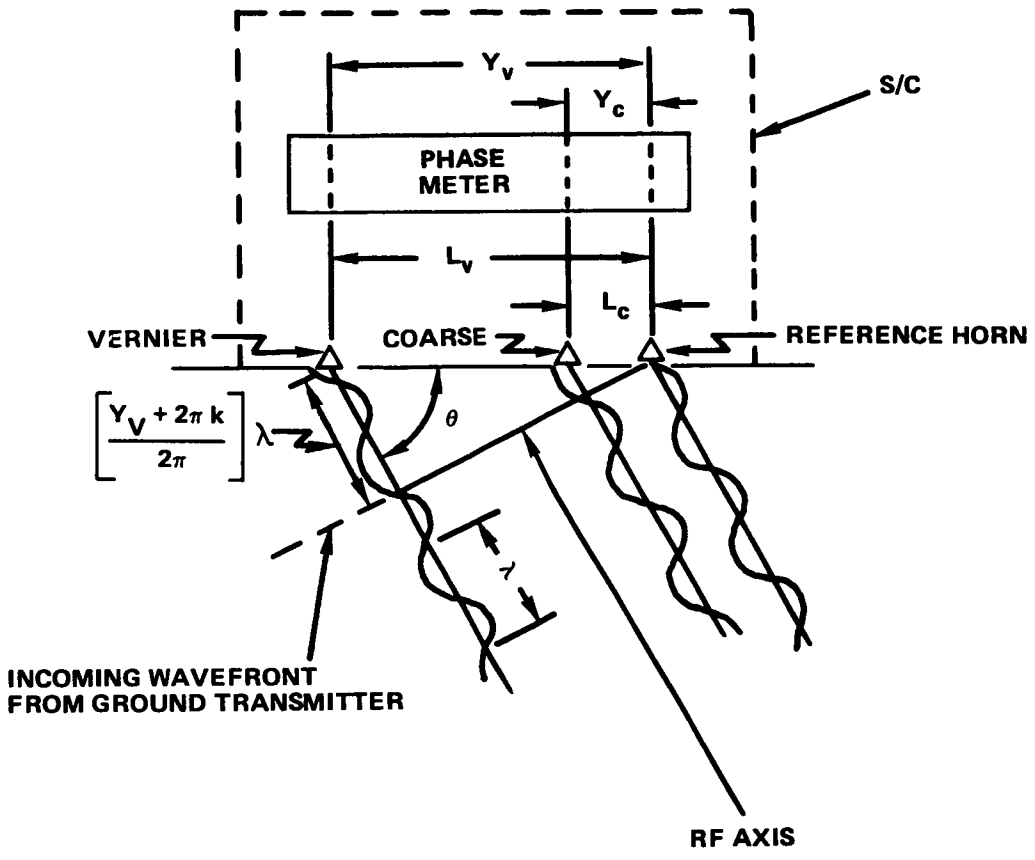

$$Y_V + 2\pi k = 2\pi \left(L_V/\lambda \cos\theta\right)$$

$$k = \frac{1}{2\pi}\left[\left(\frac{L_V}{L_C}\right) Y_C - Y_V\right] (RTNI)$$

$$\cos\theta = \frac{1}{2\pi\left(L_V/\lambda\right)} \left(Y_V + 2\pi k\right)$$

$$\Delta\theta = \frac{-1}{2\pi\left(L_V/\lambda\right)} \frac{\Delta Y_V}{\sin\theta} = \frac{-1}{125} \frac{\Delta Y_V}{\sin\theta}$$

Figure 3-3. Basic Method of Phase Measurement

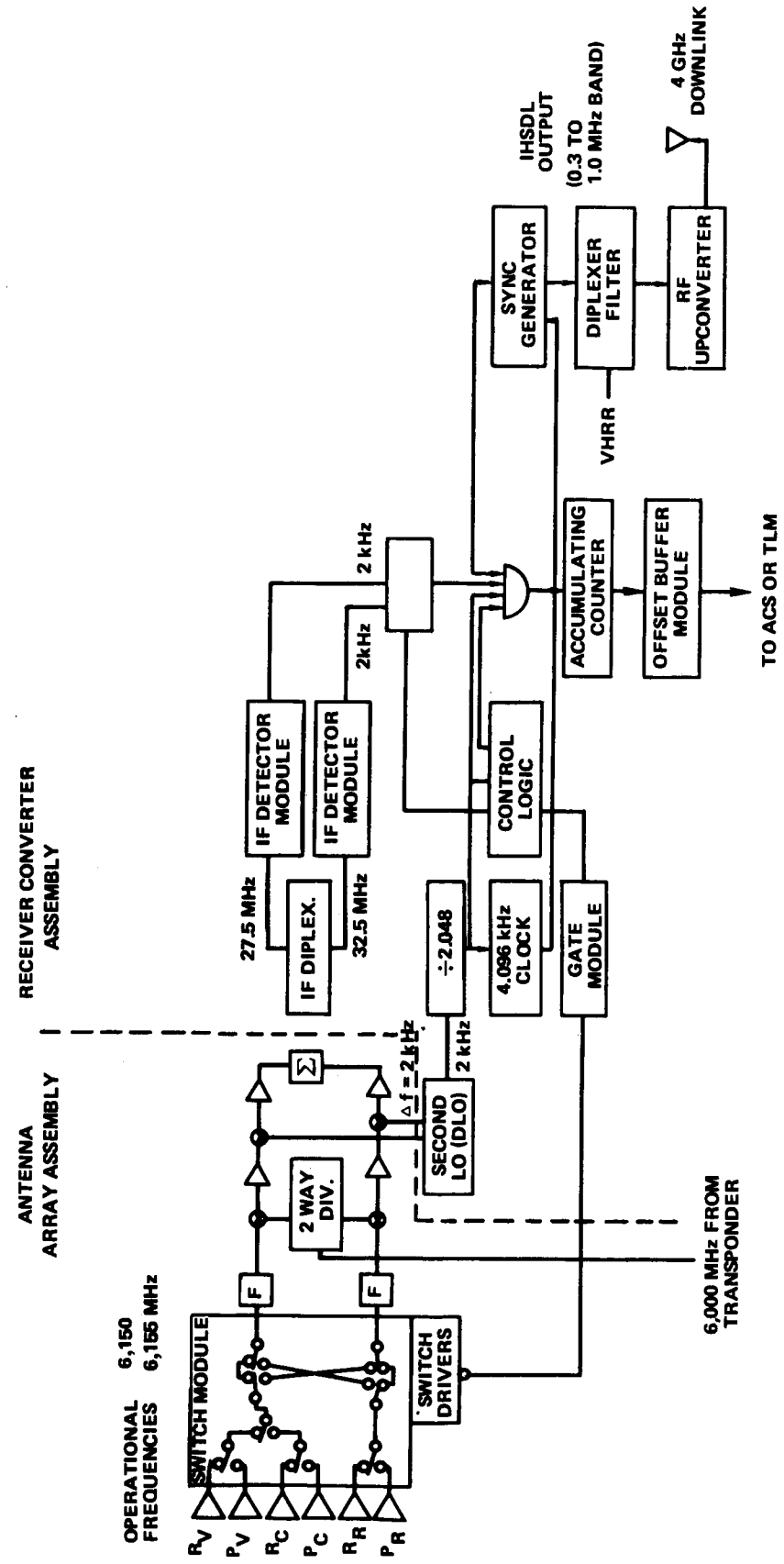

Figure 3-4. Block Diagram of Interferometer Subsystem

The primary ATS-6 interferometer parameters were as follows:

Type of Receiver:	Dual-conversion, dual-channel switched antenna elements
Input Frequency:	6.150 and 6.155 GHz
Noise Figure:	15 dB
Vernier Baseline:	38.292 in. (19.95 λ)
Coarse Baseline:	3.191 in. (1.66 λ)
Configuration:	Crossed baselines
Antenna Gain:	+12 dB
Angle Accuracy (pitch, roll):	0.018° (3σ) over ±12.5° angle range 0.025° (3σ) over ±30° angle range
Antenna Element:	Compensated horn
First I.F./I.F. Bandwidth (BW):	150 MHz/15 MHz
Second I.F./I.F. BW:	(Dual) 32.5 MHz and 27.5 MHz/1 MHz
Output Frequency/BW:	2 kHz/600 Hz
First Local Oscillator Frequency:	6.000 GHz
Second Local Oscillator Frequency:	122.5 and 122.502 MHz
Post-Filter SNR:	+41 dB at +73 dBW ground e.i.r.p.
Vernier Clock Frequency:	1024 kHz
Coarse Clock Frequency:	1024 kHz
Counter Input Rate:	2 kHz
Vernier Averaging:	64 samples
Telemetry Output:	Digital 72 bits/3 sec (1 or 2 sta modes)
Weight:	18.5 lb
Power:	15.5 watts

Ground Station Facilities

The two ground stations that provided the two C-band frequency channels were Rosman (North Carolina) and Mojave (near Barstow, California). At the Rosman station a 26-meter (m) parabolic antenna and a 4.5-m PLACE/interferometer parabolic antenna were employed. The 26-m antenna provided an uplink C-band (6.150 GHz) transmission at a peak power of 8 kW and the 4.5-m antenna provided an uplink peak power of 2 kW. The composite data received by Rosman was processed to extract the 512-kHz interferometer data. This data was time multiplexed with status settings and GMT readings that were then recorded on magnetic tape for subsequent analysis.

The Mojave station used the 12-m antenna and provided an uplink C-band peak power of 8 kW.

A two-frequency interferometer, with orthogonal baselines, established the complete attitude of ATS-6 by first determining the line-of-sight vectors to the transmitting ground stations. With the two line-of-sight vectors known, a set of axes relative to a reference were next determined. From this information the spacecraft attitude was then established.

When the interferometer was used in conjunction with the Earth sensor, which provided a line-of-sight vector to the center of the Earth, the spacecraft position and its attitude was established. The spacecraft, the two ground stations, and the center of the Earth formed a tetrahedron that contained three apex angles at the spacecraft. With the base of the tetrahedron known, the three apex angles at the spacecraft were measured with the two-frequency interferometer/Earth sensor technique. The position of the spacecraft relative to a fixed set of axes on the Earth was then established from this information.

The primary interferometer link parameters for the Rosman ground station were as follows:

Transmitter e.i.r.p. (frequency—6150 MHz)	+73 dBW
Propagation path attenuation	-201 dB
Rainfall absorption	-1 dB
Receiver antenna gain	12 dB
Receiver signal level	-84 dBm
I.f. bandwidth	1.0 MHz
Receiver noise figure	15 dB
Signal-to-noise ratio in i.f.	15 dB
Margin improvement	+3 dB

RESULTS OF TESTS

Essential tests that were first performed consisted of the two-axis phase measurements for both frequency channels with unmodulated carriers. In this test the automatic gain control (AGC) signal levels of the two frequency channels were measured as a function of the e.i.r.p. from each ground station. The Rosman station used the 26-m antenna at an e.i.r.p. of +81 dBW while the Mojave station used the 12-m antenna at an e.i.r.p. of +83 dBW. Results of this test are presented in Figure 3-5 where the measured AGC signal level is plotted against the ground station e.i.r.p. Curves in the graph indicate that a good agreement was obtained at the high e.i.r.p. values with small differences between 2 and 3 dB occurring at the low signal levels. The measured phase values for both frequency channels remained essentially constant over the range of signal levels down to the threshold level of the phase meter. During this test the onboard digital operational control system was maintained in the low-jitter mode and held the spacecraft three-axis attitude excursions to less than 0.05 degree. The measured roll and pitch offset phase angles to the Rosman station boresight, for a closed loop test, were -0.0252 degree and +0.0182 degree respectively for an input-signal level of -96.1 dBm.

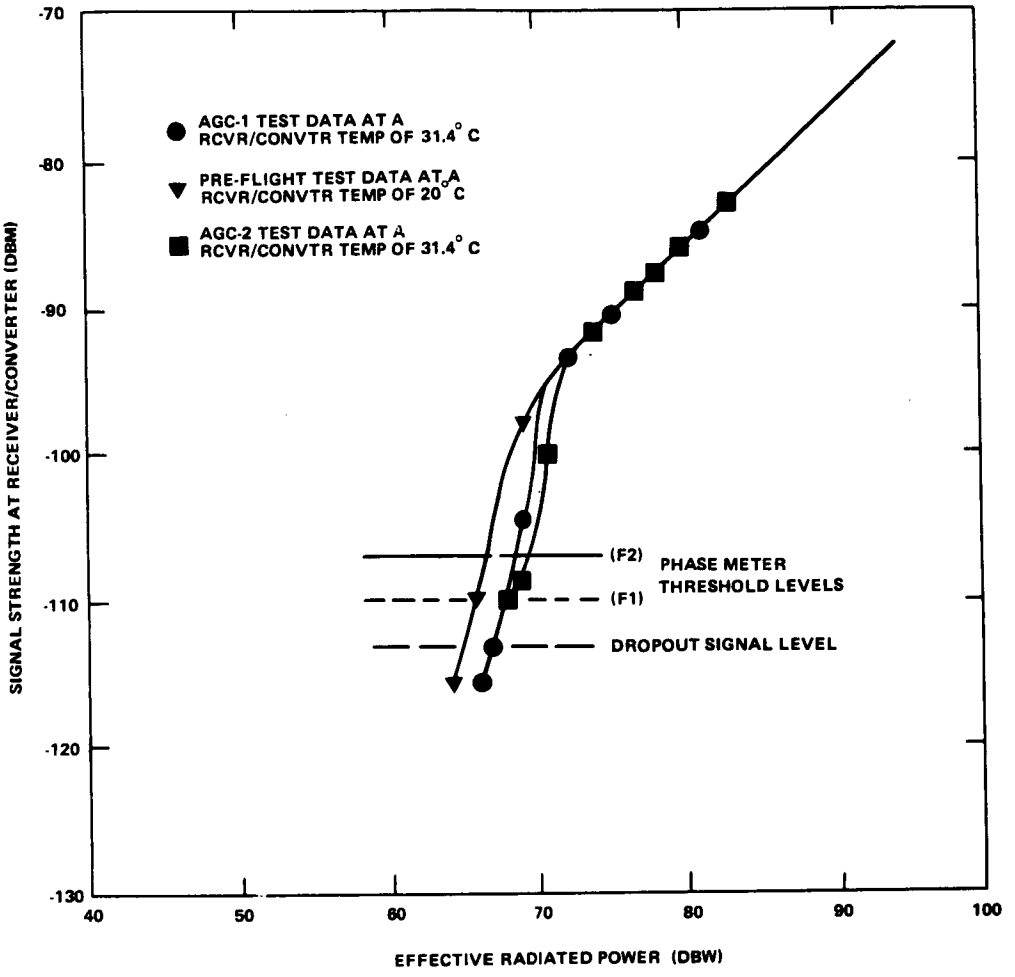

Figure 3-5. Signal Strength Characterization

The next set of tests performed consisted of an fm modulated Rosman carrier using narrowband and wideband signals. For the narrowband test, the ground attitude control command encoder provided digital data at a rate of 1200 bits per second to modulate the Rosman uplink carrier. With an output power of 2 kW and using the 4.5-m antenna, the received signal level from an unmodulated carrier was -94.4 dBm. The presence of digital data modulation had no effect on the accuracy of the spacecraft axis phase measurement nor upon the received signal level. In this test the attitude of the roll and pitch angles were controlled within ±0.015 degree with the interferometer system.

The wideband modulation test was performed with the Rosman carrier using the 26-m antenna that provided an uplink received unmodulated signal level of -73.1 dBm. Fm modulation signals that were used consisted of the Satellite Instructional Television Experiment video and the Health, Education, Telecommunications Experiment video having peak deviations of 6 MHz and 10 MHz respectively. Transmission standards that were employed for transmission of the television video consisted of CCIR type M with a 75 μs pre-emphasis/de-emphasis network. Television standard test patterns and program material were also used in this test. The television signals were relayed back from the spacecraft to Rosman where it was visually monitored for picture quality. This wideband

modulation produced fluctuations as high as -9 dBm in the received uplink signal level. With the interferometer in the closed-loop control mode, the measured attitude of the pitch and roll axis varied within 0.2 degree when the wide angle modulation was used.

In another test the apex angles were determined from the line-of-sight vectors by using the two-frequency interferometer and the Earth sensor. These angles were then compared against the reference angles that were derived from orbit parameters that were established from ranging data. The angle obtained with the two-frequency interferometer agreed to within 0.01 degree of the reference while the two angles measured with the Earth sensor indicated a maximum deviation of 0.06 degree from the reference.

The online spacecraft position was also determined by using the two-frequency interferometer and the Earth sensor. Results of this test indicated that the cross-track and the in-track errors were within 9 kilometers and within a radial error of 2 kilometers for a test period of two minutes. Over an extended period of time it was estimated that the operational position error for this sensor combination would be limited from 80 to 100 km. If three ground station transmitters were employed, the position error could potentially be reduced to less than 10 km.

When the uplink transmitter e.i.r.p. of the ground station was above 72 dBW, the phase-angle measurements of the tests performed were virtually noise free down to the quantization limit where the space angle was approximately 0.0014 degree. The stability in performing the attitude measurements was shown to be 0.002 degree for time periods of 5 minutes and 0.004 degree for periods on the order of 1 hour.

CONCLUSIONS

The ATS-6 interferometer tests proved the system to be a precision attitude sensor having a wide field of view of 35 degrees and providing a space angle resolution of 0.0014 degree. These tests also demonstrated that the stability of phase measurements was 0.002 degree and 0.004 degree for time periods of over 5 minutes and 43 minutes respectively. The test results obtained from online spacecraft position measurements indicated that with the use of three separated ground station transmitters, a position error of 10 km appeared feasible. With the existing equipment capability, it was observed that the substitution of a line-of-sight vector derived from the Earth sensor data in place of one line-of-sight vector proved to be noisy and resulted in excessive position errors. To reduce the errors for this combination of sensor data would have required a modification of the existing interferometer equipment.

The interferometer test results indicated that attitude dependent biases did not require calibration. However, the frequency dependent biases required frequent calibration to minimize the attitude and position errors. Phase-measurement errors caused by system noise was not observed for uplink e.i.r.p. values above 70 dBW.

During the early stages of the test program, one frequency channel (6.155 GHz) of the spacecraft equipment failed and resulted in only preliminary evaluation of the two-ground station interferometer calibration system for diurnal characteristics. The loss of one frequency channel necessitated the use of a single frequency channel by time sharing for the two ground stations to perform the interferometer tests.

Part B
Spacecraft Propulsion

CHAPTER 4

SPACECRAFT PROPULSION SUBSYSTEM

INTRODUCTION

The 16-jet, catalytic hydrazine propulsion subsystem that controlled orbit and attitude motion and absorbed accumulated momentum for ATS-6 for 5 years, was the forerunner of low-thrust, redundant, multitank systems for three-axis stabilized, communications satellites. At the time of its qualification, the subsystem was one of the most complex ever developed. Division into two redundant half systems provided a basic subsystem redundancy with attitude control redundancy in all axes and north-south and east-west stationkeeping. Independent electronic strings for command/control and telemetry/monitoring, provided an end-to-end overall redundancy of propulsive functions. Systems of similar complexity were subsequently used on the Communications Technology Satellite, the RCA Satcom, the (Japanese) Broadcast Experiment Satellite, the Global Positioning Satellite, and the Fleet Communication Satellite. Low-thrust catalytic hydrazine remains the baseline system for three-axis synchronous and lower attitude missions, providing proven technology in competition with electrothermally enhanced hydrazine thrusters and the resurgent bipropellant systems.

The six chapters of this part provide an overview of the ATS-6 propulsion subsystem; its attitude control, momentum unload and orbit transfer requirements; its fluid-mechanical, electrical, command/telemetry, and thermal design; and its power, mass, and fuel budgets. The development, qualification, and acceptance tests that validated the design are described. Details are provided of its in-orbit functional operation, propulsive performance, anomalies, heater and thruster failures, and alternative control procedures that supported experiment operation following failures. Comparisons are made between orbital performance and analytically predicted and ground test demonstrated performance. Based on the comparisons, and the analysis of in-flight anomalies and failures, conclusions are drawn as to necessary design and procedural changes for, and the applicability of, the ATS-6 technology to future satellite and spacecraft programs.

The spacecraft propulsion subsystem was designed and built by Rocket Research Corp., under contract to Fairchild Space and Electronics Company, prime contractor for ATS-6.

FUNCTIONAL REQUIREMENTS

The three-axis stabilized design of ATS-6 required both steady-state and pulse-mode thrusting at a relatively low level of thrust.

Steady-state thrusting was required for orbit correction, east-west stationkeeping, a proposed one-month demonstration of north-south stationkeeping, and two-station reposition maneuvers (to the Indian subcontinent and return).

Pulse-mode operation, using a number of duty cycles, was required for three-axis attitude control, including an initial and subsequent acquisition of reference attitude, attitude stabilization during orbit control thrusting, momentum wheel unloading, and jet-only backup to the three momentum wheels of the attitude control subsystem.

For most of these operations, the spacecraft propulsion subsystem (SPS) was directly controlled by ground command from the Applications Technology Satellite Operations Control Center (ATSOCC). Onboard control by the digital or analog controllers in the attitude control subsystem (ACS) was also used for long-term automatic stabilization during steady-state thrusting, jet-only attitude control, or during the mixed wheel-jet modes introduced to compensate for a partial wheel failure.

The criteria used in selecting the nominal 0.445-Newton (0.1-pound force) thrust level included: short pulse performance, repeatability and life, steady-state performance, reasonable burn and orbital maneuver times, development status, flight experience, and probability of successful schedule and cost performance. At the time ATS-6 was being specified, catalytic hydrazine thrusters at the 22.24-N (5-lbf), 4.448-N (1-lbf), and 0.445-N (0.1-lbf) thrust levels were available from a number of suppliers. The 0.445-N thruster produced by Rocket Research Company was selected because it attained the best score when compared to other designs.

Subsystem and Control Interfaces

The ATS-6 configuration in space with its center-of-mass between the high-gain antenna and the Earth-viewing module (EVM), and the redundant configuration of the SPS led to a fairly complex structural interface between the subsystem and the spacecraft. Two orbit control jet bars, each with a set of yaw and east or west firing thrusters, were mounted at the center-of-mass station on the antenna support truss legs. These assemblies were plumbed to the two-tank feed system centrally located in the EVM. Redundant pairs of thrusters mounted on the east/west and north/south sides of the EVM provided control torques about the roll and pitch axes, respectively.

Figure 4-1 illustrates the location of the orbit control and yaw (or north-south) thrusters in the plane of the center of mass while Figure 4-2 shows one of the centrally located tanks and the roll and pitch pairs on the north and west faces of the EVM.

The propulsion feed system and the eight roll and pitch thrusters were closely coupled to the EVM and did not require heaters or thermal insulation. The orbit control jet thrusters and lines were thermally isolated from the external spacecraft structure, and their temperature was actively controlled with heaters and electronic thermostats. The two figures do not show the multilayer super-insulation blankets that covered the externally mounted thrusters and propellant lines.

Power for the heaters, latching valves and thruster valves, and pressure and temperature sensors was supplied directly from the power subsystem using combinations of its solar panels, batteries and shunt, and charge and boost control elements.

The two remaining subsystem interfaces were with the telemetry and command and the attitude control subsystems. The former provided a direct path from ATSOCC for manual ground control

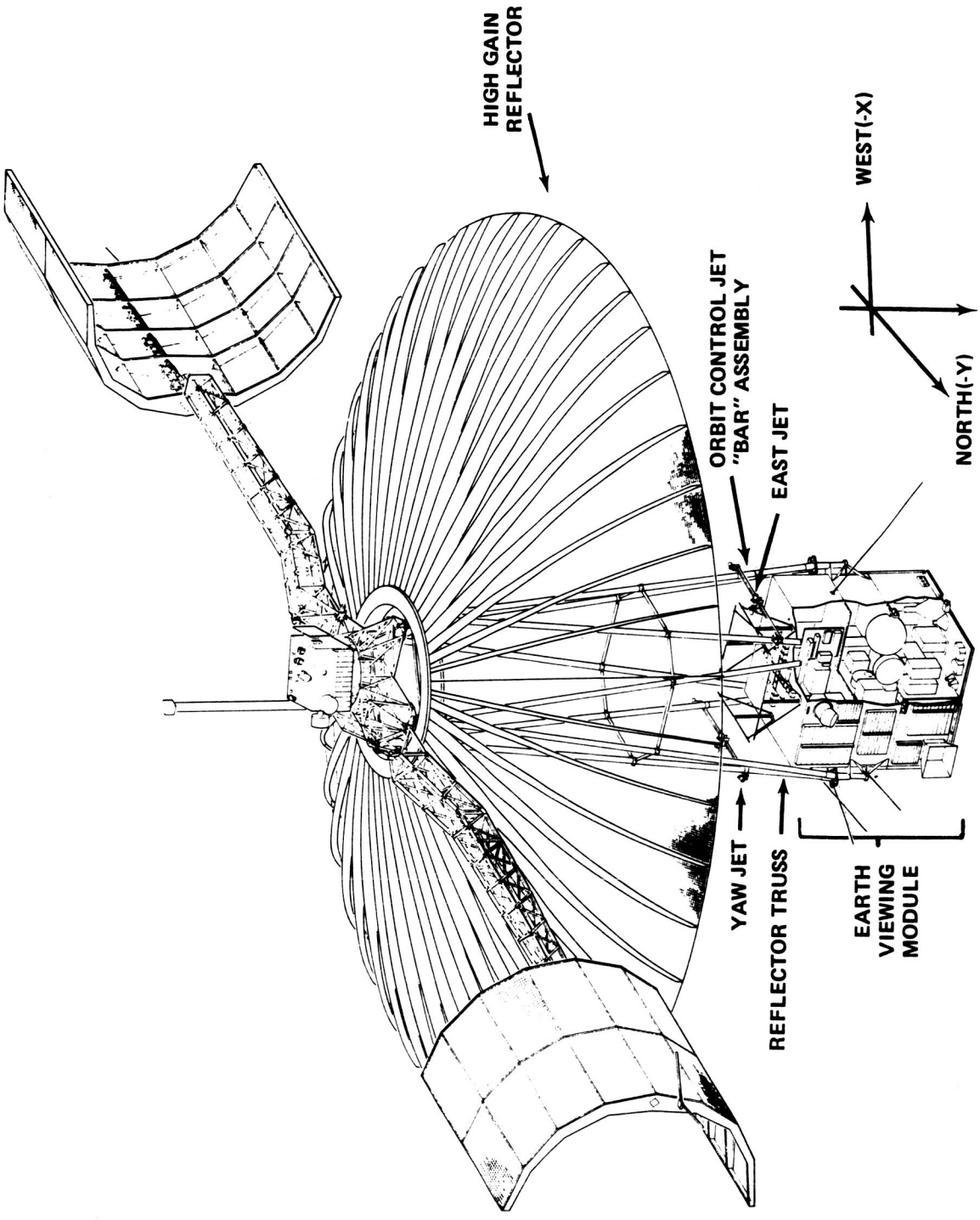

Figure 4-1. External SPS Elements

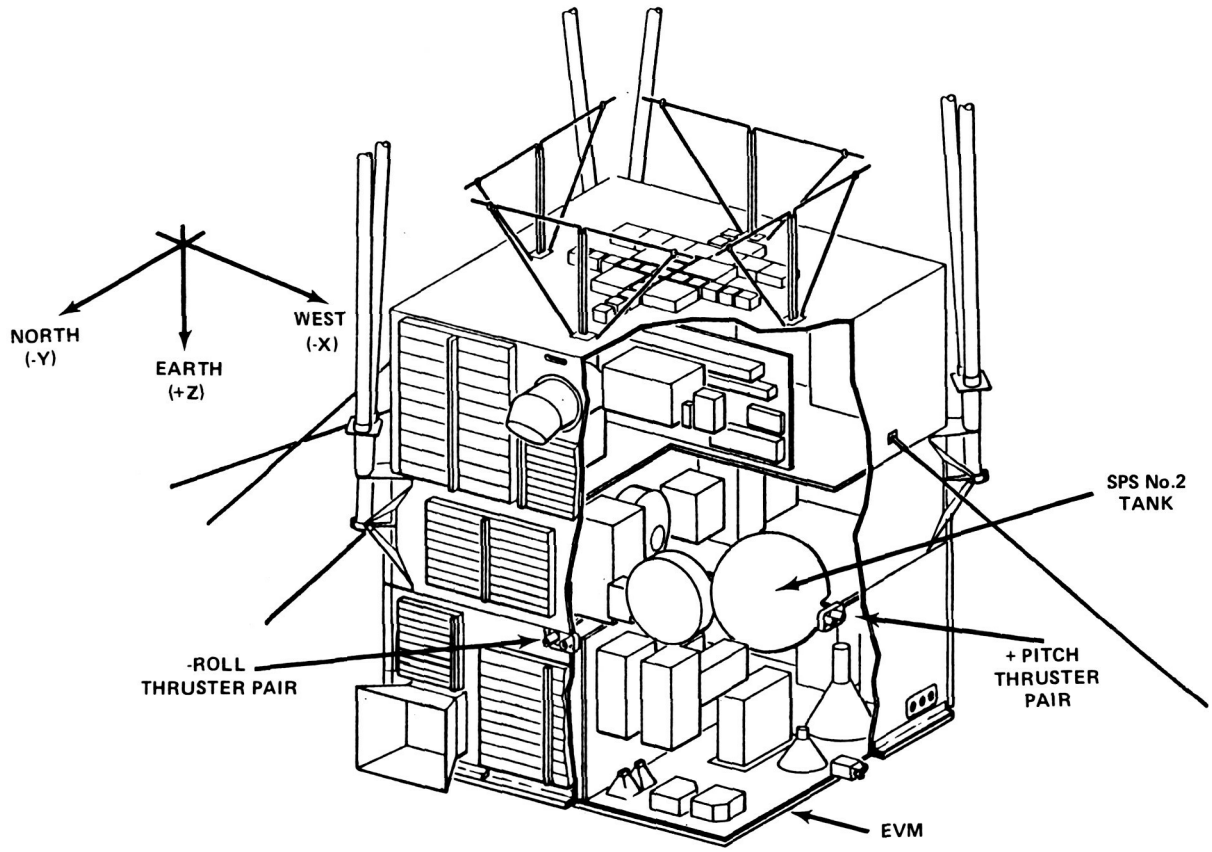

Figure 4-2. SPS Components Internal to EVM

of propulsion functions while the latter provided the critical interface for onboard control of the jets.

PROPULSION REQUIREMENTS

Table 4-1 is the propellant budget established by Fairchild Space and Electronics Company to meet the attitude and orbit control requirements of ATS-6.

Orbit correction requirement was based on 3σ (sigma) + 10 percent inplane injection errors for the Titan launch vehicle. East-west stationkeeping was provided for 1 year each at 94°W and at 35°E plus margin. The station relocation budget assumed 40 days for eastward moves and 120 days for return westward moves, and 14 feet per second were included for a proposed 1-month north-south stationkeeping demonstration.

The budget assumed an initial 3-axis acquisition from Titan 3σ handoff rates of 1 degree per second reduced to 0.5 degree per second following deployment (subsequent reacquisitions assumed relatively high rates of 0.1 degree per second), stabilization during orbit-control thrusting, and took into

Table 4-1
5-Year Propulsion Requirements/Propellant Budget

SPS Function	Velocity Impulse (ΔV) (m/s)	(ft/s)	Impulse (N·s)	(lb·s)	Propellant Weight (kg)	(lb)
E-W Orbit Control:						
Orbit Correction	13.7	45	18313	4115	8.67	19.11
Stationkeeping	3.4	11	4473	1005	2.12	4.67
Station Relocation	28.3	93	37828	8500	17.91	39.48
N-S Orbit Control:						
Stationkeeping (1 mo demo)	4.3	14	5696	1280	2.70	5.95
Subtotal	49.7	163	66311	14900	31.43	69.30
Attitude Control:						
Ref. Attitude–(Once 0.5 deg/s;			5527	1242	3.52	7.76
15 times 0.1 deg/s)			2688	604	2.10	4.64
Stabilize Orbit Control			3600	809	2.82	6.22
Wheel Unload (54 mo)						
Jet Only Backup (6 mo)			3133	704	3.55	7.82
Attitude Hold			4215	947	2.69	5.92
Slew/Offset Point			1179	265	1.33	2.94
Crosscoupling			–	–	1.27	2.80
Unallocated Reserve						
Subtotal			20343	4571	17.28	38.10
Total Required/Useable			86654	19471	48.71	107.40
Propellant Residuals					0.36	0.80
Total Load (less 0.8 kg N_2)					49.07	108.20

Definitions

ΔV – Velocity impulse
m/s – meters per second
ft/s – feet per second
N·s – Newton second
lb·s – pound second
kg – kilogram
lb – pound
N_2 – nitrogen
mo – month
demo – demonstration

account jet misalignment, lateral and vertical center-of-mass shifts, center-of-mass uncertainty, and mismatch of north-south thruster pairs.

Pitch wheel momentum unload was estimated by taking 5 percent of the peak solar torque and by assuming a constant gravity gradient corresponding to a 0.1 radian offset of the Z-axis from local vertical. The roll/yaw momentum unload was based on computer simulations. The orbital coupling of the roll and yaw axes allowed unload of either axis, but roll unloading was employed because of the longer moment arm of the roll jets (2.5 times yaw).

Six months of jet-only contingency control were included and cross-coupling effects were accounted for.

The timeline of the budget, including both orbit and attitude control propellant quantities, is shown in Table 4-2. Subsequent discussion in Chapter 7 compares the budgeted and actual 5-year consumption.

Table 4-2
Five-Year Propellant Budget Timeline

Item	Propellant Weight (kg)	(lb)
Reference attitude and orbit acquisition	9.6	21.2
1 year at 94° W	2.6	5.8
40-day move to India	14.6	32.1
1 year at 35°E	2.1	4.7
120-day move to 105° W*	5.2	11.4
2½-years at 105° W*	5.4	12.0
Attitude control contingency	7.9	17.5
Unallocated reserve	1.3	2.8
Onboard residual	0.4	0.8
Weight budget	49.1	108.3

*Changed to 140° W longitude after launch
Note: Spacecraft total budget includes 0.8 kg of nitrogen pressurant.

CHAPTER 5

SPS DESIGN DESCRIPTION

GENERAL

The propulsion subsystems for the ATS-6 were designed, built, tested, and qualified by Rocket Research Company (RRC) of Rockcor, Inc., Redmond, Washington, under contract to Fairchild and were supplied as integral units for integration into ATS-6.

The subsystem was designed for a 5-year life in orbit and the 49-kg hydrazine propellant load provided a total impulse of 88,654 Newton seconds (N·s).

The key features of the spacecraft propulsion subsystem can be summarized as follows:

- Integral fluid-mechanical brazed unit
- Two interconnected functionally redundant feed/thruster half systems
- Sixteen 0.445-N (0.1-lbf) catalytic thrusters, isolated in groups of four
- Two titanium tanks with elastomeric positive expulsion diaphragms (blow-down mode)
- A group of seven latching valves that controlled and isolated the propellant feed between the two positive expulsion tanks and the groups of thrusters
- Redundant heaters on all catalyst beds, truss thruster valves and external propellant lines
- Temperature sensors on the tanks and all catalyst beds, truss valves, and lines; tank pressure sensors and latch-valve position indicators
- Valve actuation and valve/bed heater control by the actuator control electronics units. Line heater control by the temperature control unit.

SCHEMATIC AND COMPONENTS

Figure 5-1 illustrates the fluid interconnection among the tanks (42-centimeter (cm) diameter titanium with EPT-10 diagrams), the fill and drain valves, the 7 latching valves, and the 16 nominal 0.445-N thruster assemblies. Temperature, pressure, and position sensors are indicated. Table 5-1 lists the source and identifying part number of the components.

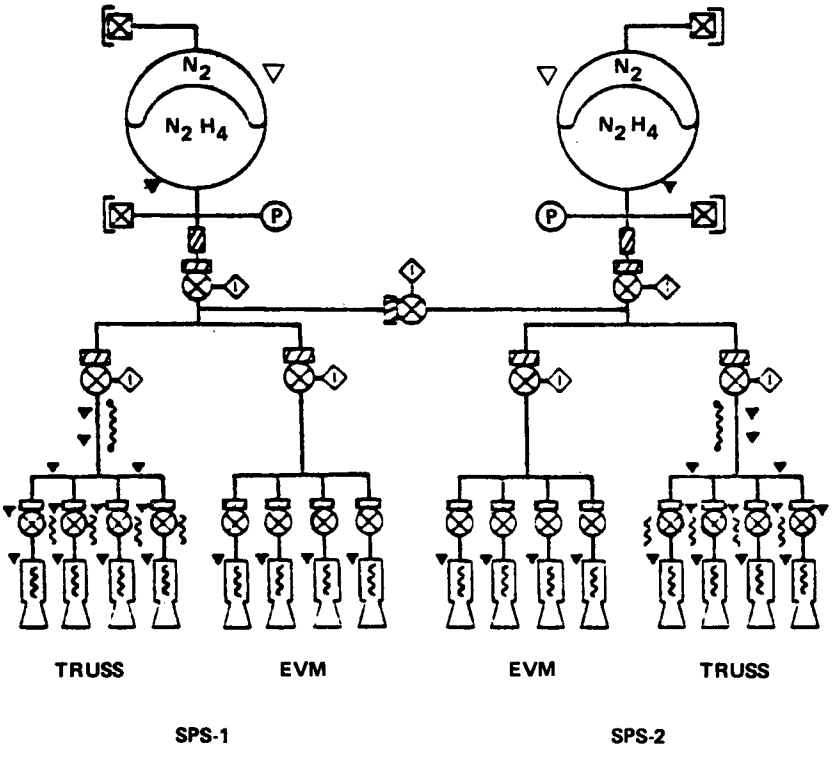

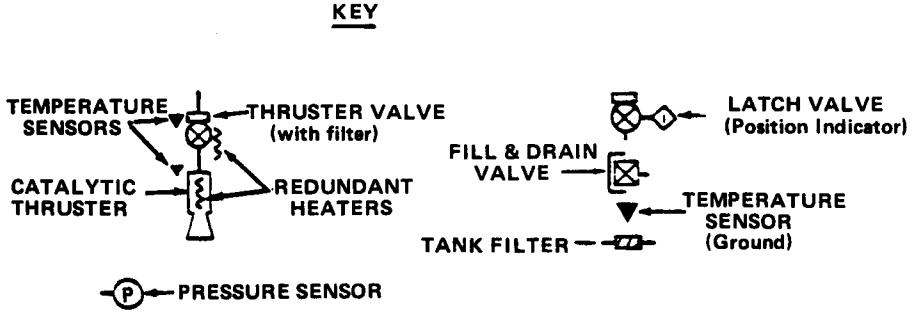

Figure 5-1. Spacecraft Propulsion Subsystem Schematic

Table 5-1
Spacecraft Propulsion Subsystem Components List

Quantity	Item	Vendor	Identification
2	Propellant Tank	Pressure Systems	PN 80177 (RRC 26331-503)
2	Transition Joint	Nuclear Metals	RRC 25185 (6 AL4V Ti to CRES 347)
7	Latching Valve	Carleton Valve	PN 2504-0001 (RRC 26328-503) (Balanced and Relieving Configs.)
16	Catalytic Reactor Assy.	Rocket Research	RRC 26311-304, 305
16	Thruster Valve	Parker Valve	PN 5700060 (RRC 26334)
16	Fluid Resistor (Viscojet)	Lee	EX 43455 (RRC 26371)
4	Fill and Drain Valve	Rocket Research	RRC 25039-19, -29
2	Tank Filter	M/S Filters (Vacco)	RRC 26355-503
68	Braze Fittings	Aeroquip	AE-506-& AE-517-Series
1	Honeycomb Panel	Rocket Research	RRC 26303
2	Pressure Transducer	Dynascience	Model 1025-0092 (RRC 26324)
14	Thermistor	Fenwal Electronic	K 1589 (RRC 26325)
4	Resistance Thermometers	Rosemont Engr.	FI 852C7474-01-020
16	Thermocouple	American Standard	RRC 26354-502
32	Catalytic Bed Heater	Clayborn Labs	RRC 26353-502
8	Thruster Valve Heater (Dual Redundant)	Clayborn Labs	RRC 26352
4	Line Heaters	Clayborn Labs	FI 862-4110-101

All thruster catalyst beds and the externally mounted thruster valves and lines had redundant heaters. In addition to the 16 catalyst bed thermocouples and 14 valve and tank thermistor sensors for telemetry, 4 platinum resistance thermometers were used as redundant sensors for thermal control of the external lines. The propellant filters were 25 micrometer (μm) absolute and 10 μm nominal. The lines were 3/16-inch diameter stainless steel, and titanium to stainless transition joints were used at the tanks.

Figure 5-2 is a close-up view of an internally mounted Earth-viewing module thruster (+/-roll and pitch), while Figure 5-3 illustrates a truss thruster. The main structural member of the thruster assembly is an L-shaped bracket. The Parker single-seat valve was bolted to one side of the bracket with the thruster body on the other side thermally isolated by three thin-walled tube legs between the bracket and the injector flange. Two bed heaters were bolted and the bed thermocouple was welded to this flange. A cylindrical heat shield covered the thruster body and its attachments and was fastened to the bracket by three welded tabs. The heat shield on the EVM thruster was gold plated while the externally mounted assemblies were black, and their valves incorporated redundant heaters and a thermistor sensor. Both photographs show a pressure chamber tap used during ground test that was cut off and welded shut before flight.

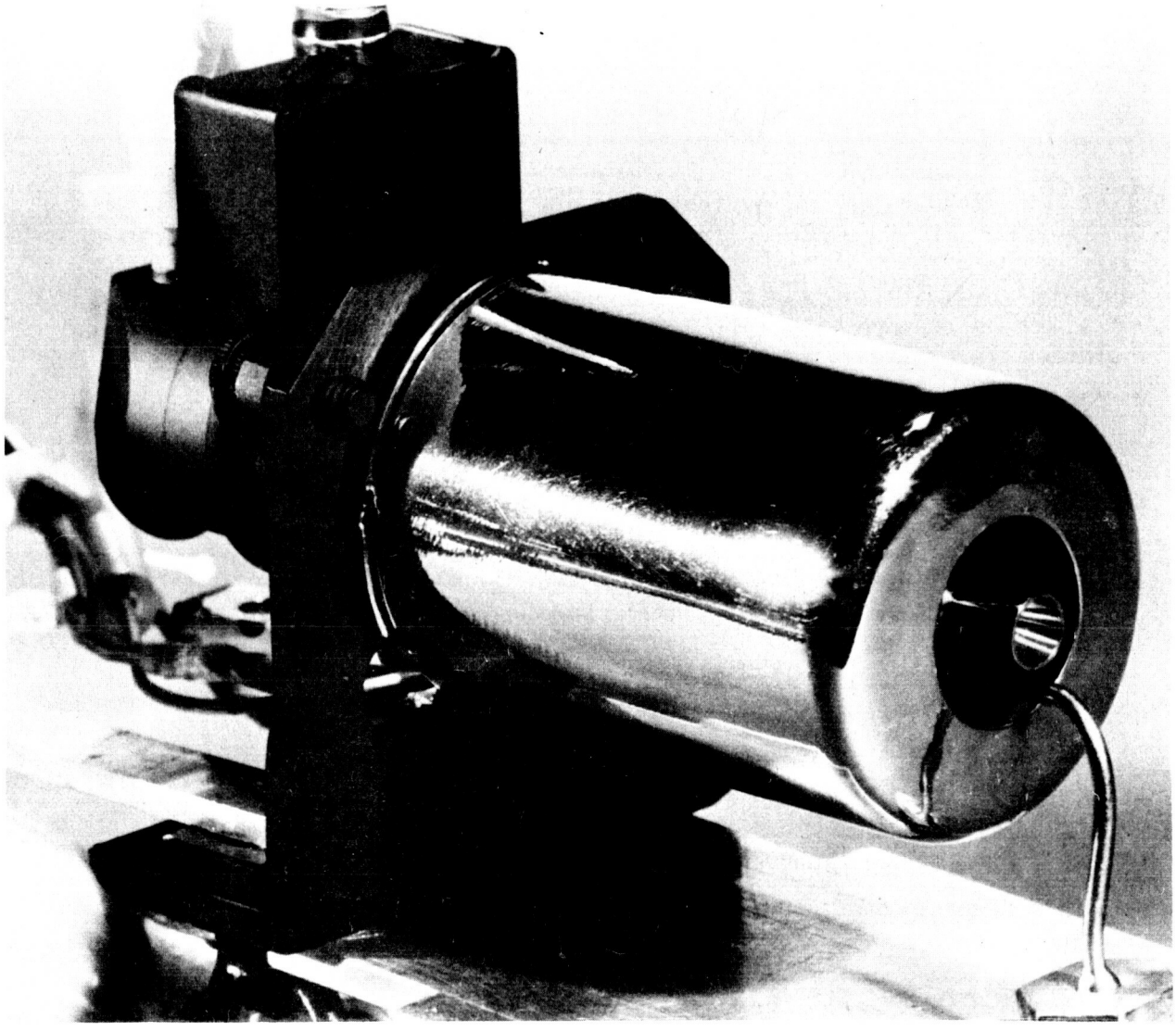

Figure 5-2. Roll/Pitch EVM Thruster

MECHANICAL INTEGRATION

Figure 5-4 is an isometric view of the subsystem feed assembly mounted on the bottom of the service module of the EVM, with the two yaw/orbit control jet assemblies attached to the truss legs. The three axes and associated attitude control jets are indicated, and the general orientation in relation to the 9.14-meter (m) parabolic reflector and the Earth is seen. Eastward orbital motion was effected by jets 7 and 8 and westward motion with jets 15 and 16. The location of the electronics that controlled subsystem functions, the actuator control electronics (ACE) and temperature (control) and signal (conditioning) unit (TSU), is also shown. The feed assembly was bolted to the bottom X-frame of the service module. The pitch and roll jets were bolted and pinned to the edge frame and the orbit control jet bars were held with clevis fittings to the graphite reinforced plastic truss legs. The thermal wrap assembly, covering the two orbit-control jet propellant manifolds and the transfer tubes, is not seen in the figure, but is described in the following paragraphs.

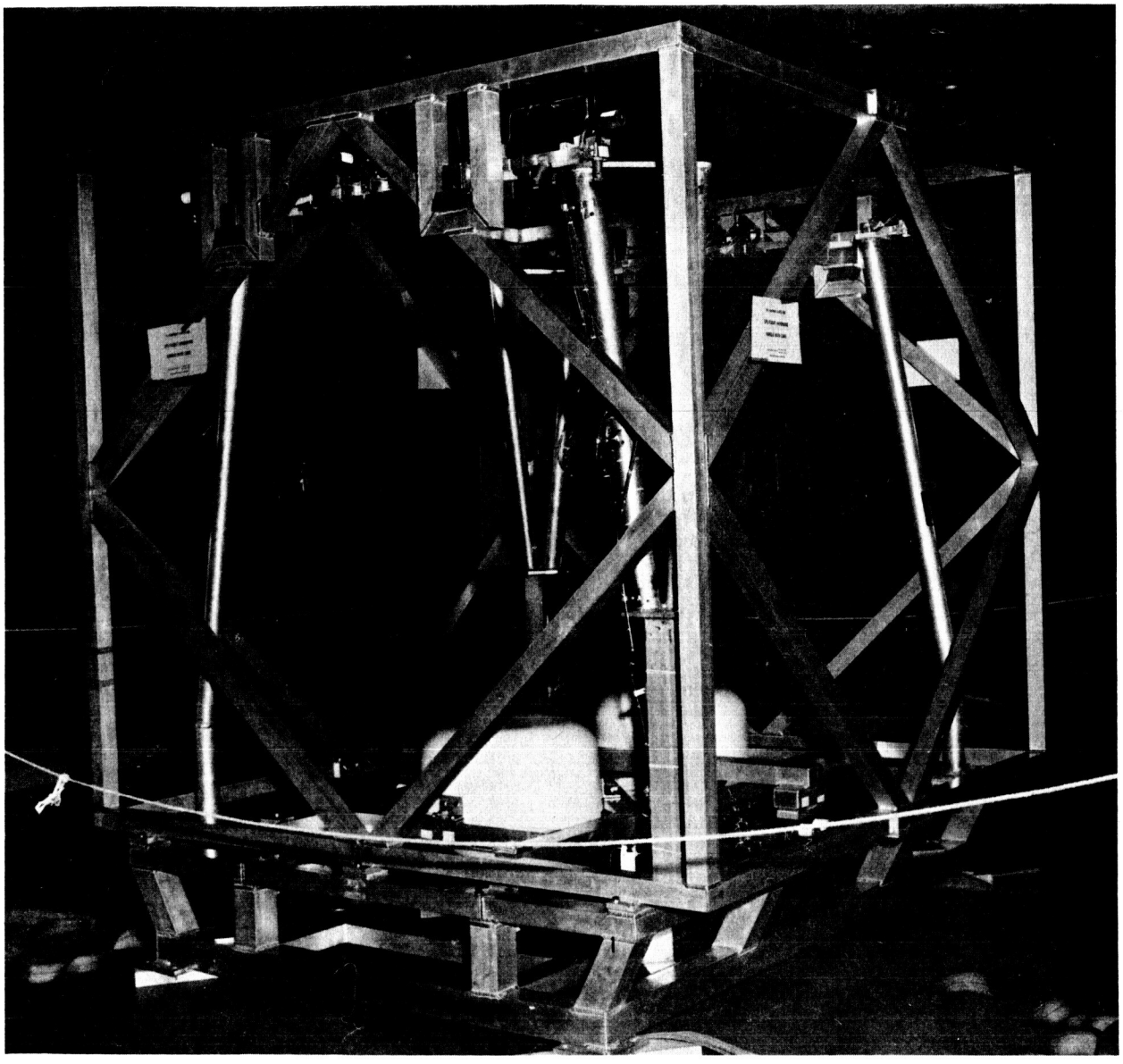

Figure 5-3. Truss Thruster

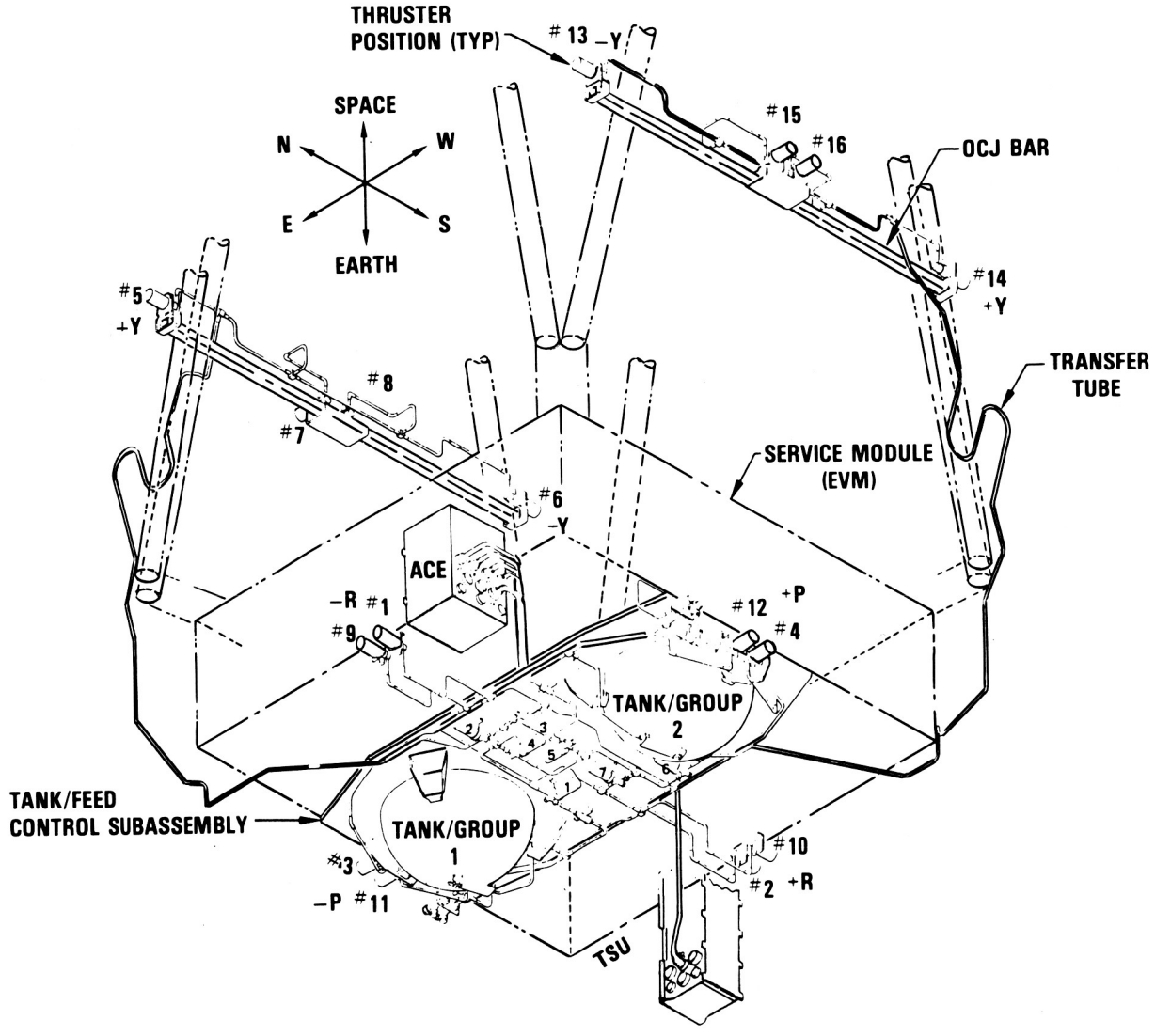

Figure 5-4. Spacecraft Propulsion Subsystem

The integral nature of the subsystem is illustrated by the way it was shipped from Rocket Research to Fairchild. The integrated subsystem in its support frame is shown in Figure 5-5.

The complex process of installing the subsystem in the spacecraft involved lowering the middle section (service module) of the Earth-viewing module onto the subsystem in its support fixture.

Temporary aluminum legs on the service module supported the orbit-control jet assemblies for subsequent transfer to the reflector support truss legs on the spacecraft. Final bolt-down of the feed assembly is seen in Figure 5-6. Following temporary support of the orbit control jet assemblies and various harness elements, the service module and attached propulsion subsystem was lifted out of the support fixture. The service module with the attached subsystem was subsequently integrated with the communications and experiments modules to form the Earth-viewing module.

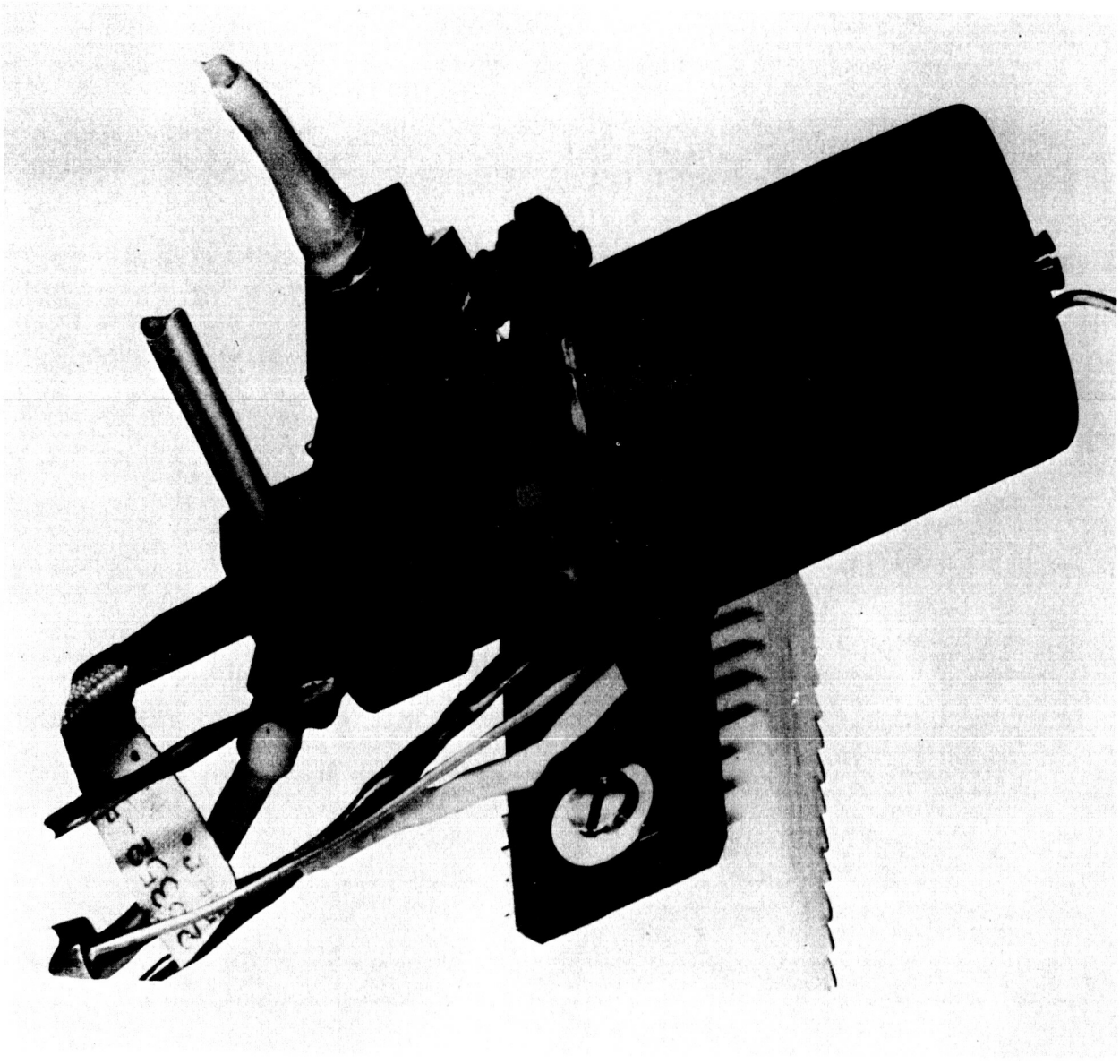

Figure 5-5. SPS Support/Integration Frame

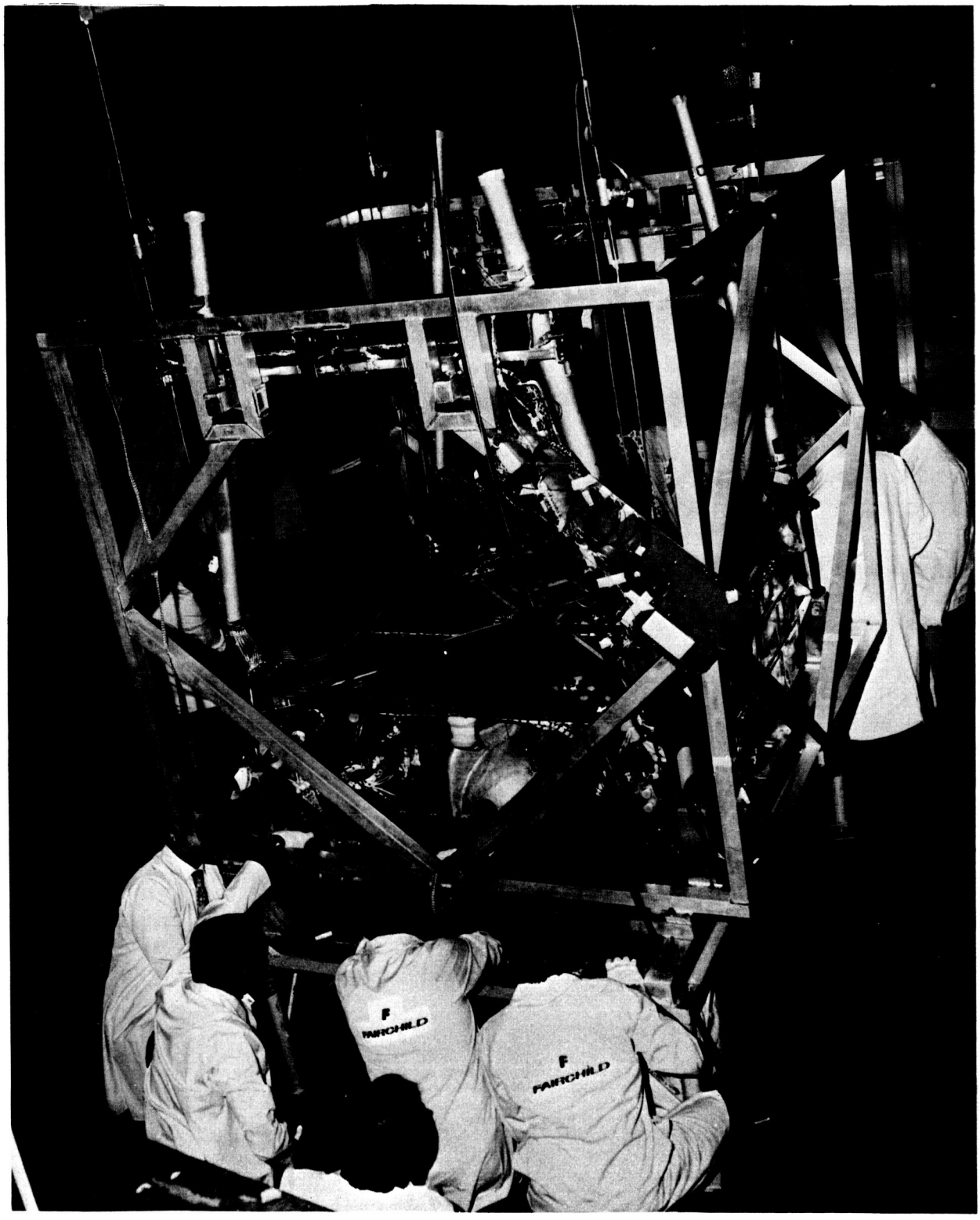

Figure 5-6. Mechanical Integration of SPS and Service Module

ELECTRICAL INTERFACE

The basic electrical block diagram of the spacecraft propulsion subsystem is shown in Figure 5-7. Groups of power input and telemetry output functions are shown connected to subsystem components. As previously indicated, part of the function of the TSU was to regulate the line heaters and process line temperature, heater, and jet-on status.

The ACE controlled the three momentum wheels and the remaining propulsion subsystem functions including jet activation, latch-valve position, and bed and valve heater activation. In addition, bed, valve, and tank temperatures; tank pressure and power; and latch-valve status data were processed by it for telemetry transmission to the ground.

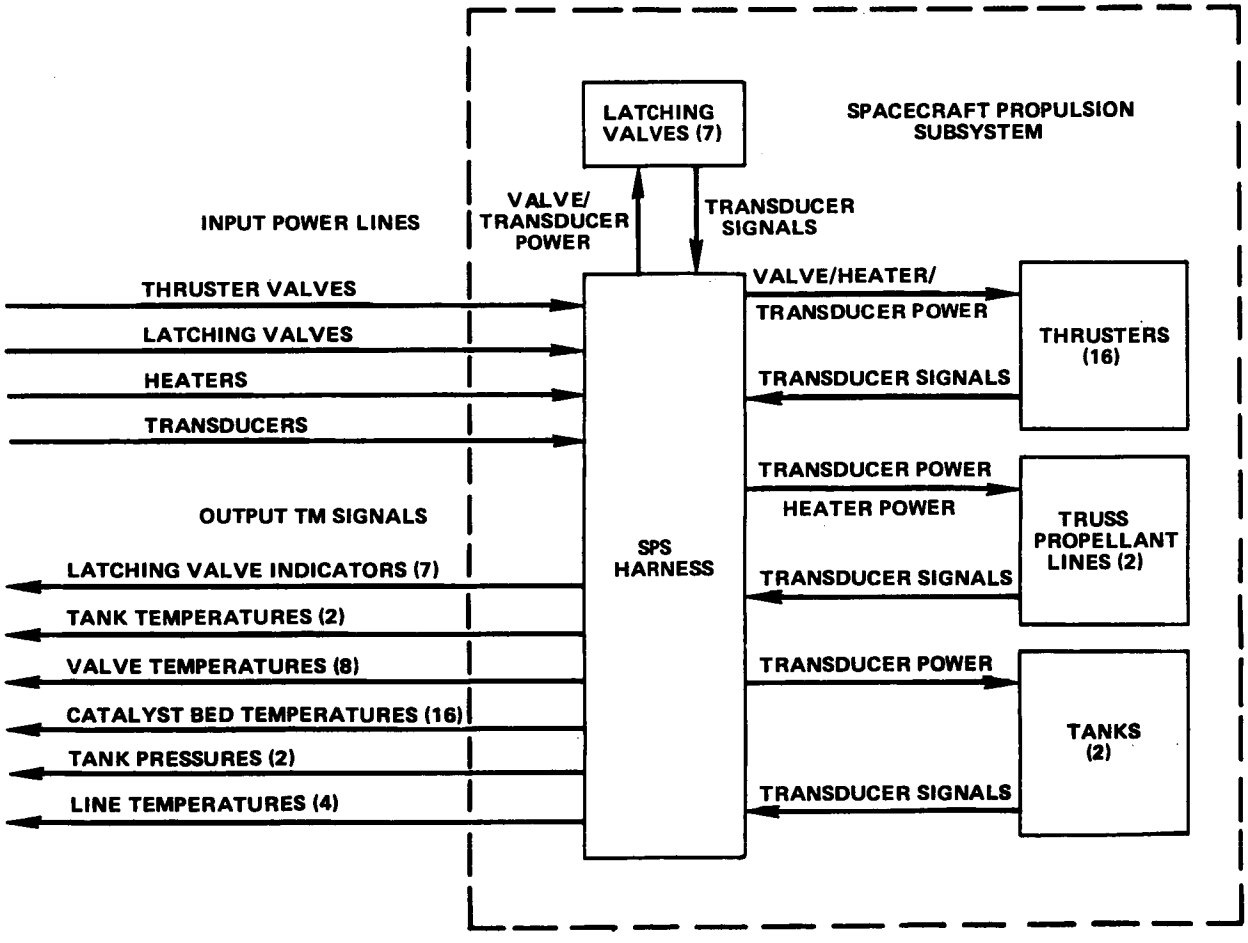

Figure 5-7. Spacecraft Propulsion Subsystem Electrical Block Diagram

CONTROL AND MONITORING FUNCTIONS

The set of 68 commands and 93 telemetry channels are summarized in Table 5-2. The control functions were divided into two identical groups (SPS-1, SPS-2). Both groups could be commanded to function simultaneously, but, in most cases, the same function (e.g., jet actuation) could not be caused to operate simultaneously in both groups. For example, the jets from the group last powered on were in control at any time, while the heaters and the EVM latch valves and truss latch valves were powered only when their particular group was activated. The tank and interconnecting latch valves and telemetry were powered when either group was activated. The jet controls were more complex, using latching drive circuits for orbit maneuvers and logic circuits to prevent opposed jet firings or to set up mixed modes where a particular jet in one group could be selected to replace a failed jet in the other.

Telemetry monitoring consisted of 32 analog temperature and pressure measurements; 37 discrete indications of power, valve position, and jet actuation status; and 24 derived discrete indications of command status. The analog signals were 0 to 5 volts direct current (Vdc) with 9-bit resolution and the discretes were 0 or 5 Vdc.

Figure 5-8 shows the location of the telemetered temperature and pressure sensors.

THERMAL DESIGN

Redundant heaters provided thermal control for all catalyst beds, for the external thruster valves, and for the external propellant lines. A particularly critical aspect was the thermal design of the external lines. The center-of-mass of the spacecraft was located between the Earth-viewing module and the reflector. This condition fixed the mounting of the orbit control and yaw jets external to the thermally-controlled Earth-viewing module in the plane of the center-of-mass.

The transfer tubes and the orbit-control jet manifold were exposed to a complex and varying pattern of Sun and shadow along their length as the Sun circled the spacecraft, and at the same time experienced a variable thermal interface with the orbit-control jet bar and truss legs.

The solution to the problem of maintaining the lines above freezing and below about 100°C under these conditions was a thermal wrap assembly containing heaters that could be automatically controlled at a low (about 2-watt) or high (about 8-watt) level by thermostatic circuits in the temperature control and signal conditioning unit. A backup manual ground-control mode was incorporated (constant on or off).

The wrap consisted of a layer of copper wires, parallel to the 4.8-millimeter (mm) lines, held by metallic straps; spiral wrapped tape heaters; an electromagnetic-radio frequency interference tape shield; a multilayer aluminized Mylar superinsulation blanket; and an outer cover of black painted Kapton. Control and telemetry sensor leads were routed inside the tape shield. The wrapped lines were supported on the legs and on the orbit-control jet bars with fiberglass thermal standoffs.

Table 5-2
Command/Telemetry Summary

Commands							Telemetry
		SPS-1		SPS-2			32 Analog Channels
Power		ON		ON			16 Bed Temp - 30° to 980°C
		OFF		OFF			8 Valve Temp -20°to 150°C
LV OPEN / CLOSE	(1) (2) (3) (4) (5) (6) (7)						4 Line Temp -20°to 150°C
							2 Tank Temp - 20°to 70°C
							2 Tank Press - 0 to 500 psi
Valve Htr.	ON / OFF	PR	BU	PR	BU		37 Discretes
Bed Htr.	ON / OFF	PR	BU	PR	BU		2 SPS Power
Line Htr.	ON (Hi)						7 Latch Valve Position
Man to Auto		PR	BU	PR	BU		2 Ground Control Jets
OFF (to Man)							12 AC Jet Actuation
							12 Line Heater Status
							2 E/W Jet Actuation
Ground Control:							24 Derived Discretes
Jet Enable / Wheels Enable	/Disable						2 SPS Power Status
							4 Bed Heater Status
Jets Only: +R -R +P -P +Y -Y							4 Valve Heater Status
							6 Mixed Mode Select
							6 Mixed Mode
Mixed Mode: ±R ±P ±Y				±R ±P ±Y			1 + R/P/Y Jet
							1 - R/P/Y Jet
Orbit Control:							
WPr, WBu, StopW, EPr, EBu, StopE, N,S							

Figure 5-9 shows the thermal wrap partially applied to a high-fidelity thermal test model of the orbit control jet assembly.

Figure 5-10 illustrates the implementation of the high/low and automatic/manual control of both the prime and backup line heaters. Combinations of high, low, and off conditions of the prime and backup circuits provided five steps of steady-state heater power; 2, 4, 7½, 9½, and 15 watts. Operating with various combinations of manual (either or both heaters steady-state) and automatic (either or both cycling on and off), various values of average power could be obtained.

In-orbit experience with line thermal control indicated that the line thermal control was overly complex.

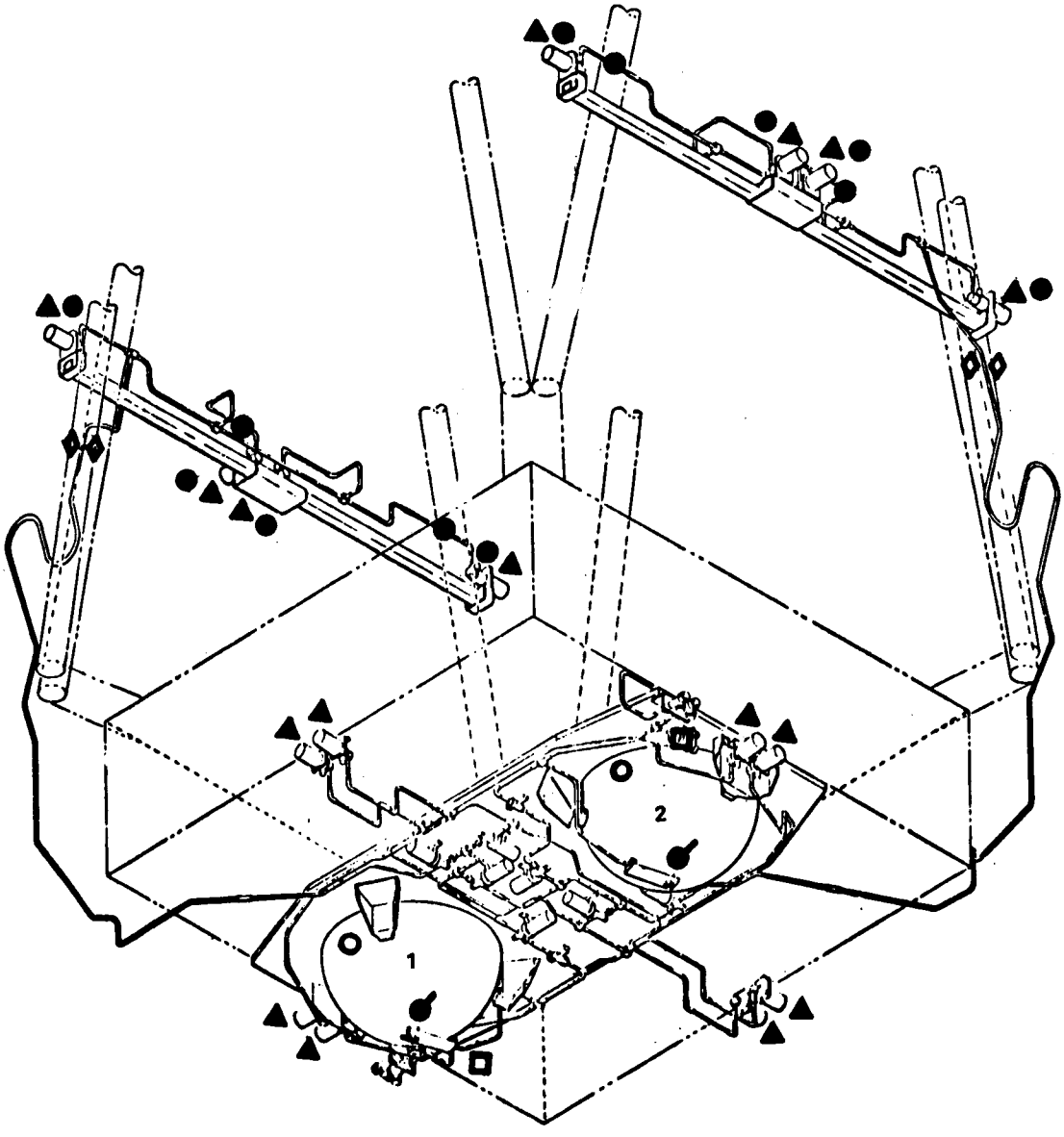

Figure 5-8. SPS Sensor Locations

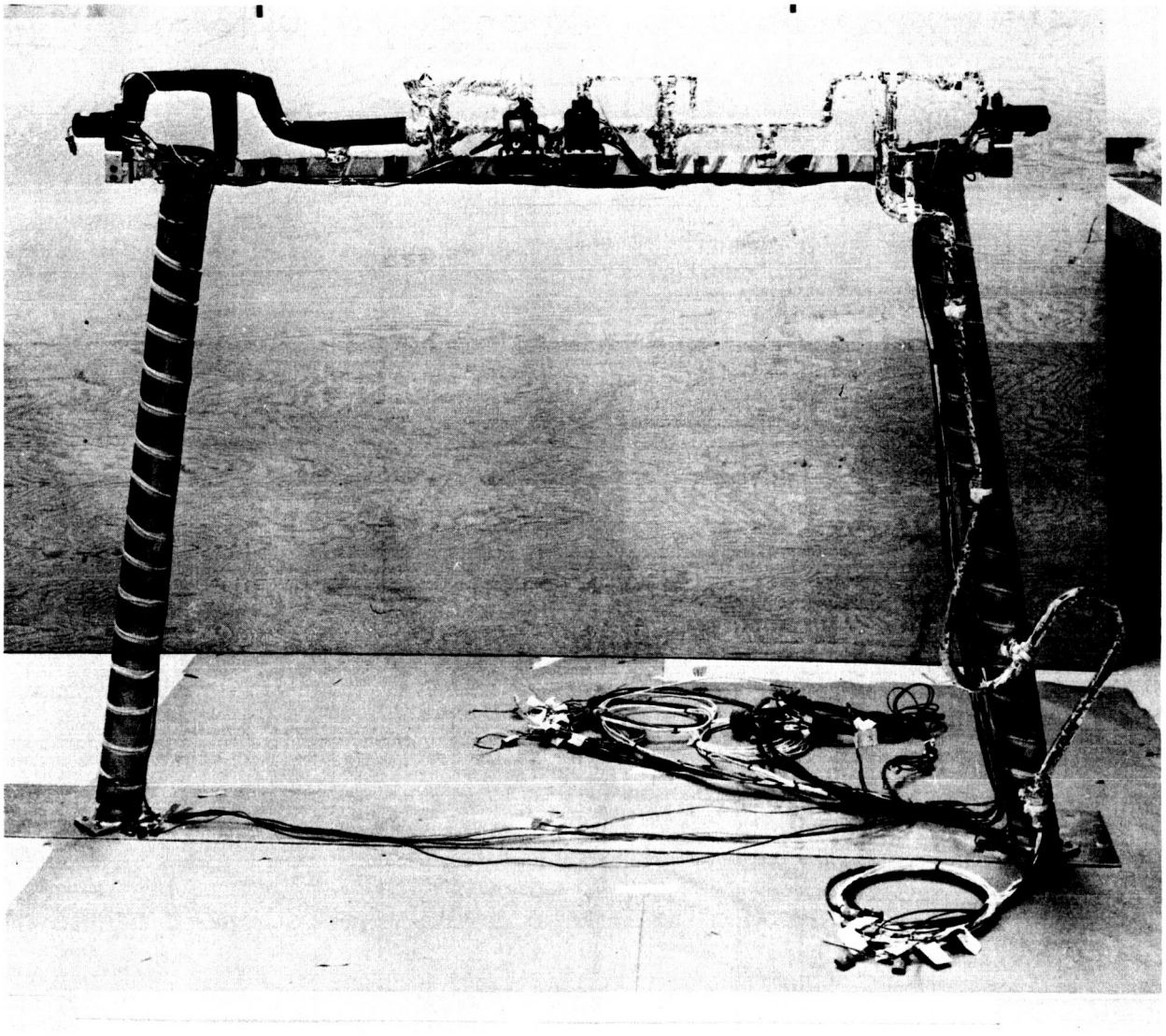

Figure 5-9. Orbit-Control Jet Thermal Test Model (Partial Wrap)

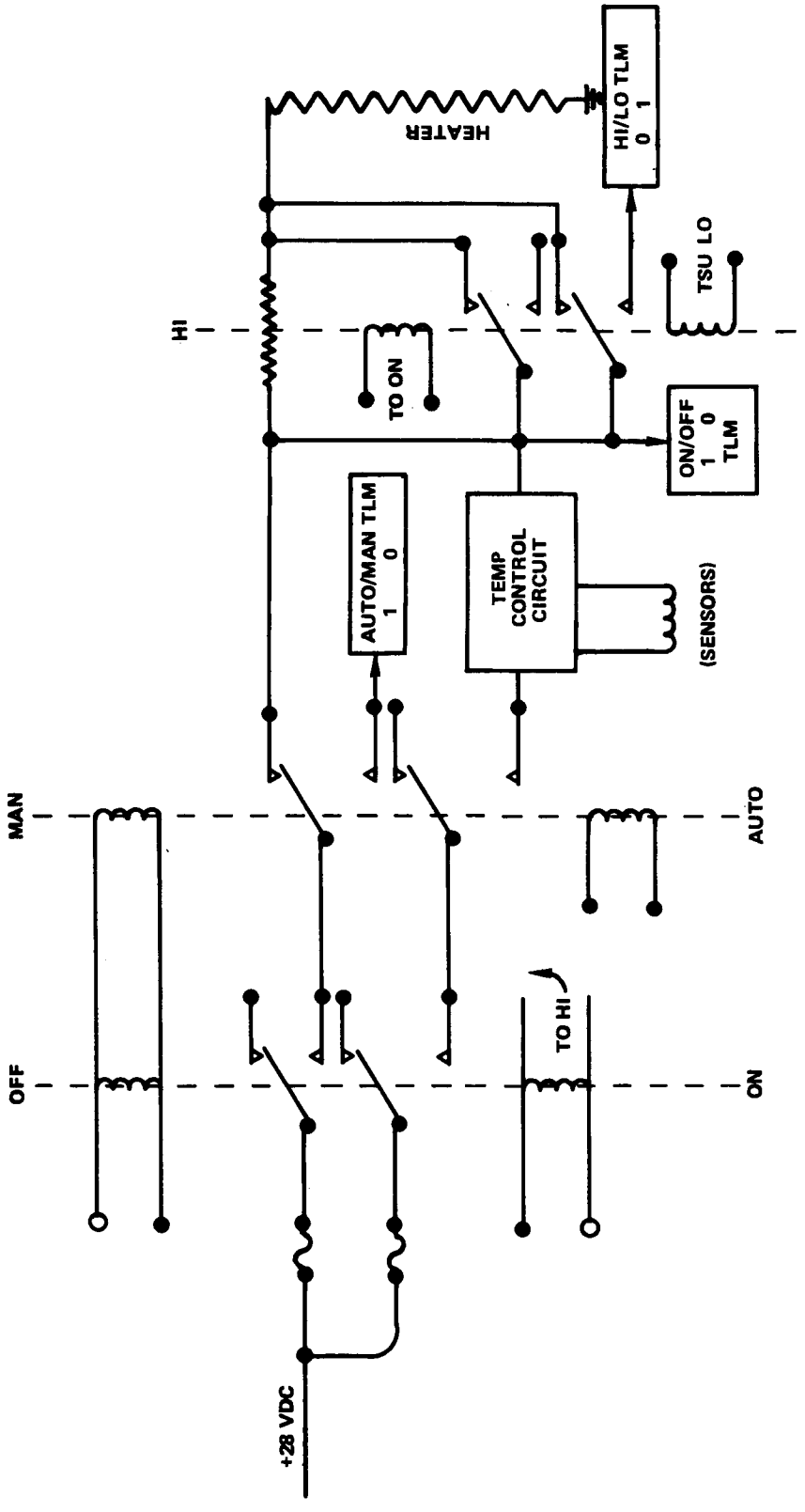

Figure 5-10. Spacecraft Propulsion Subsystem Line Heater Control

SUBSYSTEM WEIGHT AND POWER

Table 5-3 summarizes subsystem weight and component power requirements.

The subsystem dry weight was 43 percent of total wet weight with a complementary propellant/pressurant mass fraction of 0.57. It should also be noted that the weight (actual and allocated) of the truss line thermal control elements was 28 percent of the dry weight; a result of the particular ATS-6 design with externally mounted orbit control thrusters.

The nominal steady-state power with all components operational was:

SPS-1 and -2, valve heaters = 8 X 2.5	=	20.0 watts
SPS-1 and -2, prime and backup line heaters (low automatic) = 4 X 2.3	=	9.2
Sensors (2 pressure + 34 temperature)	=	0.6
Total	=	29.8 watts

Duty cycling of the line heaters resulted in an average power something less than that shown. During jet firing periods, there was an additional bed heater load of 8 X 1.5 = 12 watts and an intermittent 3 watts for thruster valves. Details of heater operation with failures is discussed later.

BLOWDOWN OPERATION AND THRUSTER PERFORMANCE

The subsystem operated in a blowdown mode over a tank pressure ratio of 2.8 to 1 (Figure 5-11). The curves were derived with temperature as a parameter, based on the actual flight propellant load.

The two types of ATS-6 0.445-N (0.1-lbf) thrusters were seen in Figures 5-2 and 5-3. Three points from the nominal steady-state performance curves over the blowdown range at a feed temperature of 21°C were as follows:

P_t, Tank Pressure	P_c, Chamber Pressure	F, Thrust		I_{sp}, Specific Impulse	
(psia)*	(psia)	(N)	(lbf)	(s)	(N·s)/kg
375	240	0.56	0.125	223	2187
285	192	0.44	0.100	220	2158
134	103	0.24	0.053	214	2099

*psia—pounds per square inch absolute

Table 5-3
SPS Weight and Power Summary

Component		Weight, kg (lb)	Power, Watts
Propellant Tanks		2 X 4.06 = 8.12 (17.90)	
Tank Brackets		2 X 0.85 = 1.70 (3.76)	
Latching Valves		7 X 0.27 = 1.89 (4.20)	46 (0.028 s)
Thruster Assembly	8 (truss)	X 0.30 = 2.40 (5.28)	3.0 (thruster valve)
	8 (EVM)	X 0.29 = 2.32 (5.12)	1.5 (bed heater)
Fill and Drain Valves		4 X 0.10 = 0.40 (0.88)	2.5 (valve heater, truss only)
Tank Filters		2 X 0.05 = 0.10 (0.23)	
Pressure Transducer		2 X 0.08 = 0.16 (0.35)	0.30
Temperature Sensors		= 0.11 (0.25)	0.043 (thermistors)
Honeycomb Panel		= 3.73 (8.22)	External line heaters
Lines and Fittings		= 1.37 (3.01)	Auto / Manual
			High 8.2 / 9.5
			Low 2.3 / 2.7
Brackets and Fasteners		= 1.28 (2.83)	
Electrical Harness		= 3.34 (7.37)	
Delivered Subsystem		= 26.94 (59.40)	
Truss Line Thermal Control (Fairchild) OCJ bars = 4.96 (10.93) Truss legs = 3.99 (8.80) TCU (allotment) = 1.68 (3.70)		= 10.43 (23.00)	
Dry Weight		= 37.38 (82.4)	
Hydrazine Propellant (Nom Budget)		= 49.08 (108.2)	
Nitrogen Pressurant		= 0.81 (1.8)	
Wet Weight		= 87.27 (192.4)	

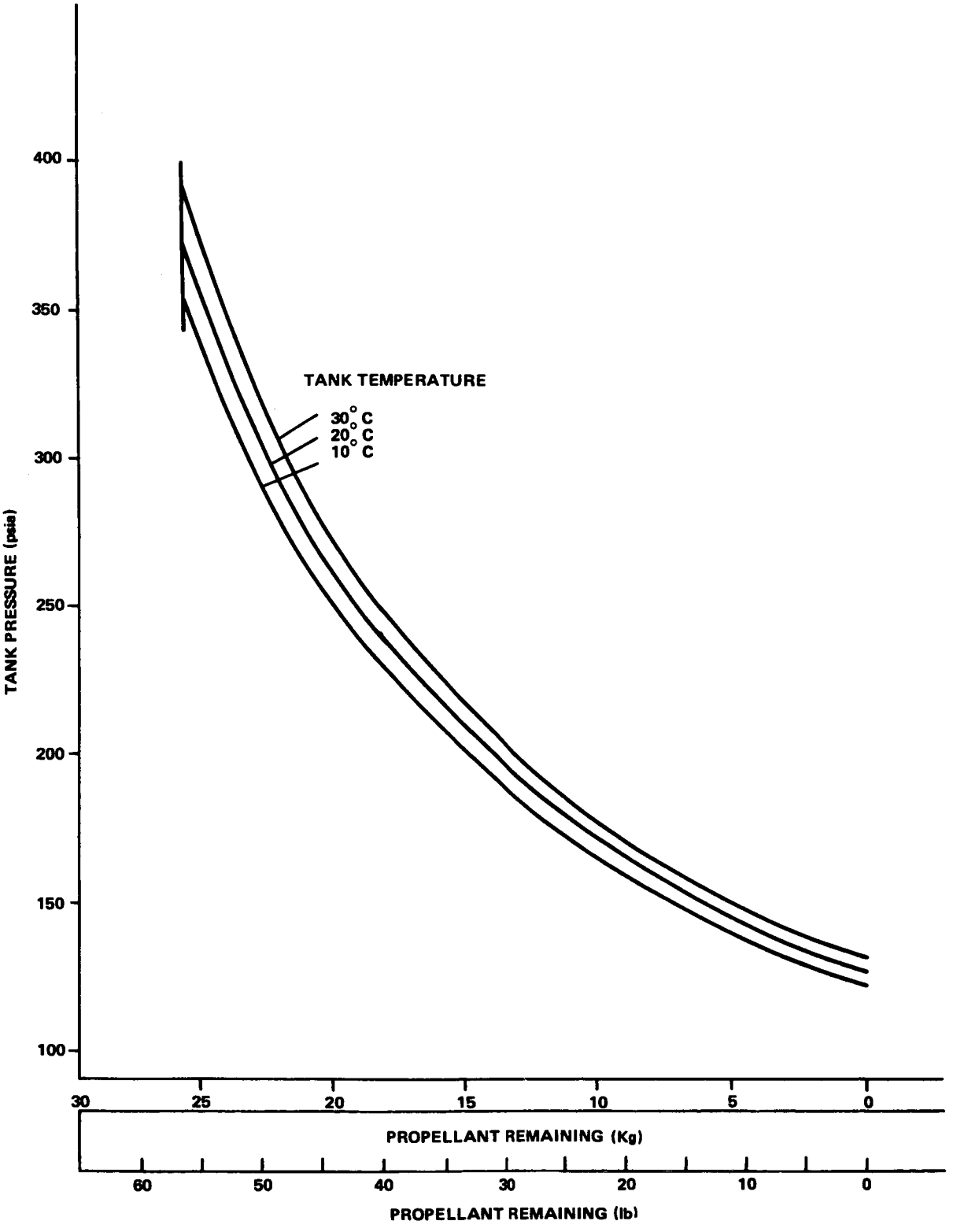

Figure 5-11. Blowdown Curve

The extremes of the nominal performance envelope at high and low combinations of feed temperature and pressure were:

	High	Low
Tank pressure, P_t	395 psia	125 psia
Feed temperature, T_f	35°C	5°C
Chamber pressure, P_c	250 psia	96 psia
Thrust, F	0.59 N (0.132 lbf)	0.22 N (0.050 lbf)
Specific impulse, I_{sp}	2197 $\frac{N \cdot s}{kg}$ (224 s)	2040 $\frac{N \cdot s}{kg}$ (208 s)

Each thruster was tested at high and low feed pressure before and after the acceptance vibration test using a set of baseline performance duty cycles consisting of 5 pulses (0.1 second on, 200 seconds off [0.1/200]), 25 pulses (0.2 second on, 10 seconds off [0.2/10]), and a single run of 200 seconds.

The steady-state acceptance data for the east-west thrusters are listed in Table 5-4 with the thrust data plotted in Figure 5-12. The small scatter of the data are well within that specified over the blowdown range. The maximum thruster-to-thruster variation in specific impulse at steady-state was ±2.8 percent at high thrust and ±5.6 percent at low thrust. Also, there was a 2 to 4 second increase in performance following acceptance vibration. The thrusters reached 90 percent of steady-state specific impulse in about 40 seconds. The maximum thrust uncertainty at any given tank pressure over the blowdown range was less than ±5 percent.

The 0.2/10 automatic momentum wheel unload duty cycle showed, on the average, a 20 percent increase in specific impulse during the first 25 pulses at high thrust and a similar 10 percent increase at low thrust. It also displayed a variable increase following the acceptance vibration test. The average thruster-to-thruster specific impulse uncertainty was fairly constant at about ±8 seconds, which translates to about ±7 percent for a first low-thrust pulse and about ±5 percent for the 25th high-thrust pulse. Figures 5-13 and 5-14 illustrate performance data for the SPS-1 No. 2 roll control thruster under a variety of conditions.

The minimum on-board pulse width during computer initiated jet-only attitude control was 0.100 second, while the normal ground commanded pulse width was 0.250 second. The 0.1/200 ground-test data indicated a total range of bit impulse for the first five pulses between 0.039 and 0.060 N·s at 0.49 N and between 0.022 and 0.040 N·s at 0.22 N. For any given pulse the maximum bit uncertainty at high thrust was ±20 percent and at low thrust was ±23 percent.

For short pulses at or below 0.1 second duration, specific impulse for the first pulse or for pulse trains at low-duty cycles was almost exclusively a function of bed temperature. For ATS-6 type

Table 5-4
East-West Thruster Performance

Parameter		Value (Pre- and Post-Vibration Test)	
		No. 7	
		Pre-	Post-
Thrust: (lbf)	– High	0.1268	0.1259
	– Low	0.0558	0.0563
Specific Impulse (s)	– High	228.2	226.9
	– Low	214.1	210.5
		No. 8	
Thrust (lbf)	– High	0.1243	0.1235
	– Low	0.0567	0.0548
Specific Impulse (s)	– High	220.1	215.7
	– Low	221.5	206.8
		No. 15	
Thrust (lbf)	– High	0.1220	0.1255
	– Low	0.0550	0.0544
Specific Impulse (s)	– High	221.2	228.3
	– Low	221.0	214.0
		No. 16	
Thrust (lbf)	– High	0.1240	0.1246
	– Low	0.0540	0.0533
Specific Impulse (s)	– High	217.5	216.2
	– Low	209.2	198.3

Note: Thrust (lbf) × 4.448 = Thrust (N)
I_{sp} (s) × 9.807 = I_{sp} (N·s)/Kg

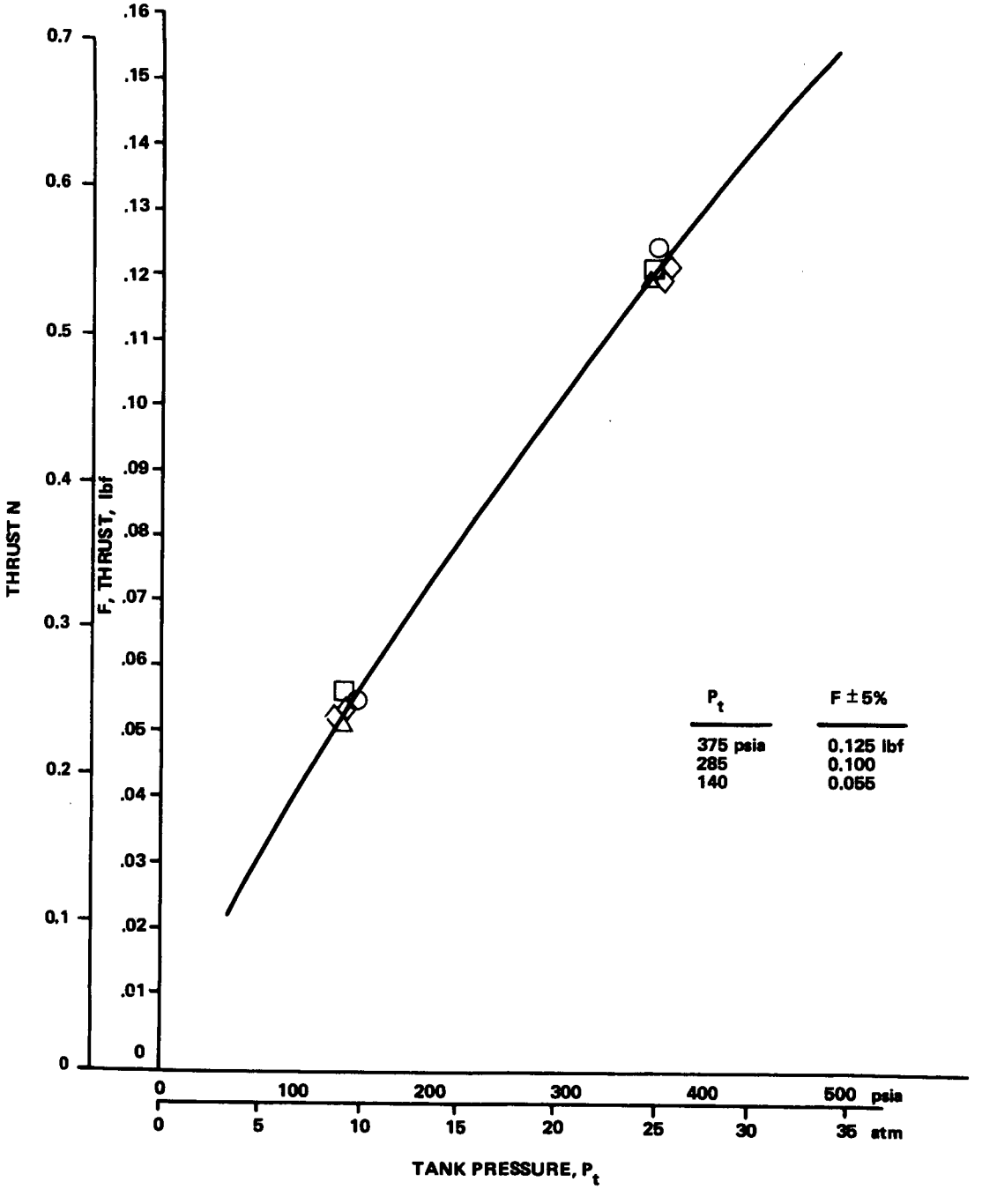

Figure 5-12. Pressure-Thrust Curve (Flight Thrusters)

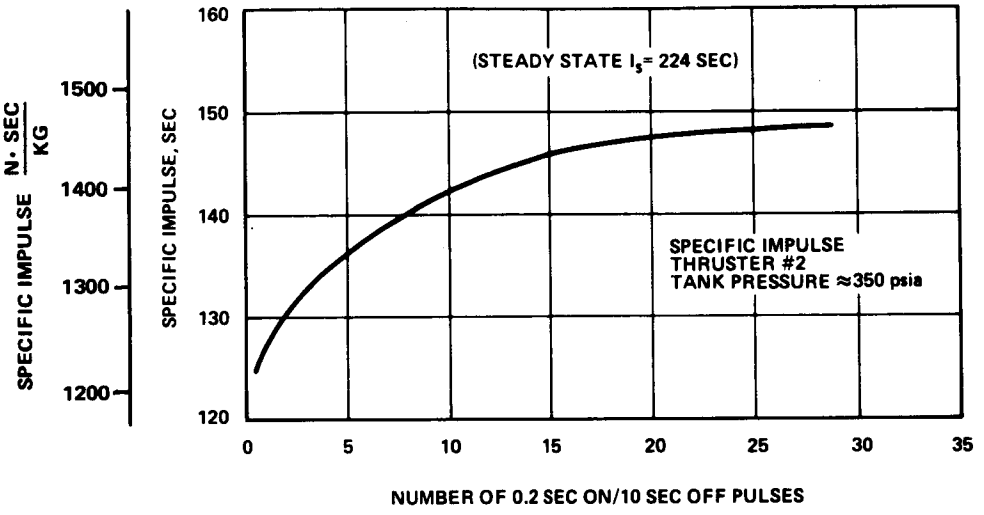

Figure 5-13. Typical Wheel Unload Performance
(Specific Impulse, Thruster 2)

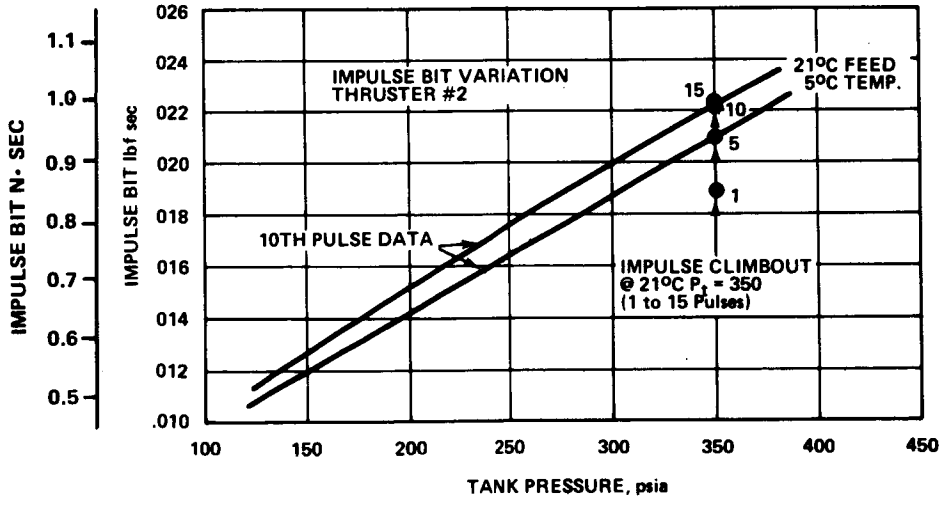

Figure 5-14. Typical Wheel Unload Performance
(Impulse Bit Variation, Thruster 2)

0.445-N thrusters, the average specific impulse for pulses having durations between 0.020 and 0.100 second was:

T_b, Bed Temperature		I_{sp}, Specific Impulse	
(°C)	(°F)	(N·s)/kg	(s)
93	200	1128	115
204	400	1226	125
316	600	1344	137
538	1999	1667	170

In-orbit performance is discussed in Chapter 7.

PROPULSION GROUND SUPPORT EQUIPMENT

The sets of test and service equipment used at Rocket Research during assembly and subsystem level testing, and at Fairchild during subsystem integration and spacecraft level testing included mechanical, electrical, and fluid equipment.

The central piece of mechanical ground support equipment was the fixture shown in Figures 5-5 and 5-6. This complex multiple-use fixture was used for component and subassembly support during initial subsystem assembly and brazing, support during checkout and environmental qualification and acceptance tests, crosscountry shipment, thermal control assembly installation at Fairchild, and subsystem integration in the spacecraft.

Electrical checkout and functional operation of the subsystem at Rocket Research was accomplished using an electrical test set and pressurization panel. All functional circuits of the subsystem including thruster valves, latch valves, heaters, and the pressure and temperature sensors could be checked individually with the test set. The pressurization panel regulated the flow of helium or nitrogen gas to the subsystem for proof, thruster flow, and leak tests.

Hydrazine propellant, water (as a flush fluid for the propellant or as a refree fluid for vibration testing) and isopropyl alcohol (a flush fluid for the water) were loaded into or unloaded from the subsystem tanks using a service cart designed and fabricated by the Ford Aerospace Company (then Philco-Ford). Figure 5-15 shows the control panel of the cart. The 2,361 kg (3,000 lb) cart incorporated a full set of hand operated pneumatic control valves; pressure gages; pressure regulators; a self-contained, high-pressure gas supply; a digital-readout tank weight transducer; a vacuum pump; and necessary interconnecting tube manifolds and high capacity micron filters. Figure 5-16 is a fluid schematic of the cart. Experience with the cart at Rocket Research, Fairchild, and at the Cape Kennedy launch site, where the spacecraft propulsion subsystem was filled with hydrazine on the tenth level of the Launch Complex 40 service tower, indicated that it was overly complex, large, heavy, and cumbersome to move and manipulate.

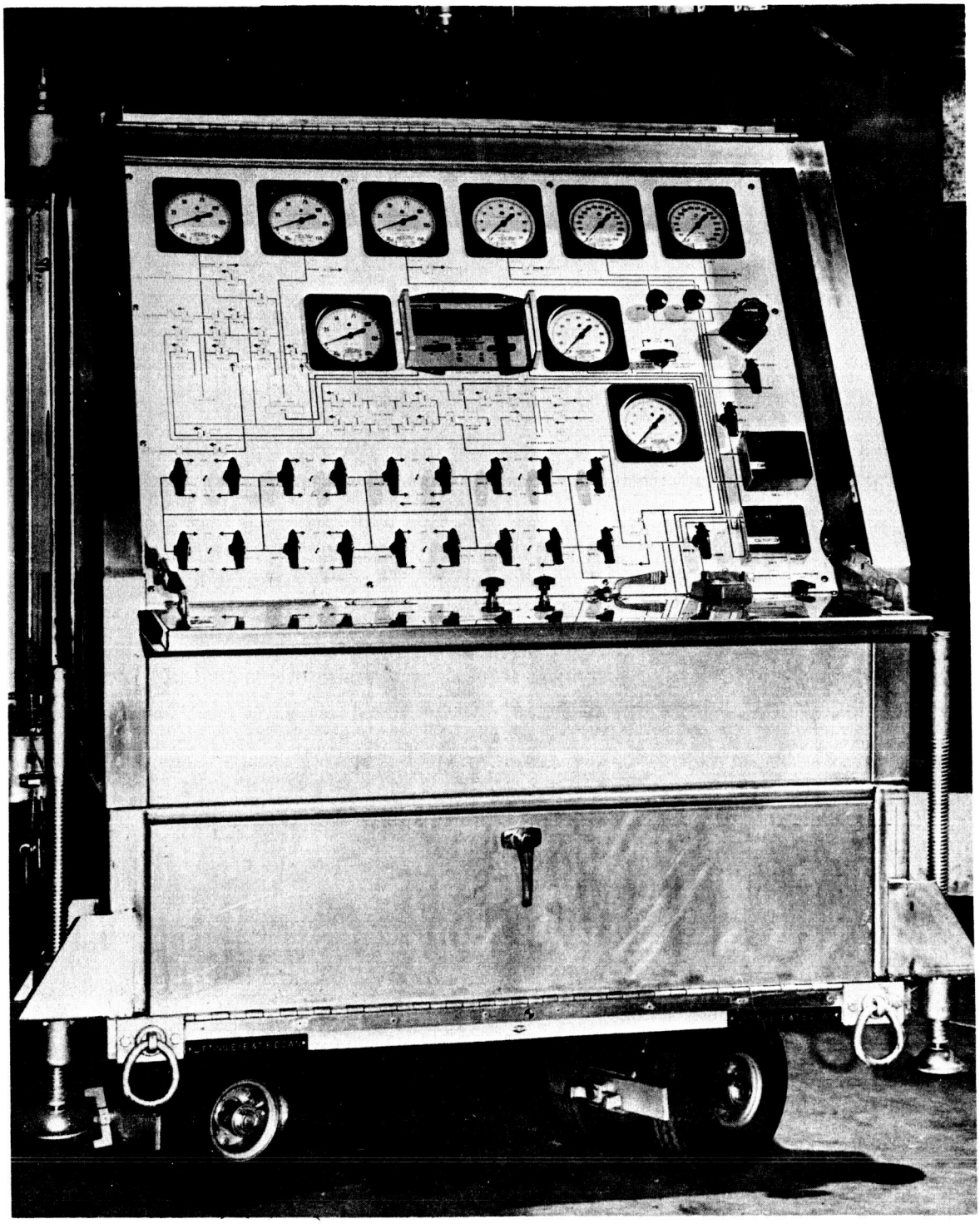

Figure 5-15. Service Cart, Front

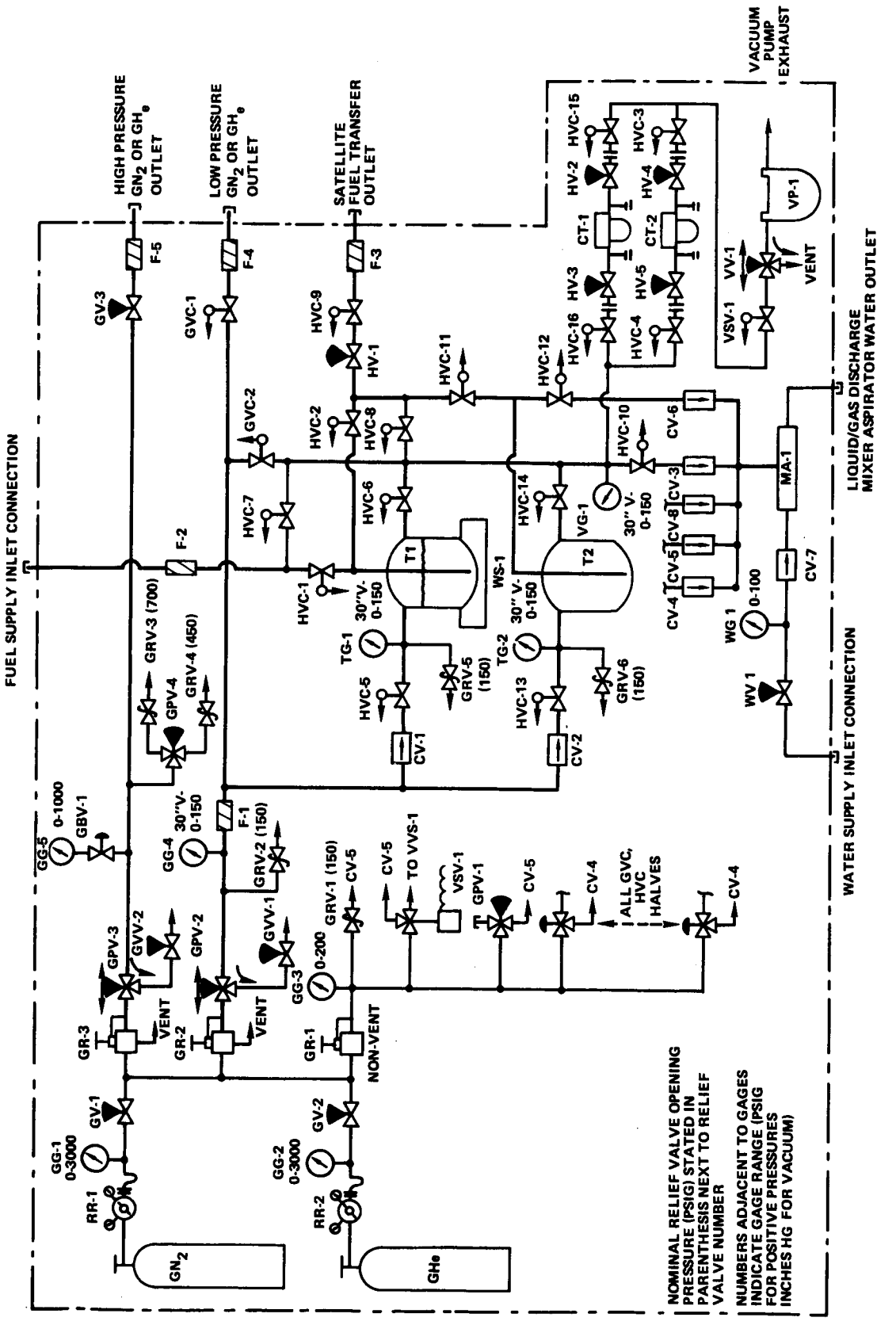

Figure 5-16. Plumbing Schematic, SPS Service Cart

Due to schedule constraints, an additional pressure test console was fabricated at Fairchild for use during thruster and valve leak tests at the spacecraft level. Figure 5-17 shows a specialized piece of mechanical ground support equipment, two of which were required to support the orbit-control jet assemblies on either side of the Earth-viewing module during transfer from the temporary support legs (Figure 5-6) to the reflector support truss legs during spacecraft assembly and integration.

In addition to the above items and laboratory multimeters, the spacecraft propulsion subsystem required a number of other ground support items including (1) a dew point indicator (Alnor Dewpointer) to determine moisture content of the gases inside the subsystem, (2) a set of low-flow gas rotometers for steady-state flow at low tank pressure (as indicative of clear thruster cap tube and catalyst bed passages and for indicating thruster operation during ambient or vacuum testing), and (3) a set of liquid pipettes to measure valve internal leakage by observing movement of a small water plug in the pipettes. Miscellaneous custom-made wrenches, fluid adapters, interconnect hose sets, and electrical components completed the subsystem ground support equipment.

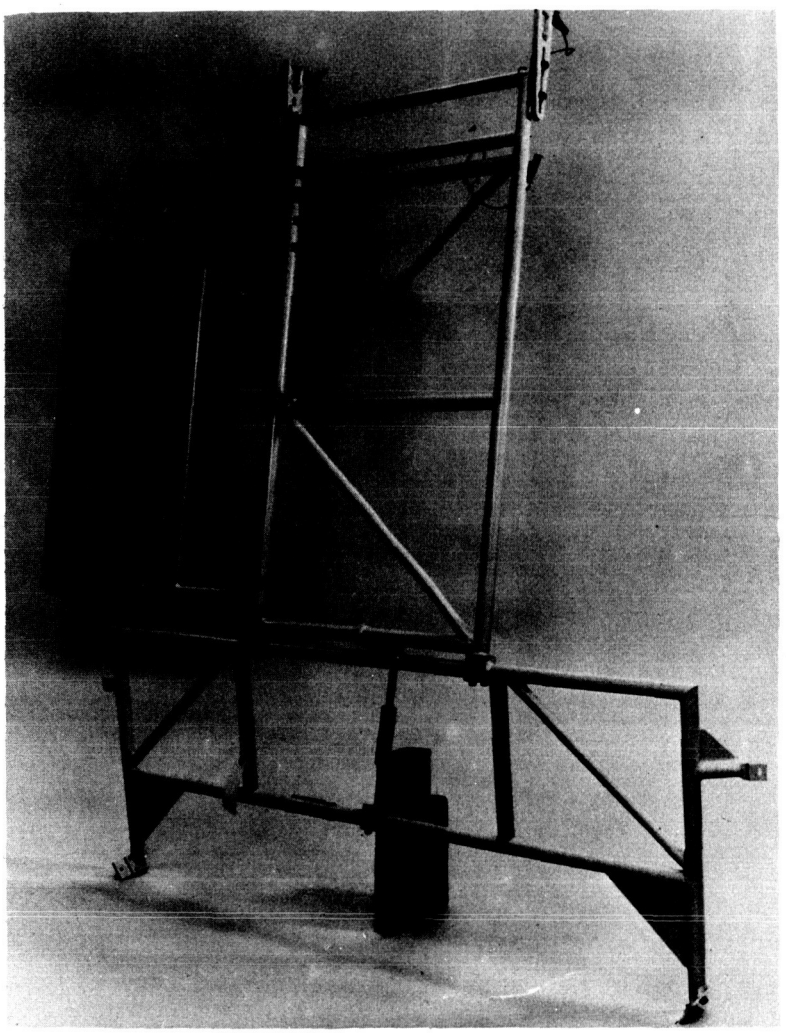

Figure 5-17. Orbit Control Jet Bar Support Fixture
(Fairchild)

CHAPTER 6
SPS DESIGN VALIDATION

OVERVIEW

Flight readiness of the ATS-6 propulsion subsystem was assured by a detailed and comprehensive ground test program that involved all subsystem components, an engineering model, a prototype for subsystem and spacecraft level qualification (the latter based on tests of the prototype installed in the thermal structural model of the spacecraft), thermal and structural models of the critical external thrusters and their manifold, a number of special assemblies and mockups to confirm various design areas, and the flight units during their acceptance tests.

Supporting the test program was a comprehensive set of documentation, a number of analytical studies, and a set of certified ground support equipment.

The extent of this effort is outlined in Table 6-1 that includes items discussed in the following paragraphs. To provide some perspective of the time span of the development test program, Table 6-2 lists the dates for a number of significant events from subsystem assembly through the ATS-6 launch. The contract to Rocket Research Company was let early in 1971.

SPECIFICATIONS, PROCEDURES AND PROCESSES

The basic requirements specification from Goddard Space Flight Center (862-1100) was translated by Fairchild into a procurement specification (862-PR1100) and placed with Rocket Research. The subcontractor in turn generated a set of component procurement specifications, design drawings, manufacturing and materials processes, assembly/integration procedures, and test procedures. All operations were under quality surveillance and control, including comprehensive documentation, through delivery of the subsystem to Fairchild.

At the spacecraft level, Fairchild generated a complete set of procedures covering the subsystem from receiving inspection at Germantown through launch at Kennedy Space Center, and drawings and material processes for the orbit-control jet thermal control assembly. The following list illustrates the comprehensive nature of the procedures, all of which were under quality-assurance control.

Number*	Title
862-PS-3010	SPS receiving inspection
862-PS-3011	SPS propellant line thermal wrap assembly
862-PS-3012	SPS installation in service module

Table 6-1
SPS Design Verification Test Outline

Analysis	Development Test	Prototype Qualification	Flight Unit	GSE Certification
Reliability	Components	Components Qualification	Acceptance	RRC Test Equip & GSE
Functional redundancy	Thruster assembly Thruster-valve life Latch-valve life	Acceptance	Components Tank/feed assembly Thruster baseline	FSEC GSE
Propellant isolation	Tank–qualification Catalyst bed heater	Components Tank/feed assembly Thruster baseline	Proof Pressure, Leak & Electrical	Launch Site Equipment
Command/ telemetry	Engineering Model	Proof Pressure, Leak & Electrical	Mech & Thermal Environmental Accept Tests	Documentation
Performance	Component test Subassembly test Mission prequal	Mech & Thermal Environmental Qual Tests	Storage/Shipment Protection	• Subsys Spec • Component Specs • Matl. Specs • Mfg. Processes • Test Procedures
Blowdown Thruster duty cycle Increased N_2H_4 load Fluid dynamics	OCJ Assemblies	Spacecraft Thermal Structural Model		
	Thermal qual model (EMI testing) Structural qual model	SPS thermal SPS vibration Practice fueling		
Structural	Special Tests			
Subsystem assembly SPS/spacecraft interaction OCJ bar	Nozzle-up vibration Valve freeze/thaw Valve thermistor Plume impingement Feed line "S" bend			
Thermal				
SPS/SC interaction OCJ thermal control Capillary feed tube Plume heating (and forces)				

Definitions

N_2H_4	– hydrazine
SPS	– spacecraft propulsion subsystem
SC	– spacecraft
OCJ	– orbit-control jet
Qual	– qualification
EMI	– electromagnetic interference
Mech	– mechanical
GSE	– ground support equipment

Table 6-2
Propulsion Subsystem Assembly/Test Dates

	Prototype (SN 1001)	ATS-F (SN 1003)	ATS-G (Spare) (SN 1002)
Begin Assembly at RRC	Nov 1971	Apr 1972	Feb 1972
Subsystem Integration Complete	Mar 1972	Aug 1972	July 1972
First Hydrazine Load	Apr 1972	Sept 1972	Oct 1972
Qualification/Acceptance Complete	May 1972	Sept 1972	Oct 1972
Receiving Inspection at Fairchild	Feb 1973	Apr 1973	Oct 1973
SPS/SM Integration	Apr 1973	June 1973	NA
Launch	NA	May 30, 1974 (ATS-6)	NA

Number* (cont)	Title (cont)
862-PS-3016	Special operations, SPS components removal from the TSM
862-TP-1139	SPS-response test set – ATS-F BTE
862-CP-1001	SPS – mechanical AGE (service cart), certification/calibration procedure for gas use
862-CP-1002	SPS – Electrical BTE (propulsion system test sets)
862-CP-1003	Certification of SPS pressure test console
862-CP-1004	Validation of spacecraft propulsion subsystem service cart at Fairchild after Cape Kennedy operations
862-CP-1005	SPS nonmetallic, low-pressure pressurization manifold assembly and proof test
862-TP-1110	SPS leak and electrical tests test procedure
862-TP-1111	TSM SPS pre/post-vibration test operations
862-TP-1112	Procedure for pressurization of SPS to support spacecraft tests
862-TP-1155	SPS latch valve, thruster valve, leak test and flow verification
862-CK-1044	Leak check of SPS at Launch Complex 40 (also for post-vibration and preship test)
862-CK-1051	Prelaunch loading of SPS with hydrazine and pressurization to flight pressure with gaseous nitrogen
862-CK-1072	Inspection and validation of spacecraft propulsion subsystem service cart and hose sets at Cape Kennedy
862-CK-1073	Hydrazine cart servicing at Cape Fuel Storage Area #1

Number* (cont)	Title (cont)
862-CK-1074	Hydrazine sample and analysis at Fuel Storage Area #1
862-CK-1075	Transport loaded hydrazine cart from Cape Fuel Storage Area 1 to Launch Site Complex 40, Level 10 of MST
862-CK-1076	Receiving inspection and validation of SPS pressure test console, pressure hose set, and electrical bench test equipment
862-CK-1078	SPS hydrazine service cart decontamination
862-CK-1094	SPS spacecraft off-loading procedure

*Note: PS = Process Specification TP = Test Procedure
CP = Certification Procedure CK = Cape Kennedy (Procedure)

In addition, there were many procedures generated for specific operations such as "Procedure for Repair of Open Circuit in Thruster Valve Position 13 (S/N 121) on FI-SPS" (862-PS-3017). Essentially all planned or unplanned work on the propulsion subsystem during spacecraft test flow was documented with written procedures.

ANALYTICAL BASELINE

Study reports, test data analyses, laboratory investigations, and recommendation memos formed the analytical documents that supported implementation of the propulsion subsystem design. They can be grouped in five areas: reliability, performance, structural design, thermal sizing, and electrical interconnection.

Considerable effort was expended in determining component arrangement to provide a functionally redundant subsystem. All orbit and attitude control thrusters and thermal control circuits had back-up elements, with all elements commanded by independent circuits. While each of the two tanks contained only one-half of the mission budget (with margin), either could be isolated in case of failure, allowing the mission to continue with reduced capability.

Operation and performance of the thrusters and of the integrated feed/thruster subsystem was analyzed in detail to ensure compatible operation of the 0.445-N thrusters with the blowdown feed system. The analytically determined duty cycles (derived from planned spacecraft maneuvers) along with postulated thermal and vibration conditions were then used in specifying the qualification and acceptance test programs. The dynamics of filling evacuated manifolds was investigated to ensure the existence of benign water-hammer effects.

Detailed structural analyses were made of all critical mechanical elements including the thruster-valve assembly, tank-mounting tabs, the feed-components support plate, the orbit control thruster-manifold-support bar assembly, and the subsystem spacecraft attachment interface.

Considerable effort was expended on thermal analyses including the thruster assemblies for steady-state, pulsing, and soak back conditions; the thrusters mounted on the Earth-viewing module to ensure they did not require heaters; and the complex Sun-shadow environment of the externally mounted orbit control thrusters. The latter analyses formed the basis for the complex orbit-control jet thermal control assembly that included copper conductor wires around the propellant lines, full length line heaters, multiple temperature sensors, and superinsulation blankets. The level of detail of the thermal studies included, for example, temperature profiles along the thruster capillary feed tube under pulsing and steady-state conditions. These temperature profiles would identify flow conditions possibly leading to pulse decay.

The original design had pairs of opposed orbit-control jet thrusters on each side of the spacecraft, with the inward facing thrusters of each pair exhausting over the antenna farm on top of the Earth-viewing module. Questions of heating of antenna elements and of plume forces generated on the reflector mesh by the outward facing thrusters were raised and a subcontracted plume analysis was let to Lockheed Missile and Space Company at their Huntsville, Alabama, operation. The sizable distances between the east-west thrusters, the antenna, and the reflector produced insignificant analyzed levels of heating and force moments during thruster operation. However, distrust of such analyses led to a decision to turn the inward facing thrusters 180 degrees, which produced the final east and west parallel sets on each side of the spacecraft. This arrangement had less than full redundancy, and when subsequent orbital operations required both eastward and westward maneuvering with a single half-system, the spacecraft had to be yawed 180 degrees to accomplish thrusting in either one or the other of the two directions.

The electronic circuits controlling and monitoring propulsion system functions were analyzed by Honeywell as part of their attitude control subsystem subcontract. They also reanalyzed particular control circuits following the heater failures discussed in Chapter 8. A qualitative analysis of harness interconnect requirements resulted in an electrical interface control drawing subsequently used as a functional and wiring checklist.

DEVELOPMENT TESTING

Development tests that confirmed the design and investigating problem areas will be outlined in four groups: components, the engineering model, orbit-control jet assemblies, and special tests.

A number of components, some of which were used in the engineering model, were subjected to life/cycle tests to establish confidence that the subsystem would successfully complete qualification. The following are abbreviated summaries of these tests.

A titanium propellant tank containing an EPT-10 elastomeric diaphragm was pressure cycled between 4.4 psi and 385 psi 2025 times at a rate of 90 cycles per hour. External leakage was zero before and after the test, while internal leakage (across the diaphragm) decreased from 4.0 to 3.5 standard cubic centimeters per hour (scc/hr) of gaseous nitrogen.

A latching isolation valve was "dry" cycled open and closed 100,223 times at 10 cycles per second (cps) while pressurized with nitrogen at 21.09 kg/cm^2 (300 psi). The internal leakage across the seat decreased from 0.06 to zero scc/hr (of helium).

A thrust chamber valve was tested at the vendor's facility through one million cycles with a resultant increase in leak rate from 0.0 to 0.16 scc/hr helium. The specified leak rate was 1.6 scc/hr.

A catalyst bed heater was energized for 68 hours at 454°C and for 31 hours at 650°C. Post-test inspection revealed no change in resistance, cracking, or deterioration of wire.

A number of thruster assemblies, some rebuilt, were hot fired at Rocket Research under a variety of inlet and ambient conditions. Initial testing on thruster assembly serial number (SN) 005 accumulated 57.2 hours of steady-state firing and 30,000 pulses over a propellant temperature range from 4°C to 71°C. Thruster assembly SN 001A, used to determine the nozzle thrust characteristics, accumulated 50 hours of steady-state firing. SN 002C provided further thrust data and accumulated 70,000 warm (bed heater activated) starts at various duty cycles and 30,000 pulses at 1 cps. SN 003A was subjected to 20,000 pulses at 4°C and confirmed the cold start capability of the thruster. Figure 6-1 shows SN 042 during abbreviated tests at Goddard Space Flight Center to provide additional confirmation of steady-state and pulse performance.

The engineering model, a half subsystem consisting of a single-feed tank and eight thrusters with a layout, valve arrangement, and manifold like the flight design, was put through a full mission prequalification test. The eight thrusters were given performance baseline firings and the tank/feed control subassembly was given a qualification-level vibration test before integration into the model. The vibration test revealed several weak brackets supporting the pressure transducer and fill and drain valves that required modification.

The engineering model test consumed 49 kilograms (kg) of hydrazine for a total impulse of 94,058 N·s. An orbit control thruster (No. 7) ran 24 hours steady-state and it and its backup (No. 8) were subjected to 500 pulses (90 seconds on, 300 seconds off) to demonstrate short burn capability. The attitude control thrusters accumulated in excess of 37,500 pulses, and in all cases the thrusters were within specification performance and showed no increase in chamber pressure roughness.

The test sequence was as follows:

- Proof, leak, and electrical check
- Performance baseline
- Cold soak at -10°C
- 24-hour thermal vacuum soak/firing at +5°C
- Thermal vacuum at +50°C
- Performance mapping
- Mission simulations
- Leak and electrical check.

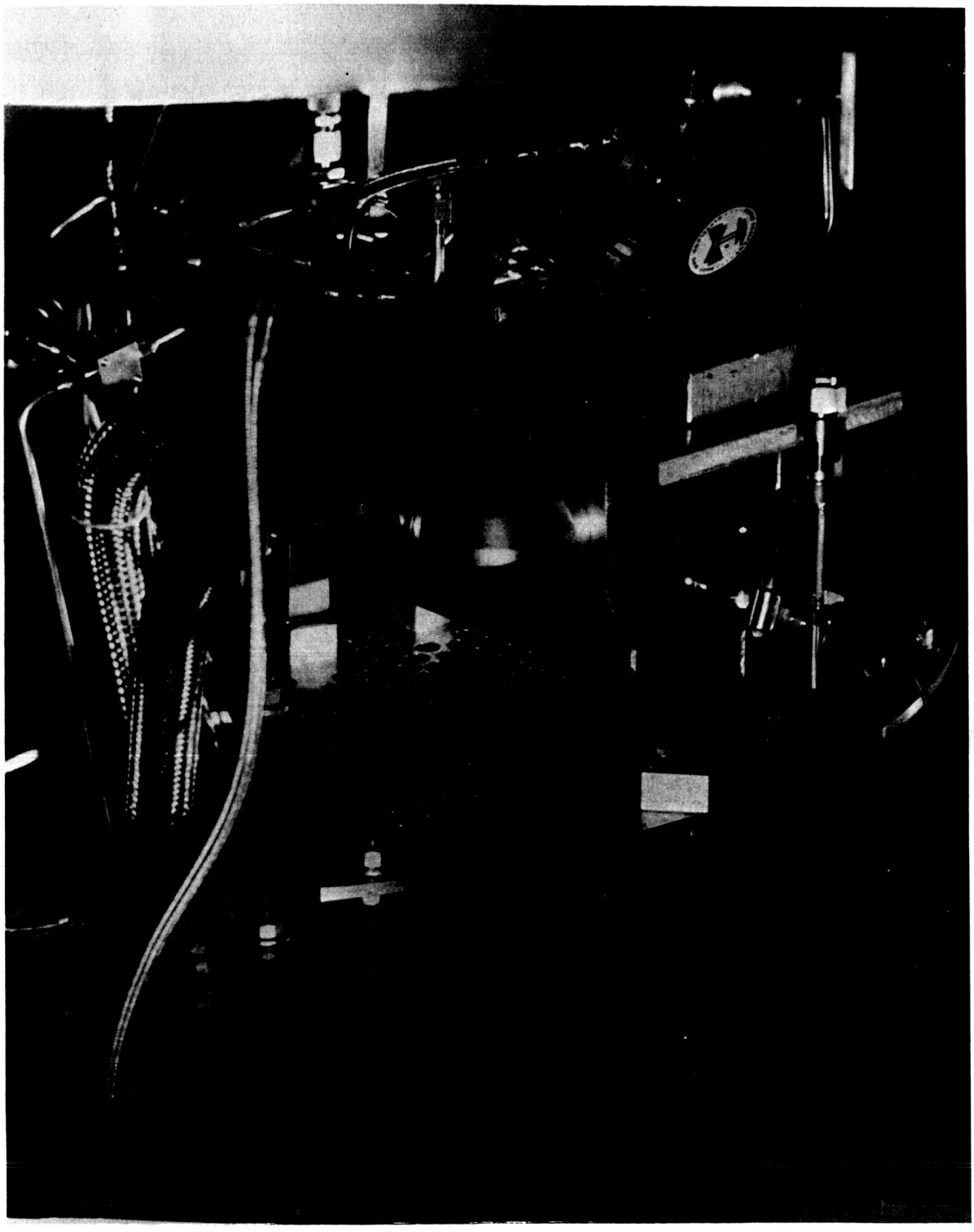

Figure 6-1. SN 042 Thruster Assembly Test at Goddard Space Flight Center

The problems that surfaced during the engineering model test were either minor or were investigated through analysis or by further development tests.

A critical area was design of the externally mounted orbit-control jet assemblies. Two high-fidelity models were fabricated to prove thermal control and structural capability. Figure 5-9, Chapter 5, shows another view of the thermal model partially assembled with its four thrusters and insulated feed manifold. Figure 6-2 shows an orbit-control jet bar configuration mounted for vibration testing, illustrating the fiberglass standoffs supporting the wrapped manifold. Test results, indicating that the bar was too flexible, led to a redesign incorporating damping strips ("Rigidamp") on all four sides of the square bar. Subsequent model and spacecraft level tests of the design indicated good margin.

The thermal model is shown being prepared for test at Fairchild in Figure 6-3 (with a thermal louver). The same model was also tested at Goddard Space Flight Center under solar simulated conditions including: equilibrium hot and cold, transients with heaters on and off, and control using all temperature control unit command combinations. Additional vacuum testing confirmed adequate venting area in the superinsulation blankets.

Further ambient testing of the orbit-control jet thermal model and a single thruster/valve assembly (SN 042) at National Science Laboratories investigated the three areas of electromagnetic interference (EMI) and radio frequency interference (RFI). They were:

1. Rf field susceptibility (valves, leads and drives)

2. Conducted susceptibility (spikes and coupled audio)

3. Conducted emissions (valve transients).

Both the orbit-control jet thermal model and the thruster assembly were somewhat out of specification during several of these tests, suggesting that additional shielding wrap-around should be applied to the thermal control assembly. This was accomplished but, as discussed in Chapter 8, the bed temperature circuits remained susceptible to the rf fields generated by the communications subsystem. No effects due to spikes, coupled audio, or valve transients were noted during the mission.

A number of tests, grouped for convenience here as special tests, investigated a number of problems associated with the thruster assembly and the interconnect line between the feed assembly in the Earth-viewing module and the orbit-control jet thrusters.

Previous experience with tenth-pound thrusters launched with their nozzles up (i.e., in the launch direction) contained instances where catalyst fines had worked their way into and plugged capillary-size feed tubes. While none of the ATS-6 thrusters was so oriented, one of the development thrusters was vibrated under qualification level conditions to ensure that no such problem existed with the ATS thrusters. Pre- and post-vibration hot firing of the vibrated thruster produced the same performance.

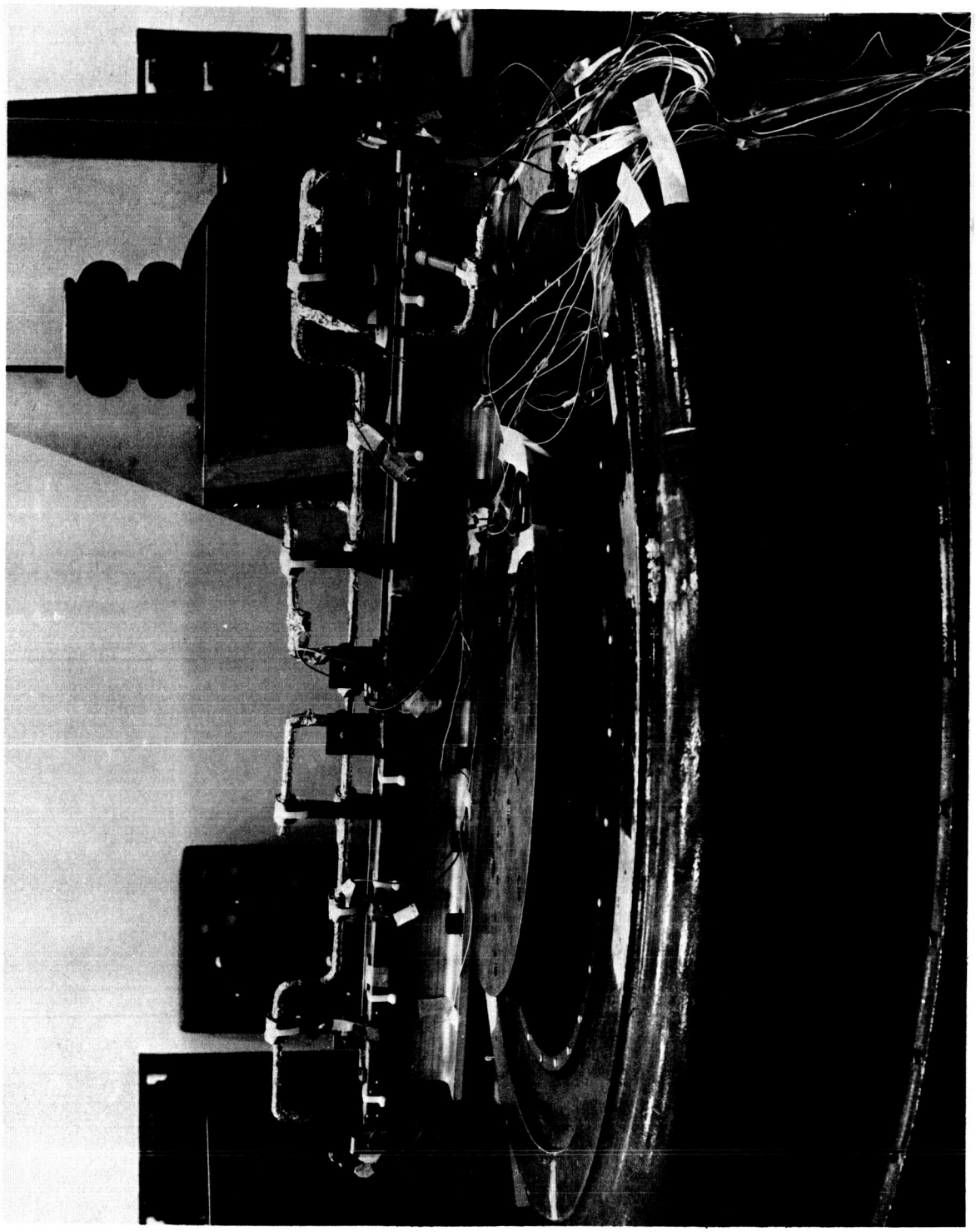

Figure 6-2. Orbit-Control Jet Structural Model Test

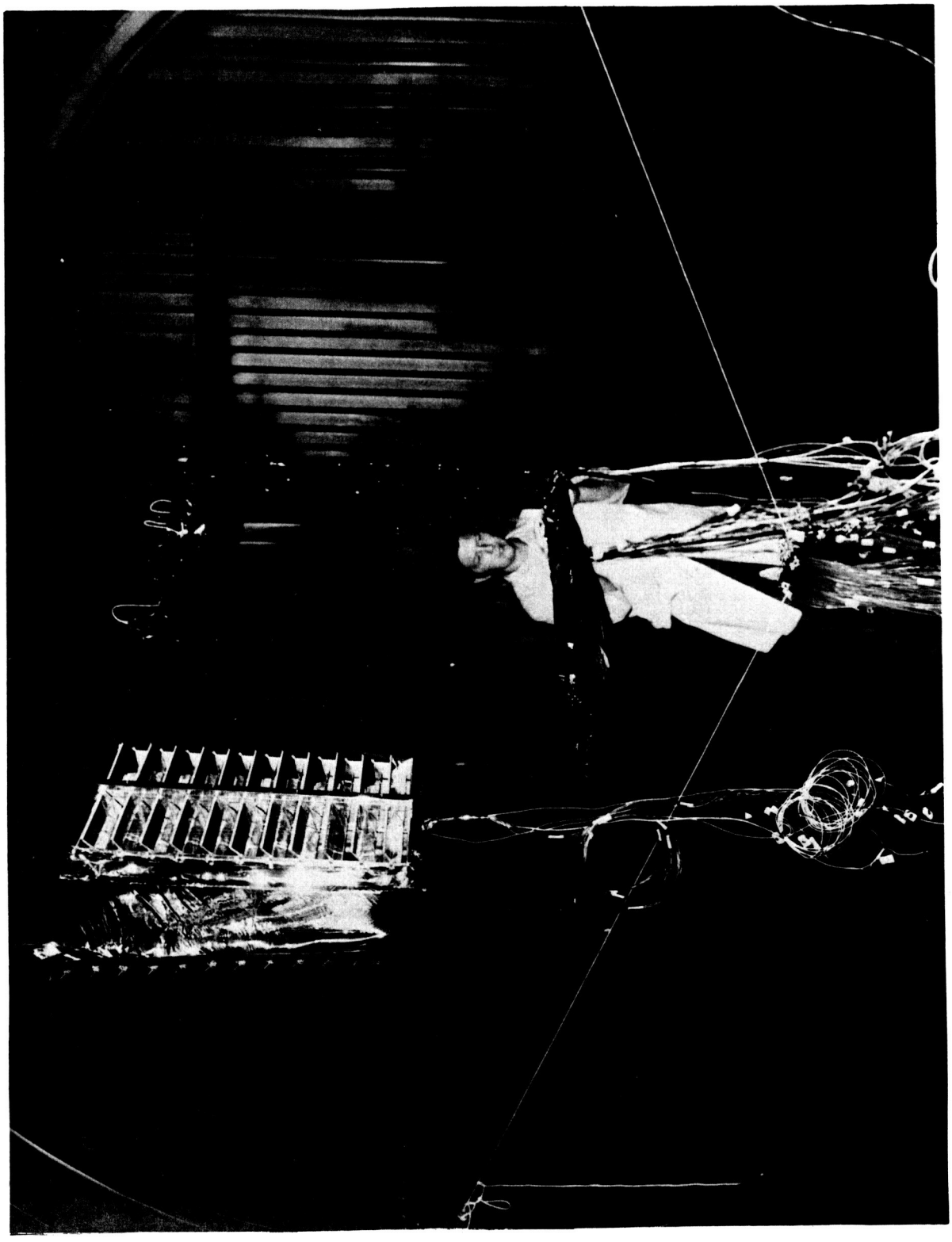

Figure 6-3. Orbit-Control Jet Thermal Model Test (With Thermal Louver)

Hydrazine, unlike water, contracts when it freezes and on remelting can produce large pressures if constrained by unmelted material. The orbit-control jet thrusters were of particular concern in this regard because of their exposed location. A thruster/valve assembly was filled with hydrazine and put through a number of freeze-thaw cycles, without actuating the valve, so that the hydrazine progressively froze and thawed from the valve (seat) end of the test setup toward the feed tube. Results indicated that the valve was unharmed after three cycles, but that the circumferential weld holding the armature/seat section to the midsolanoid section cracked between 3 and 9 cycles indicating that a valve heater failure in the orbit-control jet thrusters could lead to a major leak path. A heater failure, with freezing but without leaking, is described in Chapter 8 that addresses in-orbit anomalies.

The active element of the valve thermistor was embedded in multiple layers of epoxy and other plastics inside a steel body that was threaded for insertion in the valve body. There was some concern that differential expansion and contraction of the layers and shell could lead to failure of the sensing element. Thermal cycling of three thermistors between -96°C and 99°C for 100 cycles showed no change in thermoelectrical properties.

The thruster plume analyses discussed in Chapter 6 treated heating and force effects but not contamination from the thrusters. This latter effect is not usually important with hydrazine thrusters, except in the case of extremely cold surfaces found in proximity to the jets such as the Earth-viewing module north wall components and the roll jets. A high-fidelity mock-up was planned for test at the Lewis Research Center, including a quartz-crystal microbalance (QCM), the radiometer cooler, a Polaris sensor assembly, thermal louvers, and a number of surface material samples. However, problems with obtaining spare units, with the schedule, and the general complexity of the test setup led to a simplified and abbreviated test of a thruster with an array of QCM's as detectors. The data were somewhat variable but indicated an acceptable low level of back flow from the thruster and a good probability of no interference with cold surfaces on the north wall.

The last special test verified that the S bends, incorporated in the lines connecting the Earth-viewing module feed assembly with orbit-control jet thruster/manifold assemblies, could be straightened and rebent should any adjustment of the orbit-control jet assembly position be necessary to accommodate a shift in the center-of-mass of the spacecraft. A replica of the S-bend portion of the line was straightened (slight remaining curvature) and rebent three times, vibrated, and checked for any particulate contamination developed during the bending operation. No significant particulates were found and a pressure test at 1034 atm produced no deformation.

PROTOTYPE QUALIFICATION

The major effort in verifying acceptability of the spacecraft propulsion subsystem design for the ATS-6 was the qualification test of the prototype model at Rocket Research Company and its subsequent incorporation in the thermal structural model spacecraft and further thermal, vibration and launch-site compatibility testing.

The starting point for subsystem design was the selection of components with the required performance characteristics and a history of flight and/or development experience. Table 6-3 lists the propulsion components, their source, and an indication of previous usage on systems developed by Rocket Research Company and other programs.

Table 6-3
Component Source and History

Component	Vendor	History
Propellant Tank (2)	Pressure Systems, Inc.	Pioneer, HPM and ERTS
Latching Valve (7) (Filter)	Carleton Valve Co.	Intelsat IV
Thruster Valve (16) (Filter)	Parker Valve Co.	HPM (dual config.)
Fill and Drain Valve (4)	Rocket Research Co.	HPM, ERTS, Ranger
Tank Filter (2)	Vacco Industries	HPM and ERTS
Pressure Transducer (2)	Dynascience	Apollo LEM, HPM and ERTS
Thermistor (14)	Fenwall	REM Mono
Thermocouple (16)	American Std.	REM Mono
Thruster Heater (32)	Clayborn	HPM and ERTS
Valve Heater (8) (prime + backup)	Clayborn	HPM and ERTS

Legend: HPM – Hydrazine Propulsion Module
ERTS – Earth Resources Technology Satellite
REM Mono – Classified Satellite

The qualification program at Rocket Research required several months of effort and consisted of component, subassembly, and subsystem testing under qualification-level thermal and vibration environments for duty cycles and propellant throughputs beyond those required for the mission.

In addition, a thruster was subjected to a vibration test beyond the qualification levels because of uncertainties in the actual levels at the center of the orbit-control jet bar where the east-west thrusters were located. Strain-gage measurements during this severe test (2.3 inches double amplitude to 17 hertz (Hz) and 34 g's maintained to 25 Hz) indicated adequate margin existed in the design. Pre- and post-test hot firings showed no significant change in thruster performance variables. Another thruster valve, in addition to the development component, was subjected to a life-cycle test after the acceptance level vibration test. Functional tests following 10,000 dry cycles at 6 cps in nitrogen at 28.12 kg/cm^2 (400 psi) and a million wet cycles (water) at 6 to 12 cps at 28.12 kg/cm^2 (400 psi) agreed with pretest data. The post-test leak rate was zero.

The 16 thruster subassemblies used in the prototype subsystem were subjected to the normal acceptance test sequence involving functional, leak, vibration, and hot-firing baseline performance tests. In parallel, the tank/feed control subassembly was vibrated at sine and random qualification levels at Wyle Laboratories. Some fixture problems lead to notching of the Y-axis random test, but extensive strain-gage measurements at critical areas showed adequate structural margin. The three fundamental frequencies found were 165 cps (X), 185 cps (Y), and 185 cps (Z).

The total integrated subsystem was proof-pressure tested and then subjected to a lengthy series of functional and electrical tests and internal and external leak checks of all fluid components. The unit was loaded with hydrazine and combinations of thrusters were hot fired at three sets of steady-state and pulse-mode duty cycles at three feed pressures. The duty cycles consisted of a baseline set repeated throughout the test sequence, a duty-cycle set that thoroughly explored the limits of required mission duty cycles, and a mapping set that investigated those duty cycles sensitive to thermal effects.

The bare outline of the sequence of thermal vacuum temperature conditions and thruster firings was as follows:

Sequence	Temperature	Duty Cycle
1	21°C	Baseline
2	24-hr soak at 5°C	Duty cycle
3	5°C	Cold map
4	24-hr soak at 50°C	Duty cycle
5	35°C	Hot map
6	21°C	Baseline

The prototype was vacuum cycled among the four temperature levels in verifying subsystem design and performance using actual in-situ thruster firing data. Following the thermal vacuum test, electrical, leak, and functional tests were repeated. Analysis of test results showed that (1) thrust remained within 5 percent of the nominal blowdown curve over the qualification temperature range; (2) impulse bit values were linear with feed pressure; (3) EVM thruster-to-thruster repeatability (at 21°C) of impulse bit (I_{bit}) was ±7.4 percent maximum and of centroid time was ±8.1 percent maximum; and (4) the same criteria for the truss thrusters (at 43°C) were ±16.5 percent maximum and ±12.8 percent maximum, respectively.

Following the full vibration and thermal qualification test in Redmond, Washington, the subsystem was shipped to Fairchild where it was integrated into the spacecraft thermal structural model and subjected to further vibration and thermal testing as the thermal structural model was used to verify overall spacecraft design.

As a means of shortening the schedule and reducing costs, it was planned that ATS-6 would be given a brief checkout on arrival at Cape Kennedy and then integrated with the Titan III-C launch vehicle on the gantry where the prelaunch sequence, including flight fueling, would take place.

To ensure that such planning would work out in practice, the thermal structural model was shipped to Florida and put through the same sequence. Propulsion subsystem related operations during this activity were as follows:

1. Bench test equipment checkout

2. Hydrazine service cart checkout

3. Hydrazine shipment and analysis
4. Hydrazine cart loading at propellant storage area
5. Transport cart to level 10 on Launch Complex 40
6. Leak and electrical test of the subsystem in Hanger AE (transport the thermal structural model to Launch Complex 40 and integration to Titan III C launch vehicle)
7. Fluid/electrical hookup of the propulsion subsystem (in thermal structural model)
8. Flight load of hydrazine in the subsystem
9. Unload and decontaminate the subsystem
10. Decontaminate hydrazine cart.

The results of this practice checkout and propellant loading operation were very successful in bringing to light a number of problems that resulted in several changes as follows:

1. The fill and drain lines incorporating sample valves were modified to eliminate possible traps for contaminates as indicated by several particle counts that were out-of-specification.
2. The "scupper" design (drip collectors under the fill and drain valves) was modified to simplify line hookup.
3. Variations in the results of propellant chemical analyses performed at Rocket Research and at Cape Kennedy led to a thorough study of analytical methods and a tightening of requirements for the propellant to be used in the flight load.
4. Increasing thruster valve-leak rates took a dramatic jump following decontamination of the subsystem, prompting a major review of leak rates during the program and removal of one orbit-control jet manifold/thruster assembly on Launch Complex 40 (LC40) for shipment to Rocket Research to be part of an experimental investigation into the cause of the leaks.

Other more minor operational problems and anomalies were noted for correction prior to the ATS-6 operations a year later.

The thermal structural model was subsequently shipped to Houston, Texas, for vacuum deployment tests of the reflector and on to Germantown, Maryland, where other fluid components were removed to become part of the leak investigation. Few propulsion systems received such extensive qualification testing as that experienced by this subsystem.

GENERIC CONCERNS

During the development and qualification test programs, three areas became of critical concern as they could affect thruster operation and performance. They were: (1) control and measurement of particulate contamination in the fluids entering the system and in the system components themselves; (2) prevention and measurement of internal valve leakage (through the valve sealing interface; i.e., poppet/seat interface); and (3) measurement of chemical contaminants in the propellant.

Contamination control was a concern from the beginning and all fluids, including water, isopropyl alcohol, hydrazine, nitrogen, and helium were filtered, sampled, and counted for particulate contamination before introduction into the subsystem each time a new fluid hookup was made. All fluid equipment including lines, hoses, fittings, and the service cart, were liquid-flush cleaned and certified better than the following limits expressed as maximum allowed number of particles (of a size range in micrometers):

Size Range (μm)	Maximum Number Particles Allowed	Note
5 to 10	460	–
11 to 25	128	–
26 to 50	10	–
51 to 100	2	No metal
101 and greater	0	–

In general, the procedures and precautions for particulate contamination control were very effective and only in a few instances was it necessary to reclean or impose extra through flushing to reduce particle counts to values within specification.

As alluded to in the description of the qualification program, thruster and latch valves developed sizable leaks in the prototype and to a lesser degree in the flight units.

The original maximum allowed leak rate across thruster and latch-valve seats was 1.8 scc helium per hour at 272 atm. Toward the end of the program this was increased to 6.0 scc helium/hour at the spacecraft level. The flight subsystem was launched with leak rates for a latch valve and three thrusters valves at 18, 9, 10 and 15 scc helium/hour, respectively.

Seat leakage can be due to a number of causes, including wear, poor design, particulate contaminates or chemical contaminants generated within the system. Valve-leak rates in the prototype subsystem had progressively increased to a point where an extensive investigation into the cause was undertaken. As indicated above, components were removed and cut apart and chemical tests on residues, microscopic examination of parts, electron beam microprobe analysis, and synthesis of similar materials confirmed that the contaminants were iron, chromium, and nickel carbazates containing smaller amounts of metallic oxides. Carbazates are easily formed from the reaction of hydrazine and atmospheric carbon dioxide.

Each of the assembled units had been loaded with hydrazine, and their thrusters fired during acceptance testing. After unloading any remaining fuel, the subsystems were flushed with water and alcohol and vacuum dried. However, because of lack of information concerning the effect of flush fluids on the catalyst bed, the process did not include through flushing of the valves. The operations described with the prototype propulsion subsystem in the thermal structural model also involved partial disassembly to turn the inward pointing east and west thrusters around to avoid impingement on the antenna elements and repeated checks for leaks. These operations exposed subsystem elements to the atmosphere. The development of sizable leak rates in the subsystem were attributed to the consequent formation of carbazate contaminants. The two flight units experienced considerably reduced exposure to the atmosphere and had fewer leaks at much lower levels, as shown in Table 6-4.

The results of these effects and other internal reactions in the spacecraft propulsion subsystem during the flight of ATS-6 are described in Chapter 8 on anomalies and failures.

Propellant was procured to MIL-P-26536C, but additional detailed analyses were made of all drums and off-load samples from the service cart and the prototype and flight-ready subsystems. A full analysis of the flight load indicated: hydrazine (N_2H_4), 98.9 percent; water (H_2O), 0.6 percent; ammonia (NH_3), 0.1 percent; unsymmetrical-dimethyl-hydrazine (UDMH), 3 ppm; monomethyl-hydrazine (MMH), less than 40 ppm; aniline, 0.4 percent; nonvolatile residue, 7 ppm; particulate (1 mg/1) corrosivity, 5 ppm (iron); chloride, 0.5 ppm; and total organics, isopropyl alcohol, toluene, etc., 33 ppm. These values were well within acceptable limits. During the analyses, considerable discussion arose concerning the gas chromatographic method for monomethyl-hydrazine and unsymmetrical-dimethyl-hydrazine. Different column sizes, packing and detectors (thermal conductivity and flame ionization) used at the Air Force Eastern Test Range, Rocket Research Company, and Olin Manufacturing led to varying sensitivities and results. This problem was never fully resolved and is an area requiring further study. Propellant purity is discussed further in Chapter 8.

GROUND SUPPORT EQUIPMENT CERTIFICATION

It should be noted that all service equipment used with the propulsion subsystem passed approved certification test procedures. This included mechanical fixtures and support equipment, the hydrazine service cart, the electrical test set, electrical breakout boxes, the pressurization panels, flow meters and interconnect hose sets, and wire harnesses.

FLIGHT UNIT ACCEPTANCE

The flight subsystem for ATS-6 followed a test sequence similar to that of the prototype but at acceptance environmental levels.

Component acceptance tests, tank/feed assembly vibration tests, and thruster assembly baseline performance firings were completed before integration into a subsystem. The series of proof, leak, and electrical tests then established a pre-environmental baseline of data.

Table 6-4

Valve Leak Data (scc/hr helium @ 27.2 atm, 400 psig)

Thruster Control Valve	Prototype				Flight				Flight Spare	
	RRC	FI	POST-VIB	KSC	RRC	FI	SC	KSC	RRC	PRE-SHIP
1	0 0	0	0	0 0	0 +	+	+	+	0 0	0
2	0 0	0	0	0 0	0 0	0	+	+	0 0	0
3	0 0	0	0	0 0	0 0	+	11	9	0 0	+
4	0 0	0	0	0 0	0 0	0	0	0	0 0	0
5	0 0	0	0	0 0	+ 0	+	0	0	0 +	+
6	0 0	+	+	0 0	0 0	0	0	0	0 0	0
7	0 0	0	0	0 0	0 0	0	0	0	0 0	73
8	0 0	0	162	41 0	0 +	+	+	+	+ 0	0
9	0 0	0	0	0 0	0 0	+	+	+	0 0	0
10	0 0	0	0	0 0	0 0	+	+	+	+ 0	0
11	0 7	0	0	0 0	0 +	+	8	10	+ +	0
12	0 0	+	8	41 9	0 0	0	+	+	0 +	0
13	0 0	+	16	11 9	0 0	0	0	0	17 16	7
14	0 0	0	108	270 324	0 0	0	0	0	0 0	0
15	0 0	+	0	+ +	0 0	+	0	0	0 0	0
16	+ 0	+	+	+ +	+ 0	14	10	15	0 0	0
Latch Valve										
1(T)*	0 28	564	32	201 3000	0 0	0	0	0	0 0	NA
2(OCJ)	0 0	0	0		0 0	0	0	0	0 0	NA
3(EVM)	0 0	0	180	155 20	0 0	0	+	18	0 0	NA
4(F)	0 0	1630	+	+ +	0 0	+	+	+	0 0	NA
4(R)	0 0	2060	29	25 7	0 0	0	0	0	0 +	NA
5(T)	0 +	0	14	12 14	0 0	0	0	0	0 0	NA
6(OCJ)	0 0	0	+	+ 53	0 0	0	+	+	0 0	NA
7(EVM)	0 0	0	+	+ +	0 0	0	0	0	0 0	NA

* T = Tank, F = Forward, R = Reverse

Note: 0→1 = 0
1→6 = +
>6 = actual scc/hr helium @400 psig

The sequence of the thermal vacuum test with thruster performance firings was as follows:

Test	Temperature	Duty Cycle Set
1	21°C (70°F)	Baseline
2	24 hr soak @ 5°C (41°F)	Duty cycle
3	5°C (41°F)	Cold map
4	24 hr soak @ 45°C (113°F)	Duty cycle
5	45°C (113°F)	Hot map
6	21°C (70°F)	Baseline

The test data and post-test checks were within those limits established by the prototype and specifications. The flight unit was decontaminated, cleaned, and packed for shipment to Fairchild. The subsystem was acceptance inspected upon arrival and subsequently integrated with the flight spacecraft. The various procedures completed at the integrated spacecraft level were listed on page 149. Figure 6-4 shows the flight tank/feed assembly integrated in the Earth-viewing module and ready for initial checkout using breakout boxes. Protective covers for one of the tanks, fill and drain valves, a pair of pitch thrusters are seen and (on the right) the interconnect propellant line and electrical harness (up) to the orbit-control jet manifold/thruster assembly. The electronics box in the upper left quadrant of the Earth-viewing module is the actuator control electronics unit that controlled the space propulsion subsystem (and wheels).

Following a full environmental vibration and thermal vacuum test sequence at Fairchild and Goddard, the spacecraft was flown to Cape Canaveral on a C-5A aircraft and, except for limited mechanical operations on the transporter, was taken directly to LC40 and mated to the Titan III-C launch vehicle. Propulsion subsystem leak and electrical checks were performed as part of the overall prelaunch flow, using the electrical test set and propellant cart on level 10 of the gantry.

The propellant loads for tanks 1 and 2 were 25.2 and 24.9 kg. Instability in the service cart digital-weight scale readout prior to the final loading procedure prompted a checkout of its electronic circuits but resulted in no permanent solution. A year after launch a number of loose pins were found in the digital assembly connector.

During tank pressurization for leak tests at Fairchild, it had been noted that the rise in tank temperature was evidently more than was indicated by the tank-temperature thermistor at the liquid outlet. As a result, a ground-test thermistor was bonded to the "gas side" of the tank to allow a more accurate flight pressurization. Tanks 1 and 2 were pressurized to 26.01 kg/cm^2 (370 psi) and 26.43 kg/cm^2 (376 psi) at 20°C using these sensors. Their leads were cut before launch and the liquid-side thermistor was used for in-flight sensing.

The spacecraft was launched on May 30, 1974, and the operation, performance, and anomalies of the spacecraft propulsion subsystem are described in subsequent sections.

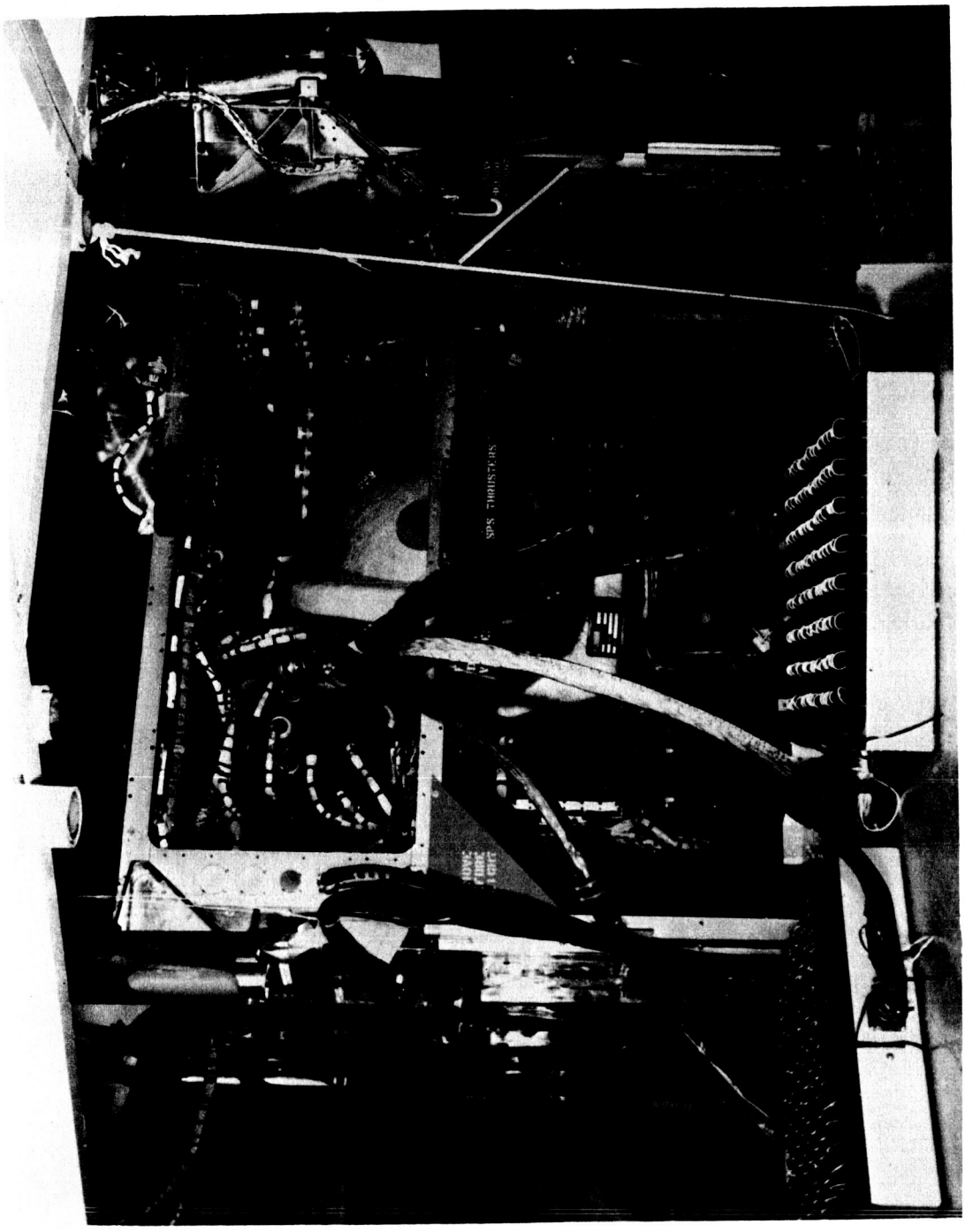

Figure 6-4. Flight Unit Tank/Feed Assembly Integrated with the EVM

EPILOGUE

Of interest, in light of the extensive qualification and acceptance program outlined above, is the fact that there were less than fifty malfunctions/failures serious enough to be reported (per Goddard Space Flight Center procedures).

The following list summarizes them in eight categories with an abbreviated explanation:

Type	Number	Note
Thruster valve leakage	18	>1.8 scc/hr helium
Latch valve leakage	5	>1.8 scc/hr helium
Low performance	6	Specific impulse (I_{sp}), bit impulse (I_{bit}), chamber pressure (P_c) valve response, latch valve relief pressure
Mechanical failure	5	Bed heater leads, panel inserts, loose latch valve indicator
Mechanical damage	3	Minor tank surface gouge, fill/drain valve needle and nose
Electrical failure	4	Thermocouple no signal, pressure transducer overvoltage, valve thermistor
Wiring error	1	Bed thermocouples
Test equipment failure	5	Accelerometer, overlevel, valve
Total	47	

Hindsight suggests that the development, qualification, and acceptance test programs for ATS-6 were more than fully adequate to verify the design. Unfortunately, the program contained a flaw that eventually cut short subsystem life. It was the subsystem level fueling and thruster firing tests that undoubtedly played a substantial role in the process that led to in-orbit thruster degradation and failure, stopping the mission after five years of extremely successful operations.

CHAPTER 7

ORBITAL OPERATIONS AND PERFORMANCE

INTRODUCTION

Following the successful lift-off on May 30, 1974, aboard a Titan III-C launch vehicle, the ATS-6 propulsion subsystem performed the required tasks of initial orbit acquisition and trim, east-west stationkeeping, wheel momentum unloading, station repositioning, and backup attitude control. System operation and performance level, overall propellant consumption history and thermal control during these various mission operations are discussed in the following paragraphs.

The discussion begins with the launch and ascent operation, including the initial orbit acquisition maneuvers, followed by typical wheel unloading cycles and a discussion of all 67 orbit control burns. Propellant, pressure, and temperature histories follow, and the chapter is concluded with an in depth discussion of the final de-orbit and depletion burns. During the presentation of the data, only passing reference to the various component anomalies and failures will be made. Their full details are presented in Chapter 8.

ASCENT AND ACQUISITION

The propulsion subsystem was launched with the Earth-viewing module latch valves, truss latch valves, and interconnect latch valves closed, the tank latch valves open, the prime valve heaters on, bed heaters off, and prime and backup line heaters on low automatic. During ascent, line temperatures warmed as predicted and soon after arriving in orbit, the thermostats established a 24-hour on/off cycle.

The spacecraft separated from the transtage with rates of about 0.1 degree per second in all three axes. Following deployment of the solar arrays and reflector, the attitude control subsystem and spacecraft propulsion subsystem (SPS) were activated and the SPS-1 lines, downstream of the latch valves, were evacuated and filled with propellant. Wheels and jets were then used for Sun, Earth, and Polaris acquisition, consuming 0.65 kg of hydrazine. Subsequent full reacquisitions have been more efficient, consuming only 0.14 to 0.18 kg of propellant.

Prelaunch/Launch

Launch configuration of the spacecraft propulsion subsystem is illustrated in Table 7-1.

The tank pressures at launch were 26.08 kg/cm^2 (371 psia) and 26.50 kg/cm^2 (377 psia) nitrogen gas at 20°C. Temperature telemetry was checked periodically from the time the tanks were loaded with hydrazine on May 18, (25.2 kg in Tank 1 and 24.9 kg in Tank 2) until launch. The prelaunch data indicated anomalous telemetry values for the SPS-2 orbit-control jet bed temperatures.

Table 7-1
Launch Configuration

	SPS-1 On and In Control	SPS-2 On
EVM Latch Valves	Closed	Closed
Orbit-Control Jet Latch Valves	Closed	Closed
Cross Latch Valve	Closed	
Tank Latch Valves	Open	Open
Valve Heaters	Prime On	Prime On
Line Heaters (prime and backup)	Low Automatic	Low Automatic
Bed Heaters	Off	Off
Ground Control of Jets	Enabled	

The predicted warming trend of the SPS propellant lines and thruster valves due to the decrease of atmospheric pressure was observed during the ascent phase. All line heaters were on at launch; the SPS-1 and -2 backup heaters went off at T+2:30 and T+2:45 hours and the prime heaters went off at T+2:46 and T+3:32 hours. The prime heaters came back on within a half-hour and stayed on for one hour. This cycle was repeated before separation. Once in-orbit operations began, the primary heater on-and-off times increased to 12 hours on/12 hours off for SPS-1 and 16 hours on/8 hours off for SPS-2, while the backup heaters had a much shorter duty cycle. The different on times were due to the different daily Sun-shadow patterns on the two half subsystems.

Tank pressure remained steady throughout the ascent while cat-bed temperatures varied as a function of Sun angle and Earth shadow.

Line Evacuation/Propellant Bleed-In

In preparing the SPS-1 for jet operation, the 0.67 atm nitrogen in the EVM and orbit-control jet manifolds downstream of the EVM and truss-latching valves was evacuated. The method was to be automatic by commanding the attitude control subsystem to Sun-acquisition mode using jets before the latch valves had admitted hydrazine to the jet manifold lines, thereby producing attitude errors to open roll, pitch, and yaw jets. However, only roll and pitch errors were large enough to activate the appropriate thruster valves, so that only the manifolds within the EVM were evacuated. It was necessary to command open the No. 7 jet (prime westward) for 5 minutes to accomplish evacuation of the orbit-control jet manifold.

The SPS-1 EVM and truss-latch valves were then opened, bleeding propellant into the manifolds. The initial tank-1 pressure drop seemed excessive at latch valve opening, but a closer estimate of the internal manifold volumes of 206 cc, equivalent to 0.21 kg of hydrazine, accounted for the 0.4 atm pressure drop from 25.2 to 24.8 atm (26.08 kg/cm^2 [371 psia] to 25.66 kg/cm^2 [365 psia]).

The evacuation and bleed-in of SPS-2 was to be delayed for 1 day to assess in-orbit temperature cycling before allowing hydrazine into the backup system. Evacuation was then to be accomplished by commands from the ground to roll, pitch, and the eastward prime thrusters. However, as a thermal safety measure, SPS-2 propellant bleed-in was not done until the backup system was actually needed.

Spacecraft Acquisition Maneuvers

Table 7-2 lists the total jet on times for the three axes for each maneuver during the initial acquisition covering May 30 to May 31, 1974, and the reacquisition maneuvers on June 10, 1974. The length of individual jet firings was distributed as shown in Table 7-3.

The on times were fairly long with most firings over 10 seconds. Because of this, an average specific impulse of 2060 N·s/kg was used in calculating the quantities of propellant used. The reacquisition did not require a Polaris (yaw) maneuver, but even if fuel were added to account for it, the amount of fuel used was significantly less (by a factor of 4) than during the initial acquisition.

Table 7-2
Acquisition Jet Usage

Initial Acquisition:	Roll		Pitch		Yaw		Total On Time, (sec.)	Wt* Propellant, (kg)	(lb)
	+R	-R	+P	-P	+Y	-Y			
Sun (sec)	131	50	166	94	220	35	696	0.18	0.40
(GMT)	(150:21:10 to 16:00)		(21:10 to 21:19)		(21:10 to 21:21)				
Earth (sec)	737	759	81	105	0	0	1682	0.44	0.96
	(150:23:10 to 24:02)		(23:18 to 23:20)						
Yaw (sec)	0	0	0	0	75	45	120	0.03	0.07
					(151:01:46 to 02:20)			0.65	1.43
Reacquisition:									
Sun (sec)	9	0	51	69	108	186	423	0.11	0.24
(GMT)			(161:11:48 to 12:01)						
Earth (sec)	39	87	0	6	0	24	156	0.04	0.09
			(161:12:01 to 13:11)					0.15	0.33

*Jet thrust = 0.53 N (0.12 lbf)
Specific Impulse = 2060 N·s/kg (210 s)

Table 7-3
Distribution of Jet Firings

Jet On Time, sec	Number of Jet Actuations	
	Initial Acquisition	Reacquisition
200	1	0
100 to 200	3	0
75 to 100	9	0
50 to 74	5	4
25 to 49	7	5
10 to 24	14	1
4 to 9	34	20
0 to 3	13	29

Initial Orbit Correction

The highly accurate orbit attained by the Titan III-C transtage required only small corrections by the SPS. In general, the spacecraft was west of the desired 94°W station with a small westward drift. Two correction firings of jet No. 7 were initiated on June 6 and 7, 1974. The first was an 8-minute calibration firing followed the next day by a 31.5-minute run.

Table 7-4 shows the pertinent data. The deviations between the calculated correction and the actual orbit change were very small as follows:

	Measured Deviations	
	1st Burn	2nd Burn
Drift rate, deg/day	0	0.0011
Semimaj. axis, km	0.196	0.30
Eccentricity	0.0001	0.000044
Inclination, deg	0.0004	0.0002
RA node, deg	0.06	0.06
ΔV, m/sec (ft/sec)	0.0003 (0.001)	0.007 (0.024)

The No. 7 orbit-control jet thrust vector is canted in the -Y direction above the spacecraft center-of-mass causing minus pitch jet components. The No. 3 (-P) jet contributes about 2.4 percent of the total orbit correction impulse (approximately equal to duty cycle); first burn = 2.1 percent, second burn = 2.4 percent (Table 7-2). The theoretical duty cycle calculated from the ratio of No. 7 and No. 3 (-P) jet moment arms about the spacecraft center-of-mass is 1.7 percent. Uncertainties in

Table 7-4
Initial Orbit Correction

	Burn #1		Burn #2	
	Start	Stop	Start	Stop
Orbit Data:				
Semimaj Axis, km	42186.4	42181.2	42180.9	42160.7
Eccentricity	0.0007	0.0006	0.000624	0.000156
Inclination, deg	1.749	1.748	1.748	1.748
RA Node, deg	266.12	266.06	266.06	265.97
Drift Rate, deg/day	0.271 W	0.203 W	0.205 W	0.0536 E
Subsatellite Long., deg	96.45	96.44	96.52	96.53
Spacecraft Wt., kg (lb)	1347.6 (2971.0)	1347.5 (2970.7)	1347.5 (2970.7)	1347.0 (2969.7)
Jet #7 Duration, s	480		1888.4	
ΔV, m/sec (ft-s)	0.19 (0.63)		0.74 (2.42)	
Wp, kg/(lb)	0.12 (0.27)		0.46 (1.01)	
Thrust, N (lbf) (ave)	0.54 (0.122)		0.54 (0.122)	
Tank 2 Press, atm (psia)	24.4 (359.4)	24.1 (355.4)	24.3 (357.4)	23.5 (345.4)
Tank 1 Temp.°C	26	25	26	25
Remaining Fuel, kg (lb)	24.6 (54.2)	24.5 (54.1)	24.5 (54.1)	24.1 (53.1)
AC Jet 1-sec Pulses				
-Pitch [I, N·s (lb-s)]	103 [5.43 (1.22)]		460 [24.1 (5.42)]	
+Yaw	2		43	
-Roll	0		15	

location and cant angles of the jets, center-of-mass location and jet impulse all contribute to the difference.

The total fuel used for the orbit correction was 0.58 kg, while 0.65 kg was used for reference attitude acquisition. A total of 9.62 kg had been allocated for these maneuvers, thus providing an extra reserve of 8.39 kg (18.5 lb).

WHEEL MOMENTUM UNLOADING

A two-day roll wheel momentum unload cycle was established early in the mission, during which the constant momentum buildup and exchange increased yaw and roll wheel speeds to a point where they approached the established speed limit of ±1200 rpm. Figure 7-1 illustrates a cycle typical of any on-station, two-day period with a minimum of offset maneuvering. When enabled by ground command, unloading was done automatically by the attitude control subsystem using roll jets (nearly equal to twenty 0.2/10 pulses) to reduce roll wheel speed when the yaw speed was near zero.

Manual command unloading was also tried to reduce roll wheel speed below 300 rpm, resulting in the 4-day cycle of Figure 7-1. A number of manual operations were performed at yaw speeds around zero to reduce cross-coupling. It was concluded, initially, that the reduced number of unload operations did not justify the greater complexity associated with manual unloading. However, this unloading technique later became the standard mode of operation.

The center of the 2-day momentum spiral is at a yaw wheel speed of about 300 rpm. This offset, or yaw bias, is due to solar pressure and shifts with the seasons, being maximum at the solstices and near zero at the equinoxes.

Pitch wheel momentum unload operations occurred less frequently, generally once every 5 to 7 days.

Figure 7-2 illustrates the accumulation of roll, pitch, and yaw jet pulses used to unload the associated wheels during the first 100 days of flight. Cumulative consumption of propellant is shown along the right ordinate. Based on the trend indicated in this figure, approximately 0.32 kg per year of hydrazine was required for wheel unloading.

ORBIT CONTROL

Four orbit control thrusters were provided on the spacecraft—two for eastward and two for westward thrusting. Each thruster was intended for long duration firing as opposed to the pulsed operation of the twelve attitude jets.

A total of 67 in-plane, orbit-control jet maneuvers were executed over the 5-year plus lifetime. The thruster performance for each maneuver is summarized by Figure 7-3, which gives the mean thrust for each maneuver according to date and compares this value with the nominal thrust level calculated from current tank pressure. The mean thrust was determined from the change in the mean

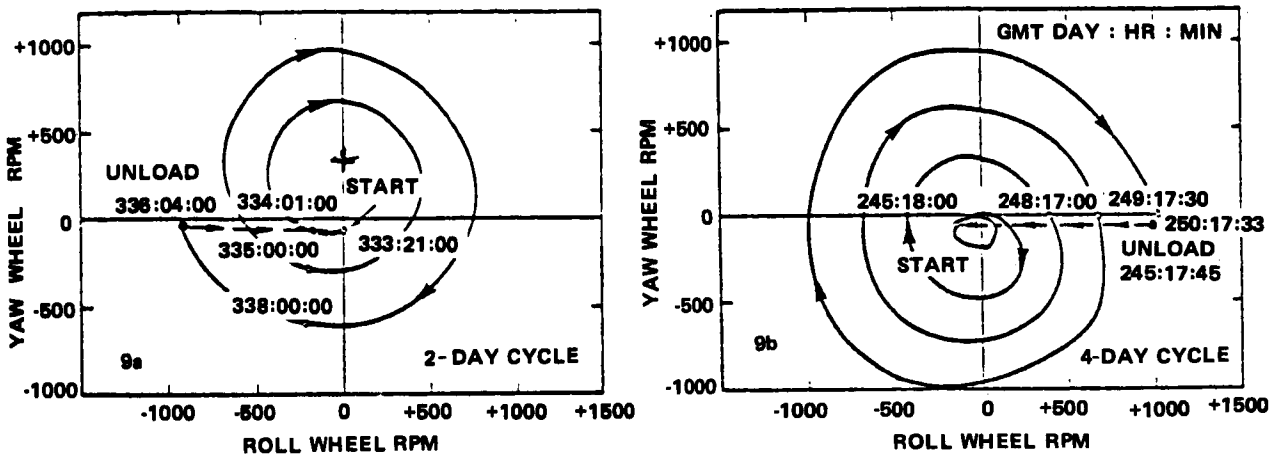

Figure 7-1. Typical Wheel Loading/Unloading Cycles

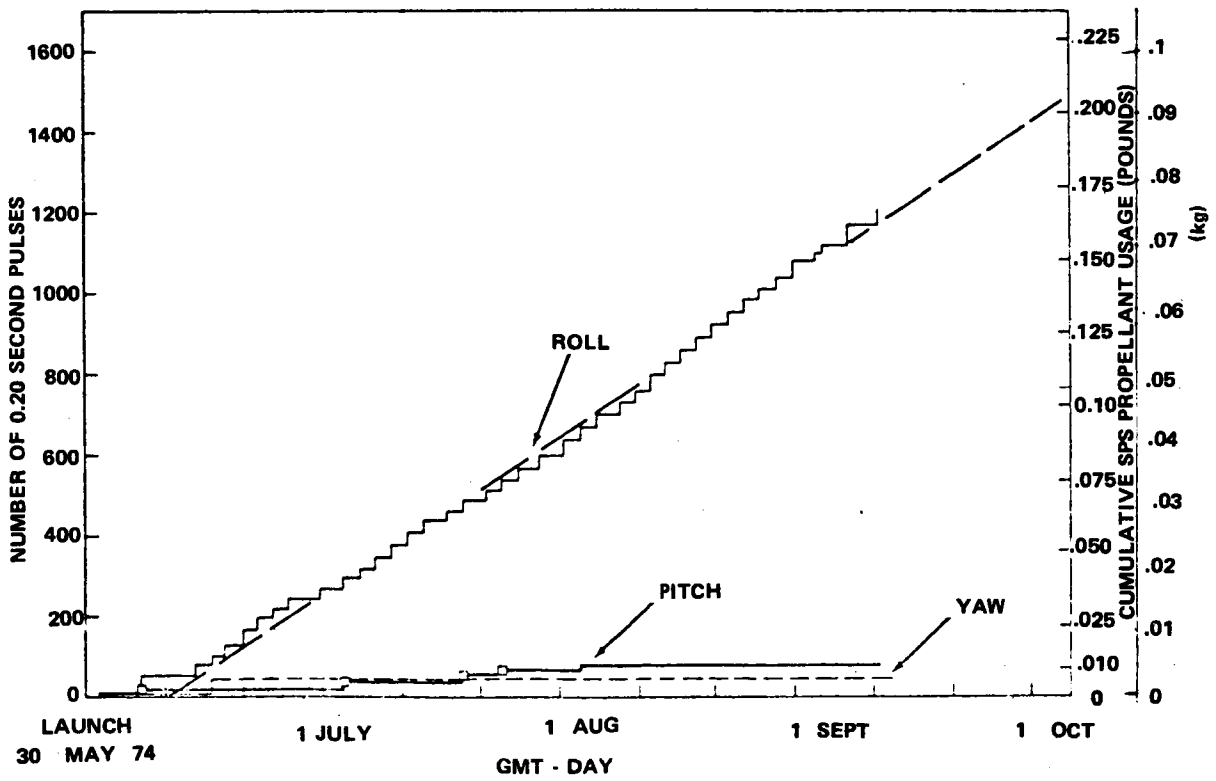

Figure 7-2. Wheel Unload Propellant Usage
(0.2/10 Duty Cycle, I_s = 140 sec)

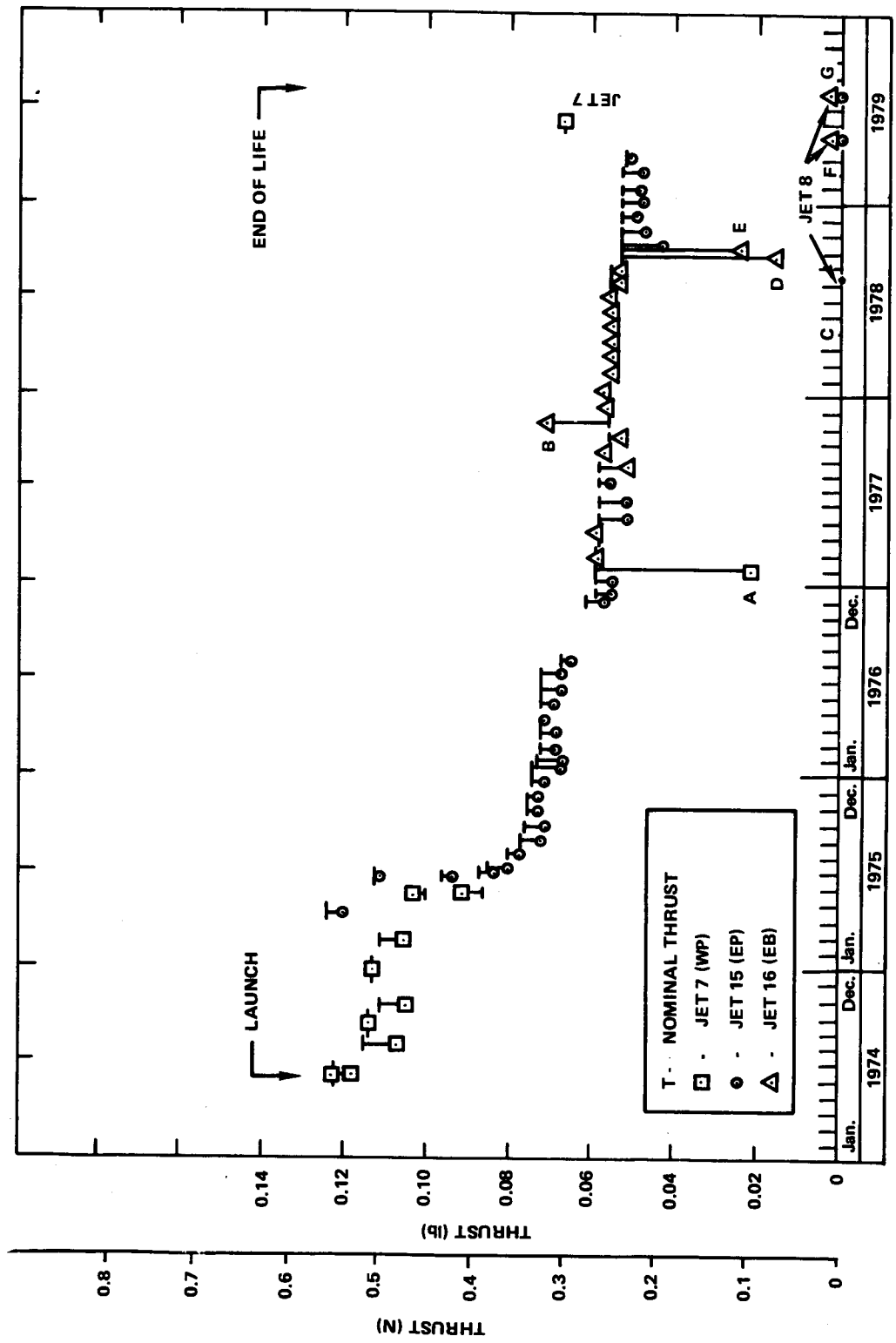

Figure 7-3. Orbit-Control Thruster Performance

daily longitudinal drift rate based on pre- and post-maneuver orbits, the mean spacecraft mass, and the actual burn time.

All but seven thruster firings are seen to be close to nominal thrust levels. Of these seven, two disagree due to poor pre- or post-maneuver orbits while the remainder reflect orbit-control thruster malfunction. See Table 7-5 for a summary of anomalous firings.

Jet No. 7 (west prime) was the only orbit-control thruster to function nominally throughout the lifetime of the spacecraft. The final maneuvers starting July 31, 1979, and ending August 3, 1979, could not be evaluated.

Jet No. 8 (west backup) never did produce thrust. During the truss line evacuation starting August 12, 1978, it was determined that Jet No. 8 was dead. Bed temperature data from the initial line evacuation in January 1977 showed that Jet No. 8 did not respond then either. Subsequent attempts to fire this jet proved futile.

Jet No. 15 (east prime) functioned normally through the March 28, 1979, maneuver, but was found to be completely dead on May 6, 1979, and on subsequent attempts. This jet failed abruptly without warning.

Jet No. 16 (east backup) functioned very well through the August 24, 1978, maneuver—tracking the nominal thrust levels very closely. During the maneuvers of September 27 and October 5, 1978; however, the jet operated intermittently, behaving as though the jet was alternately partially blocked then cleared. The catalyst bed temperature rise failed to follow a smooth curve. This jet failed to function during subsequent attempts.

Table 7-5
Summary of Anomalous Firings

Anomaly	Jet No.	Comment
A	15	Orbit perturbed by truss line evacuation before maneuver. Jet seemed normal.*
B	16	Post-maneuver orbit definition was poor. Jet seemed normal.*
C	8	Jet was dead.*
D, E	16	Erratic jet operation.*
F, G	8, 15, 16	Jets were inoperative.*

*Evidenced by catalyst bed temperature

Thruster firing data for each of the four orbit-control jets are summarized by Table 7-6 which illustrates the wide difference in operational usage among the four jets over the lifetime of ATS-6.

The salient maneuver parameters for each of the 67 individual maneuvers are presented in Table 7-7. It may be noted that most of the orbital maneuvering was devoted to small stationkeeping maneuvers. The largest single maneuver was used to drive ATS-6 to its final below-synchronous drift orbit. When the spacecraft was powered down on August 3, 1979, it was drifting eastward at a rate of 6.05 degrees per day.

The performance of the propulsion system for orbital maneuvering is summarized according to maneuver phase in Table 7-8. It is interesting to note that only 3.92 kg of hydrazine were expended for east-west stationkeeping during 4.6 years of on-station operations, whereas 13.49 kg of fuel were required just for the 39-day orbital repositioning from 94°W to 35°E longitude.

Orbit control impulse (I), incremental velocity (ΔV), and propellant consumption were normally calculated from pre- and post-maneuver states. The best estimates of spacecraft mass thruster efficiency and specific impulse were used in each case. Propellant consumption for attitude control was taken as the difference between the actual total consumption and the estimated propellant expenditure for orbit control.

Table 7-6
Orbit Control Thruster Firing Data

Thruster No.	Usage	No. Times Fired	Total Firing Time (Hrs)	Longest Continuous Burn (Hrs)	Service Life (First use to last use) (Yr)	Total Throughput (kg)	(lb)
7	West prime	12	47.7	28.1	5.2	20.8	(45.9)
8	West backup	–	–	–	–		0.0
15	East prime	37	25.5	4.1	4.0	14.6	(32.1)
16	East backup	18	3.4	0.3	1.6	1.4	(3.0)
Total		67	76.6	–	–	36.7	(81.0)

Table 7-7
Orbit Control Maneuver Data

Type of OC Maneuver	Date	Jet No.	Burn Time (s)	OC Fuel Consumed (kg)	(lb)	Tank Pressure (psia)	Incremental Velocity (mps)	(fps)	Thrust (N)	(lb)
Insertion at	6 Jun 74	7	480	0.14	0.3	359 – 355	0.20	0.64	0.54	0.122
94°W	7 Jun	7	1,888	0.45	1.0	357 – 345	0.73	2.41	0.52	0.118
	8 Aug	7	265	0.05	0.1	335 – 333	0.09	0.31	0.47	0.106
Stationkeep.	14 Sep	7	260	0.05	0.1	331 – 329	0.10	0.32	0.51	0.114
at 94°W	19 Oct	7	295	0.09	0.2	325 – 323	0.10	0.33	0.47	0.105
	28 Dec	7	323	0.09	0.2	329 – 327	0.12	0.39	0.50	0.113
	22 Feb 75	7	203	0.05	0.1	319	0.07	0.23	0.47	0.105
	11 Apr	15	197	0.05	0.1	371 – 369	0.08	0.26	0.53	0.120
Reposition	21 May	7	14,828	3.08	6.8	317 – 261	5.06	16.60	0.46	0.103
94°W to	21 May	7	19,627	3.49	7.7	265 – 221	5.94	19.49	0.40	0.091
35°E	21 Jun	15	14,712	3.40	7.5	361 – 291	5.46	17.90	0.49	0.111
	25 Jun	15	13,297	2.63	5.8	293 – 255	4.16	13.66	0.42	0.094
	29 Jun	15	5,058	0.91	2.0	251 – 239	1.42	4.65	0.37	0.084
Stationkeep.	3 Jul	15	179	0.05	0.1	239	0.05	0.16	0.36	0.080
at 35°E	3 Aug	15	583	0.09	0.2	223 – 221	0.15	0.50	0.34	0.077
	31 Aug	15	592	0.09	0.2	217	0.14	0.47	0.32	0.072
	28 Sep	15	690	0.09	0.2	213	0.16	0.54	0.32	0.071
	25 Oct	15	577	0.09	0.2	211	0.14	0.46	0.32	0.073
	22 Nov	15	561	0.09	0.2	211	0.14	0.45	0.32	0.073
	20 Dec	15	720	0.09	0.2	208	0.17	0.57	0.32	0.072

Table 7-7
Orbit Control Maneuver Data (Continued)

Type of OC Maneuver	Date	Jet No.	Burn Time (s)	OC Fuel Consumed (kg)	OC Fuel Consumed (lb)	Tank Pressure (psia)	Incremental Velocity (mps)	Incremental Velocity (fps)	Thrust (N)	Thrust (lb)
Stationkeep.	18 Jan 76	15	208	0.05	0.1	206	0.05	0.15	0.30	0.067
at 35°E	31 Jan	15	440	0.09	0.2	204	0.10	0.32	0.30	0.067
(cont)	21 Feb	15	664	0.09	0.2	202	0.15	0.50	0.30	0.068
	21 Mar	15	651	0.09	0.2	200 – 198	0.15	0.49	0.30	0.068
	18 Apr	15	531	0.09	0.2	200	0.13	0.42	0.31	0.071
	14 May	15	626	0.09	0.2	200	0.14	0.47	0.31	0.069
	13 Jun	15	735	0.09	0.2	201 – 199	0.16	0.54	0.30	0.067
	11 Jul	15	581	0.09	0.2	199	0.13	0.43	0.30	0.067
Reposition	2 Aug 76	15	10,894	1.54	3.4	196 – 186				
35°E to	4 Aug	15	8,689	1.18	2.6	184 – 176	4.25	13.94	0.29	0.065
140°W	29 Nov	15	7,648	1.00	2.2	179 – 175				
	30 Nov	15	10,501	1.27	2.8	173 – 165				
	2 Dec	15	3,643	0.41	0.9	167 – 163	4.20	13.78	0.28	0.057
Stationkeep.	12 Dec	15	387	0.05	0.1	165	0.07	0.24	0.25	0.056
at 140°W	9 Jan 77	15	705	0.09	0.2	164	0.13	0.43	0.24	0.055
	1 Feb	15	325	0.05	0.1	162	0.02	0.08	0.10	0.022
	20 Feb	16	938	0.09	0.2	162 – 160	0.19	0.61	0.26	0.059
	6 Apr	16	580	0.09	0.2	160	0.12	0.38	0.26	0.059
	3 May	15	873	0.09	0.2	160	0.15	0.50	0.23	0.052
	7 Jun	15	904	0.09	0.2	160	0.16	0.52	0.23	0.052
	15 Jul	15	855	0.09	0.2	158	0.16	0.52	0.24	0.055

Table 7-7
Orbit Control Maneuver Data (Continued)

Type of OC Maneuver	Date	Jet No.	Burn Time (s)	OC Fuel Consumed (kg)	(lb)	Tank Pressure (psia)	Incremental Velocity (mps)	(fps)	Thrust (N)	(lb)
Stationkeep.	18 Aug	16	635	0.09	0.2	158 – 156	0.11	0.36	0.23	0.052
at 140°W	12 Sep	16	646	0.09	0.2	156 – 154	0.12	0.41	0.25	0.057
(cont)	12 Oct	16	501	0.05	0.1	154	0.09	0.30	0.24	0.054
	7 Nov	16	847	0.09	0.2	154	0.20	0.66	0.32	0.071
	9 Dec	16	513	0.05	0.1	152	0.10	0.32	0.25	0.056
	11 Jan 78	16	795	0.09	0.2	154	0.15	0.50	0.25	0.057
	15 Feb	16	777	0.09	0.2	152	0.15	0.48	0.25	0.056
	17 Mar	16	552	0.05	0.1	150	0.10	0.34	0.24	0.055
	14 Apr	16	703	0.09	0.2	152 – 150	0.13	0.43	0.25	0.056
	11 May	16	540	0.05	0.1	150	0.10	0.33	0.25	0.056
	7 Jun	16	580	0.09	0.2	152 – 150	0.11	0.35	0.24	0.055
	6 Jul	16	746	0.09	0.2	150	0.14	0.46	0.25	0.056
	2 Aug	16	454	0.05	0.1	150	0.08	0.27	0.24	0.054
	24 Aug	16	946	0.14	0.3	150 – 148	0.17	0.57	0.24	0.054
	27 Sep	16	619	0.05	0.1	146	0.03	0.11	0.07	0.016
	5 Oct	16	752	0.05	0.1	146	0.06	0.20	0.11	0.024
	11 Oct	15	590	0.05	0.1	148	0.09	0.28	0.19	0.043
	8 Nov	15	534	0.05	0.1	148	0.09	0.28	0.21	0.048
	6 Dec	15	870	0.09	0.2	148	0.15	0.48	0.22	0.049
	4 Jan 79	15	445	0.05	0.1	148	0.07	0.24	0.21	0.048

Table 7-7
Orbit Control Maneuver Data (Continued)

Type of OC Maneuver	Date	Jet No.	Burn Time (s)	OC Fuel Consumed (kg)	(lb)	Tank Pressure (psia)	Incremental Velocity (mps)	(fps)	Thrust (N)	(lb)
Stationkeep.	28 Jan	15	796	0.09	0.2	146	0.13	0.43	0.21	0.048
at 140°W	28 Feb	15	787	0.09	0.2	146 – 144	0.13	0.42	0.21	0.048
(cont)	28 Mar	15	640	0.05	0.1	144	0.11	0.36	0.23	0.051
	9 May	7	669	0.09	0.2	185	0.15	0.50	0.30	0.067
Change Orbit	31 Jul	7	101,134	12.07	26.6	183 – 130	17.08	56.04		
Deplete Fuel	2 Aug	7	31,836	1.09	2.4	134 – 20		0		

Table 7-8
Orbital Maneuver Summary

Orbital Maneuvers					Performance				Propellant Consumed, Wp kg (lb)	
			Incremental Velocity ΔV		Impulse					
					I_I		I_{sp}			
Phase	Thruster No.	Duration of Phase (mo)	m/s	(ft/s)	N·s	(lb-s)	N·s/kg	(s)	Attitude Control	Orbit Control
Orbital insertion at 94°W longitude	7	2.1	1.02	(3.35)	1374	(309)	1981	(218)	1.10 (2.42)	0.64 (1.42)
East-west station-keep. at 94°W	7+ 15	9.6	0.47	(1.54)	632	(142)	1954	(215)	0.32 (0.71)	0.30 (0.66)
Reposition from 94°W to 35°E	7+ 15	1.3	22.03	(72.29)	29492	(6630)	2026	(223)	1.39 (3.06)	13.49 (29.74)
East-west station-keep. at 35°E	15	13.2	1.97	(6.46)	11512	(2588)	1926	(212)	3.99 (8.80)	1.26 (2.77)
Reposition from 35°E to 140°W	15	4.0	8.44	(27.72)	11174	(2512)	1917	(211)	0.51 (1.13)	5.40 (11.91)
East-west station-keep. at 140°W	15+ 16	31.9	3.77	(12.36)	4960	(1115)	1945	(214)	4.11 (9.06)	2.36 (5.21)
Change to lower orbit	7	–	17.08	(56.04)	22326	(5019)	1717	(189)	0.48 (1.05)	12.06 (26.58)
Deplete propellant (end of life)	7	–	–		–		–		1.66 (3.65)	1.10 (2.43)
Total		62.1	54.78	(179.76)	81,470	(18,315)	1890	(208)	13.56 (29.88)	36.61 (80.72)

PROPELLANT CONSUMPTION

Prior to launch, 50.17 kg of hydrazine were loaded into the spacecraft—25.22 kg in SPS-1 and 24.95 kg in SPS-2. Propellant utilization through the end of the mission is compared to the budgeted consumption in Table 7-9. The relative consumption from SPS-1 and SPS-2 over the mission is presented in Figure 7-4. Propellant remaining was calculated using tank volume, pressure and temperature, blowdown characteristics, and initial state. The pressure sensor, although actually measuring hydrazine pressure, also indicated nitrogen pressure since the pressures were equalized as long as the diaphragm was floating. The temperature sensor, located on the liquid side of the tank, provided only an approximate measure of nitrogen temperature. The indicated temperature was a function of Sun angles and electrical loading and generally lagged the true gas temperature. Application of the gas law to the nitrogen pressurant was accomplished by taking the daily mean of pressure and temperature readings at two-hour intervals. A calibration correction was then applied to the mean pressure. The corrected mean values were used to compute the propellant remaining in each tank. Such a procedure smoothed the data and provided a consistent calculation of onboard fuel.

Table 7-9
Hydrazine Propellant Consumption
(Comparing 5-Yr Budget to Actual Usage)

	Budget		Actual	
	kg	(lb)	kg	(lb)
Load at Launch	49.08	108.2	50.17	110.6
Ref. Attitude/Orbit Acquisition	9.6	21.2	1.7	3.8
1 Year @ 94°W	2.6	5.8		
10 months @ 94°W			0.6	1.4
40-day move to India	14.6	32.1		
39-day move to India			14.9	32.8
1 Year @ 35°E	2.1	4.7		
13 months @ 35°E			5.3	11.5
120-day move to 140°W	5.2	11.4	5.9	13.0
2½ year @ 105°W	5.4	12.0		
32 months @ 140°W			6.5	14.3
AC Contingency	7.9	17.5		
Deorbit			12.5	27.6
Unallocated Reserve	1.3	2.8		
Propellant Depletion			2.7	6.1
Residual	0.4	0.8		

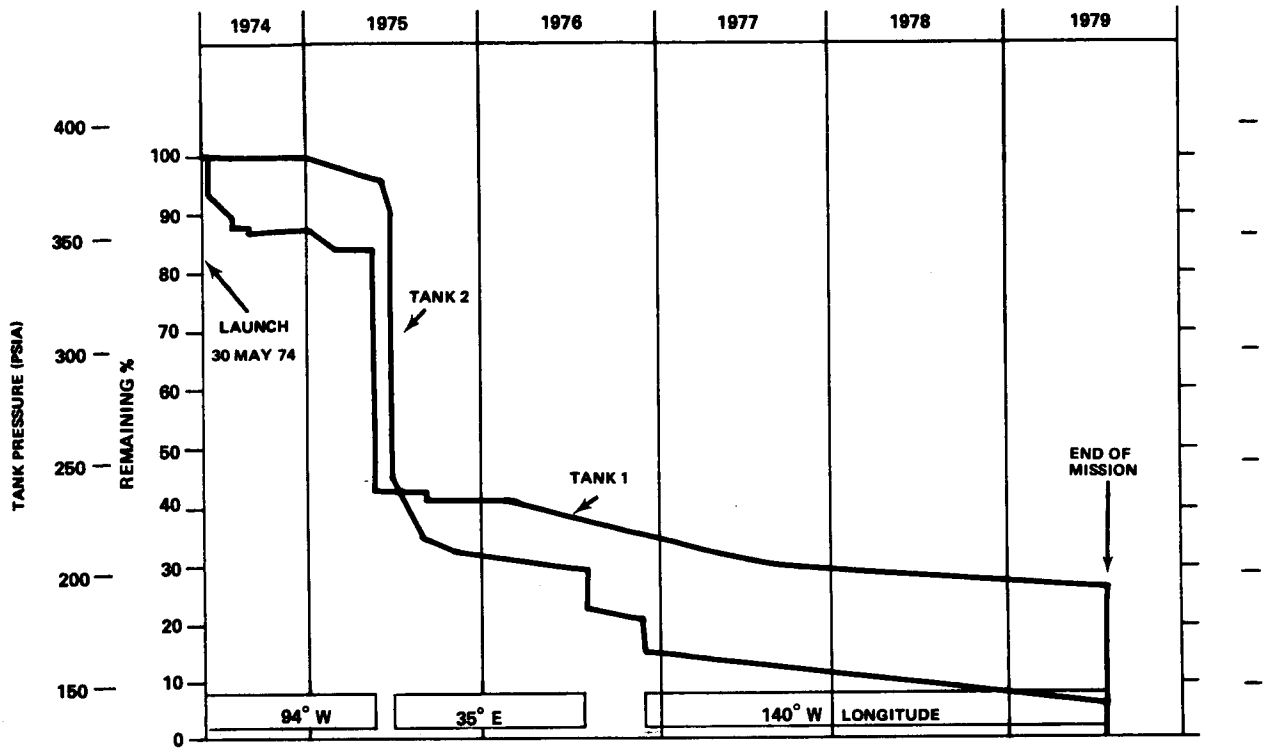

Figure 7-4. Propellant Consumption Summary

A typical day's readings are illustrated by the temperature/pressure plot of Figure 7-5. The solid line in the figure is the pressure/temperature characteristic that represents the existing state of the fuel in that tank. On this particular day the tank pressure and temperature variations were 8 psi and 13°C.

Deviations of 1.47 psi and 1°C in the mean pressure and temperature values influence the calculation of propellant remaining by 0.14 kg (full tank) to 0.73 kg (empty tank).

Propellant consumption during the several mission phases over the life of the spacecraft is shown by the plots in Figure 7-6 that indicate propellant usage for attitude control and orbit control. The consumption rate (slope of curve) was quite low for most of the five-year, two-month lifetime. The periods of high consumption included the two sets of repositioning maneuvers, the final change to a lower orbit, and fuel depletion.

Commencing June 1, 1978—four years after launch—propellant was used very sparingly in the support of attitude control. Special conservation measures were taken by the operating personnel to unload the reaction wheels at the most effective times, to maneuver on wheels as much as possible, and during idle time, to point the spacecraft to take advantage of solar torques.

The thrusters were used extensively for attitude control in the middle of 1975 when a roll-wheel drive problem appeared, followed by Apollo-Soyuz support. Prior to the deorbit maneuver of July 31, 1979, 15.0 kg of propellant were still available—equivalent to 7 years of normal operation.

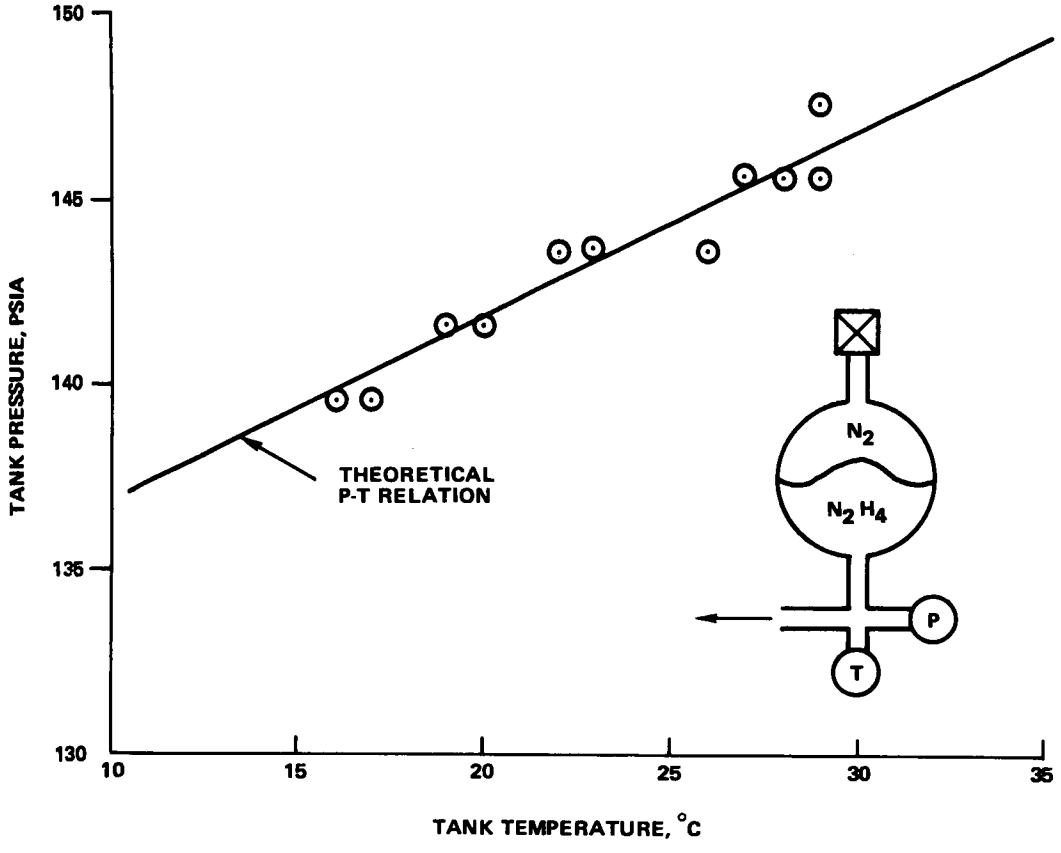

Figure 7-5. Daily Cycling of Tank Pressure and Temperature

THERMAL CONTROL

Figures 7-7 through 7-10 are typical 24-hour cycles of the thruster valve, propellant line, catalyst bed, and tank temperatures. The data was taken while SPS-1 and -2 prime valve heaters were on, the prime and backup line heaters were in the low-automatic mode, and catalyst bed heaters were off.

Predictions had indicated a daily temperature range for the valves of from 5°C to 75°C. The actual initial cycle was from 25°C to 96°C with the prime catalyst heaters on. This was considered somewhat high and the bed heaters were turned off. The valve temperatures then cycled between approximately 12°C to 88°C depending on the angle of the Sun.

The difference in shape of the SPS-1 and -2 component cycles was due partly to the daily sequence of exposure of sunlight and shadow as the spacecraft Sun angle changed. The line temperatures were under thermostatic control and consequently exhibited a much narrower cycle. The pronounced difference in temperature between the two SPS-2 orbit control thrusters that is reflected in their valve temperatures was checked during the special radio frequency compatibility test and found to be anomalous. The minimum catalyst-bed temperature of about -15°C was not a problem, considering that temperature cycle tests at GSFC and Fairchild were run to -50°C without damage.

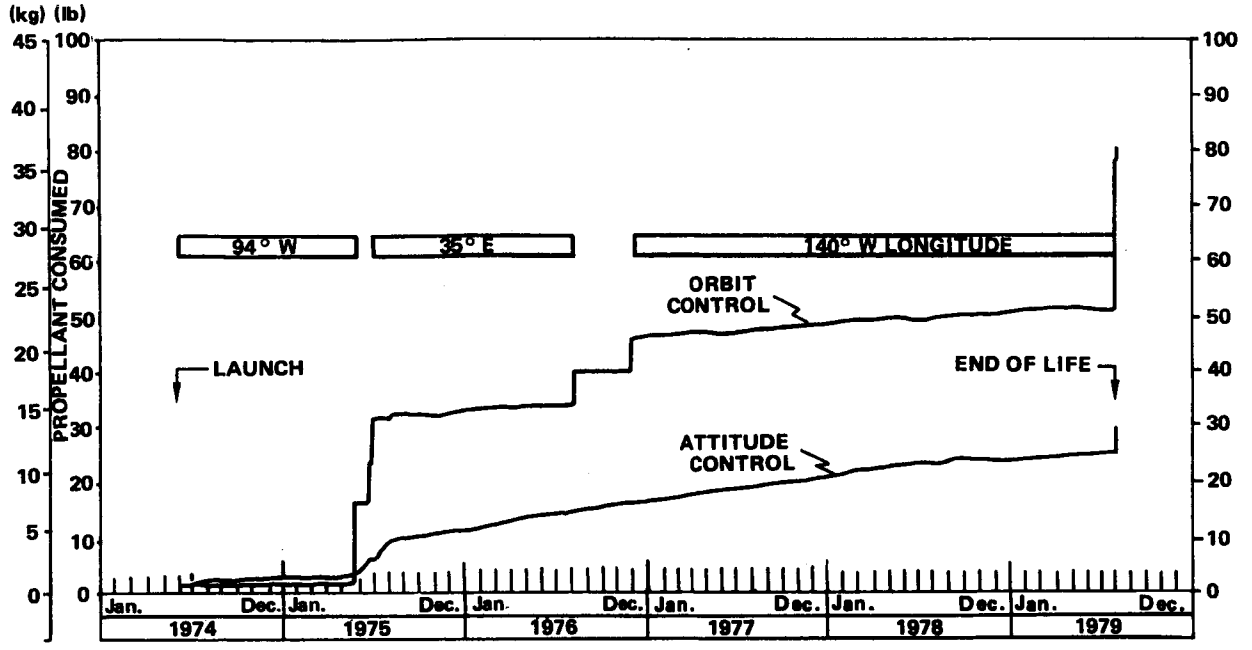

Figure 7-6. Propellant Consumption History

The temperature rise of the No. 7 catalyst bed during steady-state jet firing was as predicted, reaching a steady-state value of 650°C in 90 seconds. The -pitch thruster (2.4 percent duty cycle) reached 450°C during the 8-minute burn and 505°C during the 31-minute burn. Minor pulsing of attitude jets is clearly evident from the bed-temperature telemetry. The No. 7 thruster valve cooled down from an initial temperature of 66°C to 46°C during the long steady-state burn and after jet cutoff increased to a maximum value of 78°C.

Figure 7-11 shows SPS-1 valve temperature data for September 4 and September 5, 1974 (fourth day of shadow), with an occult period between 5:55:02 and 6:31:45 and an umbra condition between 5:59:41 and 6:27:06. The temperature of valves 7 and 8 dropped to 8°C and 9°C. Because of the exposure to sunlight during the daily cycle, SPS-2 valve temperatures were 20°C and 60°C greater than those of SPS-1 at the time the spacecraft entered occult and they did not approach the freezing level during the shadow period.

Because of the need to conserve electrical power during occult, it was decided to warm the SPS-1 valves to the SPS-2 level using the backup heaters, turning them off just before entering shadow. Figure 7-12 illustrates the warmup for the case where the backup heaters were left on during occult, and for the case where they were turned off. The minimum temperature was 10°C (freezing point of hydrazine = 2°C). The warmup, using the SPS-1 backup heaters, was standard operation during the occult season.

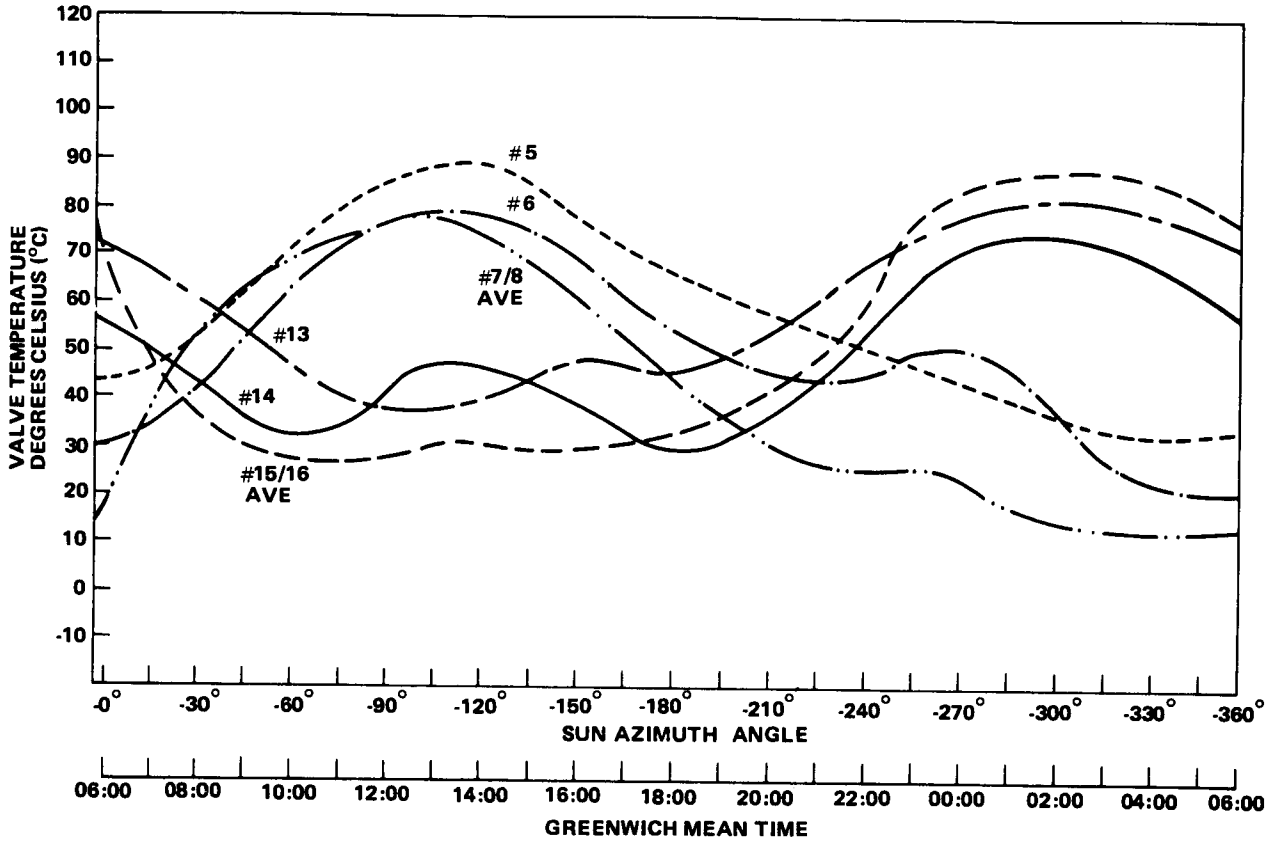

Figure 7-7. Thruster Valve Temperatures (24-Hour Cycle)

PROPELLANT PRESSURE

Propellant pressure was measured by a pressure transducer installed on the liquid hydrazine side of each tank. Daily pressure excursions of several psi resulted from temperature variations of the nitrogen pressurant. As propellant was consumed, the hydrazine pressure dropped accordingly. Since this was a blowdown system, incremental pressure dropped rapidly at first then tapered off as propellant was expelled.

The curves of Figure 7-4 portray the pressure history of each tank from launch to end-of-life some five years later. It will be noted that the largest pressure changes occurred during repositioning maneuvers, the final orbit change maneuver, and at end-of-life when propellant was deliberately depleted. The final pressure drop occurred on August 3, 1979, when the second tank (tank 1) diaphragm bottomed out. At that point the nitrogen pressurant could no longer pressurize the hydrazine and the pressure dropped rapidly toward zero.

The crossfeed latch valve connecting the two systems was first opened on August 1, 1979, as the tank pressures were equal at approximately 10.12 kg/cm^2 (144 psia). This valve was left open thereafter to ensure depletion of the hydrazine in tank 2. Because of the initial hydrazine loading and nitrogen pressurization, tank 2 emptied first at equal pressure on August 2, 1979.

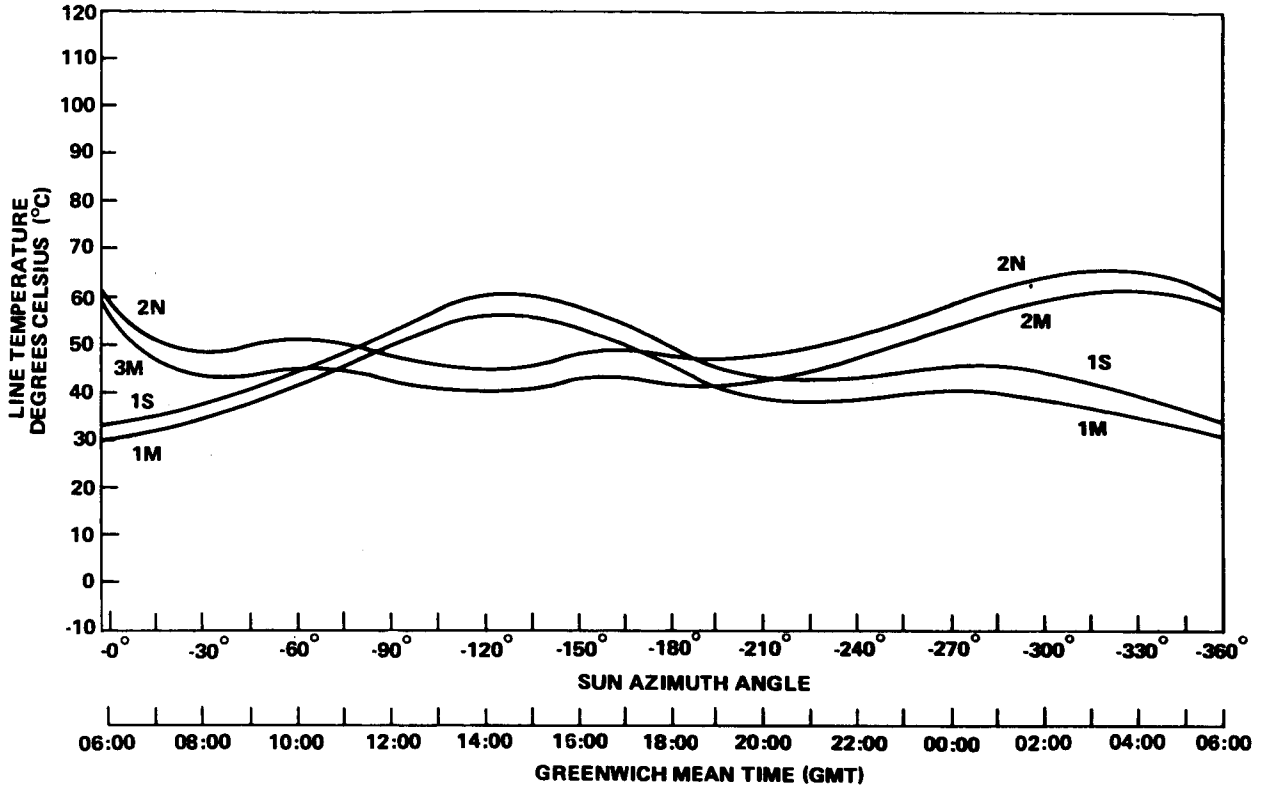

Figure 7-8. Propellant Line Temperatures (24-Hour Cycle)

TERMINAL MISSION MANEUVERS

Orbit Change

This next to last maneuver was designed to place ATS-6 in an orbit significantly below synchronous altitude. An orbit above geosynchronous altitude was preferred, but due to telemetry and attitude jet problems, it was deemed prudent to proceed to a lower orbit that would afford extended visibility from Rosman. The maneuver was to continue without interruption until all but 2.27 kg of hydrazine had been expended or until attitude control could no longer be maintained. The 2.27 kg of propellant was deliberately held in reserve for the final roll spinup maneuver.

The actual orbit change maneuver lasted for 28.1 hours with large roll, pitch, and yaw excursions developing due to inoperative attitude jets and the continued anomalous performance of the roll wheel drive. The positive yaw jet (No. 5) fortuitously revived just when needed.

The indicated pressures of tanks 1 and 2 and the catalyst bed temperature of the orbit control jet (No. 7) during the course of the orbit-change maneuver are illustrated in Figure 7-13. The pressure readings change in increments of 0.14 kg/cm^2 (2 psi)—the resolution of the telemetered pressure.

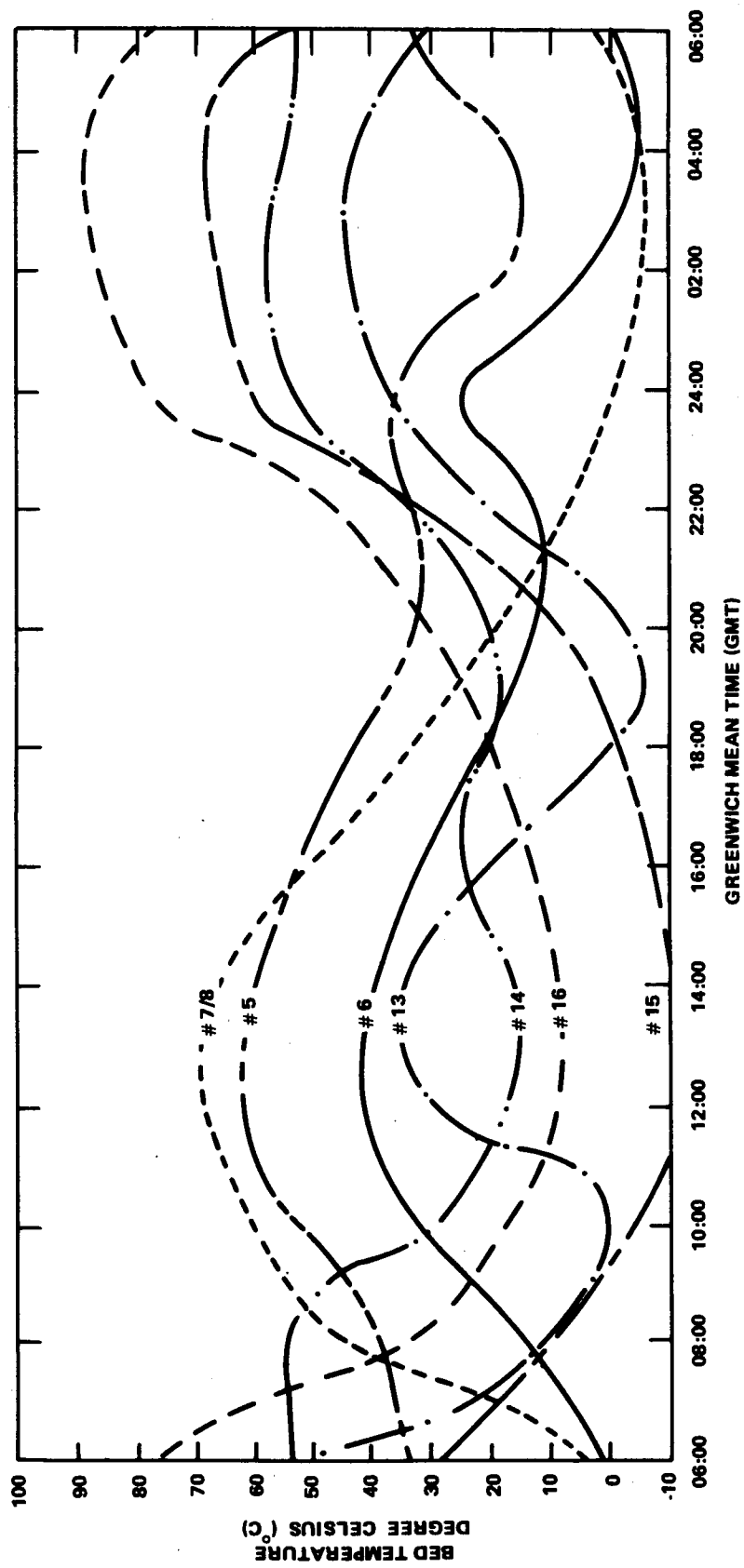

Figure 7-9. Catalyst Bed Temperatures (24-Hour Cycle)

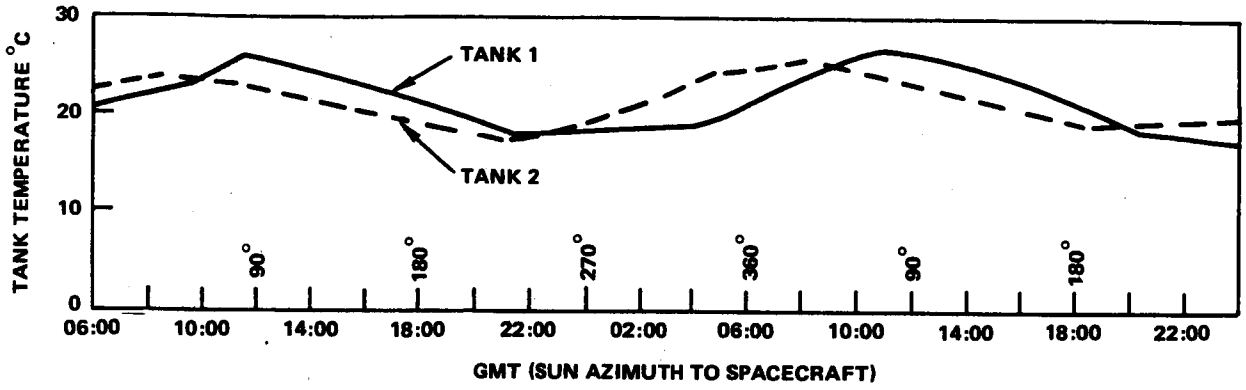

Figure 7-10. Tank Temperatures (24-Hour Cycle)

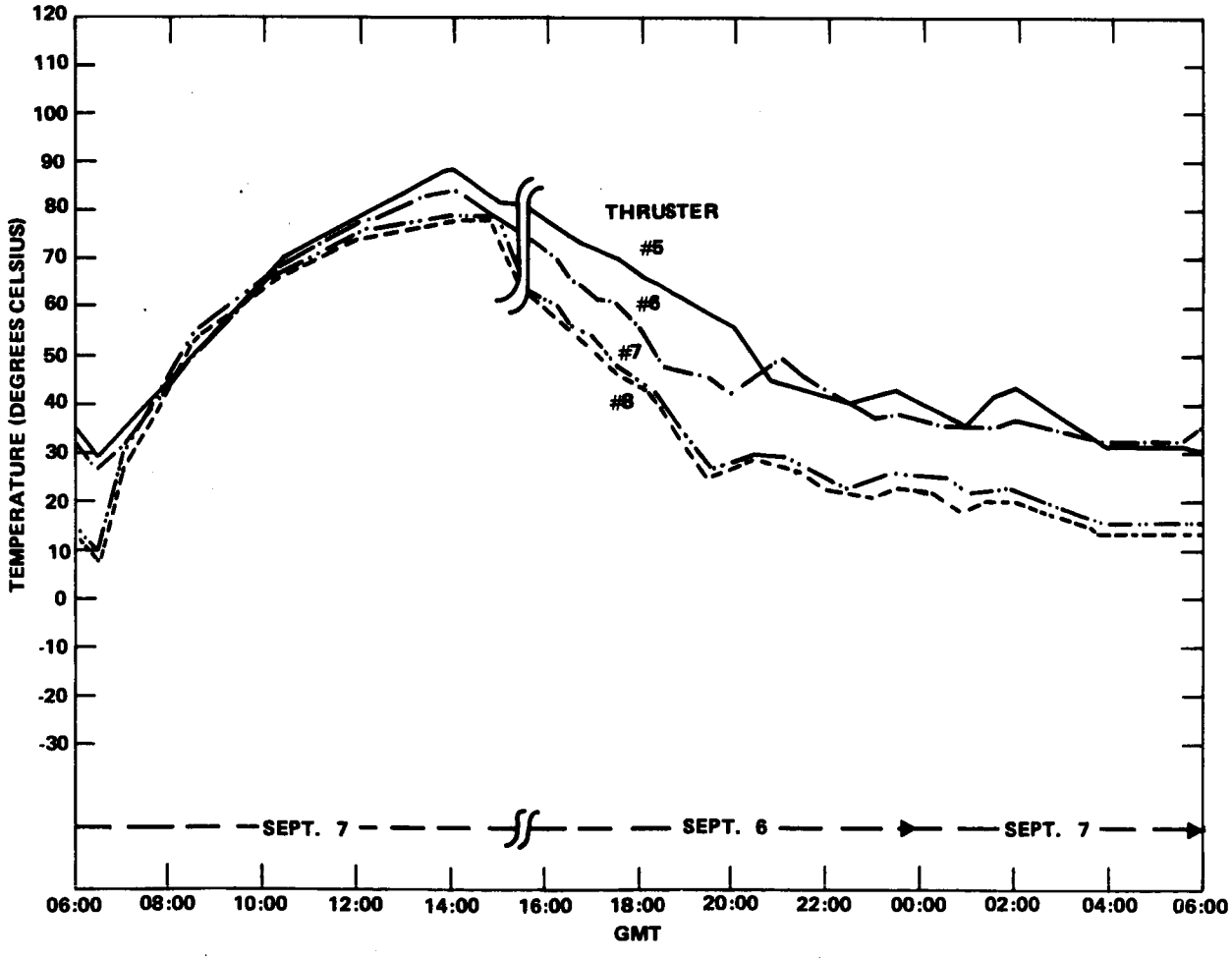

Figure 7-11. SPS Valve Temperatures vs. GMT During Occult

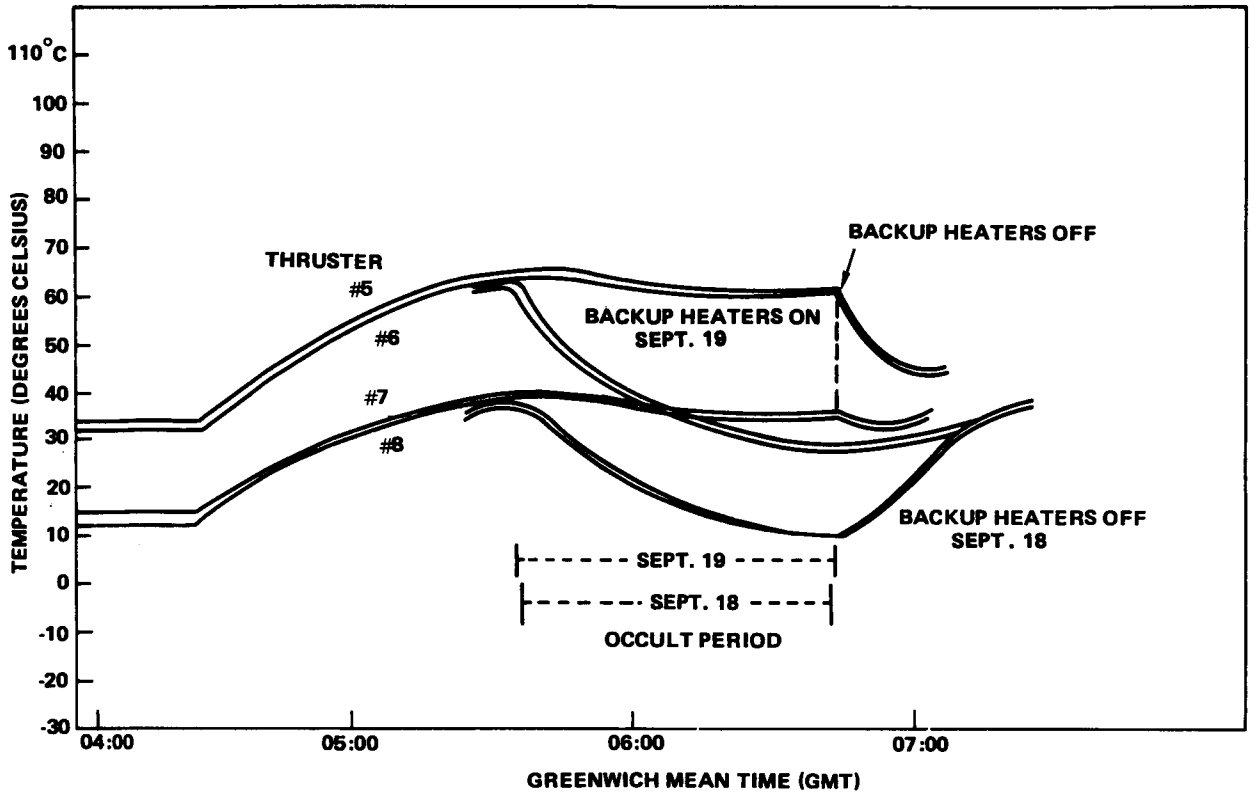

Figure 7-12. SPS-1 Valve Temperatures (Prime Valve Heaters On)

During the first portion of the maneuver, the tank-1 pressure dropped steadily as fuel was consumed. The tank-2 pressure increase was due to a tank-2 nitrogen temperature rise. Based on an expected 0.21 kg/cm^2 (3-psi) calibration pressure differential between the two tanks, the cross-latch valve was opened (for the first time) as soon as the tank-1 pressure, p_1, indicated 0.28 kg/cm^2 (4 psi) below the tank-2 pressure, p_2. In reality there was a 0.42 kg/cm^2 (6-psi) differential pressure as shown in Figure 7-13.

Roll Spinup and Propellant Depletion

The final ATS-6 maneuver was designed to spin the spacecraft about the roll axis (X-axis) oriented along the sunline and to deplete the 2.7 kg of onboard propellant.

Starting at 1429Z, the spacecraft +X axis was first pointed at the Sun, then the positive roll jet (No. 2) was commanded on in a continuous mode. When the roll rate reached a value of 2 degrees per second, the west prime orbit-control jet (No. 7) was commanded on and burned steadily for 8.8 hours. Due to the orientation of No. 7, the time interval over which the orbit-control jet fired—while the spacecraft was solar-oriented—probably had little effect on the semimajor axis, but undoubtedly did slightly increase the eccentricity of the final orbit.

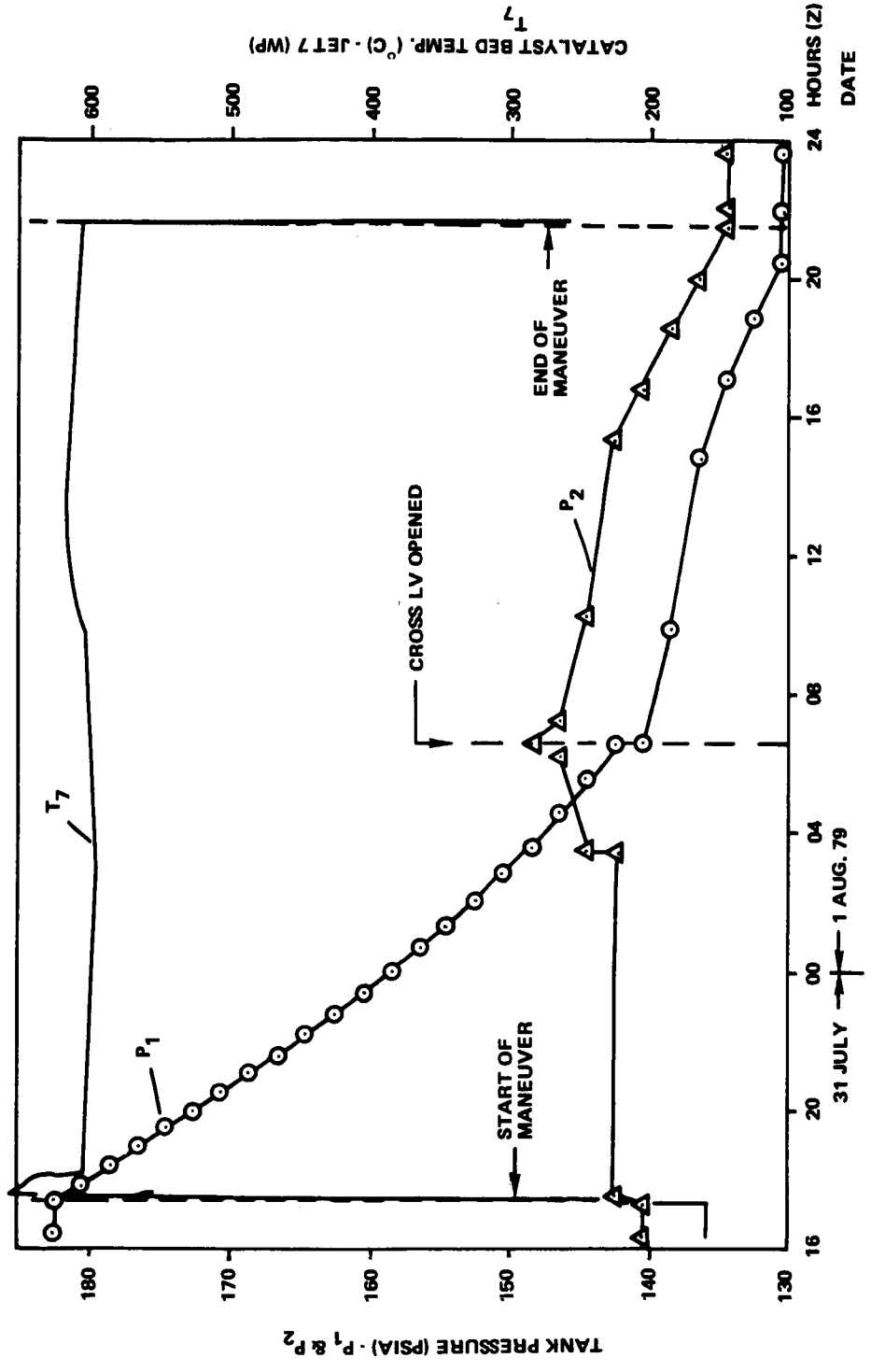

Figure 7-13. ATS-6 Orbit Maneuver (July 31/August 1, 1979)

When the roll rate reached a value of 4 degrees per second, the positive yaw jet (No. 5) was turned on in the continuous mode to aid in the fuel depletion process. It was judged that the spacecraft was sufficiently roll-rate stabilized to avoid perturbing the spin-axis orientation with a yaw jet firing. From this point on, all three thrusters (the only functional jets left on the spacecraft) fired continuously for approximately 5 hours.

Since the cross-latch valve had been open from the previous maneuver, fuel was drawn from both tanks even though all three firing jets were on system 1. At 1844Z on August 2, 1979, the tank-2 diaphragm bottomed out, thus the nitrogen in that tank could no longer pressurize the liquid hydrazine. From this point on both pressure readings were supported solely by the pressurant in tank-1.

The indicated tank pressure readings and the significant maneuver events are presented as a function of time by Figure 7-14. The most interesting part of the entire 11.1-hour maneuver occurred at 0022Z on August 3, when the diaphragm of tank-1 bottomed out. As soon as this happened, the pressure readings immediately started a rapid fall. When the diaphragm stopped floating, the catalyst bed temperature of jet No. 7 (the orbit control thruster) was 618°C. At 0109Z the nonessential bus was turned off for 9 minutes—shutting off all three jets. At the time of turnoff, the catalyst bed temperature had dropped to 280°C but the tank pressures were also low (1.687 kg/cm^2 [24 psia] and 1.968 kg/cm^2 [28 psia]). Only jet No. 7 was again turned on at 0119Z. The catalyst bed temperature rose to a peak value of 465°C at 0127Z then gradually decreased to 280°C at 0137Z at which time all telemetry was turned off. Jet No. 7 was left on, however, to get rid of the last bit of hydrazine.

As a result of this final spinup maneuver, ATS-6 was left spinning about its X-axis (with positive roll rate) at a rate of 9.6 degrees per second (1.6 rpm). The final spin-axis orientation was estimated to be:

right ascension	132.1 degrees
declination	17.8 degrees

ATS-6 was given an eastward drift rate of 6.05 degrees of longitude per day.

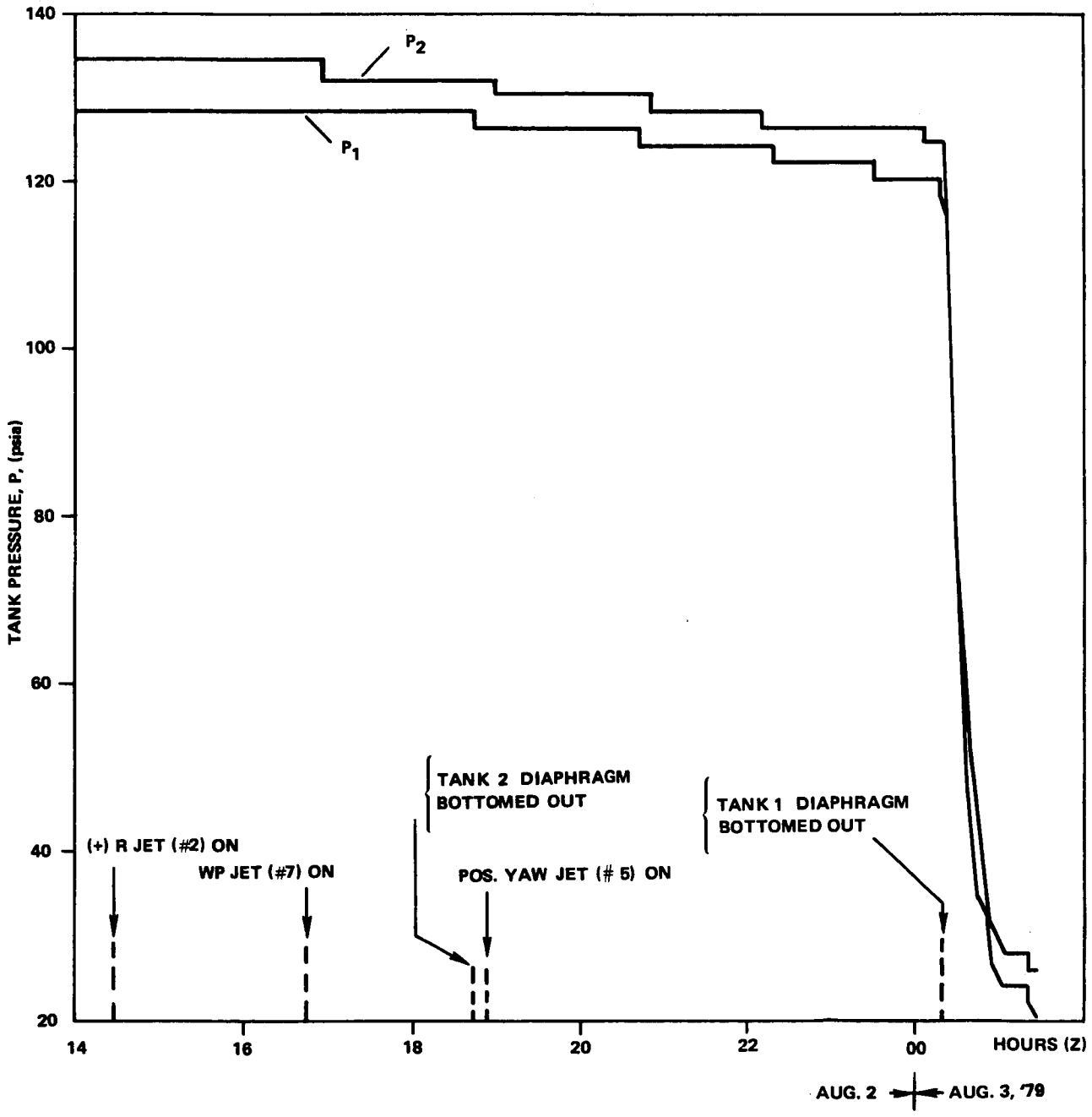

Figure 7-14. Roll Spin-Up and Propellant Depletion Maneuver

CHAPTER 8

IN-ORBIT ANOMALIES AND CONTINGENCY OPERATIONS

INTRODUCTION

The following discussion of anomalous behavior and failures concerns test and operational problems encountered during the mission lifetime of the ATS-6 spacecraft propulsion subsystem. The first two items involve failures of heater elements. The first of these was the loss of a primary valve heater that the backup heater was able to replace, while the second was a failure of both prime and backup valve heaters that required a change in normal operations. The third item is an instrumentation anomaly caused by rf susceptability of a thermocouple circuit that had little impact on system operation. The final section is devoted to discussion of the many thruster failures that occurred as the flight progressed, finally prompting a decision to terminate the mission before all orbit control was lost. Factors contributing to the thruster failures are discussed in detail with contamination being identified as the most probable cause.

Contingency operations that were necessary to continue the mission are discussed, and design conclusions to be drawn for the benefit of future programs finish each section.

SPS-2 VALVE HEATER DRIVE FAILURE

During temperature checks on July 31, 1974 (GMT 212:12:40), it was noted that the four SPS-2 thruster valve temperatures were very low (No. 13, -16°C; No. 14, -4°C; No. 15, -22°C; and No. 16, -20°C). Data for the previous day at the same time indicated values between 25°C and 40°C. Commanding the SPS-2 prime heaters on (again) produced no change in temperature. The backup heaters were then commanded on, and valve temperatures rose to their normal values within three hours.

Subsequent flight data and flight test data analysis showed the failure to be in the prime heater driver circuit and associated with a random electronic component failure. The valve heater system is described in the next paragraph followed by a description of the failure, an analysis, the consequences of failure, and the design conclusion.

Valve Heater System Background

The ATS-6 spacecraft propulsion subsystem (SPS) featured 16 catalytic hydrazine thrusters arranged in two functionally redundant half-subsystems (SPS-1 and SPS-2) fed from two propellant tanks (Figures 5-1 and 5-4, Chapter 5).

Liquid hydrazine was fed to the SPS-1 and SPS-2 truss thrusters through separate propellant lines, each wrapped with independently powered line heaters to keep the liquid hydrazine in the lines

from freezing (2°C). The line heaters were normally thermostatically controlled, although low (2.5 watts) and high (8.8 watts) constant-power modes were available on command. Prime and backup line heaters were provided for SPS-1 and SPS-2.

Prime and backup valve heaters were provided for the SPS-1 and SPS-2 truss thrusters to keep them from freezing as well (Figure 8-1). The four primary valve heaters and the four backup valve heaters for SPS-1 (SPS-2) were wired in parallel (in sets of four) from separate heater drive circuits located in the actuator control electronics. A simple constant power on-or-off command mode was provided for each set of four heaters. Thermister temperature transducers were provided for the eight truss thruster valves.

No valve heaters (nor valve temperature sensors) were provided for the eight thrusters located in the thermally-controlled Earth-viewing module. Prime and backup catalyst bed heaters were provided for the eight SPS-1 and eight SPS-2 thrusters. Single on (constant power) and off commands were available for each of the four sets of eight parallel-wired heaters.

The SPS contained seven latching valves for isolating the two tanks and combinations of the eight thrusters located in the Earth-viewing module and the eight thrusters located on the truss.

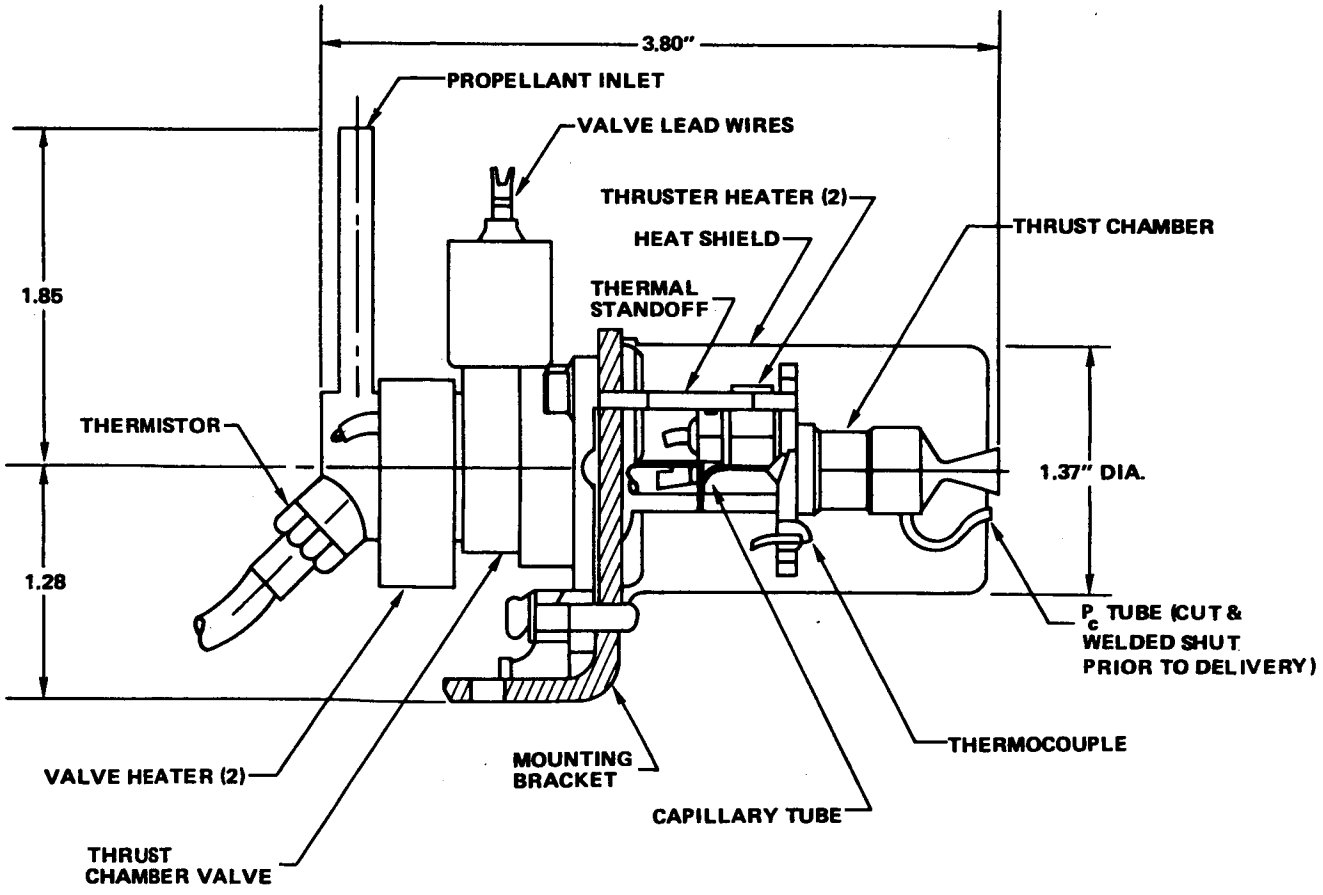

Figure 8-1. SPS Thruster Subassembly—Truss Configuration

Description of Failure

SPS valve temperatures, SPS power status, spacecraft load bus current, and all spacecraft commands were evaluated for the 24-hour period covering the failure. Figure 8-2 is a plot of the temperature data from this period and shows the time of failure and the subsequent temperature variations.

During this period no commands that could have affected the SPS had been executed, and the spacecraft bus current showed no abnormalities.

The failure analysis focused on the nature and history of the heaters and on the design of driver circuits in the attitude control electronics.

Malfunction Analysis

The test history of the valve heaters was reviewed. No failures had occurred, and no anomalous operation had been observed either at Rocket Research Company or Fairchild. Resistance, high potential, and response-on-activation measurements had all been normal (resistance = 294 to 304 ohms, specification: 296, ±30 ohms; high potential = 35 k to 80 k megohms, specification: equal to or greater than 100 megohms).

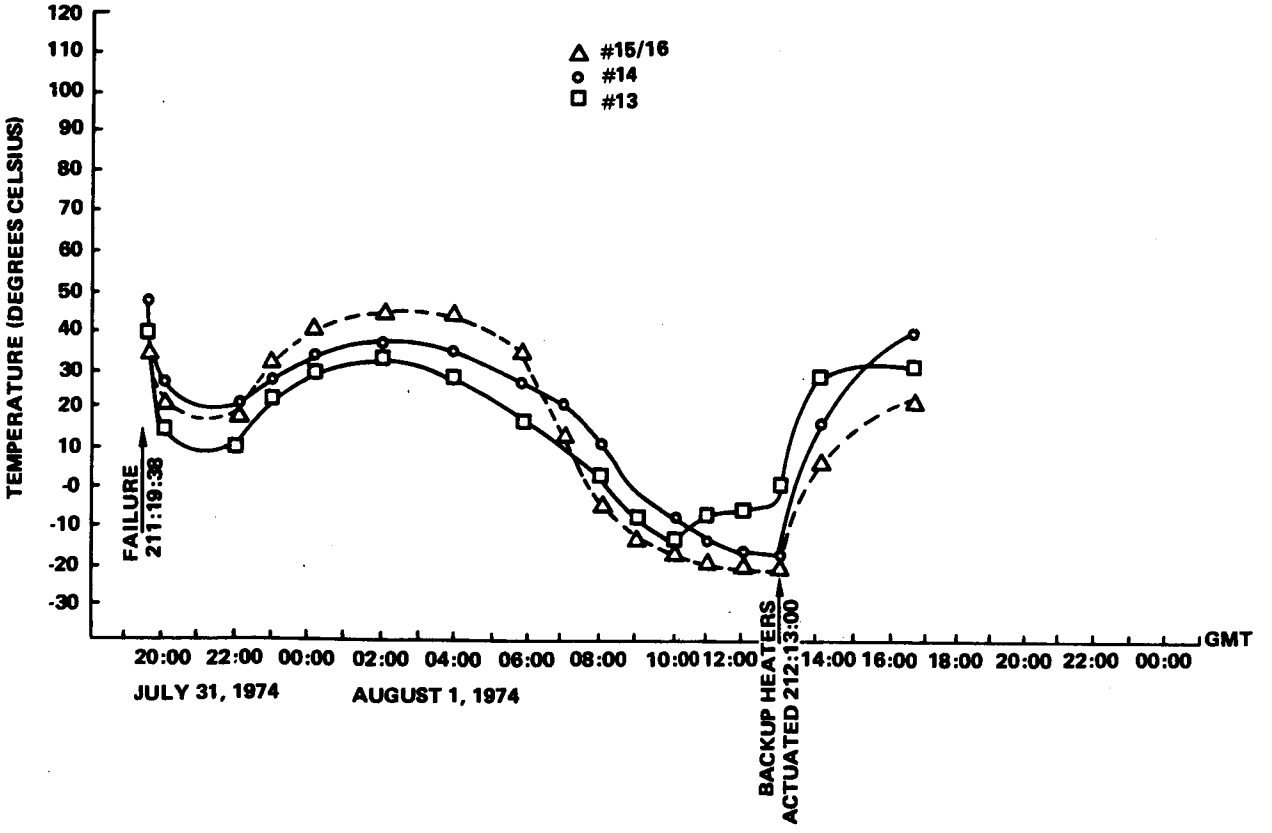

Figure 8-2. SPS-1 Truss Valve Temperatures vs. GMT

The prime and backup heater elements for each valve were potted together in a C-shaped cylinder that was bonded to the valve body. The two lead wires from each heater element ran from the heater to connector J-9 (SPS-1) or J-10 (SPS-2) on the actuator control electronics box. Inside the actuator control electronics, the eight leads from either a prime or backup set of four heaters (SPS-1 and -2) were wired in parallel on a terminal board and connected to a single driver circuit. The driver was a solid-state switch with associated current limiting and latch circuits.

The fact that an external open failure of any single valve heater would not prevent operation of the remaining heaters eliminated such a failure from consideration. An internal or external short would cause current limiting in the circuit and prevent heater operation. An internal open or circuit component failure would lead to the same result.

Current was limited by the circuit to 0.5 to 0.6 ampere, and a short would result in a similar increase in the spacecraft bus current for the 250-ms heater command period. If no change in bus current occurred, an internal open failure would be implied. In addition, if the heater malfunction was the result of a failure of the latching function of the circuit, the normal current of approximately 0.3 ampere would be drawn during the command pulse.

For the test, the communications subsystem was configured to draw enough power to discharge the batteries. In this configuration, changes in load current could be detected using the battery discharge current (telemetry channel 57) that was about three times as sensitive as channel 65 (the spacecraft load current). In addition, the wheels were taken out of the control loop, eliminating their influence on load current. When the SPS-1 backup valve heaters were commanded on, the normal current of 0.3 ampere was clearly evident on the stripchart recorder. The SPS-2 prime valve heaters were commanded on four times over a 25-minute period. No current transients were visible on the recorder, nor were any seen in the channel-57 digital printout.

After a review of the circuit design by Fairchild and Honeywell, it was concluded that, while the driver circuit was specifically designed for the ATS program and had not been used on other programs, it was fully adequate for the application. This conclusion was reinforced by the fact that there were no malfunctions recorded during component and subsystem testing at Honeywell or during Fairchild integration and spacecraft level tests.

It was concluded that the prime heater driver circuit was open probably due to a random failure of an unknown part.

Consequences of Failure

Operation with the SPS-2 backup valve heaters on (with the prime heaters failed) left no backup. The bed heaters were normally off except for periods when jet operation was anticipated.

The temperature data shown in Figure 8-2 indicate that operation with the SPS-2 backup heaters was the same as with the prime heaters. Since propellant was not bled into the SPS-2 manifold yet, it was possible to operate with the backup heaters off, allowing the dry valves to go to temperatures below the freezing point of hydrazine.

The valve vendor, Parker Hannifin, had no low temperature cycle data on the valve. Rocket Research Company had subjected one dry valve to 25 cycles between -100°C and +38°C. Before-and-after leak and electrical checks indicated no change in performance. Freeze-thaw tests at Rocket Research Company during the ATS program subjected a valve filled with hydrazine to 3 cycles between -45°C and +66°C. The valve was operational and visual inspection showed no external damage; however, an additional six cycles caused a circumferential valve-body weld to crack allowing external leakage of hydrazine.

Discussions with Rocket Research indicate that neither they nor Parker Hannifin were concerned about dry-valve temperature cycles between approximately -25°C and +50°C (as compared to +10°C to +90°C with the valve heaters on). The sensitive area where the poppet rests on the valve seat was under spring compression force and would tolerate any minor motions due to thermal expansion. However, temperature cycling of a wet valve below the freezing point of hydrazine (2°C) could rupture the valve body and cause possible internal damage.

With the manifolds filled, the backup heater and the higher solar heat input to the SPS-2 thrusters was adequate to maintain valve temperatures above the hydrazine freezing point throughout the rest of the mission.

Design Conclusions

No changes to the SPS heater system are recommended as a direct result of this failure. Ground testing of the heater drive circuit was free from malfunction and backup heater performance was adequate to maintain valve temperatures above 10°C throughout the rest of the mission. The random nature of the failure pointed up the desirability of backup capability on critical system elements.

SPS-1 VALVE HEATER FAILURES

On October 11, 1976 (2 years, 4 months into the mission), the SPS-1 truss valve heaters failed during a combined prime and backup heater powered mode. The failure was characterized by a rapid increase in the number 8 thruster-valve temperature followed by a decay in all four truss thruster-valve temperatures during the eclipse period. Analysis and ground testing has shown that combined powering of the prime and backup heater elements probably caused gradual degradation of the heater element insulation. This led to local shorting in the number 8 thruster-valve heater that eventually cascaded into a failure of both prime and backup heater driver transistors and loss of all SPS-1 truss thruster-heater power.

Malfunction Analysis

A limited command test was performed, starting on 03:51 on October 12, 1974. The purpose of the test, which was patterned after a similar test performed following failure of the SPS-2 prime valve heaters on July 31, 1974, was to establish whether a short or open condition existed in the affected SPS-1 actuator control electronics-heater circuitry. No current turn-on transients were observed during repeated executions of the prime and backup valve heater-on commands. This implied that an open condition existed in the associated circuitry.

A second SPS-1 valve heater command test was run on December 5, 1976. The lack of any current transients on the spacecraft power bus during execution of heater on commands verified that the affected actuator control electronics-drive circuitry had failed in an open condition. This was concluded to have been precipitated by partial shorts in thruster number 8's prime and backup valve heaters.

An investigation was performed of valve heat-up flight data during the usual combined use of the prime and backup valve heaters just prior to each eclipse period. The study revealed that until the Fall 1976 eclipse season, the heat-up patterns of the SPS-1 positive and negative yaw thruster valves (number 5 and number 6) and the prime and backup west orbit-control thruster valves (number 7 and number 8) closely matched each other. At the start of the Fall 1976 eclipse season, the valve of thruster number 8 started to heat up faster and hotter than that of number 7 (Figure 8-3). This differential heating pattern became more and more pronounced until, on October 10, 1976, the temperature of the number 8 valve sky-rocketed to a very high value just prior to the loss of the prime and backup valve heater functions for SPS-1. These facts supported the conclusion that the backup valve heater of thruster number 8 developed a partial short early in the Fall 1976 season, that this short became progressively worse, and that ultimately (through internal overheating during the combined heater use prior to the eclipse period) it caused a partial short to develop in the prime valve heater as well. The resulting overdrive load condition caused a failure of the associated actuator control electronics drive transistors, leaving the affected circuitry in a failed open condition (i.e., no prime or backup heater power).

A study was conducted on three flight spare and one engineering model SPS valve heater assemblies. X-rays revealed that the one engineering model heater and one flight spare heater were wired in an inconsistent manner. Internal heater leads, with evidently no insulating tape between them, were alternately wired to +28 V and ground external leads. Only the varnish coating on the wires and surrounding epoxy in the heater assembly would prevent an internal short of 28 V to ground. Two other flight spare heaters were wired in a consistent manner.

A 200-cycle thermal vacuum test was conducted on the three flight spare units to simulate the temperature cycles and combined primary/backup heater power ON phases (all considerably foreshortened in time). There was no evidence of severe damage to any of the three heater modules after the 200-cycle test. Outgassing and some thermal distortion were noted however.

An over power/voltage stress test was then performed to precipitate a failure; the voltage level to the backup heaters during their powered on phases being increased by 3 volts during each succeeding temperature cycle. One heater module (S/N 89) failed catastrophically after 10 such cycles (causing the drive electronics to fail in the process) at a voltage level of 52 volts compared to a maximum rate voltage of 33 volts. The failure was a result of a partial short from the 28-volt lead of the primary heater to a point on the coil of the backup heater near its ground lead. Coil resistance changes were noted on all three heater modules after the test, indicating some shorting of turns in each of the heater coils. Severe overheating was experienced by the failed heater module resulting in melting of the varnish coating on its heater wires, its epoxy casing, and the insulating kapton film between the heater coils. Considerably less damage was evidenced by the other two heater modules, involving some melting of the epoxy case and the heat sink bond, and some of the varnish coating of the heater coils.

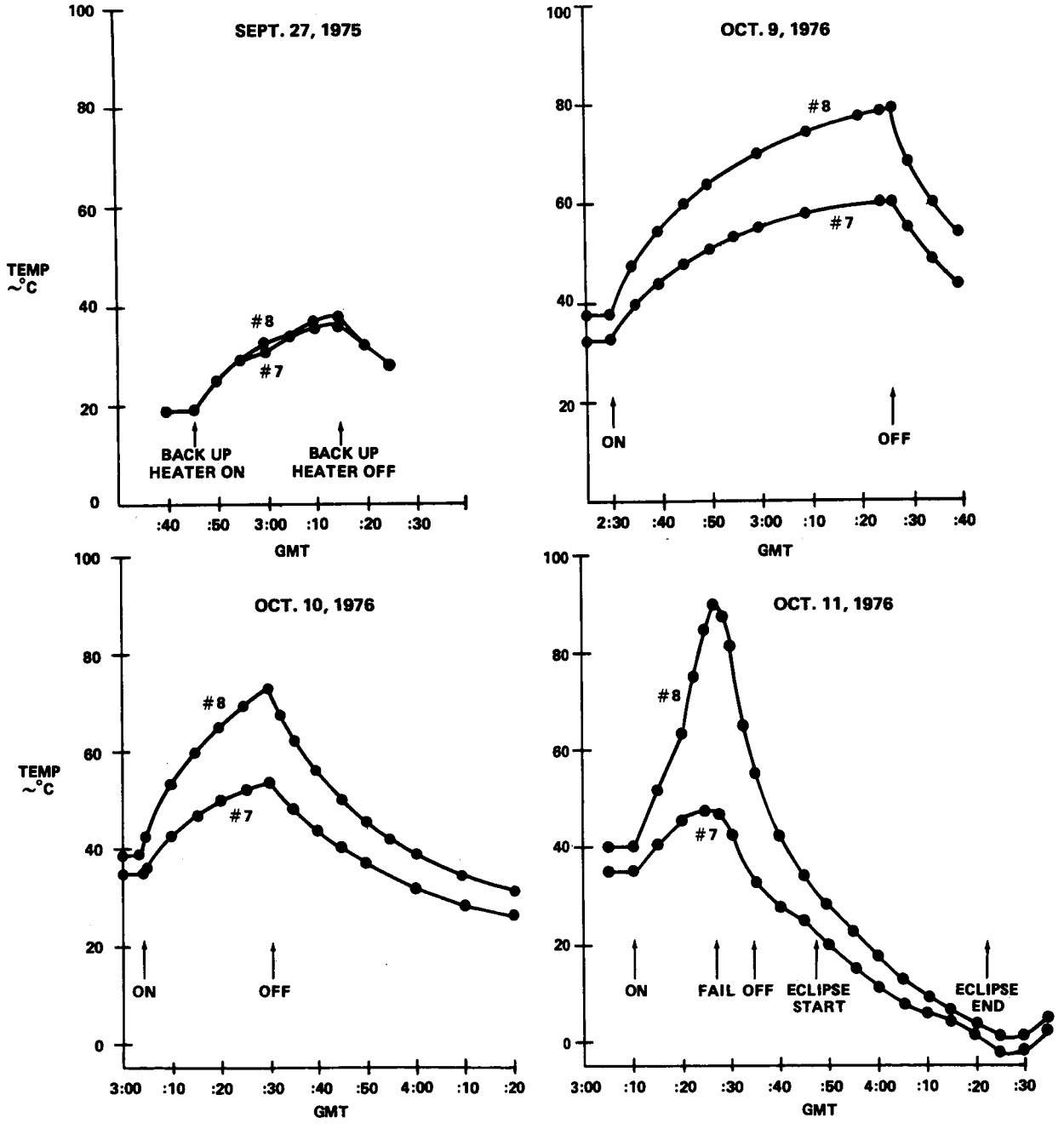

Figure 8-3. Thruster No. 7 and No. 8 Valve Temperature Profile

A thermal evaluation/analysis of a heater module subjected to voltages above the nominal 28-V level was performed. The analysis showed that if gaps or voids developed in the epoxy or Kapton/adhesives adjoining the backup heater wire, then the elevated temperature of the wire, produced at an input voltage of about 50 volts, could cause the insulating Kapton to deteriorate and permit a short to develop. With regard to the actual in-orbit failure of an SPS-1 heater module at a 28-V level, a similar analysis showed that if a break occurred in the bond of the heater module to the valve housing (explainable by the observed deformation of heater modules after repeated thermal cycles) and a gap then developed in the conductive medium surrounding the backup heater wire, then heater-wire temperatures sufficient to cause deterioration or breakdown of the insulating Kapton film could also occur.

A study was performed of the printed circuit card wiring drawings for the valve heater drive circuits in the actuator control electronics. This study revealed that the actual wiring provisions ensure the presence of independent, redundant circuit paths for the prime and backup valve heater circuits. Hence, no single-point failure in these circuits could have caused the loss of both the SPS-1 prime and backup heater functions.

Failure Consequences

A thermal study was conducted of several possible approaches for keeping the SPS-1 truss thruster valves from freezing. It was found that by commanding the SPS-1 line heaters into a constant high-power mode, enough heat was conducted to the valves to keep them from freezing. The one exception to this was the extreme cold condition associated with periods of Sun eclipse by the Earth. An effective valve-heating approach conceived for this condition was first to vent the SPS-1 manifold prior to each eclipse season (thereby also precluding the use of the SPS-1 truss thrusters). Next, during each eclipse period, the four associated valve solenoids were to be continuously activated, providing a direct heat input to the valve body.

Subsequent SPS-1 truss line evacuation tests eliminated some (but not all) of the residual hydrazine in the lines and provided baseline data on continuously-energized valve heat-up characteristics, these data being needed to guide the indicated contingency eclipse operations.

As a result of successful reprogramming to enable the digital operational controller to output simultaneous positive, negative yaw thruster commands, it was possible to define a relatively simple and effective operational sequence for thermal control of the SPS-1 truss thruster valves during subsequent eclipse periods. The first two Spring 1977 eclipse operations confirmed the viability of this sequence and its adequacy for thermal control of dry SPS-1 truss valves, even during maximum eclipse periods. Thruster control during eclipse periods was handled by the SPS-2 thrusters that were operating properly with the backup heaters.

Design Conclusions

As a result of this failure, many conclusions relating to the design and use of similar heater units in spacecraft applications can be made.

During the first eclipse period of 1974, performance of the prime SPS-1 heaters (when entering the eclipse at 15°C) appeared marginally able to maintain valve temperatures above the 5°C design condition. Concern about freezing of hydrazine led to institution of the combined prime and backup heater mode on SPS-1 prior to each eclipse. This maintained valve temperatures at or above a more comfortable 10°C (with respect to hydrazine freezing temperature of 2°C) during subsequent eclipses. Post-failure ground testing showed that this combined mode of operation (not included in heater qualification testing) caused increased outgassing and thermal distortion of the heater. The testing also revealed design/manufacturing faults that could have contributed to an individual valve heater shorting failure. Thermal analysis showed that any unbonding of the heater elements from outgassing or thermal distortion (during a combined mode) would result in heater temperatures above the insulation degradation point. Once the insulation broke down, shorting of the elements of the design would follow. When the shorting became excessive (resistance less than 20 ohms), the heater drive circuits would unlatch or fail, resulting in loss of both prime and backup heaters.

It was concluded that proximity of the prime and backup heater elements in the design led to failure of both elements due to a failure in one. Future programs should use a more positive separation of redundant heater elements. The ATS-6 system was designed to a 5°C minimum temperature to minimize system power requirements. Future programs should design to at least 10°C (and take the power penalty) to provide adequate margin above hydrazine freezing during long eclipse periods.

As identified in the ALERT issued by GSFC on the heater, simultaneous operation of prime and backup heaters should be avoided on similar parts in use. If this heater is selected for a new program, an additional screening test using X-rays is suggested to eliminate high risk parts.

THRUSTER BED TEMPERATURE ANOMALIES

Due to the operating temperature range of 30°C to 1000°C, thruster catalyst bed temperatures were sensed by chromel-alumel thermocouples rather than thermistors. During ground test, prelaunch, launch, and initial mission phases, the susceptability of the thermocouples and associated electronics to radio frequency interference from the prime focue feed reflector caused 10°C to 100°C uncertainties in various bed temperatures (Figure 8-4). The final level of uncertainty (10°C to 30°C) did not interfere with detecting proper operation of the bed heaters or the large temperature change associated with thruster operation. However, differences of 20°C to 30°C magnitude were very noticeable and fell outside of the predicted ±15°C accuracy of the bed temperature monitoring system. The following paragraphs present a detailed description of the observed temperature anomalies, test history of the temperature circuit, consequences of the anomalies, and design conclusions.

Anomaly Description

Anomalous readings on thruster catalyst bed temperatures were first observed during ground rfi tests. Shielding was added to the SPS actuator control electronics connectors and reduced but did not eliminate the rfi influence. Further ground tests showed that anomalous readings would disappear when telemetry was transmitted by the omnidirectional antenna rather than the reflector.

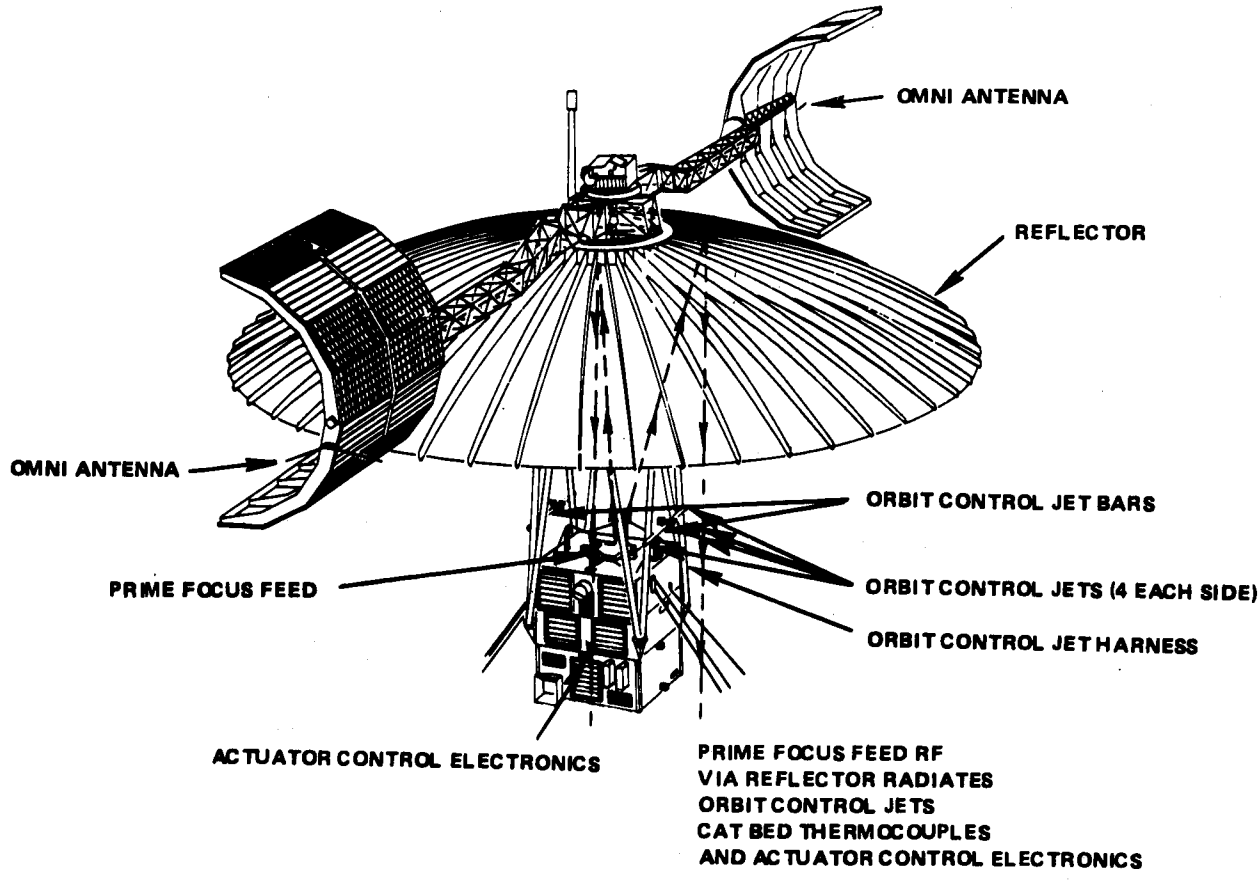

Figure 8-4. Anomaly Element Illustration

Table 8-1 presents the prelaunch, launch, and in-orbit temperature and illustrates the magnitude of the anomalies. (Note: temperature resolution is 4°C). In this table, thrusters numbers 4, 14, and 16 read 15°C to 60°C high when compared to their companion numbers 12, 6, and 15 thrusters. With no shroud and transmitting on the omnidirectional antenna, the anomalous readings disappeared. SPS-1 thruster activity after deployment interferred with any further comparison.

A special in-orbit test was conducted on July 23, 1974, to determine the effect of telemetry rf on the bed temperature readings. Table 8-2 presents temperature readings from the test with the transmitter and antenna configured five different ways. Again resolution is 4°C per unit count.

With no change in transmitter configuration (first two columns), five one-count changes occurred in 5 minutes. Times between configuration were variable and all shifts were one-count changes except when the A2 (137 MHz)/prime-focus feed combination was turned off, switching the temperature telemetry to A1 (136 MHz)/omnidirectional-2. In this case three significant shifts occurred

Table 8-1
SPS Catalyst Bed Temperatures (°C)

	JETS			5-24-74 SC PWR On	5-30-74 SC PWR On	←SHROUD→ 5:01 AM Pre-Launch	T-4 MIN Pre-Launch	←NO SHROUD (OMNI)→ T+45 Shroud Off Pre-Shadow	T+1:30 Post Shadow Cool	T+6:14 Trans-Orbit Warm	←DEPLOYED→ T+8:03 SPS 1 Bed Htr On, Sun On SPS 2	T+9:32 SPS 1 Bed Htr On, Sun On SPS 1	T+15:29 1:70 Post Yaw, Sun On SPS 2
				LC40									
SPS 1	1	-R	EVM	23	23	23	23	27	19	23	100	140	148
	2	+R		15	15	19	19	19	19	27	104	136	132
	3	-P		23	23	19	19	19	15	27	83	156	128
	4	+P		23	23	27	27	15	15	27	120	144	160
	5	+Y	OCJ	27	23	31	27	31	11	27	95	144	140
	6	-Y		15	11	19	19	23	11	23	87	132	104
	7	WP		19	15	19	19	27	11	23	79	144	112
	8	WB		15 (19)	11 (15)	15 (19)	15 (19)	23 (27)	11 (11)	19 (23)	83	160	128
SPS 2	9	-R	EVM	27 (23)	23 (23)	19 (23)	19 (23)	23 (27)	15 (19)	19 (23)	15	7	31
	10	+R		23 (15)	27 (15)	19 (19)	15 (19)	19 (19)	19 (19)	23 (27)	15	7	7
	11	-P		19 (23)	19 (23)	15 (19)	15 (19)	19 (19)	15 (15)	27 (27)	3	55	11
	12	+P		11 (23)	11 (23)	11 (27)	11 (27)	11 (15)	11 (15)	19 (27)	39	11	47
	13	-Y	OCJ	31 (27)	27 (23)	27 (31)	31 (27)	27 (31)	11 (11)	23 (27)	23	-5	47
	14	+Y		95 (15)	71 (11)	51 (19)	43 (19)	23 (23)	15 (11)	23 (23)	27	-9	23
	15	EP		35	35	43	43	15	7	19	43	-9	55
	16	EB		79 (35)	59 (35)	67 (43)	59 (43)	23 (15)	11 (7)	27 (19)	39 (43)	-5 (-9)	63 (55)

NOTE: During early first stage burning, SPS 2 OC temperatures were unstable (±30°C) while shroud was on.

Table 8-2
RF Effect on Catalyst Bed Temperatures

			Telemetry Transmitter Condition (Day 204)						
XMTR		Antenna	15:42:31	15:47:02	15:47:38	16:00:01	16:09:28	16:11:49	
136	A1	OMNI-2	ON	ON ▲	OFF ▲	ON	ON*	ON*	
137	A2	PFF	ON*	ON*	ON*	ON*▲	OFF	OFF	
136	A3	(None)	OFF	OFF	OFF	OFF	OFF	OFF	
136	A4	OMNI-1	OFF	OFF	OFF	OFF	OFF ▲	ON	
			Catalyst Bed Temperatures, °C						
SPS-1	1	-R (EVM)	47°	43°	43°	43°↓	39°	39°	
	2	+R (EVM)	15	15	15 ↑	19 ↓	15	15	"Typical Values"
	3	-P (EVM)	63 ↑	67 ↓	63 ↓	59 ⬇	51	51	
	4	+P (EVM)	15	15	15	15	15	15	
	5	+Y (OCJ)	47	47	47	47 ↓	43	43	52°
	6	-Y (OCJ)	27	27	27	27	27	27	31
	7	WP (OCJ)	51	51	51 ↓	47	47	47	49
	8	WB (OCJ)	47	47	47 ↑	51 ↓	47	47	49
SPS-2	9	-R (EVM)	39	39	39	39 ⬇	27	27	
	10	+R (EVM)	11	11	11	11 ↑	15 ↓	11	
	11	-P (EVM)	71	71 ↓	67 ↓	63	63 ↓	59	
	12	+P (EVM)	19 ↓	15	15 ↑	19	19	19	
	13	-Y (OCJ)	23 ↓	19 ↑	23	23 ↓	19	19	20
	14	+Y (OCJ)	11 ↑	15	15 ↑	19 ⬇	3	3	24
	15	EP (OCJ)	-9	-9	-9 ↑	-5	-5	-5	-7
	16	EB (OCJ)	11 ↑	15	15	15 ↓	11	11	13

*Catalyst bed temperature transmitter

Legend:

↑ = Normal Temperature Change

⬇ = Rapid Temperature Change

▲ = Transmitter Antenna Change

with thruster number 14, which has always been sensitive to rf, showing a 16°C change, thruster number 9 showing a 12°C change, and thruster number 3 showing an 8°C change. No significant changes were seen when the omnidirectional-1 antenna was activated.

Periodic monitoring of bed temperatures over 24-hour periods during noneclipse periods continued to show anomalous readings when transmitted by the reflector. Figure 8-5 shows comparison thruster bed temperatures for the 24-hour period beginning December 21, 1974. Note the 15°C to 20°C bias between thruster numbers 15 and 16, numbers 2 and 10, and the 0°C to 30°C delta between numbers 1 and 9.

Test History

Rfi testing, during spacecraft level tests, showed certain catalyst bed temperature readings to be susceptable. This was particularly true of those thermocouples directly in the beam of the prime-focus feed. Initial susceptability included instabilities and inaccuracies reaching 100°C. Corrective action involved the application of additional shielding at all thermocouple connector locations and retesting with a portable rf source. Rf sensitivity was reduced to an acceptable level (20°C) but not eliminated. Temperatures transmitted by the prime-focus feed still appeared higher than normal, but read normal when temperature data was transmitted by the omnidirectional antenna. No further ground testing was conducted.

Once in orbit, continued anomalous readings were observed. On July 23, 1974, a special in-orbit test was conducted to quantify the magnitude of the rf effect on the catalyst bed temperature (Table 8-2).

No general conclusion could be drawn from the in-orbit test data. It appeared that switching in omnidirectional antennas had little influence on data being obtained by the prime-focus feed. A significant shift occurred on a few channels when the telemetered temperatures were switched from the prime-focus feed to an omnidirectional antenna and the prime-focus feed was turned off.

The improved consistency between companion channels indicated some reduction of rf influence and the remaining inconsistencies were attributed to system accuracy. It should be noted that differences up to 22°C between companion temperatures would still be within the predicted ±15°C accuracy of the catalyst bed temperature.

Consequences of the Anomalies

The primary function of the catalyst bed temperature monitors was to assure proper operation of the catalyst bed heaters. This was indicated when a reading of 200°C to 250°C was observed. At this level 15°C to 20°C uncertainty was not significant. A secondary use of the data was to detect the large (200°C to 600°C) temperature change indicative of proper thruster operation. Again a 15°C to 20°C uncertainty was not significant.

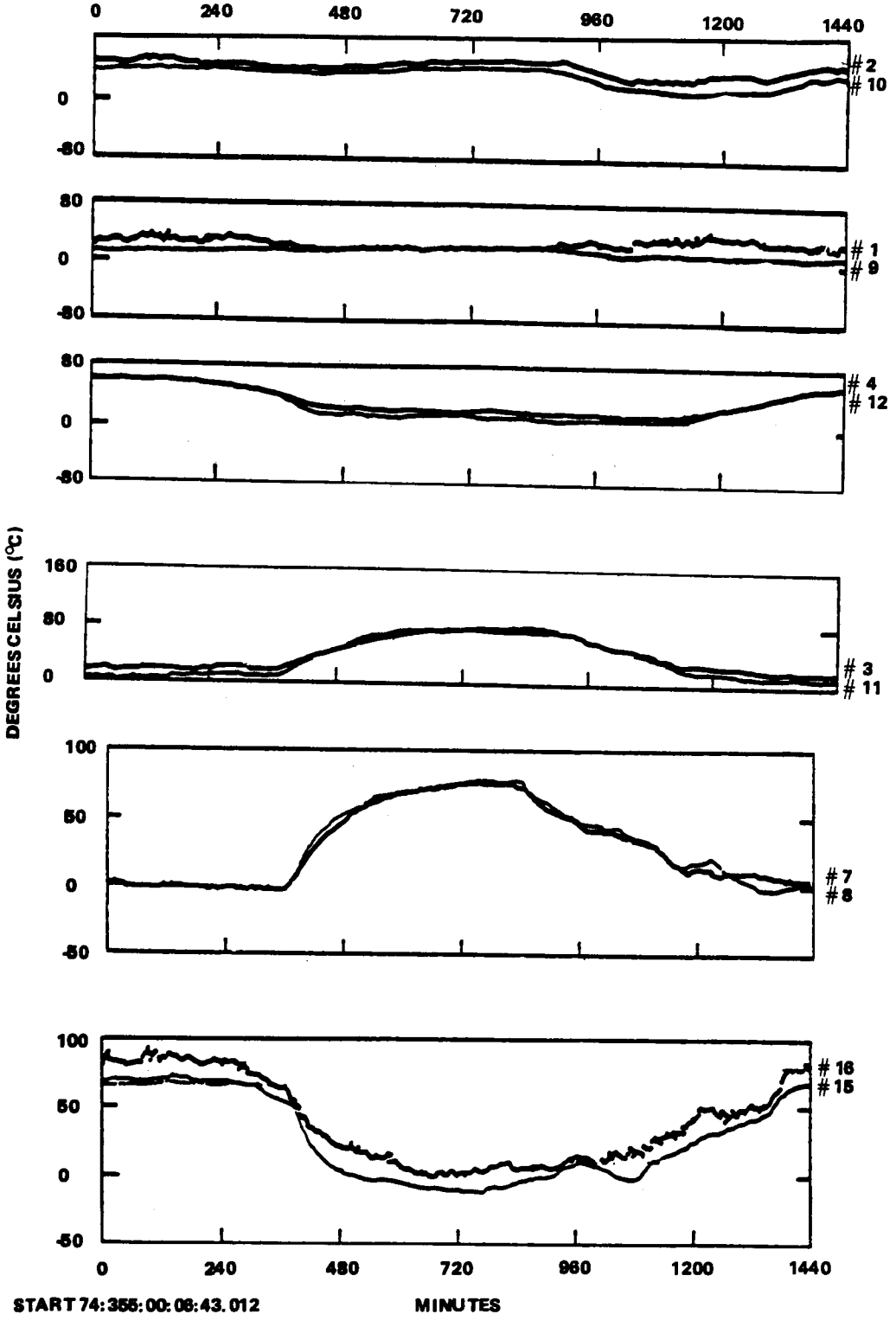

Figure 8-5. Thruster Bed Temperatures (24-Hour Cycle)

Once the in-orbit test established that the magnitude of the rf induced anomaly was within acceptable limits when related to the purposes for the temperature monitor, no further investigation was necessary. Subsequent temperature transmissions used the prime-focus feed, and all catalyst bed temperatures remained operational for the duration of the mission.

Design Conclusions

The design of the catalyst bed temperature monitor system (i.e., chromel-alumel thermocouples, connectors, harness, amplifier circuit, etc.) was adequate for the intended purposes. Rf susceptability caused 10°C to 30°C uncertainties in system elements directly exposed to the prime-focus feed rf. An in-orbit test established the temperature bias when the prime-focus feed was used. No impact on bed temperature monitoring resulted from the known uncertainties. A redesign of the amplifier circuit of the actuator control electronics package could have reduced the uncertainties beyond the reduction achieved with shielding but at the time, this would not have been cost or schedule effective.

Future missions with high rf transmission power should consider well shielded and filtered thermocouple temperature systems early in the design phase to minimize rf susceptability.

THRUSTER ANOMALIES

Beginning in February 1977, after 2.6 years in orbit, and continuing to the final de-orbit maneuver after 5.3 years, a total of 13 of the 16 thrusters experienced various combinations of intermittent leakage; low, variable, or degrading thrust and impulse bits; or failure to produce thrust upon command. At the end of the mission, three thrusters were still operating normally, and one was producing thrust at a degraded level. Figure 8-6 summarizes the chronology and nature of each of the failures. Extensive analysis and ground testing both prior to and after launch indicates the most probable cause as contaminants that either accumulated slowly in the thruster capillary tube or suddenly plugged the thruster feed. The most likely sources of the contaminants were zinc and silicon oxide (SiO_2) leached from the EPT-10 diaphragm, trace impurities in the loaded hydrazine, or residual deposits from clean and flush operations after initial ground test hydrazine exposure. The following sections present the complete description, test history, failure consequences, and design conclusions relating to the various failures.

Description of Failures

The thruster anomalies and failures are detailed chronologically as follows:

- On four separate occasions during January 1976, the SPS-2 negative roll jet number 9 exhibited abnormally high impulse in response to commands. The bit impulse increased progressively, was quantitatively erratic, and at its maximum was twice that expected. Attitude control was switched to SPS-1 until May 1976 when a special test indicated normal jet number 9 operation.

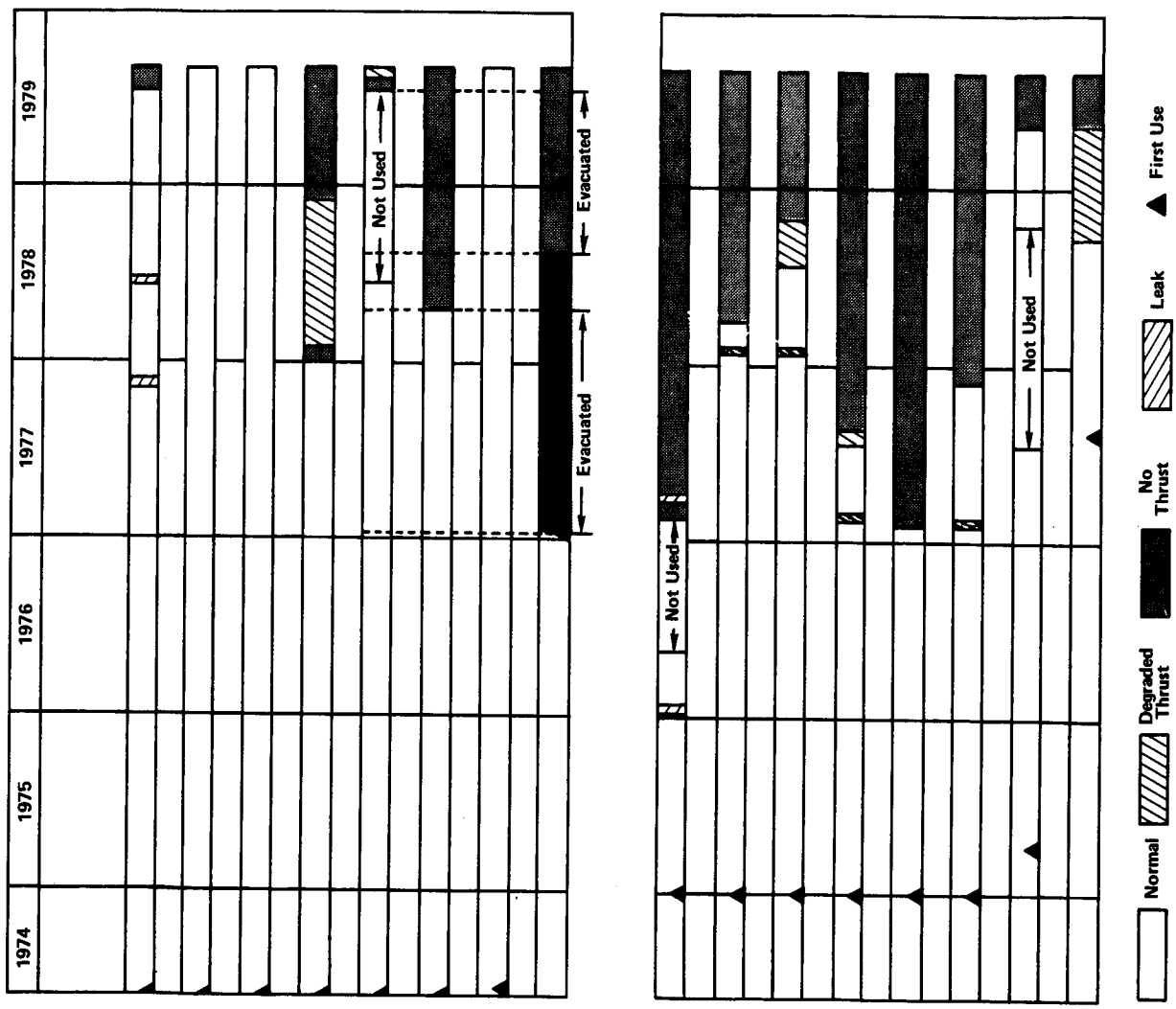

Figure 8-6. Thruster Failure Chronology

- On February 2, 1977, during a scheduled ATS-6 stationkeeping maneuver, a failure of the SPS-2 negative yaw jet number 13 was observed. Subsequent testing confirmed a propellant feed blockage as the cause of the failure. Several exercises were scheduled during the month in an attempt to free the blockage, but all results were negative.

- On February 19, a test was conducted to evaluate the performance of the other SPS-2 attitude control jets. During the test, it became apparent that the negative roll jet number 9 had also failed. The negative roll and negative yaw jet failures appeared to be similar. The discrete telemetry on both jets indicated that the actuator control electronics was firing them and the valve solenoids were heating up, indicating that they were being energized. However, the catalyst bed temperatures and inertia wheel speeds remained constant, indicating some sort of propellant feed blockage.

- During February 1977, low impulse response on initial pulse trains was indicated on SPS-2 positive yaw jet number 14 (February 1), and SPS-2 positive pitch jet number 12 (February 19). Subsequent pulse testing of the jets indicated normal operation.

- Testing of the failed jets on SPS-2 continued during the month of February. On March 4, an attempt was made to free the obstruction in the negative roll jet number 9 by pulsing it 2,000 times using a time delay between commands of 0.25 second. This test was similar to one performed on the negative yaw jet number 13 in February. The results of the negative roll jet test were negative. Additional testing of the negative roll and negative yaw jets on March 16 confirmed that both jets were still blocked. On March 30, the SPS-2 negative roll jet number 9 began to leak as evidenced by an increasing catalyst bed temperature and increasing roll wheel speed. During the ensuing 12 hours, it was necessary to issue positive roll torque commands to maintain acceptable wheel speeds. Several hours later, the catalyst bed temperature and roll wheel speed returned to normal, indicating that the leak had subsided. All attempts at getting the jet to fire on April 1 were negative.

- Because of the concern over the performance of the SPS-2 thrusters, periodic tests of these jets were initiated on June 3, 1977. Except for the inoperative negative roll and negative yaw jets, all thrusters responded normally to 5-pulse command sequences on June 3, and June 17, 1977.

- On July 15, during a routine test of the attitude control jets, it was noted that the SPS-2 positive pitch jet number 12 appeared to be firing with less than nominal performance. A nominal performance from this jet should have resulted in a change of wheel speed from 16 to 18 rpm per pulse but instead, a change of only 10 rpm per pulse was noted. Further testing of the number 12 jet was carried out on July 19. During the test the output of the jet degraded further to a thrust level of approximately 6 rpm per pulse.

- A regimen of SPS jet testing was instituted whereby the SPS-2 jets were tested weekly and the SPS-1 jets were tested biweekly. Results of the SPS-1 and -2 tests conducted on August 6 indicated that SPS-2 positive pitch jet number 12 had further degraded to approximately 1 rpm per pulse from the previous 6-rpm per pulse level. Status of all other SPS-1 and -2 jets remained the same.

- On Number 11, 1977, starting at about GMT 17:29, several operational mistakes during a routine reorientation maneuver caused the loss of Earth acquisition. Contributing to this event was the fact that the SPS-1 negative roll jet number 1 stuck partially open for some 5 minutes after it was commanded off by the onboard control electronics.

- On January 11, 1978, prior to a scheduled maneuver, an attempt to adjust pitch-wheel speed revealed that SPS-1 positive pitch jet number 4 was inoperative. The maneuver was completed satisfactorily despite the problem. This was the first time that an SPS-1 jet exhibited degraded performance. Subsequent testing of the SPS-1 pitch jet number 4 showed a resurrection of thrust response. A January 21 test revealed a thrust level of 1.44 rpm per pulse; further testing of the jet saw the thrust level reach approximately 3 rpm per pulse. The testing of the SPS-1 positive pitch jet number 4 was terminated on February 1, since the output thrust value remained constant at 3 rpm per pulse during the previous week.

- On January 25, an attempt to unload the pitch inertia wheel revealed that SPS-2 negative pitch jet number 11 was operating at approximately 40 percent of the expected value when a multiple execute command (20 executes) to fire was transmitted. A second multiple execute command was transmitted. Close monitoring of the performance of this jet indicated no recurrence of the problem.

- On January 31, in the process of unloading the roll inertial wheel, it was noted that SPS-2 positive roll jet number 10 was operating at approximately 70 percent of the expected thrust value. Subsequent firings of this jet indicated normal operation.

- On April 24 the SPS-1 truss latch valve was commanded open after which the spacecraft was carefully monitored for 1 hour to detect any possible leaks in the system. After it was determined no leaks were present, the SPS-1 positive yaw jets were pulsed in the ground-control-jets mode to determine their condition. The SPS-1 positive yaw jet number 5 was found to be operating at normal thrust but the SPS-1 negative yaw jet number 6 was completely inoperative. Testing of the number 6 jet on a regular basis, including commanding it open (by the digital operational controller) for up to 20 minutes, continued with no response.

- On June 1, 1978, while the spacecraft was in the jet-assist mode, the SPS-1 negative roll attitude jet number 1 fired. It was noted that the jet remained firing for approximately seven times longer than normal. This anomaly had been observed previously but did not repeat itself.

- A stationkeeping maneuver was performed September 27, 1978, using the SPS-2 eastward backup orbit-control jet number 16. Telemetry indication of lower than expected thrust was observed and post-maneuver tracking data revealed a thrust level 28 percent of predicted. A second maneuver was performed on October 5 using the same thruster. Post-maneuver analysis indicated a thrust level of 45 percent. On October 11, a third stationkeeping maneuver was performed, this time using the SPS-2 eastward prime orbit-control jet number 15. This thruster performed at 85 percent of the predicted thrust, which was based on its last use on July 15, 1977.

- During a scheduled stationkeeping maneuver on May 6, 1979, SPS-2 eastward prime orbit-control jet number 15 failed to fire. After repeated 'ON' commands with no response, the maneuver was cancelled. This jet performed nominally when last fired on March 28, 1979. On May 8, the maneuver was attempted again, and jet 15 did not fire. It was then attempted using the eastward backup orbit-control jet number 16, which had exhibited low erratic thrust the last few times it was used, but it too failed to fire. The stationkeeping maneuver was performed successfully on May 9 using SPS-1 westward prime orbit-control jet number 7 after doing a 180-degree yaw flip. This required pressurizing the SPS-1 truss manifold that had been evacuated since August 1978. SPS-1 westward backup orbit-control jet number 8 was test fired during this maneuver and was still inoperable. (It appeared inoperable during an SPS-1 truss line evacuation test performed early in 1977.) The three bad orbit-control jets were tested extensively on May 21 and again on May 25 with no response from any of them.

- During a routine roll wheel unload on July 13 the SPS-1 negative roll jet number 1 failed to respond. To maintain roll stability it was planned to use the SPS-1 positive yaw jet number 5 at 180-degree yaw as an alternate. However, this jet, which had not been used since June 25, 1978, also failed to fire. This left the only contingency plan of twice daily 180-degree yaw flips to maintain roll momentum management.

- Command 55150 (136 MHz TLM XMTR OFF) was executed August 3, 1979, thus ending the active life of ATS-6 after more than 5 years of in-orbit operation. Leading up to this final shutdown, a 28-hour burn of the SPS-1 westward prime orbit-control jet number 7 was completed on August 1. This maneuver consumed 12.5 kg of hydrazine and placed the spacecraft in an orbit estimated to be 520 km below synchronous with an eastward drift rate of 6.05 degrees per day. During this burn, the SPS-1 negative pitch jet number 3 and positive yaw jet number 5 (that came back to life after failing to fire July 13) performed well to help maintain spacecraft attitude. The orbit-control maneuver was followed by a continuous burn of the SPS-1 positive roll jet number 2 to fuel depletion, achieving a roll spin rate of 1.6 rpm. SPS-1 westward prime orbit-control jet number 7 was left on at final shutdown to allow any remaining hydrazine to escape.

Test History

At the component level each thruster was successfully fire tested, at high and low feed pressure, before and after acceptance vibration tests using a baseline performance duty cycle.

The results of the 200 second steady-state acceptance tests are listed in Table 8-3. No correlation with the flight anomalies and failures is evident from the data.

After installation in the subsystem, additional vacuum fire tests were performed at Rocket Research. This required loading the subsystem and subsequently unloading and decontaminating it prior to shipping to Fairchild. The decontamination procedures involved flushing with water and alcohol and vacuum drying but with no through flushing of the individual thrusters.

Following these components, assembly, and subsystem acceptance tests at Rocket Research, the flight subsystem was shipped as an integral unit to Fairchild. The SPS then proceeded through receiving inspection, installation in the service module, thermal wrap assembly, and electrical integration with the attitude control subsystem. With the SPS installed, the spacecraft level testing included the long form test, thermal vacuum cycle and balance, spacecraft acoustic, protoflight vibration, mass properties, separation, radio frequency compatibility, and finally preparation for shipment. All ATS-6 prelaunch testing and checkout at the Air Force Eastern Test Range was accomplished after mating with the Titan III-C launch vehicle on Pad 40, including final hydrazine fueling.

Throughout the prelaunch period, leak rates across the individual thruster valve seats were monitored. The original maximum allowable leak rate was 1.8 scc helium per hour at 28.18 kg/cm^2 (400 psi). Toward the end of the program this was increased to 6.0 scc helium per hour. Table 8-4 lists the measured leak rates for the flight system taken throughout the test and prelaunch period. Note that three of the thruster valves were slightly over specification leakage at the time of launch necessitating a waiver. Flight performance of these valves showed no correlation with the preflight leak rates.

All fluids, including water, isopropyl alcohol, hydrazine, nitrogen, and helium were sampled and counted for particulate contamination before introduction into the subsystem each time a new fluid hookup was made. All fluid equipment including lines, hoses, fittings, and the service cart were liquid-flush cleaned and certified better than the following limits expressed as maximum allowed number of particles (of a size range in micrometers): 460 (5 to 10 μm), 128 (11 to 15 μm), 10 (26 to 50 μm), 2 (51 to 100 μm, no metal) and 0 (101 μm and greater).

Considerable effort was expended to ensure that chemical and particulate impurities of the flight propellant were within limits mutually agreed upon by management of Goddard, Fairchild, and Rocket Research. Several drums of propellant, purchased to the basic hydrazine specification, were rejected following analysis at Rocket Research and returned to the vendor. Drum H-4413 was then selected for flight use from two drums that had acceptable analyses.

Table 8-5 documents the eight analyses performed on this propellant from the time it was first checked on April 25, 1974 until the post-flight load samples on May 17, 1974, two weeks before launch. Seven of the eight analyses were performed at the Air Force Eastern Test Range Chemical Laboratory, including the as-received drum, the loaded cart, samples from the fill lines before satellite loading, and post-load samples.

Table 8-3
Thruster Acceptance Test Performance (200 Seconds)

Thruster No.	Thruster SN	Hi Thrust SS Thrust - (lbf)	Hi Thrust SS I_{sp} - (sec)	Low Thrust SS Thrust - (lbf)	Low Thrust SS I_{sp} - (sec)	Flight Performance
1	73 Previb	0.122	215	0.054	208	Leaked twice,
	Post-vib	0.124	222	0.054	209	Plugged
2	74	0.124	224	0.054	213	Okay
		0.124	223	0.056	213	
3	76	0.123	221	0.054	211	Okay
		0.121	224	0.055	214	
4	82	0.121	219	0.054	209	Plugged, low thrust,
		0.121	219	0.054	212	Plugged again
5	50	0.123	223	0.054	214	Plugged, low thrust
		0.127	230	0.054	216	
6	51	0.124	229	0.054	204	Plugged
		0.128	225	0.056	224	
7	71	0.127	228	0.056	214	Okay
		0.126	227	0.056	211	
8	72	0.124	220	0.057	221	Plugged
		0.124	215	0.055	207	
9	60	0.122	224	0.053	218	High impulse, plugged
		0.123	221	0.055	214	Leak, plugged
10	75	0.125	221	0.053	208	Low thrust,
		0.123	225	0.054	212	Plugged
11	77	0.125	219	0.054	209	Low thrust, okay,
		0.124	222	0.056	213	Degrading thrust,
						No thrust

Table 8-3
Thruster Acceptance Test Performance (200 Seconds) (continued)

Thruster No.	Thruster SN	Hi Thrust SS Thrust - (lbf)	Hi Thrust SS I_{sp} - (sec)	Low Thrust SS Thrust - (lbf)	Low Thrust SS I_{sp} - (sec)	Flight Performance
12	87	0.124 0.126	222 221	0.055 0.057	210 213	Low thrust, okay, Degrading thrust, No thrust
13	78	0.122 0.122	222 220	0.055 0.054	212 208	Plugged
14	79	0.126 0.123	222 222	0.054 0.055	218 211	Low thrust, okay, Plugged
15	58	0.122 0.125	221 228	0.055 0.05	221 214	Plugged
16	81	0.124 0.125	218 216	0.054 0.053	209 198	Degrading thrust, No thrust

Note: Thrust (lbf) 4.448 = thrust (N)

I_{sp} (sec) 9.807 = I_{sp} $\frac{(N \cdot s)}{kg}$

Table 8-4
Thruster Leak Summary

Thruster	Thruster (SN)	Thruster Valve (SN)	RRC ATP (1)	RRC ATP (2)	Fair-child	S/C Instl	Post-TV	Post-Vib	Pre-Launch	Remarks
1	73	131	0	1.8	2.3	1.9	0	1.6	0.8	Leaked twice in flight
2	74	132	0	0	0.7	2.6	0	1.5	0.6	
3	76	132	0.2	0	2.3	11.0	4.1	21.1	15.0	Launch waiver granted, no flight problems
4	82	144	0	0	0	0	0	0.1	0	
5	50	156	1.4	0	1.1	0	0.2	0.5	0.3	
6	51	153	0	0.2	0.7	0.4	0	0.1	0.2	
7	71	111	0	0	0	0	0	0	0	
8	72	155	0	4.2	5.4	4.5	0.5	3.7	4.1	
9	60	160	0	0	2.5	3.2	0	7.6	10.1	Launch waiver granted, high impulse anomaly, leaked once in flight
10	75	133	0	0	2.3	2.4	0.2	10.9	9.3	Launch waiver granted, plugged in flight
11	77	136	0	2.3	2.3	8.0	0	0	0	
12	87	146	0	0	0.6	1.1	0.4	1.3	0.7	
13	78	137	0	0	0.5	0.5	0	0.6	0.4	
14	79	147	0	0	0.2	0.4	0	8.1	0.6	
15	58	140	0	0	1.1	0.7	0	1.0	0.7	
16	81	110	1.7	0	13.8	10.4	0.4	0.3	0.5	

Note: Leak rate in scc per hr He at 400 psig

Table 8-5
Chemical Analysis of ATS-6 Flight Propellant (April and May 1974)

		Drum H-4413		Samples from Loaded Cart		Preload (Fill Lines) 5-17-74		SPS Backout 5-17-74	
	RQMTS	RRC 4-25-74	AFETR* 5-2-74	#1	#2 (5-12-74)	SPS-1 -599-***	SPS-2 -600-	SPS-1 -601-	SPS-2 -602-
N_2H_4, percent	98.0 min	98.65	98.7	98.9	98.9	98.84	98.90	98.90	98.85
NH_3, percent	0.4 max	0.24	0.2	0.1	0.1	0.09	0.09	0.10	0.10
H_2O, percent	1.5 max	0.66	0.6	0.6	0.6	0.7	0.6	0.6	0.6
NVR, ppm	20 max	4	12	11	6	7	7	6	8
Particulate, mg/1	10 max	0	0	0	0	1.2	0.0	1.2	0.0
Corrosivity, ppm Fe	25 max	0.8	1.8	4	3	5	6	4	5
Chloride Ion, ppm	5 max	0.8	2	<0.2	0.2	0.45	0.52	0.76	0.40
Aniline, percent	0.5 max	0.45	0.4	0.4	0.4	0.4	0.4	0.4	0.4
UDMH, ppm		(0)	3	3	4	3	3	3	3
MMH, ppm		(0)	<100	<20 (ND)**	<20 (ND)	<40	<40	<40	<40
Total Organics, ppm		8	–	–	–	–	–	–	–
Toluene, ppm		–	–	<1 (ND)	<1 (ND)	–	–	–	–
IPA, ppm		–	3	20	17	52	60	33	34
CH_4 and Methyaniline, ppm		–	–	3	3	–	–	–	–

*AFETR = Air Force Eastern Test Range
** (ND) = Not Detected
*** AFETR Sample Number 4100-XXX-054

When the figures are compared to the requirements column, it is seen that all of the results are well within established limits. Most of the small variations among the results can be attributed to experimental uncertainty, with the possible exception of the corrosivity figure that indicates some increase in absorbed carbon dioxide (CO_2) with time and handling (i.e., increased possibility of atmospheric exposure). Discussions with the chemist at the time the samples were being analyzed indicated that the minimum detection level for the organic constituents was different for each species and that the numbers quoted should be used with caution. The analytical figures support the concensus that the propellant had the necessary and sufficient purity for flight use.

Failure Consequences

For the first four and a half years of the mission, the full redundancy of the spacecraft propulsion subsystem and revised attitude control system modes of operation allowed normal attitude control and orbit-adjust maneuvers despite individual thruster failures.

Full three-axis thruster control during any phase of flight was first lost in February 1977 when the SPS-2 negative yaw thruster number 13 failed. This, combined with the valve heater failures in the SPS-1 yaw and orbit-control jets, resulted in loss of negative yaw jet control during eclipse periods. Normal negative yaw jet control was totally lost April 1978 with the failure of the SPS-1 negative yaw thruster number 6. (The inertia wheels continued to provide the requisite spacecraft yaw control.)

On May 20 and 21, 1978, a special test was performed to prove that roll wheel momentum could be properly maintained even if the remaining negative roll jet failed. The test was successful and was followed on May 31 by a test to determine if the negative pitch jet could be used to maintain roll wheel momentum. Satisfactory results were obtained and further tests simulating different combinations of jet failures were planned and completed satisfactorily on June 24.

Failure of the SPS-2 negative pitch jet number 11 on November 2, 1978, completed the loss of all SPS-2 attitude control jets.

With the failure on November 21, 1978, of the SPS-1 positive pitch jet number 4, momentum management of the pitch wheel was switched to solar pressure and gravity gradient torquing by selected pitch pointings during nonexperiment periods. This failure marked the loss of normal attitude control operations; i.e., the ability to provide full 24-hour experiment support.

On May 6 and 8, 1979, failure of both the prime and backup east orbit-control jets, number 15 and number 16, required a 180-degree yaw flip maneuver to perform the normal stationkeeping maneuver with jet number 7. Testing of jet number 8 at this time revealed that it too was still inoperative, leaving jet number 7 as the only remaining orbit-control jet. Extensive testing of these three failed jets proved fruitless, prompting the decision to terminate the ATS-6 mission by mid-August.

Failure of the SPS-1 negative roll jet number 1 and the SPS-1 positive yaw jet number 5 on July 13, 1979, required the implementation of twice daily 180-degree yaw flips to maintain roll momentum management.

The final de-orbit maneuver was successfully conducted over the period from July 31 to August 1, 1979. A 28-hour burn on SPS-1 orbit-control jet number 7 was used to place the spacecraft in an orbit 520 km below synchronous. Following de-orbit, a continuous burn of the SPS-1 plus roll jet number 2 achieved a 1.6 rpm roll spin rate and, combined with jet number 7 and number 5 full-on commands, depleted the remaining hydrazine.

Design Conclusions

With the total SPS thruster's flight performance in perspective, many conclusions can be drawn relating to the causes and to the prevention in future flights of the various ATS-6 failures.

As a result of extensive literature reviews, ground testing and flight anomaly investigations, the most probable sequence of events leading to the majority of thruster failures is described in the following paragraphs.

Hydrazine containing the impurities of Table 8-5 and possibly small amounts of silicon oxide was loaded into the system where it proceeded to diffuse into and swell the tank diaphragm. Following launch, the system was activated by opening the thruster valve, evacuating the feed system downstream of the latch valves, closing the thruster valve and opening the latch valves. Hydrazine filled the feed manifold and dissolved the small amounts of residual carbazate salts in the valves leaving undissolved residual oxides that were the result of previous ground test operations. Steady-state and pulse-mode operation of the thrusters was initiated and proceeded for the first one and three-quarter years without incident and within specified performance limits.

During this period (as shown by data from ground tests of EPT-10 diaphragm/hydrazine compatibility), a major source of contaminants, notably zinc and silicon oxide, was in the constant process of being leached from the diaphragm by the hydrazine. The concentration of these contaminants in the hydrazine was constantly increasing as a function of the following variables:

1. Time was required for the hydrazine to migrate into the diaphragm and for the contaminant products to migrate out into the hydrazine.

2. An increase in temperature increased both chemical reaction rates (with zinc) and rates of physical diffusion (of silicon oxide). A common rule of thumb is that, at room temperature, reaction rates double for every 10°C increase in temperature.

3. The diaphragm (and propellant) also experienced a daily temperature cycle that influenced the rates mentioned in (2) and resulted in a small expansion/contraction cycle that assisted the physical migration of the contaminants and the silica filler into the propellant. Once in the propellant, the contaminants migrated slowly away from the diaphragm surface by concentration gradient diffusion. The greater the amount of mission time or propellant expelled from a tank, the greater the concentration of contaminants. At the other end of the system, propellant was evaporating in the thruster capillary feed tube (Figure 8-7) following either shutdown from a steady-state run or following each pulse of a train of

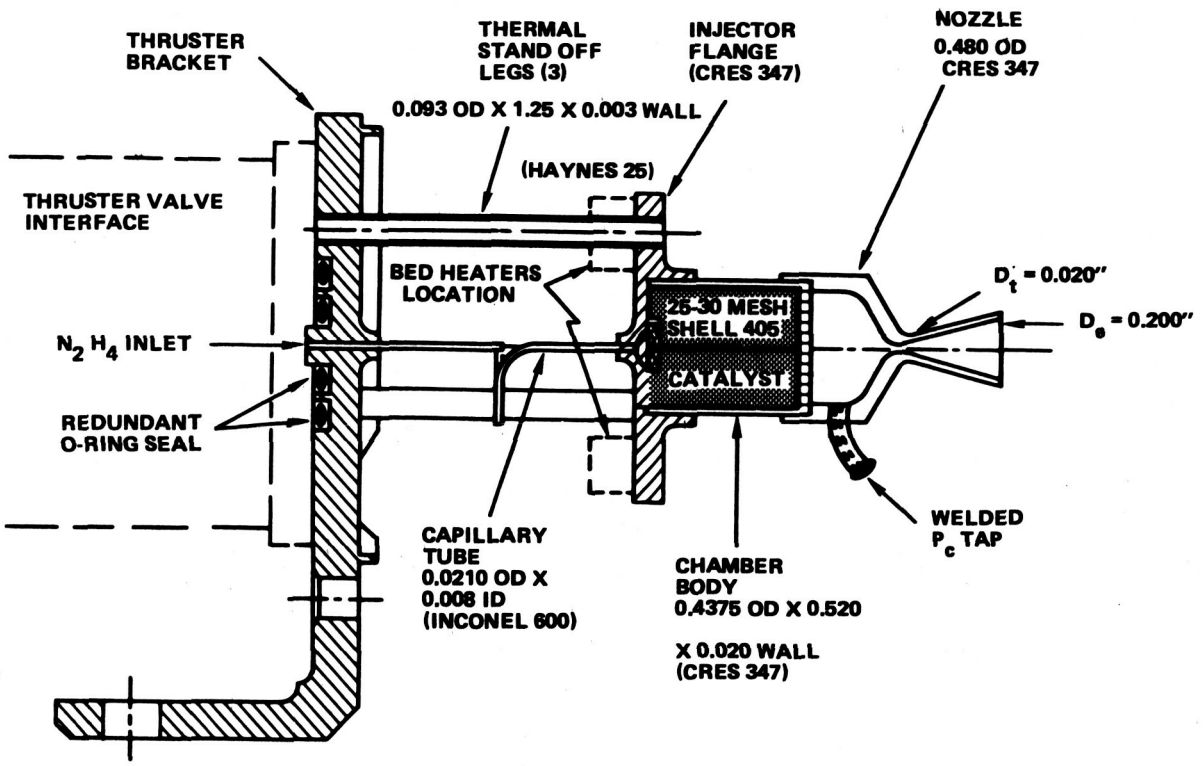

Figure 8-7. SPS Catalytic Reactor Assembly

short pulses. The volume of propellant between the valve seat and the thruster capillary entrance also evaporated but at a much slower rate. It is postulated then that as the approximately 0.001 cc of hydrazine in the tube evaporated it deposited on the interior tube wall whatever minute quantity of soluble or insoluble contaminants it contained. This process continued to add material to the irregular inside wall of the tube, progressively reducing its cross-section. Contaminant in the larger volume was also concentrated on the valve poppet (the coolest surface) as seen during prototype testing (Figure 8-8). These processes varied from thruster to thruster because of differences in their capillary tubes and thermal environments. Figure 8-9 illustrates the potential contamination buildup and plugging areas of the valve/thruster interface. Accumulation of contaminants downstream of the filter also occurred in those manifolds that were evacuated for long periods of time. Subsequent refilling washed these contaminants toward the various thrusters causing leaks or immediate plugging. The slow soluability of these contaminants also resulted in some degraded or even plugged thrusters being revived before finally failing.

Referring back to Figure 8-6 will show that combinations of the postulated plugging, leaking, degraded thrust, revived operation, and perfect operation occurred on various ATS-6 thrusters.

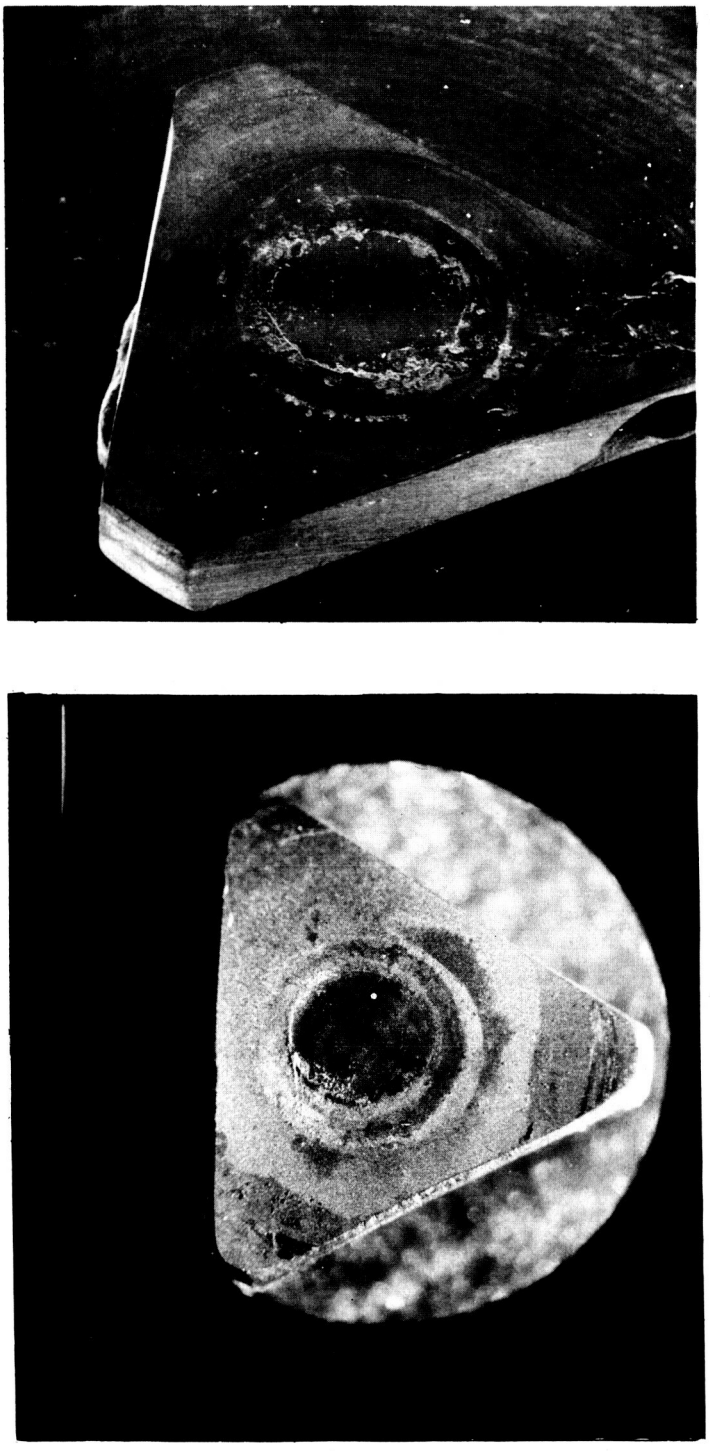

Figure 8-8. Prototype Valve Poppets Showing Accumulation of Downstream Contaminants

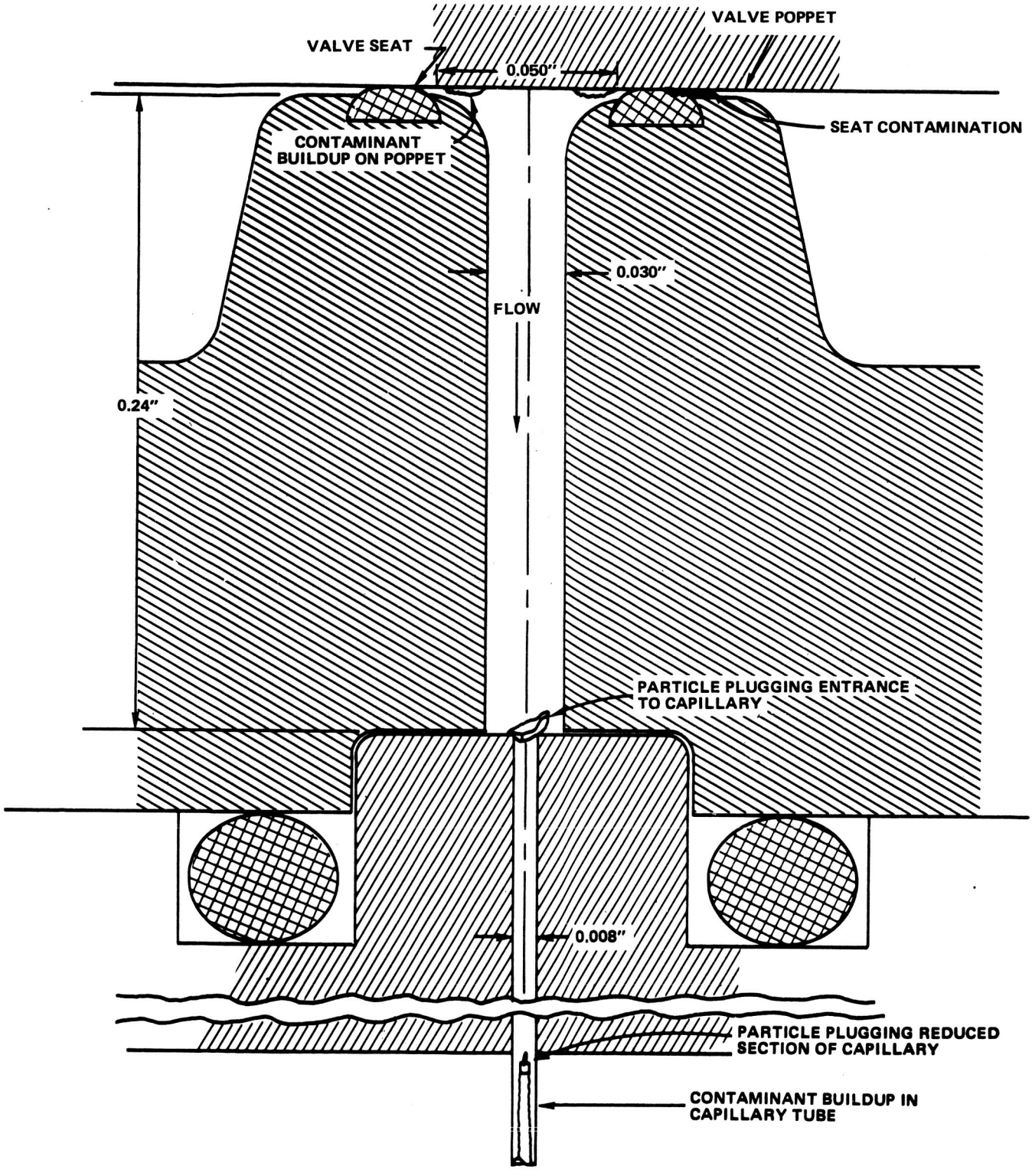

Figure 8-9. Cross Section of Valve/Thruster Interface Showing Potential Contaminant Buildup and Plugging Locations

It is concluded that the causes of these failures were contaminants: (1) left in the system as a result of previous ground hydrazine exposure and/or, (2) leached from the diaphragm and/or, (3) existing in small quantities in the loaded hydrazine.

Future long term missions using hydrazine thrusters should minimize potential contamination by:

- Specifying and controlling the purity of the flight fuel to the best state-of-the-art levels
- Not allowing flight feed system exposure to hydrazine until the flight loading operation
- Selecting diaphragm materials with proven low contaminant generation or, where flight operations allow, elimination of elastomeric diaphragms as an expulsion aid.

Susceptability of the thrusters to contamination should also be diminished by:

- Selecting higher thrust levels and, therefore, larger capillary feed tubes if allowed by mission requirements
- Using larger capillaries to feed the catalyst bed
- Minimizing the number of pulses on any particular thruster as permitted by mission attitude control requirements.

CHAPTER 9

CONCLUSIONS AND RECOMMENDATIONS

INTRODUCTION

The lessons to be learned from the ATS-6 propulsion experience are reviewed in the following paragraphs in approximate order of importance. Thruster failures due to plugging of the propellant feed passages were a major cause for mission termination and were one of the more critical generic failures on the satellite. It should also be noted that without the versatility of the attitude control subsystem and the capability for reprogramming its digital controllers that allowed implementation of unique control schemes to accommodate thruster failures, the mission would likely have been terminated before the achieved 5-year life.

Within the propulsion subsystem, thermal control was the next most critical area with several design flaws in components, rf interaction problems with the communications system and, while not flight critical, a need for more comprehensive predictions of temperature conditions during various mission phases and failure modes.

Propellant control and the propellant consumption prediction technique were fully adequate but could have used further refinement.

A fourth aspect of subsystem operation, in constant use for observation of the above three subsystem functions, was ground control and monitoring by the command and telemetry subsystem from the ATS Control Center. A few comments are made regarding technical aspects, philosophy, and operation.

This chapter is concluded with minor comments and recommendations concerning subsystem electrical and mechanical design, launch site operations, the development program, and the process of subsystem procurement.

THRUSTER CONFIGURATION AND PERFORMANCE

Aside from thrust failures and assuming, as appears reasonable, no inherent mechanical or catalytic bed design flaws, the Rocket Research in-orbit thruster performance met specification requirements and confirmed ground test data on steady-state and pulsing thrust, impulse bit, and specific impulse. The precision of inflight steady-state performance measurement was variable, depending on the position of the satellite and the accumulated number of ranging measurements. Pulsing performance on the other hand was quite accurately determined by the sensitive response of wheel speed. Incorporation of chamber pressure transducers to improve the measurement of thruster performance, instead of, or in addition to, the catalyst bed temperature sensors, would have been an expensive and unneeded option.

The spatial layout and side-by-side redundancy of the 16 jets was a fully adequate configuration while the mechanical complexity of the orbit-control and yaw-jet assemblies was a necessary result of overall spacecraft design where the center-of-mass was between the parabolic reflector and the Earth-viewing module.

CRITICAL THRUSTER FAILURES

The extensive information recorded for each anomaly and failure, including bed temperature and wheel response data, special in-orbit tests and comparative studies attempting to relate steady-state or pulsing operation and history of usage to failure mode, were described in previous paragraphs. Fourteen of the 16 thrusters experienced one or more of the following anomalies:

1. Reduced pulse mode I_{bit}, over sustained periods that was variable and degraded followed by return to normal

2. Excessive pulse mode I_{bit}

3. Short period of low thrust after shutoff

4. Short period of spontaneous leakage (after plugging)

5. Reduced steady-state thrust

6. Plugging of steady-state thrusters after small or large propellant throughput or without any use (i.e., failure to operate the first time)

7. Plugging of pulse mode thrusters used infrequently, moderately or intensively after long periods of inactivity or during mixed steady-state and pulse tests.

The accumulated data provided no basis for a convincing correlation that explains the variety of failures that have occurred.

A review of the literature and information available in the propulsion community, reveals a long history of leaks, thrust degradation, and plugging failures attributable to impurities and contaminants in hydrazine fuel that goes back 10 to 15 years. What is unique about ATS-6 is the extent and variety of failures experienced on one flight.

What little is known of the chemistry of reactions between hydrazine containing trace impurities and subsystem fluid components, and between hydrazine and diaphragm materials, that would support the mechanism proposed in Chapter 8 has been reviewed in Reference 31 listed in the Bibliography. Figure 9-1 depicts the propellant path from tank to thruster, and Figure 9-2 summarizes what is logically concluded to be the elements involved in the contaminant process that leads to flow anomalies and thruster blockage in such a system as was flown on ATS-6. A scaled view of the passage connecting the valve seat area and the capillary tube was shown in Figure 8-9, Chapter 8, and is assumed to be the critical area in the flow path.

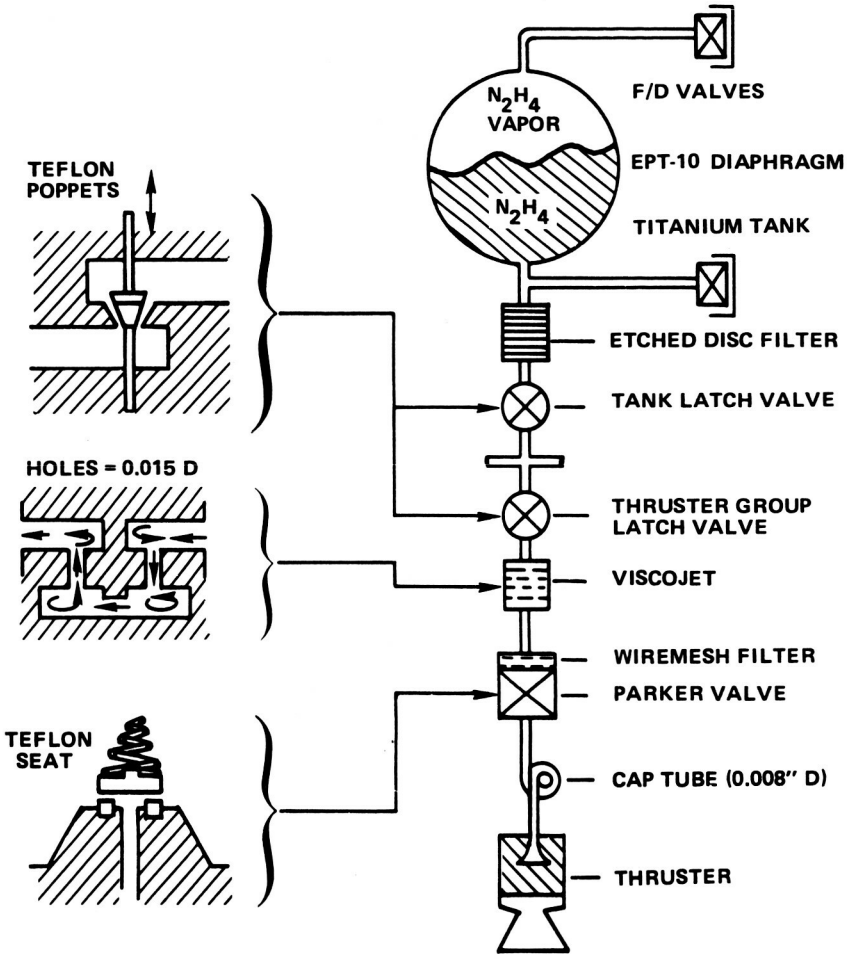

Figure 9-1. Propellant Flow Path

Based on the proposed mechanism, the recommendations of Chapter 8 follow:

1. Increase capillary feed tube diameter (possibly specifying higher thrust)

2. Minimize short pulsing (observed increase in "time-between-failures" when multiple pulse 0.2/10 wheel unload was replaced with single equivalent pulse)

3. Eliminate elastomeric diaphragms for positive propellant expulsion (consider metallic surface tension devices)

4. Stringent control of propellant purity (possible use of highly purified grades)

5. Reduce chance of chemical contamination by not introducing propellant before prelaunch operations and by strict control over loading of referee liquids.

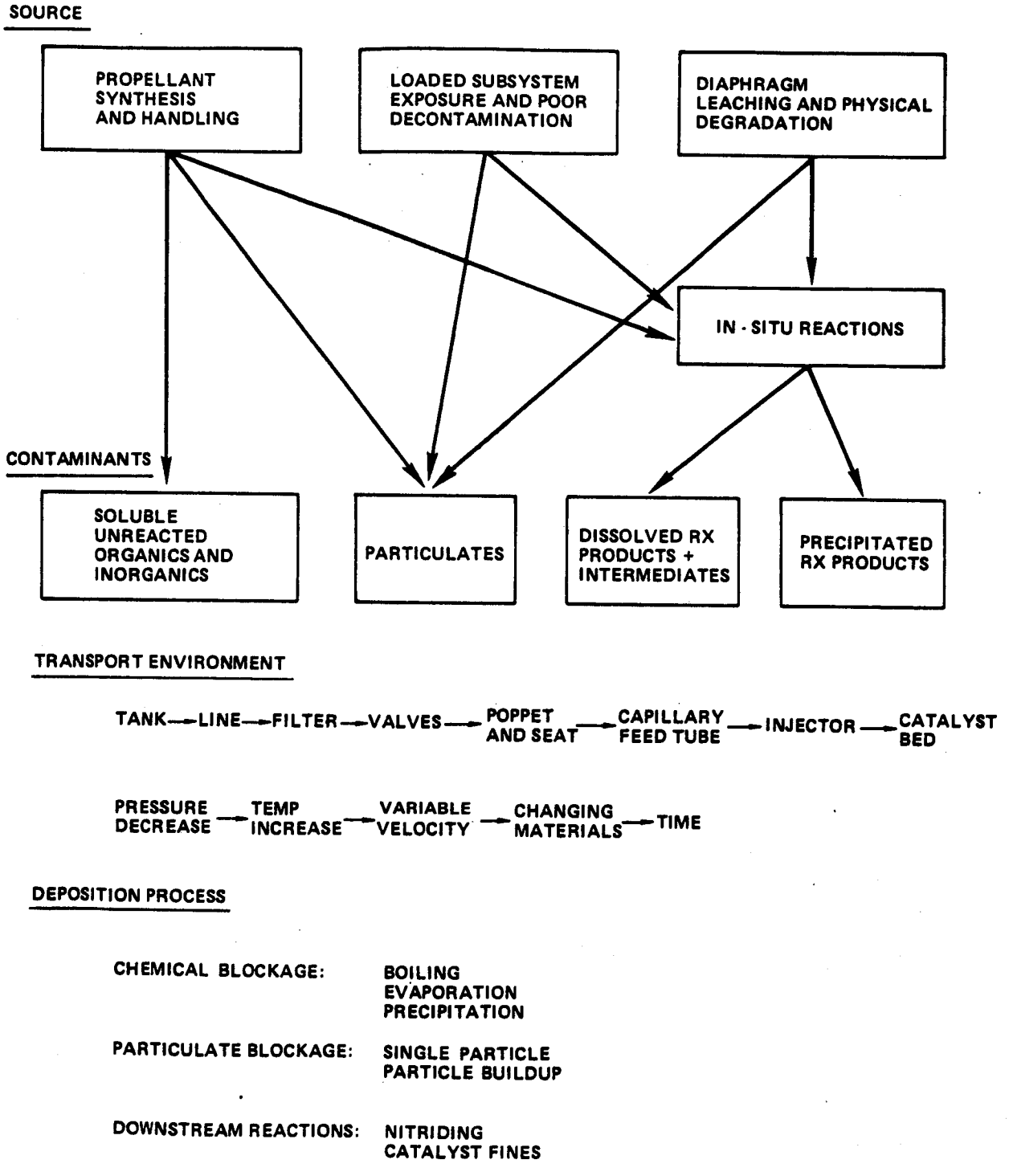

Figure 9-2. Contaminant Process Summary

It is further concluded that test and exposure of the loaded subsystem followed by inadequate decontamination was a major factor in the failures on ATS-6, and that there *might possibly* have been many fewer failures had the subsystem been handled differently while using the same thrusters, components, diaphragms, duty cycles, and propellant.

Finally, a general comment and recommendation: It is evident that design details (not always planned) and local conditions of flow and temperature (not always analyzed) produce conditions that can either promote or prevent flow blockage. Incipient problems may not surface during a test program based on particular mission requirements, and new requirements, (involving what appear to be minor changes in duty cycles, burn times or thermal conditions) can lead to anomalies or failures.

While the problem of contamination-induced flow blockage can probably be reduced by astute design and analysis and can be more completely identified by programs of extensive testing, it is felt that further work on hydrazine purity and diaphragm materials could provide the means for essentially eliminating it.

Processing steps beyond the Viking freezing procedure should be investigated, including distillation or other methods of removing trace elements, to obtain a purified grade with absolute minimum impurities for long term missions that operate under conditions where contaminants could be a problem. Possible new diaphragm materials should be investigated, including fluorocarbon elastomers derived from Teflon, that would provide a more inert method of positive expulsion for those missions that cannot use surface tension control.

Flow blockage due to impurities and contamination has a long history, is currently causing problems, and there is no reason to suppose it will disappear. Its elimination will require further coordinated effort within the propulsion community.

THERMAL CONTROL

The redundancy concept for the SPS heaters, which provided prime and backup elements for the valves, lines, and catalyst beds, was fully adequate and came into full use as the mission progressed.

Thermal control design of the orbit-control jet thruster/manifold assemblies was complicated by the lack of an early integrated design effort that could have taken into account electromechanical requirements of both the propulsive and thermal control elements and changing thermal environment inputs. As a result, the thermal control assembly was overly complicated and difficult to install because it involved multiple parallel copper wires, sensors, wrapped strip heaters, rfi shielding, heater and sensor leads, super insulation blankets, grounding strips and fiberglass standoffs, along the full lengths of the complex external manifolds. It worked well but could have been considerably simpler.

The very involved line heater controls, including high/low automatic electronic control with manual override on all prime and backup circuits, were prompted by the uncertainties inherent in the complex thermal control design.

The single string on/off circuits driving parallel groups of prime or backup valve and bed heaters worked well except for the random electronic part failure in the SPS-2 prime driver circuit. The backup circuit was activated and performed well throughout the remainder of the mission.

The observed in-orbit temperature limits were within the specified limits indicating the adequacy of the thermal models in specifying heater size and location. The thermostatically controlled lines operated as predicted. The manual backup mode provided a thermal input to thruster valves to compensate for valve heater failures. The thruster valves operated at higher temperatures (12°C to 88°C or 25°C to 96°C with bed heaters on) than predicted (5°C to 75°C), but were well within an acceptable range.

During the first series of lengthening eclipse cycles, as the SPS-1 thruster valve temperatures approached their predicted lower limit of 5°C, an overly cautious concern developed. Thus, the backup valve heaters were energized in parallel with the prime elements to provide a pre-eclipse warmup that would ensure a minimum of 10°C during the eclipse period. This concern instituted a procedure that was used prior to all eclipse cycles and eventually aggravated a design weakness leading to a combined failure of the prime and backup heaters.

The valve heaters not only contained design flaws (the inadequate thermal and electrical separation of prime and backup elements and a rigid configuration that could lead to thermal bond separation) but were also improperly fabricated. While the parallel activation of prime and backup elements was not stated or tested as a capability (a specification shortcoming), such operation would have been reasonable with adequate design and quality control of fabrication. It is unfortunate that many heaters of the same design are on other active spacecraft, but with the restriction against parallel operation, they should perform without failure.

The rfi problem with bed temperatures was not a major flaw in the design because changes in temperature rather than absolute level were more useful in determining pulse performance and the fact that the high temperature during steady-state operation is at least a semiquantitative criteria of performance. More attention should be paid to such thermocouple conditioning circuits early in the design cycle when it is easier to include filtering.

The models and temperature limit predictions were fully adequate for a successful thermal design, but considerably more efforts should have been spent on the operational aspects of thermal control. While it was known, for example, that the Sun-shadow sequence was such that the SPS-2 would not require its failed heater circuit to warm up the valves each pre-eclipse period, it would have been useful to have had predicted temperature data for the daily cycles of such components at equinox and the solstices; and for special cases of offset pointing, yaw maneuvers, and failure conditions.

PROPELLANT CONTROL

The two-tank, seven-latch valve arrangement of the feed system, separating the subsystem into two functionally redundant half systems was effective and fully adequate for the ATS-6 mission. No problems were experienced with the feed and isolation of propellant. The crossover latch valve

separating the two half systems was opened for the first time after 5 years in orbit to deplete the propellant during the de-orbit maneuver.

The comprehensive budget contained the necessary margins for unplanned maneuvers, failure mode consumption, and jet experiments. Two unused budget items, injection error correction (minor usage), and north-south stationkeeping experiment (dropped) also contributed to the margin accumulation that allowed the unplanned de-orbit maneuver at the end-of-mission.

The initial evacuation of manifold pad (gas) pressure followed by propellant bleed-in was uneventful in light of frequent cautions expressed in other programs concerning the water-hammer effect when pressurized propellant flows into evacuated lines.

The several evacuation procedures during the mission for removing propellant from the orbit-control jet manifolds were successful because the thrusters opened for evacuation showed an initial peak of hydrazine decomposition followed by decay over a period of days. However, no specific instrumentation nor ground test data was available to indicate the extent of liquid removal. Following the de-orbit maneuver, thruster number 7 was left open to fully evacuate the remaining propellant; however, a later partial reactivation of ATS-6 in November 1979 indicated increasing tank pressure (from 20 to approximately 100 psia) and, except for the number 7 valve, very low valve and line temperatures (Table 9-1). What this suggests is that the line to thruster number 7 was frozen shut and the gas on the pressurization side of the diaphragm was diffusing through the diaphragm and increasing the pressure in the trapped propellant. Presumably the frozen hydrazine would continue to sublime into the vacuum of space, eventually clearing the passages of the interconnected manifold and tank system.

The use of the pressure-volume temperature relationship to calculate propellant consumption (or remaining) was hampered by the pressure-temperature hystersis effect that would be essentially eliminated by using a gas-side rather than liquid-side temperature sensor. However, the 24-hour average procedure applied to the data was sufficiently accurate that the (cumulative) prediction of final runout was within 1 kg (1 hour longer than predicted burn of 3 of the 4 operative thrusters, 1 operating at 40 percent thrust). The point-to-point precision of prediction over the blowdown range was variable being less in the beginning (±0.15 kg) and more at the end (±0.45 kg).

An additional minor discrepancy between ground test information and inflight data was the calibration data for the two pressure transducers. The data indicated a 0.21 kg/cm^2 (3 psi) difference between the two telemetered values at the same actual pressure, whereas, the actual difference was 0.42 kg/cm^2 (6 psi) when they were connected to the same pressure source following opening of the tank interconnect latch valve.

GROUND CONTROL/MONITORING FROM ATSSOC

In general, the command and telemetry capability designed into the SPS was fully adequate for hands-on operation.

Table 9-1
ATS-6 Reactivation Telemetry
November 24, 1979

```
   POWERS    GMT  328:15:56:29:683   DACU 1   QUAL=GOOD   FRM= 0
                                     28V REG 2 STATUS          DISCON
SOL ARRAY SHT TAP V A419    15.3 V
SOL ARRAY SHT TAP V A420    15.6 V   BAT1 STATE OF CHARGE            0
SOL ARRAY SHT TAP V A421    16.0 V   BAT1: HRS LEFT TO .5 SOC -99999
SOL ARRAY SHT TAP V A422    15.9 V
SOL ARRAY SHT TAP V A423    16.5 V   BAT2 STATE OF CHARGE            0
SOL ARRAY SHT TAP V A424    14.5 V   BAT2: HRS LEFT TO .5 SOC -99999
SOL ARRAY SHT TAP V A425    15.9 V
SOL ARRAY SHT TAP V A426    21.3 V   SPACECRAFT LOAD POWER       132.5
SOL ARRAY SHT TAP V A427    17.1 V   EXCESS SOLAR ARRAY POWER    52.65
SOL ARRAY SHT TAP V A428    15.6 V
SOL ARRAY SHT TAP V A429    17.5 V   SOL PANEL A8 NORTH TEMP        0C C
SOL ARRAY SHT TAP V A430    16.1 V   SOL PANEL A3 NORTH TEMP        0C C
                                     SOL PANEL A5 SOUTH TEMP        0C C
CONV FULL SCALE TEMP CAL     0.0 V   SOL PANEL A2 SOUTH TEMP        0C C
EVM TEMP SENSOR CAL REF      0.0 V
POWER CONTROL UNIT TEMP     22.5 C   61 SUN BODY AZIMUTH             0
PWR REG UNIT TEMP           26.9 C   62 SUN BODY ELEVATION           0

28V REG 1 STATUS          DISCON
COMP PWR CNT TEMP  GMT 328:15:56:32   ACKACK          FRM=  1
INF  OFF     25.8ROFF   POFF   OFF  NO  MODE NO    CAL OFF DI OFF
PSA2 OFF     OFF  YOFF          NAQ  SS ON  ITOFF   GSOFF   ROOFF   GO OFF
YIRU30.4 IHB   0CYOFF           0CD/H     0CC   OPTEM   4CC UNCAG NO  IHB
MONO OFF          R-6.55 P-6.57       FREQ OFF      GAIN S
ESA  ON      27.38R  .00 P  .00 NAQ  RSO  RST RST  PHT 26.53
RGA1 OFF          ROFF   POFF  NSY
RGA2 OFF          YOFF         NSY   .    SPS#1/SPS#2 STATUS ERROR
CFSS OFF          P   0C Y   0C CRS  .TCA  BED 1  TANK   TCA  BED 2  TANK
DSS  OFF          P00000 Y00000 NO   .1-R   31.C  98.4P  9-R OFF  C 104.4P
AUX  OFF          A00000 B00000 NON  .2+R   35.C  20.C   10+R OFF  C  28.C
                  - NO CONTROL       .3-P    7.C         11-P OFF  C
DOC1 OFF MON 19.4 NO CONTROL         .4+P   47.C  VALVE  12+P OFF  C VALVE
DOC2 OFF MON 20.1 NO CONTROL         .5+Y   -1.C   -6.C  13-Y OFF  C OFF  C
ABC  ON  MON      SUN HOLD           .6-Y   -5.C   -6.C  14+Y OFF  C OFF  C
ACE          21.3 ON/WHL/YES         .7WP   -9.C   11.C  15EP OFF  C OFF  C
SCB 24.6     DEGC  RPM   +DC  -DC    .8WB  -25.C  -16.C  16EB OFF  C OFF  C
WHLR OFF     OFF   -OFF  0.000 0.000 .     LINE TEMPS      1/LATCH VALVES/2
   P OFF     OFF   -OFF  0.000 0.000 . 1S  -8.C 2N  29.C T O E /M/ T O E
   Y OFF     OFF   -OFF  0.000 0.000 . 1M -11.C 2M OFF  C O O O  O  O C C
                                     . JETS ON NONE        O      NONE

1  137 MHZ TLM XMTR 2 POWERN11927 5                  OFF     15:51:20
2  IE 1 BOUNDARY ANODE CUR N127O118     LO +   0. MA      15:51:02
3  SPS1 LINE TEMP SOUTH ENDN119O118     LO -   8. C       15:51:02 A
4  SPS2 TANK PRESSURE      N118O118     LO +104.4 PSIA    15:51:02 A
5  EME LIC OUTPUT VOLTAGE  N114151B     LO +   0.0 V      15:50:56
6  DACU 1 POWER            N12014 7                  ON      15:50:53
7  ERROR OVERFLOW, TOTAL OF 26 CURRENT ERRORS.                          C
   55054 137 MHZ TLM XMTR 2 POWER ON          EV  15* 58* 21
```

The CRT "pages" were crowded and would have benefited from the application of human engineering principles. Reasonable requirements for future in-orbit monitoring would be realtime graphical presentation of critical sets of cyclic temperatures; a constantly updated set of critical limits coupled with active warning; and an indication of accumulating pulses, impulse, and steady-state burn time on all thrusters that also provides propellant consumption status.

It is also recommended that failure and backup modes, procedures, and actions be documented in such a way that they are readily usable by both new and seasoned operational personnel.

A final recommendation concerns the ATS-6 prohibition against not only experimental manipulation of subsystems, which is a reasonable rule, but also checkout of all subsystem modes and redundancy options and specific tests of performance. Other experience would suggest that information and measurements in the latter three areas should be used to confirm in-orbit performance of delivered subsystems and to reduce later uncertainties when dealing with possible emergency situations.

ELECTRICAL DESIGN

From a development viewpoint, the electrical interface to the spacecraft propulsion subsystem (whereby all component leads were terminated in connectors that were subsequently connected to the actuator control electronics and the temperature control and signal conditioning unit drive and conditioning circuits) provided a direct easy way (by breakout boxes) to check out all components and activate the subsystem for leak and electrical checks.

Except for the failed heater elements and the rfi problem discussed before, all electrical components and elements performed satisfactorily.

MECHANICAL DESIGN AND INTEGRATION

Spacecraft propulsion systems are frequently mechanically complex, with their elements located at widely separated points on the spacecraft structure.

The ATS-6 spacecraft propulsion subsystem was an outstanding example of such complexity with the feed system and thrusters buried inside and half its thrusters mounted outside the thermally controlled Earth-viewing module.

In general, the support fixtures, while frequently requiring manual coordination, functioned well and were effective in assisting in the integration tasks. As previously discussed, the mechanical design of the orbit-control jets could have been simpler had all requirements been defined earlier.

The tank support tabs required considerable design effort but were fully adequate in test and flight, as were the other mechanical components including the support shelf, brackets, and fasteners.

PRELAUNCH OPERATIONS AT HANGAR AE AND LAUNCH COMPLEX 40, KENNEDY SPACE CENTER

The spacecraft propulsion subsystem was subjected to a baseline checkout at Hangar AE and to more complex leak and flow tests, fueling, and pressurization operation on Level 10 of Launch Complex 40, with relatively few problems.

The outstanding problem encountered during prelaunch activity was the size, weight, and complexity of the service cart. It was checked out in Hangar AE, fueled at the cape fueling area, and transported to and used on Level 10. Special reinforced flooring was required in the elevator and on the floor of Level 10 to satisfy floor loading limits. The manipulation of the many penumatic pilot valves controlling cart fluids was a slow time-consuming process, and at one point failure of a seal allowed hydrazine to leak at a pneumatic valve on the control panel. The electronic weight scale (with digital readout) developed a cyclic drift that led to detailed checking of cards from the electronics box just before loading of flight propellant, much to the consternation of all concerned. No fault was found with the circuits, and on reassembly, the drift returned. Manual averaging was used to determine the final scale reading. A strong recommendation would be to use the simplest and most reliable service cart with a highly accurate mechanical scale.

It should also be noted that the prelaunch practice session with the spacecraft propulsion subsystem in the thermal structural model, deemed necessary because ATS-6 was the first satellite checked out and fueled following integration with the Titan III-C launch vehicle, did much to smooth the way for the flight unit operations.

DEVELOPMENT/TEST PROGRAM

The ATS-6 planning included an extensive spacecraft propulsion subsystem test program that was substantially increased as problems developed. As one reviews testing on current satellite programs, it is evident that ATS-6 had a generous if not more than adequate amount of testing. The extensive work with the engineering model, prototype and thermal structural model provided great confidence that the system would work as designed for the 5-year goal period. In a sense, however, it was this comprehensive nature of the program (specifically as it included subsystem hot testing and state-of-the-art decontamination) that was the source of thruster failures that eventually overwhelmed the successfully performing satellite.

SUBSYSTEM PROCUREMENT

Rocket Research is to be congratulated on their performance in designing, fabricating, testing, and delivering the spacecraft propulsion subsystem. They were highly responsive to requests for, and questions about, design changes, fabrication, and test of special assemblies, data and data analysis and, in fact, all aspects of the subcontracted work. They provided an engineering team that produced quality equipment supported by comprehensive documentation.

FINAL CONCLUSION

It is clear that one can point with pride to the highly successful communications and experiment performance of ATS-6 while viewing with concern the lack of detailed experimental information about the cause of the thruster failures. Such information, if available, might alter the proposed explanation for their plugging and alter future design practices.

From a propulsion viewpoint, ATS-6 would be a very interesting spacecraft to retrieve for post-flight examination and evaluation.

CHAPTER 10

CESIUM BOMBARDMENT ION ENGINE EXPERIMENT

OBJECTIVES

The primary objective of the Cesium Bombardment Ion Engine experiment was to demonstrate a north-south stationkeeping of ATS-6, with its propulsion system over a long term of operation.

The second objective was to perform attitude maneuvers and unload the spacecraft's momentum wheels by applying the engine's thrust-vector torques about the spacecraft's center of mass. This thrust vectoring capability of the experiment could also be used to correct for thrust-vector misalignment and to track the movement of the spacecraft's center of mass.

The third objective was to determine the effect on the spacecraft experiments resulting from the discharge of cesium ions and aluminum atoms from the ion engine's exhaust impinging on the north and south surfaces of the Earth-viewing module.

The fourth objective, which was not a part of the ion engine experiment but used the ion thruster, was to demonstrate the control of the environmentally induced potential on the surface of the spacecraft. Although this experiment was a separate effort from that of the ion engine experiment, the ion thruster was involved in performing the measurements.

DESCRIPTION OF ION ENGINE SYSTEM

Ion Engine System Design

The ion engine system consisted of a thruster subsystem and a control logic/power conditioning subsystem. The two subsystems were packaged separately for convenience in mounting on ATS-6 and are illustrated in Figure 10-1.

Thruster Subsystem

The thruster subsystem configuration was cylindrical as shown in Figure 10-1 and contained 3.6 kg of cesium. A discharge chamber and electrode assembly were mounted at a 45 degree angle, with respect to the propellant reservoirs and the mounting flange, to permit the thrust-vector to pass through the spacecraft center of mass. A final thrust-vector adjustment was made during the integration of the spacecraft. A two-grid extraction system provided a thrust-vector of ±3 degrees in two directions by an accelerator electrode translation. A cesium plasma bridge neutralizer, operating at the spacecraft potential, was used to produce neutralized electrons. The thruster discharge chamber used the magnetoelectrostatic plasma containment (MESC) concept in which the bounding

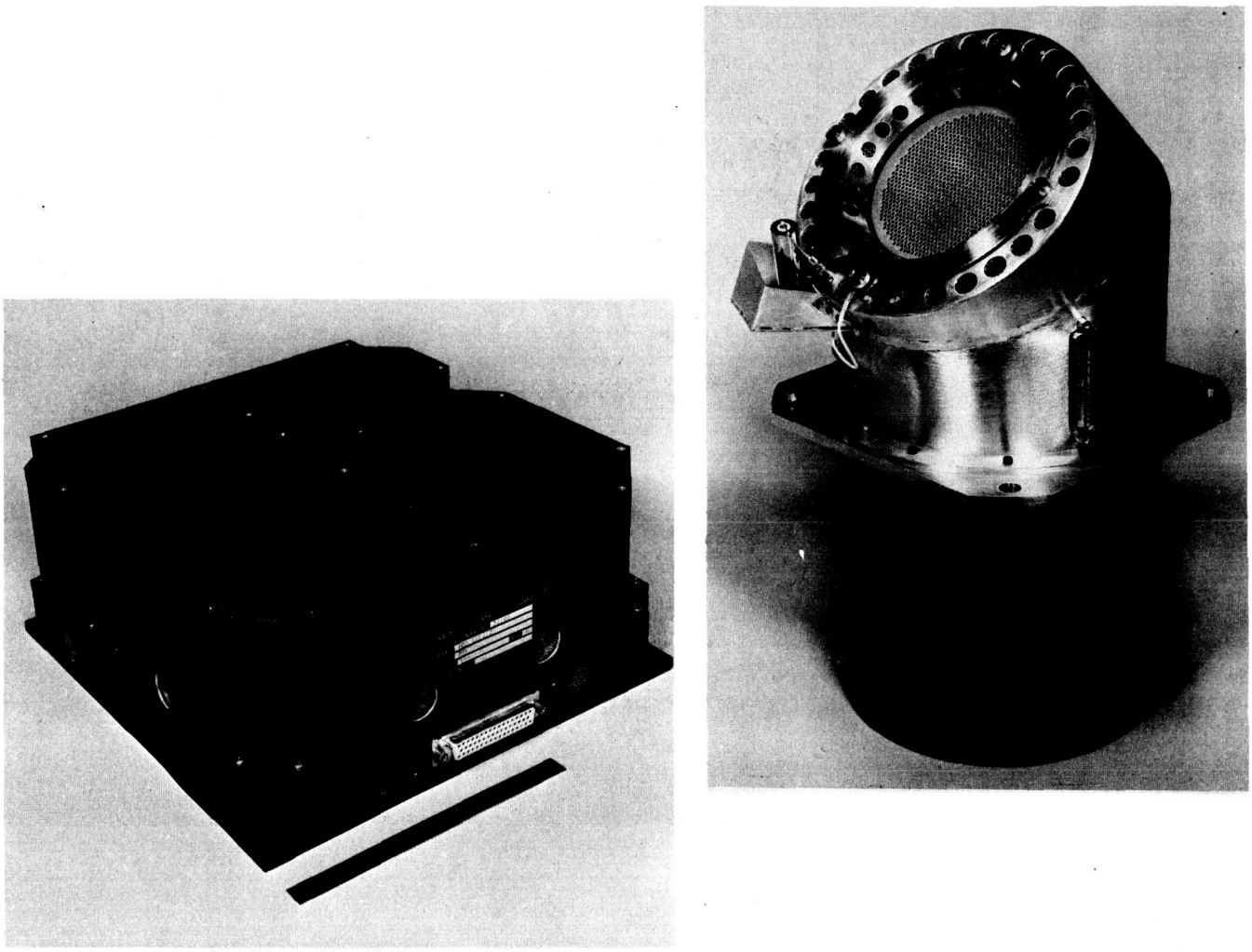

Figure 10-1. Ion Engine System

surfaces of the chamber reflected most of the ions and electrons approaching them (Figure 10-2). The magnetoelectrostatic boundary forced the plasma to maintain an electric field near the boundries that reflected the ions back into the plasma. This reduced the ion losses to the walls and increased both power and mass utilization efficiency. Another favorable aspect of the configuration was the low magnitude of the residual field variation within the discharge chamber plasma volume. Since the magnetic field was the major cause of plasma density gradients at the screen electrode, the MESC technique provided a uniform plasma density to allow efficient ion extraction with uniform geometry electrodes.

The shell of the discharge chamber was an iron ribbed hemisphere that provided the magnetic return path for the ring of seven magnets. Each of six magnets was a ring of circular cross section Plancover

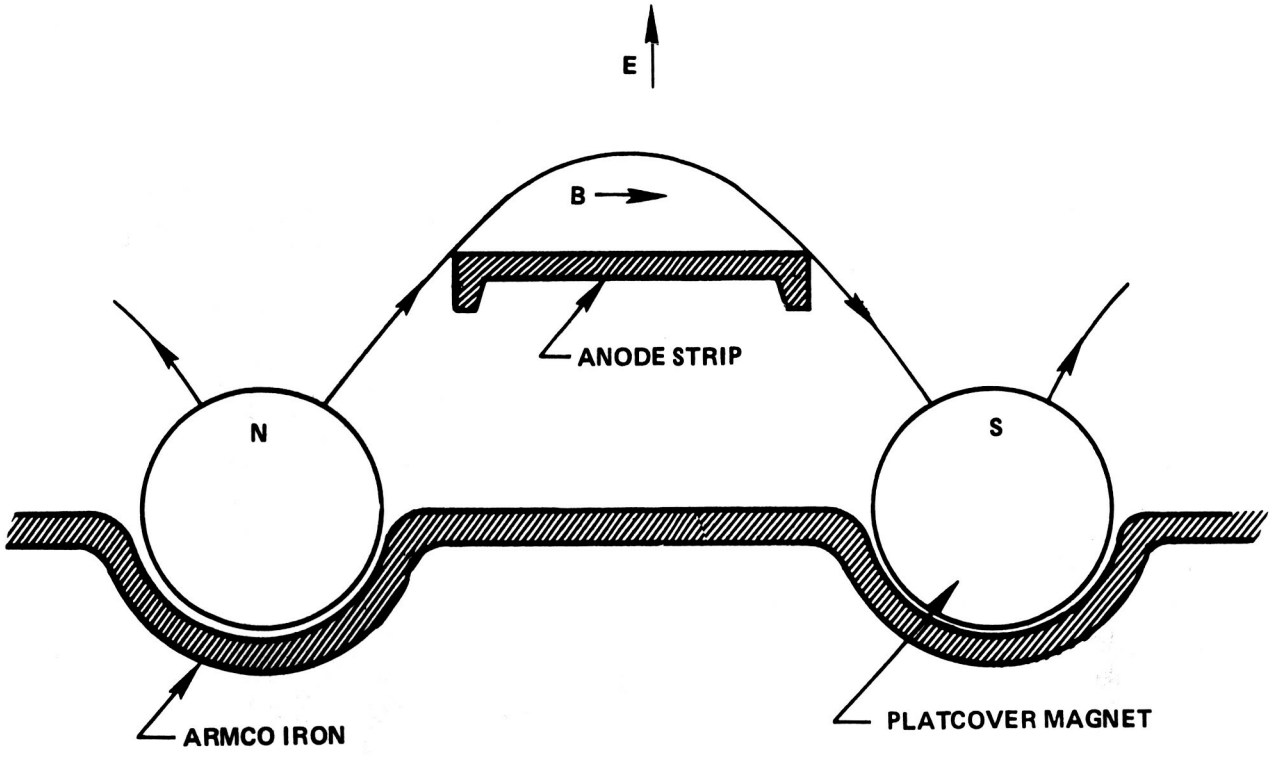

Figure 10-2. Magnetoelectrostatic Containment Geometry

magnetized normal to the shell. A seventh magnet was a part of the cathode assembly. Boundary anodes were mounted to the hemispherical shell and above the magnets. A plasma anode, consisting of a tantalum strip, was positioned in front of the cathode to provide the most desirable performance and control.

The cathode construction was a cesium hollow cathode with a small orifice that was mounted on the thruster axis and contained an internal coaxial heater. Approximately 10 percent of the cesium flow occurred through the cathode and the vaporizer feeding the cathode was automatically controlled to maintain a selected value of discharge current. The remainder 90 percent of the cesium flow was provided by the main feed ring that was biased at the potential of the boundary anodes.

The screen and the accelerating electrodes each had 1093 aperatures. The accelerator displacement method of thrust vectoring, which used the thermal expansion forces to displace the accelerator electrodes in a direction perpendicular to the thruster axis, was incorporated into the engine system. This action caused a deflection of the individual ion beams that provided the thrust vector. The accelerator electrode was supported by an array of eight legs to which electrical heating power was applied resulting in the expansion of the legs that produced a translational motion of the electrodes.

The plasma bridge neutralizer, employed in the thruster, had emission characteristics that varied with the flow of cesium through it and with the cathode temperature. External heaters were used

on both the cathode and the vaporizer. An auxiliary electrode, located near the cathode and biased 150 volts positive with respect to the neutralizer, acted as an anode probe that caused enough emission current to start the neutralizer when the thruster was off. This probe was allowed to float electrically and served as a plasma bridge potential sensing element for control purposes when the thruster was on.

Three types of propellant feed systems, the thruster cathode, the thruster anode, and the neutralizer, were used and consisted of the zero-gravity surface tension feed with a radial fin geometry to stabilize the location of the cesium within the reservoir. The feed system assembly was an annular cylinder containing the three types of reservoirs that were electrically isolated from each other as shown in Figure 10-3. Each feed system contained a thermally actuated, cadmium sealed, one-shot valve and a Pirani pressure sensor. Sealing of the propellant system was accomplished by employing a sealed valve at the end of the vaporizer.

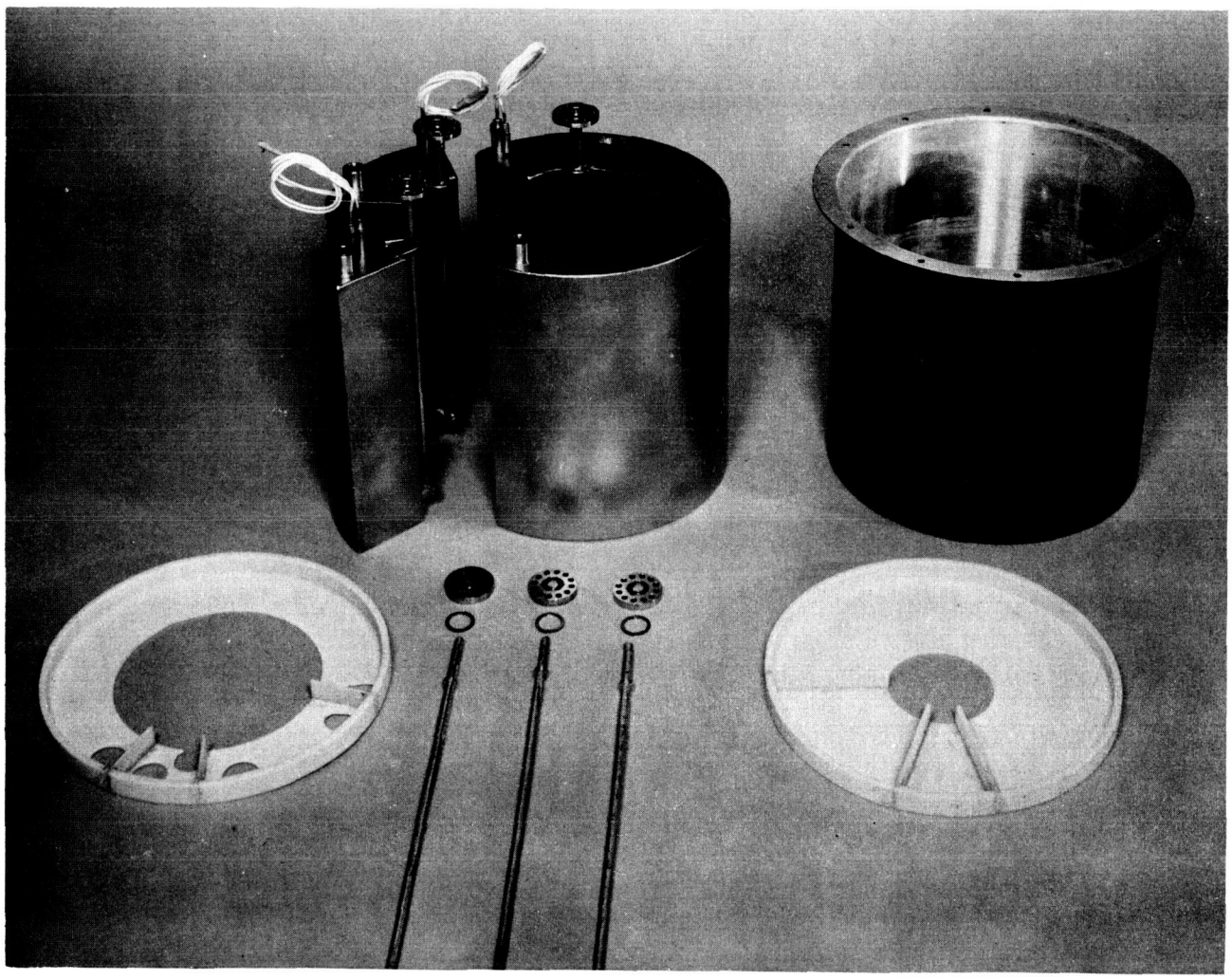

Figure 10-3. Feed System with Insulators and Ground Screen

The ion engine provided a thrust of 4.5 millinewtons (mN) or 1 millipound (mlb). Further details on the design of the ion engine can be obtained from References 1, 2, 3, and 4 listed at the end of this chapter.

Control Logic and Power Conditioning Subsystem

The primary function of the power conditioner was to convert the power at 18 Vdc to 16 power outputs required for the thruster subsystem. A control circuitry was incorporated in the unit to provide a normal startup, run, shutdown, and thrust vectoring of the thruster from the appropriate command signals that were received. Telemetry circuits in the unit performed the monitoring of the relevant system parameters. All of the power outputs were supplied by four converters of the parallel 100 percent duty cycle type and operated at a switching frequency of 10 kHz. One of the converters supplied +500 volts (V) at 113 milliamperes (mA) to the ion beam. A second converter supplied -550 V at 0.5 mA to the accelerator. Approximately 8 and 6 watts were supplied to the anode and cathode vaporizers, respectively. The third converter supplied power to the plasma anode at a voltage of +16 V and a current of 1.6 A. Power was also supplied to the boundary anode array at +3 V and 200 mA. The plasma anode supply was referenced to the beam potential at +550 V with respect to the ground, while the boundary anode supply was referenced to the plasma anode supply. The fourth converter provided power at +150 V to the neutralizer to initiate the discharge.

The command signals provided by the spacecraft for the operation of the ion engine consisted of 13 command channels that accepted 50-milliseconds (ms) positive pulses at a nominal amplitude of 20 V. These 13 channels consisted of the following:

a. Master Converter On
b. Master Converter Off
c. Neutralizer On
d. Neutralizer Off
e. Neutralizer Adjust
f. High Voltage On
g. High Voltage Off
h. Cathode Vaporizer On
i. Cathode Vaporizer Off
j. Anode Feed Vaporizer On
k. Anode Feed Vaporizer Off
l. X Deflection Adjust
m. Y Deflection Adjust

The primary parameters of the ion engine were monitored with 12 telemetry channels.

Ion Engine/Spacecraft System

Two ion-engine thrusters were employed on ATS-6, one on the north surface and the second on the south surface of the Earth-viewing module (EVM). This configuration had the capability of providing a north-south stationkeeping by maintaining the spacecraft's orbital inclination. Figure 10-4 shows the ATS-6 orbital configuration where the Z-axis or yaw axis was pointed to the center of the Earth, the velocity vector was in the X-axis or roll axis, and the pitch axis was on the Y-axis. The ion engines were mounted on the EVM so that the thrust vector formed a 54-degree angle with respect to the pitch or Y-axis in the roll rotation plane and passed through the spacecraft's center of

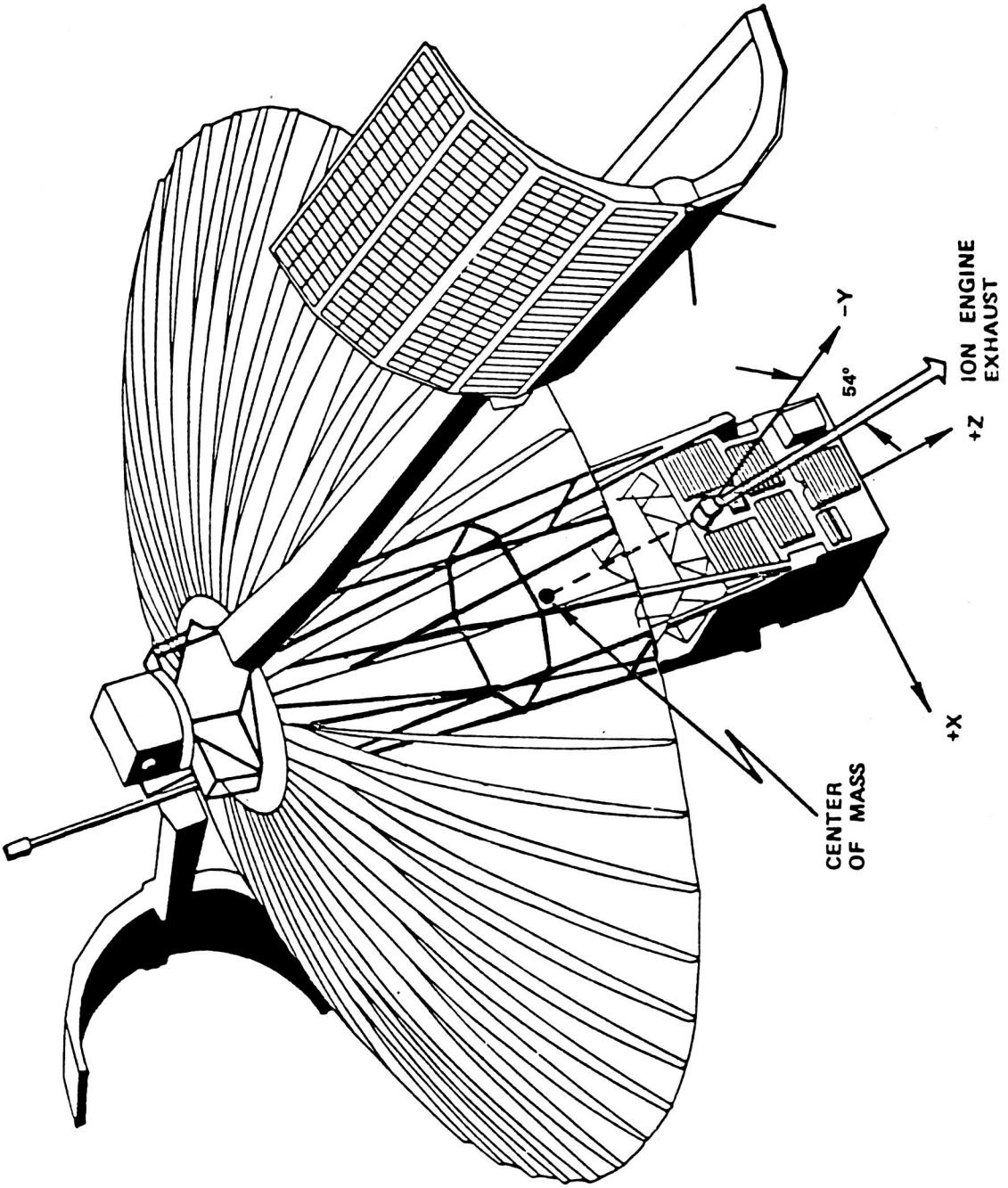

Figure 10-4. Spacecraft and Ion Engine Configuration

mass. In this configuration a thrust vector of 2.6 millinewtons (mN) was applied normal to the orbital plane and a vector of 3.6 mN was applied radially outward. To accomplish the spacecraft's stationkeeping, the two thrusters were operated alternately so that their thrust components, normal to the orbital plane, were symmeterically applied about the nodal crossings of the Earth's equatorial plane. The configuration of the ion thrusters on ATS-6 is illustrated in Figure 10-4.

Each ion engine applied 81 percent of its thrust vector (3.6 mN) radially outward resulting in a small increase in the spacecraft's altitude which caused a corresponding westward drift. This drift added approximately 20 percent to the natural drift (0.8 degree per year) of ATS-6 whose east-west stationkeeping was kept at 95° West longitude. This additional westward drift caused by the thrusters did not seriously impact on the normal stationkeeping maneuvers of the spacecraft. The system specifications for each of the two ion thrusters were as follows:

Thrust	4.5 mN (1 mlb)
Thrust Vectoring	±3° in X- and Y-axis
Specific Impulse	2500 seconds
Input Power	150 watts
System Mass	16 kg (35 lb)
Propellant Capacity	4400 hours at 4.5 mN
Command Channels	13
Telemetry Channels	12

The exhaust from the ion thruster consisted of collimated cesium ions with a half-angle of 15 degrees, and an efflux of uncollimated cesium and aluminum atoms. The collimated ion beam constituted 90 percent of the thruster exhaust and was referred to as Group 1 ions as illustrated in Figure 10-5. These ions did not interact with the spacecraft surfaces of the EVM. All of the remainder ions, referred to as Group 2 ions, were of the secondary type and were produced within the thruster accelerating structure with the capability of escaping the thruster. Some of the ions in the primary beam, external to the thruster, traveled approximately perpendicular to the beam and were referred to as Group 4 ions. The ions that were produced within the thruster, but had insufficient energy to escape, were referred to as Group 3 ions. The Group 4 ions and the neutral efflux impinged on both the north and south surfaces of the EVM and on the lower one-eighth of each solar array. Laboratory tests indicated that the temperature of the star trackers was sufficient so that the cesium would reevaporate at a rate exceeding the arrival rate. The tests also showed that the accumulation of aluminum did not affect the solar array output over the life of the experiment.

There were three areas on the EVM that were considered critical to the thruster exhaust and consisted of the cooler for the radiometer experiment that operated at 100 K (north face only), the Polaris star tracker (north face only), and the active thermal control surfaces (north and south faces). The exteriors of neither the cooler nor the star tracker were in line of sight of the thruster's ions or neutral atoms; therefore, neither the ions nor the neutral atoms from the exhaust could reach directly into the interior of the two units. There was still a possibility that a charge exchange of ions generated in the ion beam could reach these surfaces. The cone on the radiometer cooler was

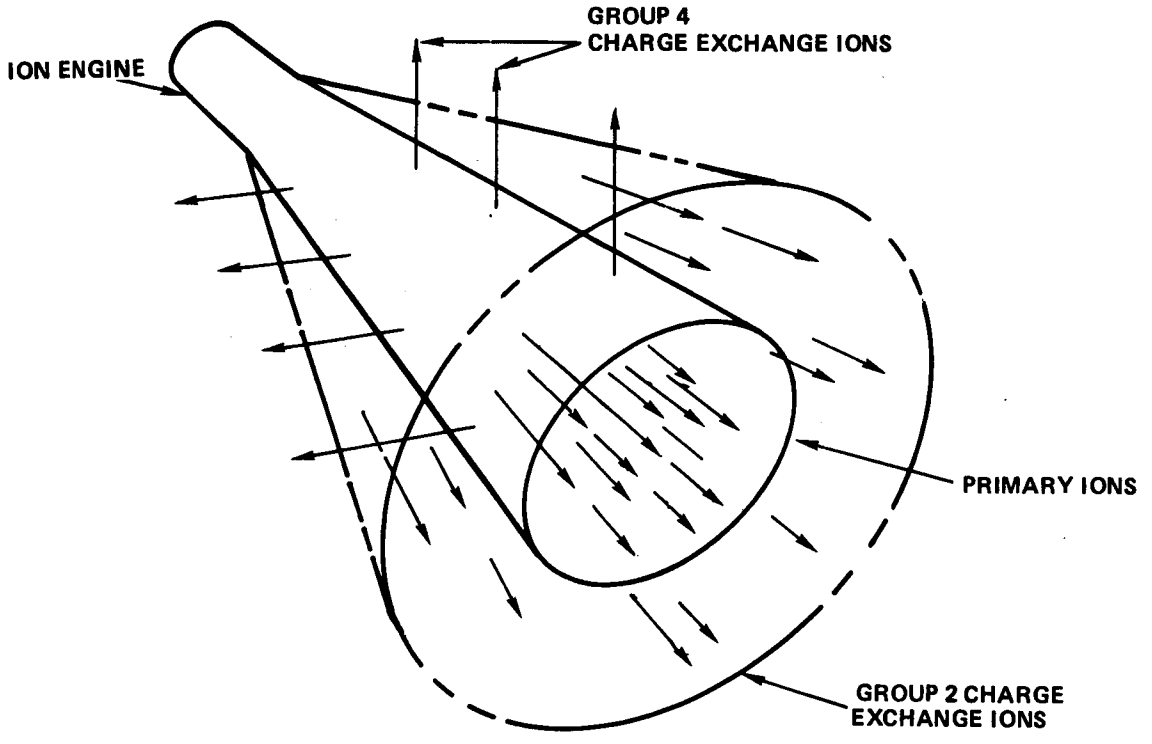

Figure 10-5. Ion Distribution

biased at 28 V positive with respect to the spacecraft structure to ensure that the charge-exchange ions would not reach the critical 100-k detector cold plate. A quartz-crystal microbalance contamination monitor was mounted on the north face of the EVM, near the radiometer cooler, to measure the actual material that might be deposited on the surface. The detector of this device operated at about 200 K and was not in the line of sight of the thruster exhaust.

An investigation was conducted on the possibility that the exhaust of the ion thruster would interfere with the illumination in the Polaris star tracker. Since the Polaris star is a point source of light, the star tracker could easily discriminate between it and the illumination of the ion-thruster exhaust.

ION ENGINE/SPACECRAFT OPERATIONAL RESULTS

Ground Operation

Two ion-engine units were integrated with ATS-6. Ground tests were conducted with the spacecraft experiments by using a thrust simulator and a flight unit power conditioning system. No interference was detected between the ion-engine systems and the spacecraft experiments. In addition to the interference tests, a life test of the ion engine was also performed. During the life test, the anode vapor feed control loop showed signs of instability. This problem was resolved by increasing the current of the anode feed ring heater.

Another problem, observed during this test, was that an increase of propellant flow was required before the discharge could be initiated. The addition of a starter power supply, which provided 65 V on the plasma anode during the predischarge period, corrected this problem.

During the test, a neutralizer cathode heater failed to open in the downstream end and an investigation considered the result as a random heater failure. However, erosion of the downstream face by charge-exchange ions was observed. Degradation of the Tophet C conductor material by grain growth was also observed. To avoid this problem the material was changed to Tophet A.

Space Operation

The final tests on the ion engine were performed under zero-gravity in space after ATS-6 was launched into orbit. Initial operational tests were conducted on the south ion engine because of its minimum interaction by being on the opposite side of the EVM from the Polaris star tracker, the radiometer, and the quartz-crystal microbalance contamination monitor. The south thruster performed very well and all of the parameters were similar with those observed during the ground tests.

The data received from a low-energy charged particle spectrometer, on board the spacecraft, indicated the spacecraft structure had a positive potential with respect to the ambient plasma when the ion engine was not operating and a negative potential with the ion engine in operation. The possibility of radio frequency interference occurring in the spacecraft communications system due to operation of the ion engine was determined by employing a receiver in the spacecraft i.f. amplifer for each of the three frequency channels that had the following characteristics:

Band	Center Frequency	Sensitivity (G/T, FOV)	Bandwidth
Vhf	153 MHz	-25 dB/K	6 MHz
S	2250 MHz	6.0 dB/K	40 MHz
C	6150 MHz	9.1 dB/K	40 MHz

No indication of interference was observed in the three frequency channels nor in the telemetry and command subsystems.

When the ion engine was shut down, all of the attempts that were made to restart it failed. The cause of the malfunction of the engine could not be determined; however, the most significant indication of the cause was that the 10 percent decrease in the neutralizer vaporizer current, observed from telemetry data on several occasions, could be produced by a shorted cathode heater. This result, in turn, could be caused by an excess of cesium in the vicinity of the thruster. Fifteen additional attempts to start the thruster produced the same result of heavy overloading of the high voltage power supplies followed by a system shutdown.

Because of the unresolved failure of the south ion engine, the north engine was then placed into operation. The initial operation of the second thruster showed that the performance was completely normal for all phases of the tests. The thruster was shut down for one hour and then a restart was

attempted similar to that performed on the south thruster. An identical failure also occurred with the second ion engine. The common malfunction that occurred for both thrusters was the continuous overloading of the high voltage power supplies that prevented the restarting of both thrusters.

An investigation indicated that an unbalance of cesium vapor pressure in the feed system resulted in liquid cesium being expelled into the discharge chamber. This caused the overloading of the discharge and high voltage power supplies. A diagram of the propellant feed system is shown in Figure 10-6. Two methods of approach were taken to resolve this problem. One method, determined in the laboratory, involved the cyclic operation of the thruster preheater and cathode heaters. The second method consisted of applying continuous power to the cathode and discharge chambers. Both methods were applied, but neither approach corrected the malfunction.

Development of New Feed Line Valve

A laboratory investigation was initiated to correct the malfunction of the thrusters. Two actions were untaken. One consisted of degassing the cesium in the reservoir to assure that all of the fin surfaces were wetted and remained in that condition. The second involved the development of a new feed-line valve that would close sufficiently tight at the end of each engine operation to prevent cesium liquid from flowing into the discharge chamber.

To ensure that the new feed-line valve would correct the engine problems, the following design requirements had to be met:

a. Minor impact (preferably none) on the existing ATS-6 ion engine electronics package

b. Minor impact on the size of the thruster package

c. Operation in a cesium vapor environment over a temperature range of -30° to +400° Celsius (C)

d. Helium leak-tight seal initially plus an acceptable cesium liquid leak rate following initial operation

e. Negligible change in opening and closing temperature over a large number of operating cycles

f. Negligible change in open dimension at normal (315°C) vaporizer temperature over a large number of operating cycles

g. Largest possible open dimension within packaging constraints.

The first requirement dictated the use of a thermally actuated design where the vaporizer heater could be employed for valve operation. By maintaining the same heater power and impedance, no changes were required within the electronics package. Requirement b dictated a tradeoff between the opening and closing temperature and the maximum open dimension obtained. Requirement c dictated an all metal design that in turn complicated satisfying requirement d.

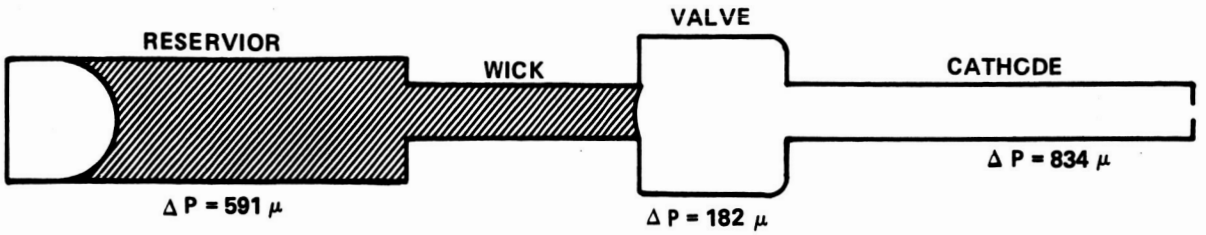

$$\Delta P = \frac{2\gamma \cos\theta}{r}$$

Figure 10-6. Propellant Feed System Schematic

Many valves of different characteristics were designed to determine the type that would meet the requirement for satisfactory operation of the ion engine. The problem with the original valve was that it would not close tight enough at the end of each engine operation to prevent the flow of liquid cesium into the discharge chamber. A series of valves were developed using bimetal discs to provide the sealing and closing force. A cross sectional view of the new valve design is shown in Figure 10-7. The opening discs provided only the plunger movement and were not required to compress the closing springs.

Two types of bimetal material (Chace No. 3600 and 4600), having different temperature characteristics, were used in the various models of valves that were developed. The two primary parameters that were considered in the development of the valves were the opening temperature from the initial closed condition and the open spacing of the discs at the typical operating temperature of approximately 315°C. These two characteristics for the valves that used the 3600 bimetal are shown in Figure 10-8. Similar characteristics were obtained for the valves using the 4600 bimetal.

Leak tightness was measured after the test was performed by using a liquid displacement method with the use of helium at 2.0265×10^5 Pa (2 atm) of pressure.

Active Control of Environmental Charging

The University of California conducted an investigation, sponsored by NASA and the Air Force, on the feasibility of actively controlling the environmentally induced potential on the surface of the spacecraft. This experiment jointly used the cesium-ion engine experiment and the auroral particles experiment on board ATS-6 to perform the measurements.

The ion engine was of the bombardment type using a low-energy cesium plasma as its neutralizer. The neutralizer served as a source of electrons to maintain a net charge neutrality when the cesium ion source was in operation. Both the ion source and the neutralizer were operated simultaneously and were used to alter the current balance of the spacecraft resulting in actively controlling the

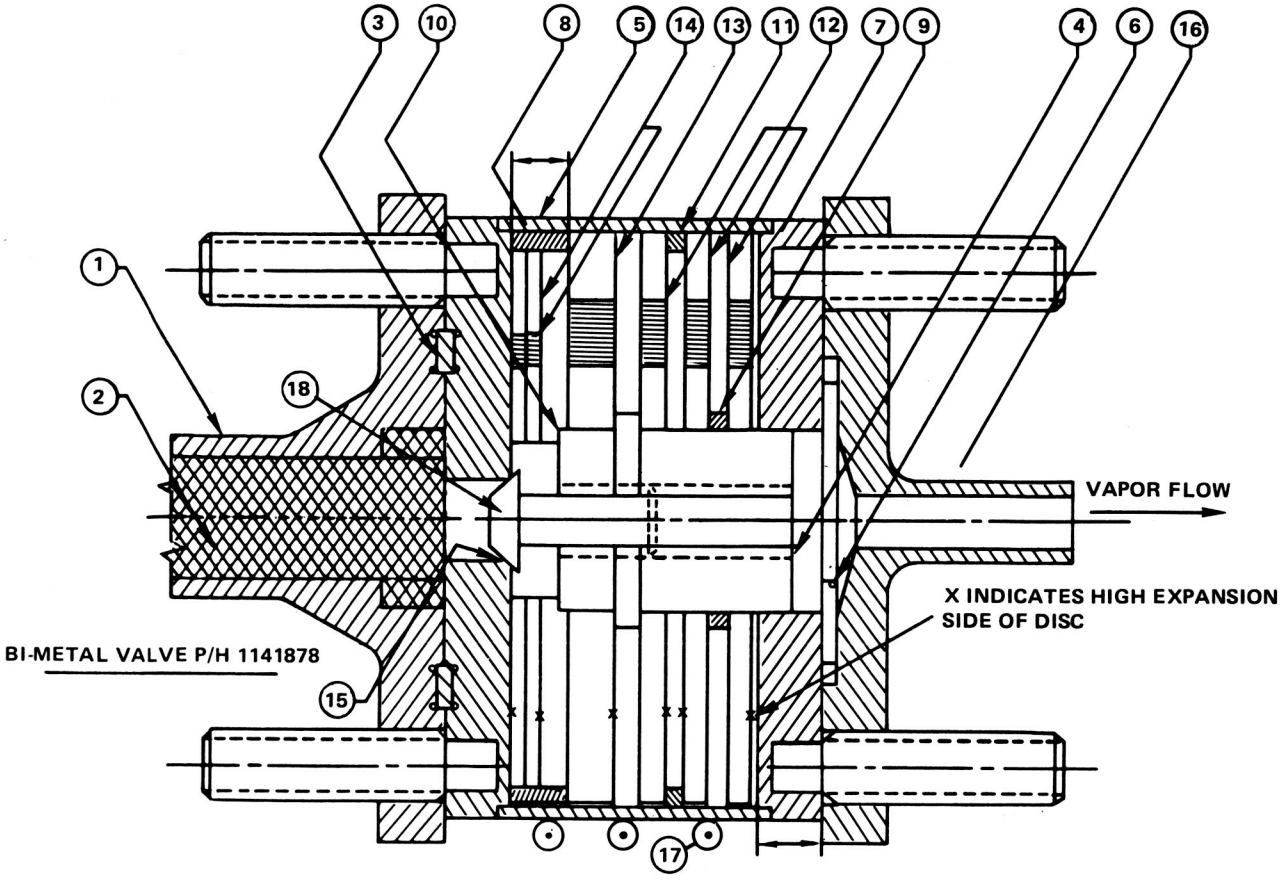

NOTE:

The parts of the assembly are:

1. Reservoir feed tube (CRES)
2. Reservoir to valve seal (copper)
3. Liquid cesium wick (CRES)
4. Plunger (DRILL ROD)
5. Body (CRES)
6. Valve to vapor feed tube seal (copper plated CRES)
7. 8, 9, 10, 11 spacers (DRILL ROD)
12. Closing discs (Chace Nos. 3600 or 4600)
13. High force disc (Chace Nos. 3600 or 4600)
14. Opening discs (Chace No. 3600 or 4600)
15. Initial seal (cadmium) (optional)
16. Vapor feed tube (CRES)
17. Valve-vaporizer sheathed heater
18. Plunger tip (nickel)

Figure 10-7. Bimetal Valve

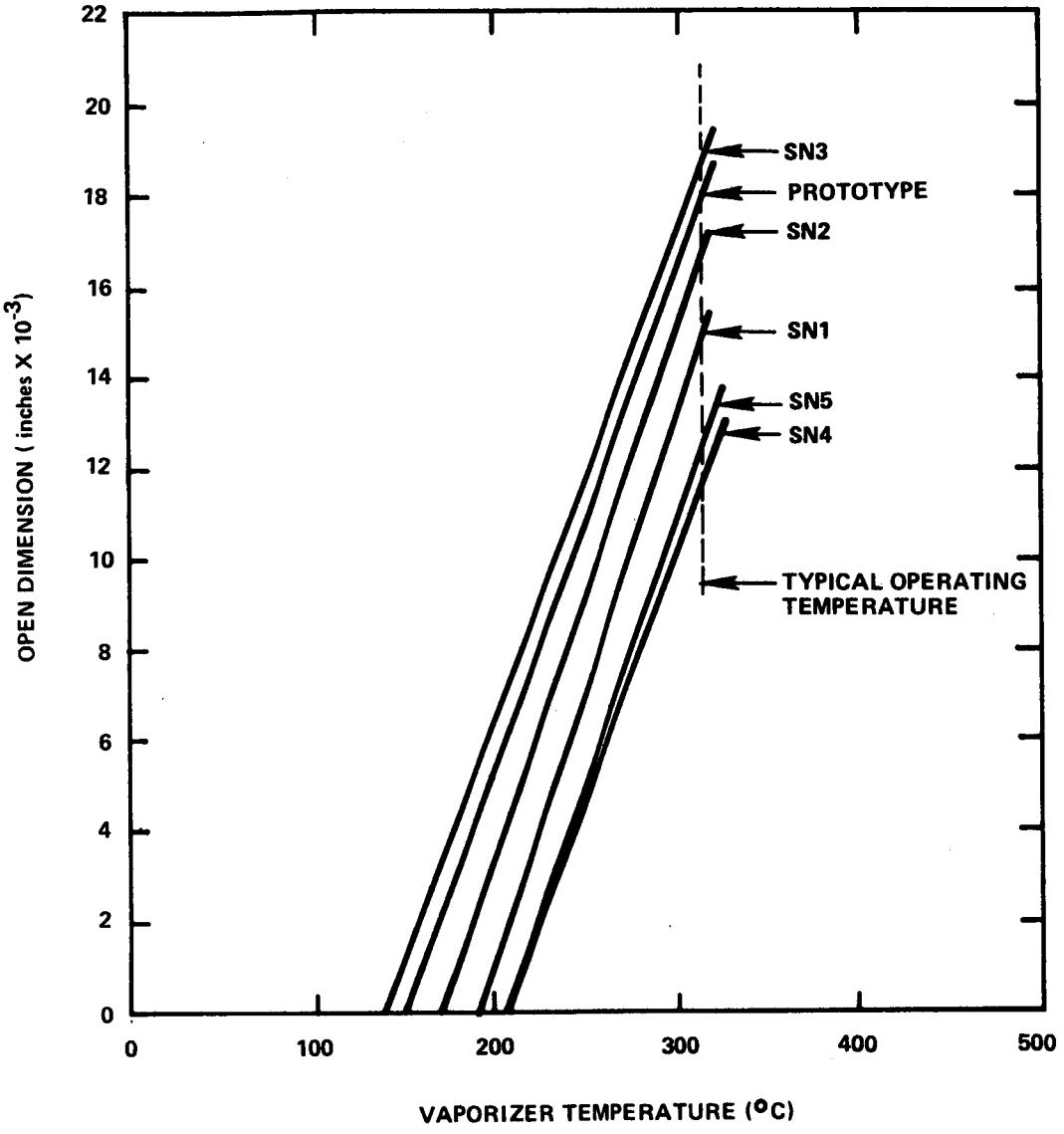

Figure 10-8. Thermal Valves (3600 MTL)

spacecraft's potential. This effect was measured with the use of the auroral particles experiment. Results of these tests were performed under the conditions of no eclipse and are presented in Figure 10-9. These data indicate that the spacecraft's potential was clamped at approximately -4 volts throughout the 4-day operation of the ion engine experiment.

The cesium vapor flow to the plasma neutralizer was regulated to control the potential of an anode probe in its discharge. The potential of the probe during the 4-day operation of the ion engine was +4.5 V relative to the spacecraft ground as measured by telemetry. Since the neutralizer cathode potential was that of spacecraft ground, the potential of the anode probe was at or very near the

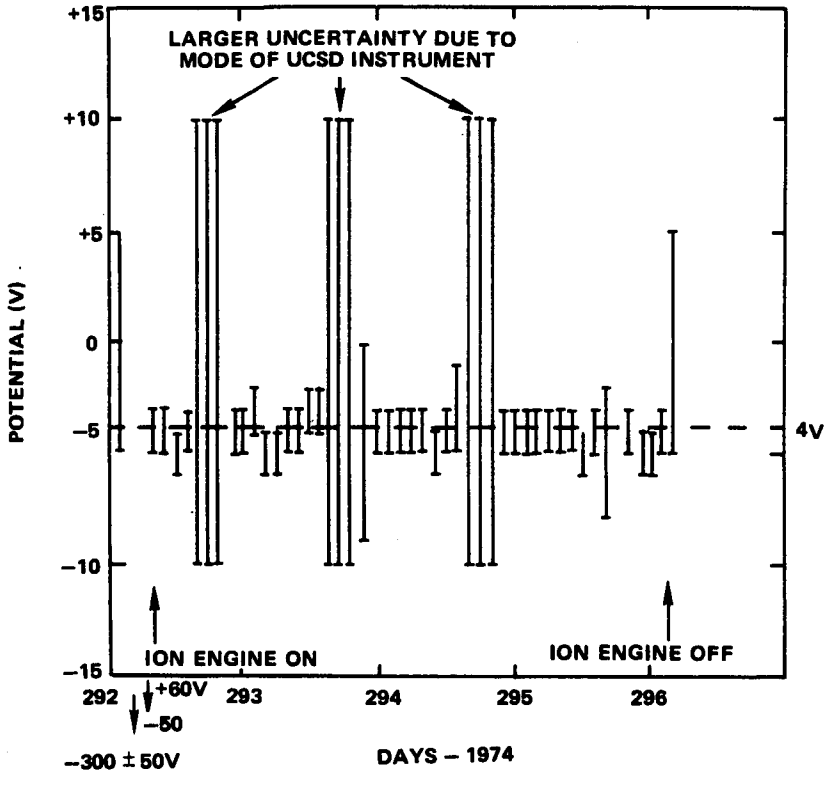

Figure 10-9. Ion Engine Operation (No Eclipse)

potential of the ambient plasma. If the probe was operated at the spacecraft potential and the cathode of the plasma neutralizer was operated with a negative bias, the spacecraft probably could have been held at the plasma potential. Since the ion engine experiment did not have the bias capability, this concept could not be demonstrated. The biasing feature was incorporated in the USAF Space Test Program and further details can be obtained from Reference 5.

A series of tests were also performed under the condition of a Sun eclipse. These tests required the use of the ion-engine neutralizer only. The results of a test are shown in Figure 10-10. These data indicate that the low-energy plasma neutralizer was sufficient to discharge the spacecraft. Due to the absence of natural low-energy ions under this condition, the exact potential to which the spacecraft was clamped could not be measured with precision. Some of the experiments of this type have shown that the spacecraft potential was clamped to approximately -5 V by the neutralizer's operation. The operation of the plasma neutralizer had also reduced the differential charging of the

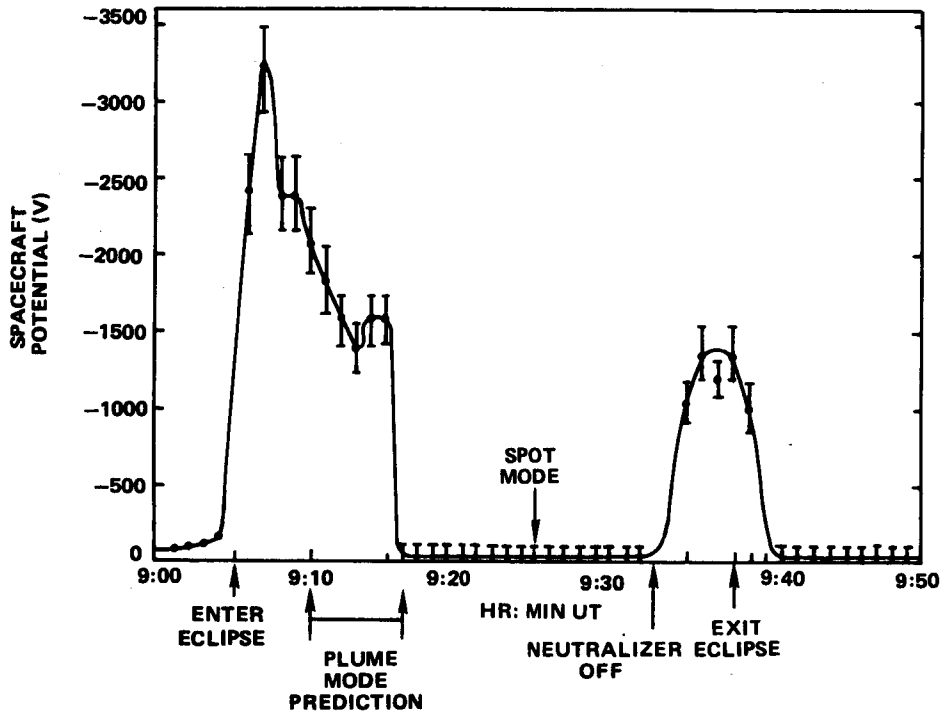

Figure 10-10. ATS-6 Neutralizer/Eclipse Operation (April 5, 1977)

spacecraft, but not to the same extent as the operation of the ion thruster. This effect was most likely due to the larger density of the free low-energy ions associated with the ion thruster's operation.

CONCLUSION

Both ion engines performed very well in their initial operation in space and met all of the time-limited objectives of the experiment. When either engine was shut down, it could not be restarted again. All of the approaches that were taken could not correct this problem.

When it was determined that the malfunction occurred in the feed-line valve, a program was initiated to design new types of valves. The family of thermally actuated valves that were developed and tested in the laboratory met all of the original design goals. On this basis the new types of valves could be included in future cesium thruster systems with confidence to provide satisfactory operation.

The experiments performed on active control of environmental charging on ATS-5 and ATS-6 provided the first known measurements on the interaction of the natural plasma and an artifically produced plasma at the geosynchronous altitude. The neutralizer plasma source on ATS-6 maintained

the spacecraft's potential within a few volts of the ambient potential for both positive and negative charging events under all observed plasma conditions. Many measurements of the environmental charging potentials performed on ATS-5 and ATS-6 indicated potentials in excess of 1000 volts. From the measurements performed in the experiments, it appeared that the spacecraft could be clamped at the plasma potential by biasing a low-energy plasma discharge to compensate for the coupling to the ambient. Operation of the ion engine showed that it suppressed the differential charging and clamped the spacecraft potential at a fixed voltage relative to the ambient plasma.

Experimental data indicated that the dominant factor controlling the equilibrium potential on the spacecraft was the consistency of the ambient plasma. These experiments have shown that the active control devices completely dominated all natural current sources. Also, the experiments have demonstrated that the task of ensuring that the spacecraft was not sensitive to electromagnetic interference potentially associated with the environmental charging was feasible.

REFERENCES

1. James, E., et al., "A One Millipound Cesium Ion Thruster System," Proceedings of AIAA 8th Electric Propulsion Conference, August 1970.

2. Moore, R., "Magneto-Electrostatically Contained Plasma Ion Thruster," Proceedings of AIAA 7th Electric Propulsion Conference, March 1969.

3. Worlock, R., et al., "An Advanced Contact Ion Microthruster System," Journal of Spacecraft and Rockets, Vol. 6, No. 4, April 1969, pp. 424-429.

4. Worlock, R., et al., "The Cesium Bombardment Engine N-S Stationkeeping Experiment ATS-6," AIAA 75-363, New Orleans, Louisiana, March 19-21, 1975.

5. Cohen, H. A., et al., "Design Development and Flight of a Spacecraft Charging Sounding Rocket Payload," Proceedings of USAF/NASA Spacecraft Charging Technology Conference, Colorado Springs, Colorado, 1978.

Appendixes and Bibliography

APPENDIX A

ACS CONTROL LOOPS

The following figures define the control laws implemented in the ACS controllers as discussed in the design description section. Outputs from these controllers (the digital operational controller [DOC], and the analog backup controller [ABC]) drove the actuators defined below. Average spacecraft inertial characteristics during operational modes were:

$$Ixx = 1.45 \times 10^8 \text{ kg-cm}^2 \text{ (10,700 slug-ft}^2\text{)}$$
$$Iyy = 8.27 \times 10^7 \text{ kg-cm}^2 \text{ (6100 slug-ft}^2\text{)}$$
$$Itt = 6.37 \times 10^7 \text{ kg-cm}^2 \text{ (4700 slug-ft}^2\text{)}$$

Products of inertia were less than 2.71×10^6 kg-cm^2 (200 slug-ft^2).

WHEEL CHARACTERISTICS

The inertia wheels each had equal spin inertias of 8.62×10^2 kg-cm^2 (0.0636 slug-ft^2) and a speed-torque relation as defined in Figure 1-14, Chapter 1.

REACTION JET CHARACTERISTICS

Reaction jet thrusts varied from 0.667 N (0.15 lbf) to 0.222 N (0.05 lbf) depending upon supply pressure. (See Part B, "Spacecraft Propulsion," for details.) The locations and orientations of the jets are shown in Figure 1-16, Chapter 1.

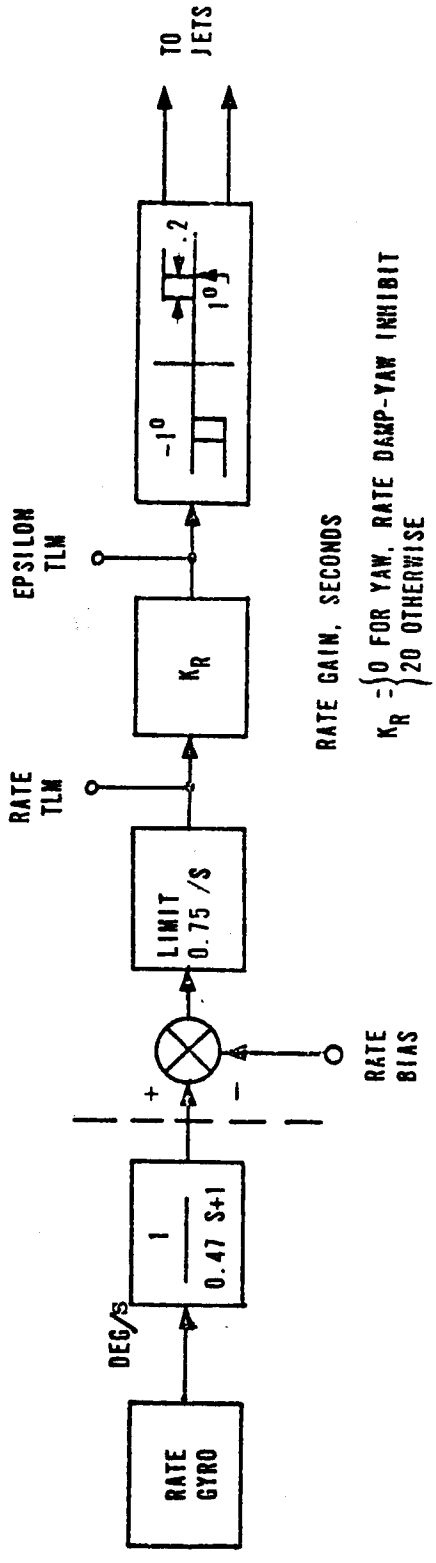

Figure A-1. Rate Damp Control Law – DOC

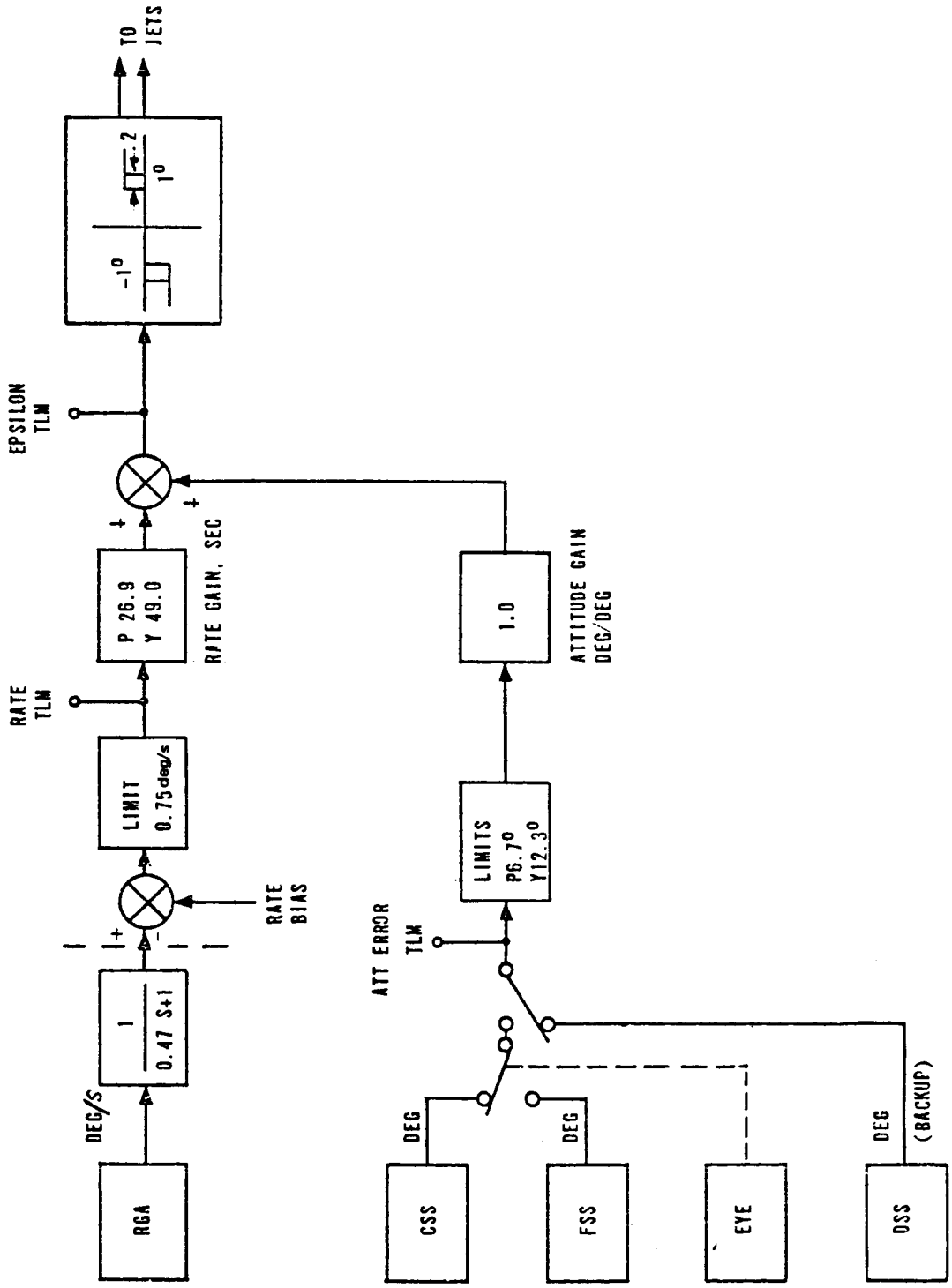

Figure A-2. DOC Sun Acquisition Control Law, DOC Earth Acquisition Control for Yaw, and DOC Earth Acquisition Control for Pitch Prior to Acquisition

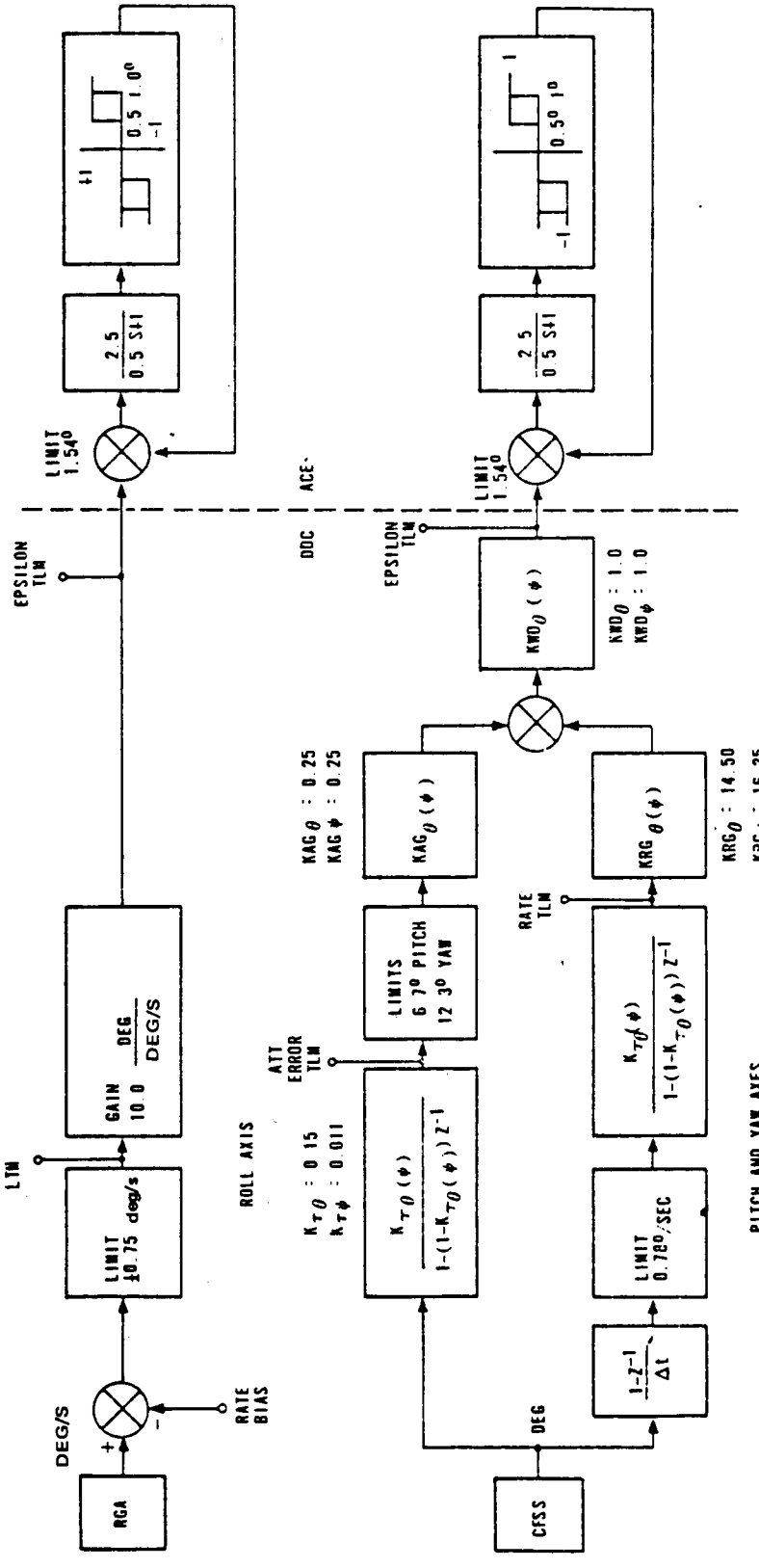

Figure A-3. DOC Sun Acquisition and Select Wheels

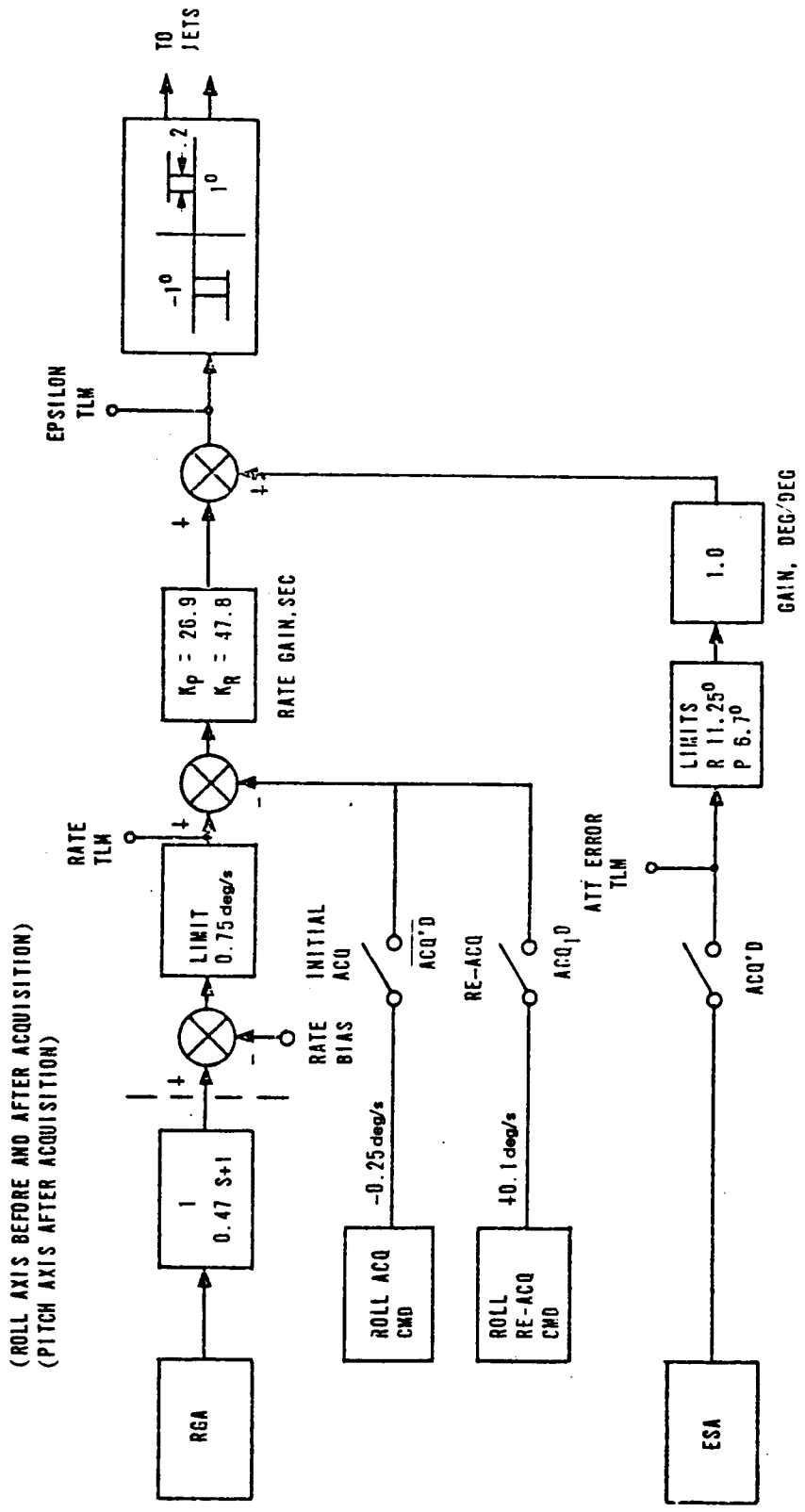

Figure A-4. Earth Acquisition – DOC

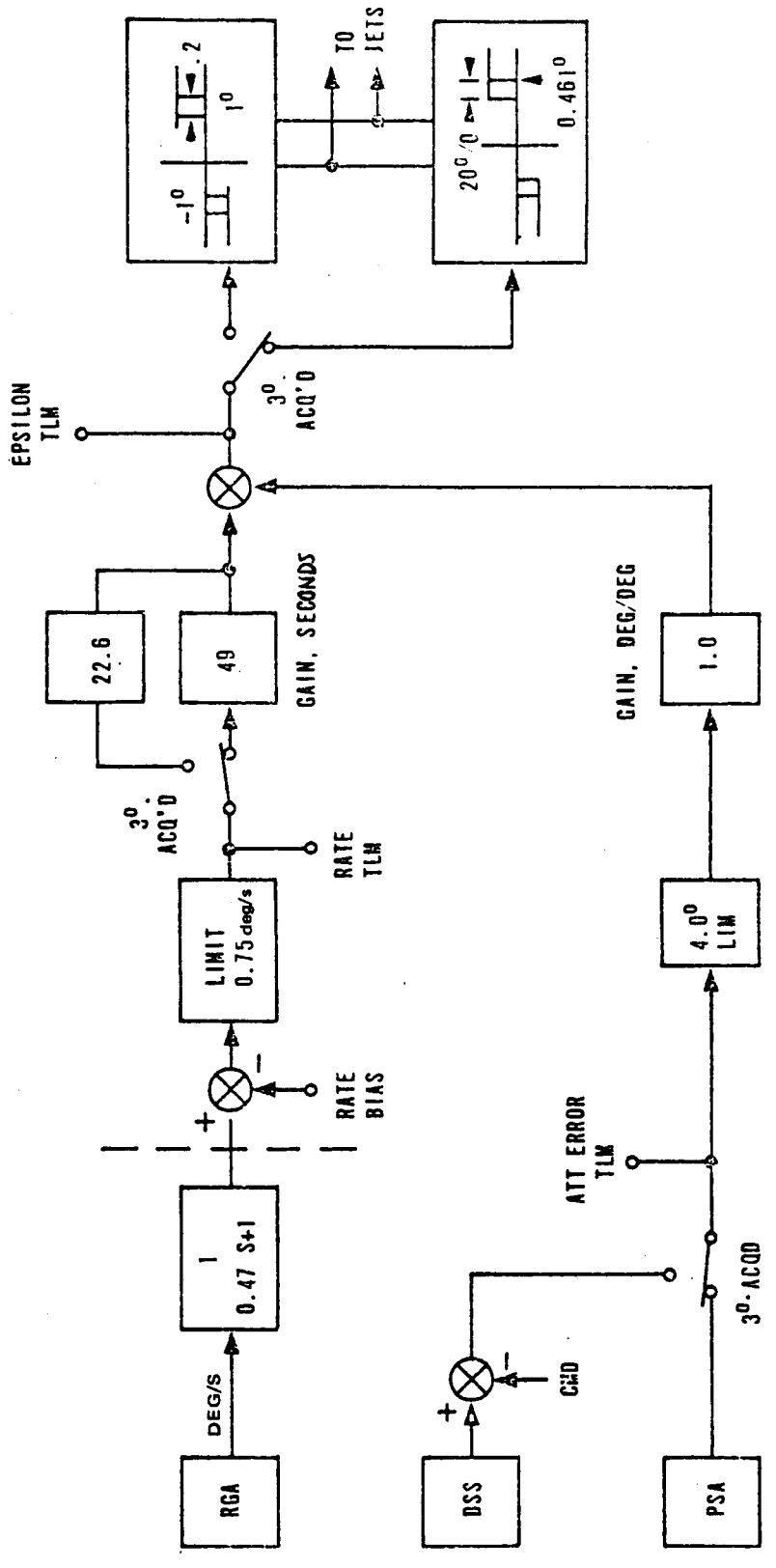

Figure A-5. DOC Polaris Acquisition Control Law

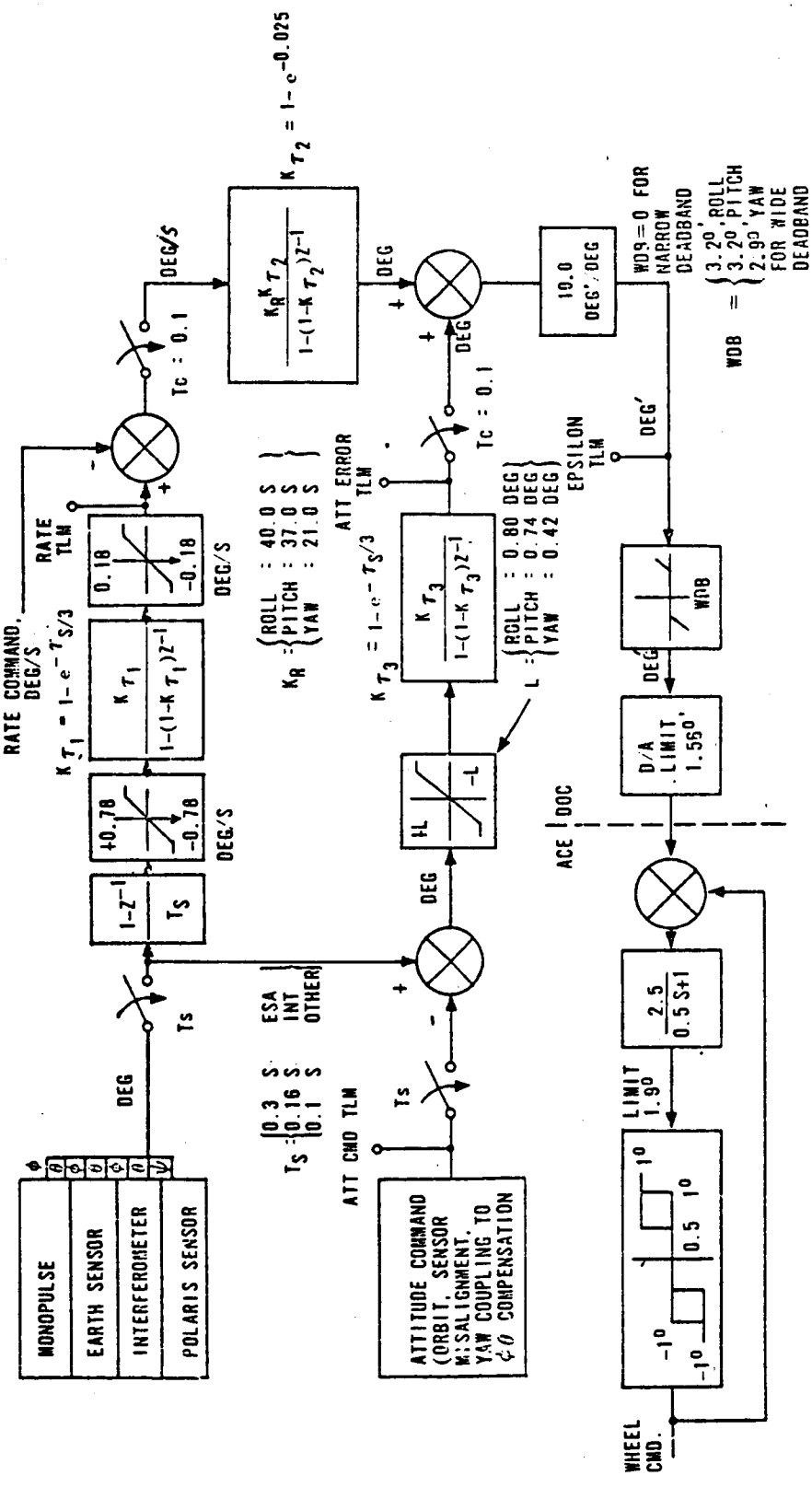

Figure A-6. DOC Standard Wheel Modes Control Law

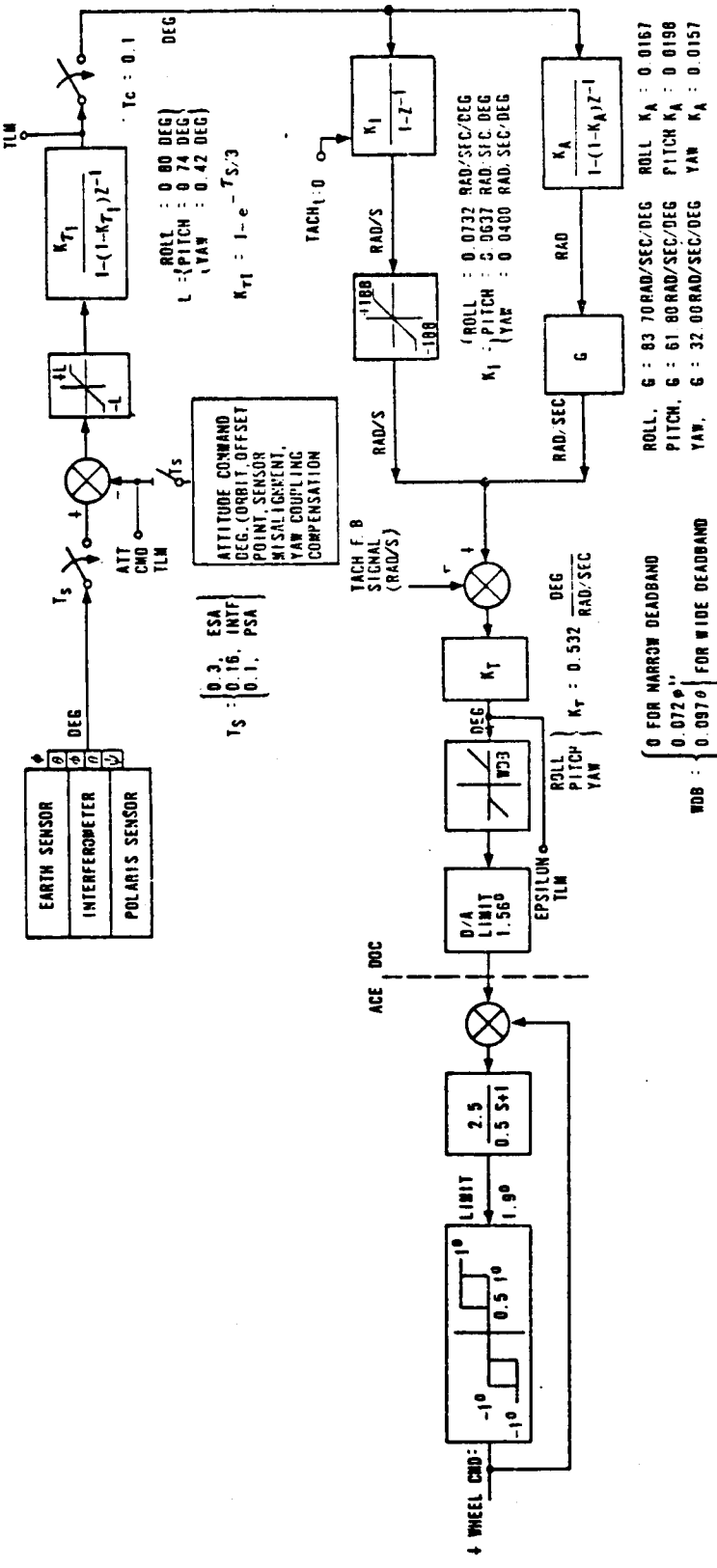

Figure A-7. DOC Low Jitter Wheel Control Law

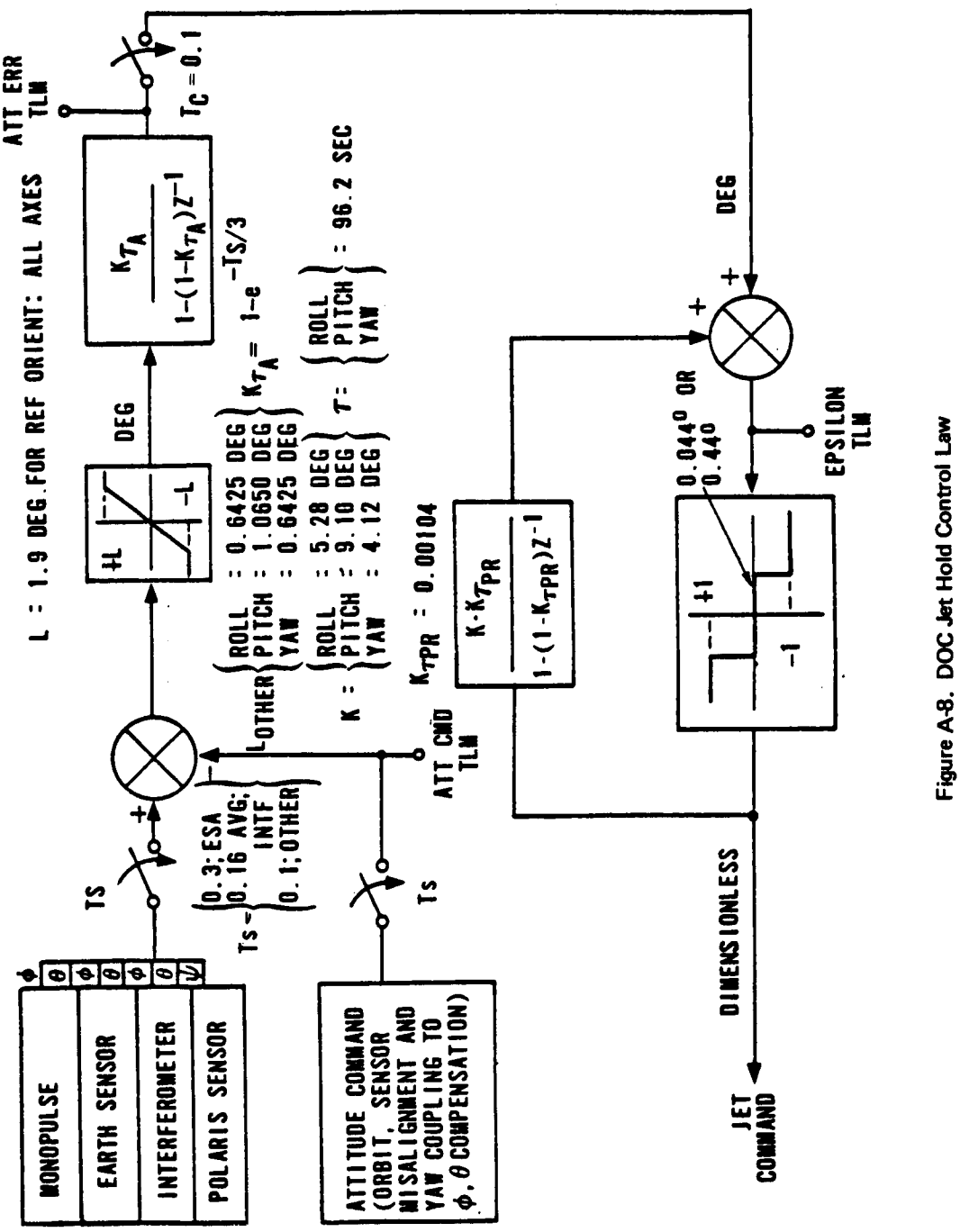

Figure A-8. DOC Jet Hold Control Law

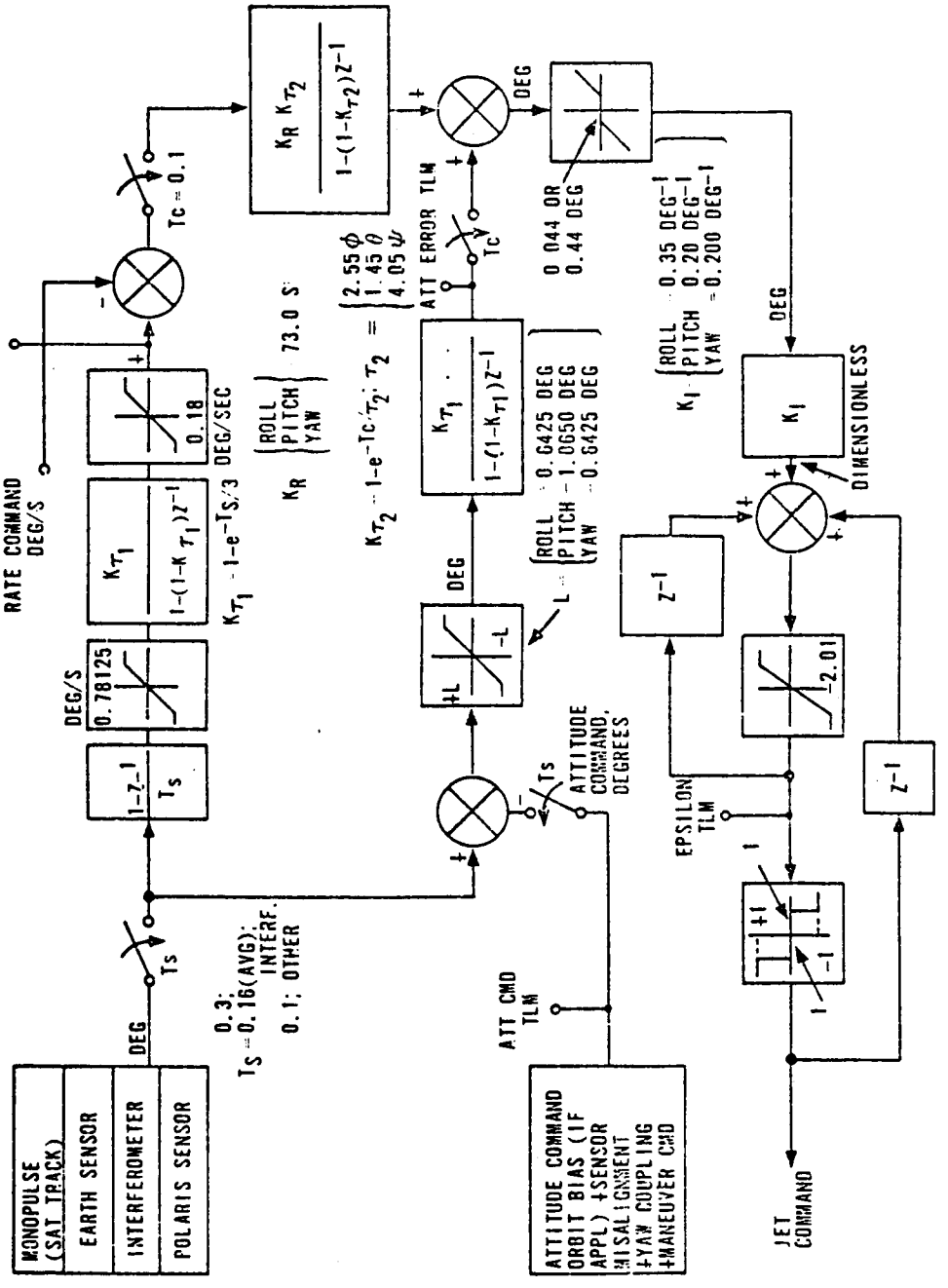

Figure A-9. DOC Jet Control Law for Maneuvering Operational Modes

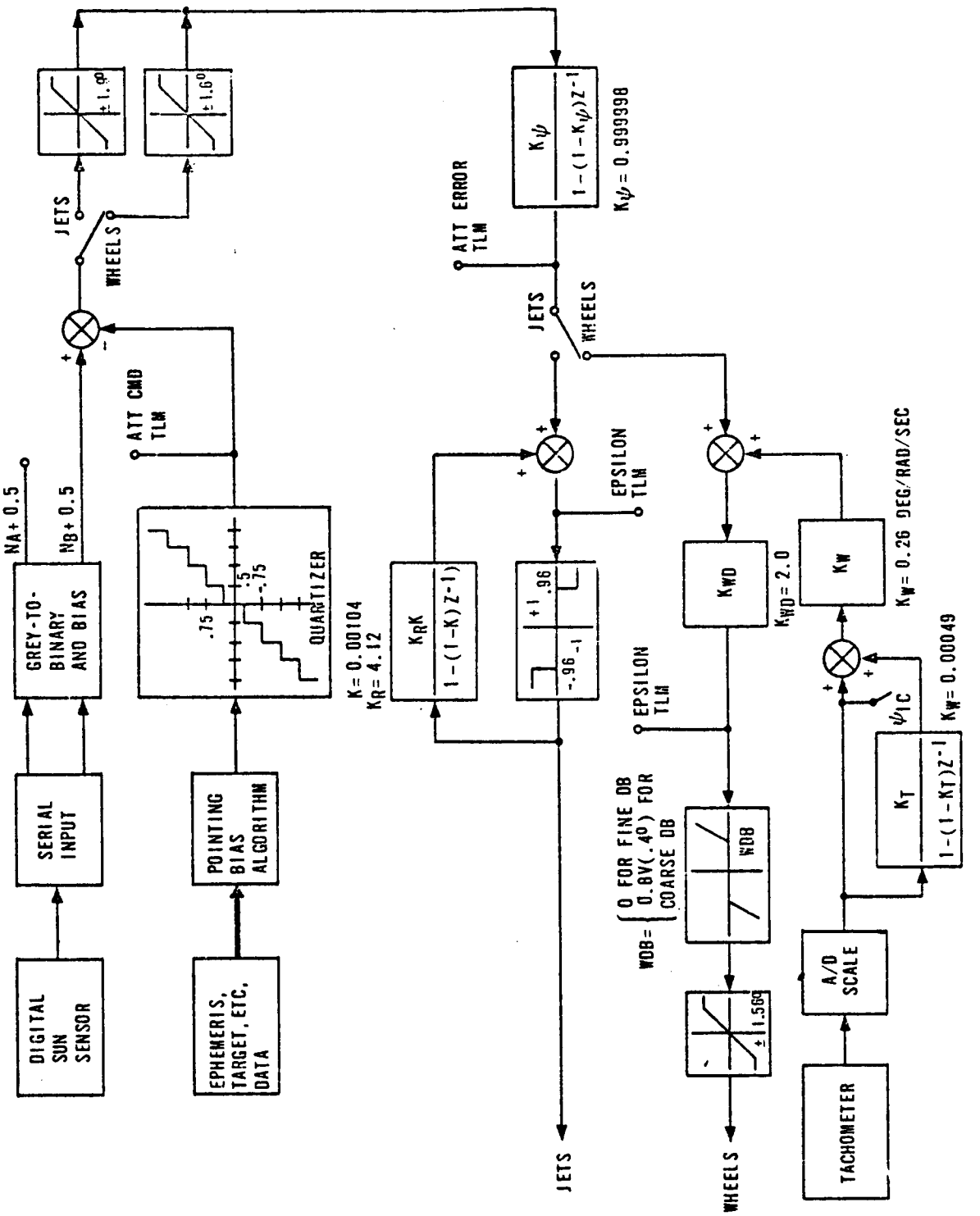

Figure A-10. Yaw Backup Mode for Jet and Wheel Control

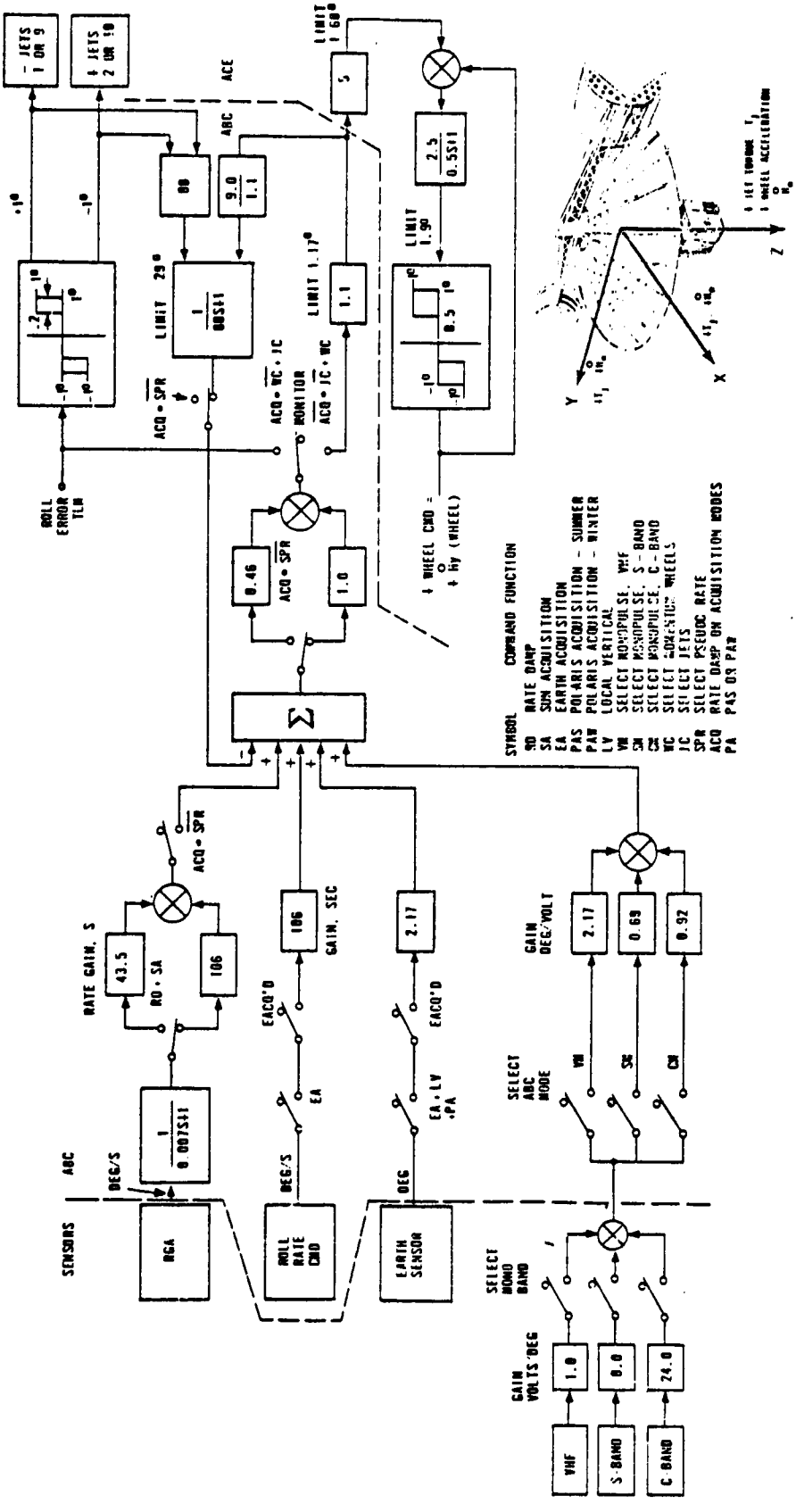

Figure A-11. Block Diagram – ABC Roll Axis

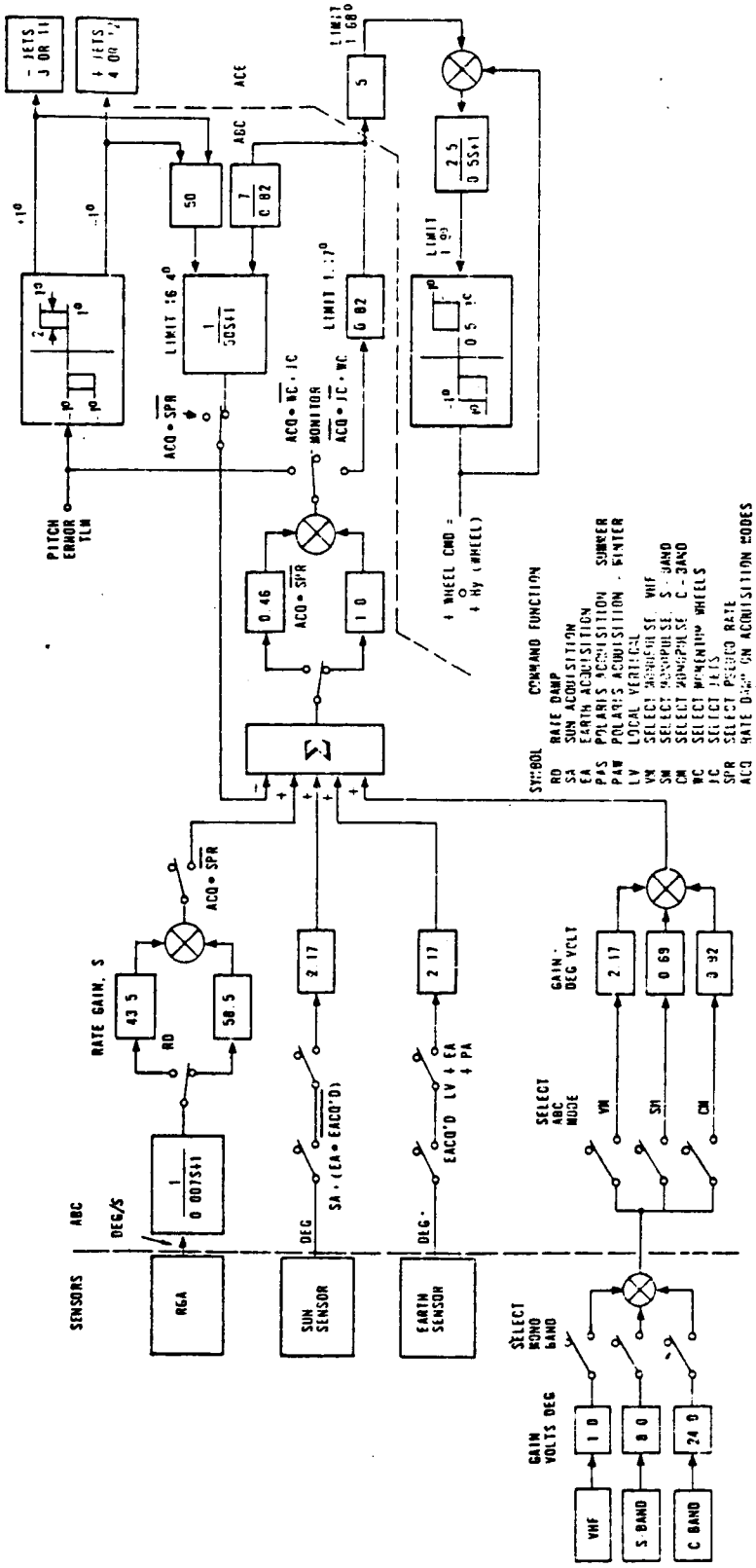

Figure A-12. Block Diagram — ABC Pitch Axis

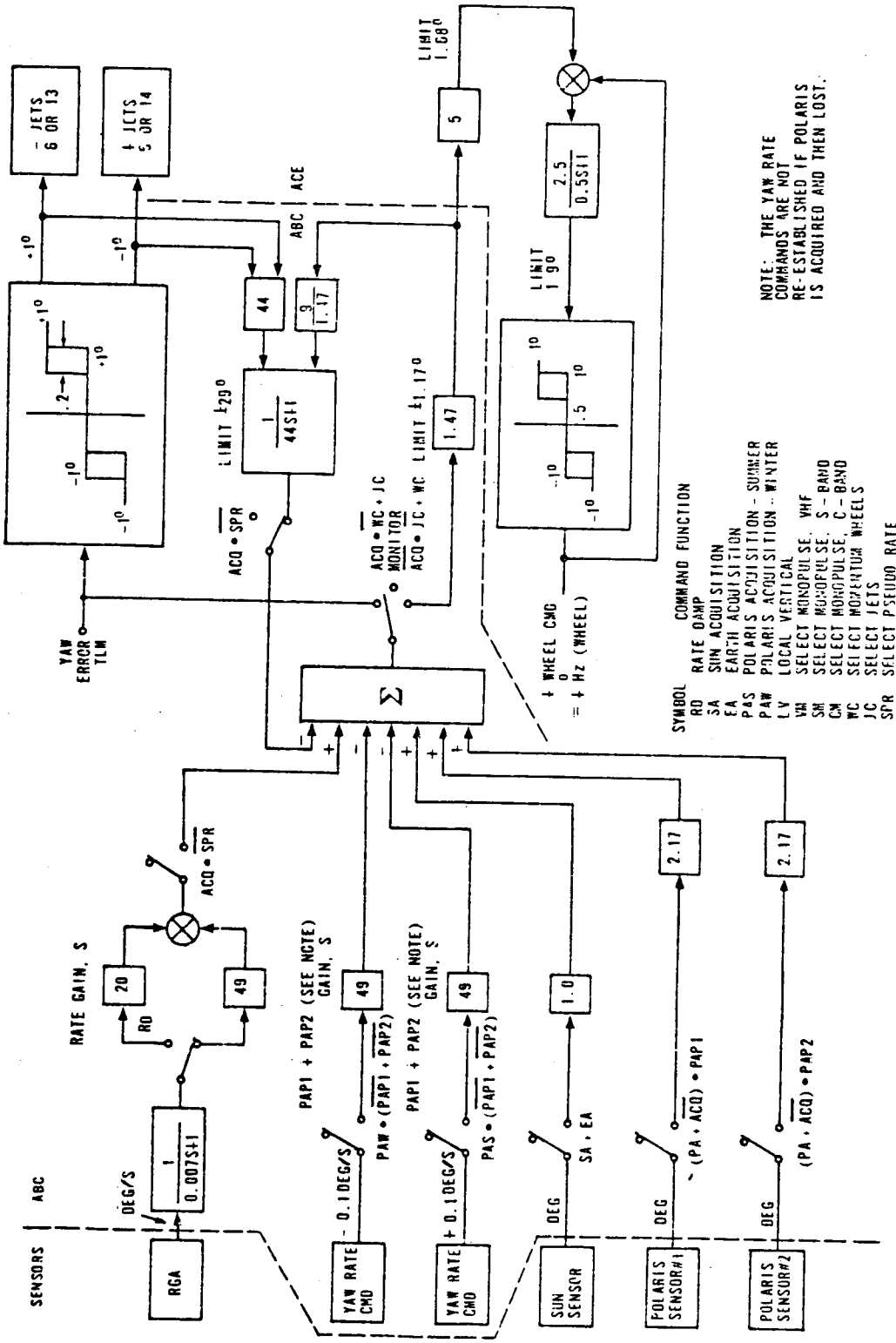

Figure A-13. Block Diagram – ABC Yaw Axis

APPENDIX B

ACRONYMS AND ABBREVIATIONS

A

A	ampere
Å	Angstrom
ABC	analog backup controller
AC	attitude control
a.c.	alternating current
ACE	actuator control electronics
ACP	acquisition control program
acq.	acquisition
ACS	attitude control subsystem
ACSN	Appalachian Community Service Network
A/D	analog to digital
ADC	analog-to-digital converter
ADPE	automatic data processing equipment
ADS	automatic deployment sequencer
ADSS	auxiliary digital Sun sensor
ADVM	adaptive delta voice modulation
A/E	absorbtivity to emissivity
Aerosat	aeronautical satellite
AES	Ahmedabad Earth Station
AESP	Appalachian Education Satellite Project
af	audio frequency
AFC	automatic frequency control
AFTE	Advanced Thermal Control Flight Experiment
AGC	automatic gain control
AGE	aerospace ground equipment
Ah	ampere-hour
AID	Agency for International Development
AIDSAT	Agency for International Development Television Demonstration
AIR	All India Radio
ALC	automatic level control
ALED	Alaska Education Experiment
am, AM	amplitude-modulation
AMP	amplifier
AOS	acquisition of satellite
APM	antenna pattern measurement

APT	automatic picture transmission
ARC	Appalachian Regional Commission
ASC	Aerospace Corporation
ASP	automated sequential processor
ASSY	assembly
ASTP	Apollo-Soyuz Test Program
ASTP-TV	ASTP television coverage experiment
ATA	automatic threshold adjust
AT&T	American Telephone and Telegraph (Spacecraft)
ATC	air traffic control, active thermal control
ATFE	Advanced Thermal Control Flight Experiment
atm, ATMOS	atmosphere(s)
ATS	Applications Technology Satellite
ATS-6	Applications Technology Satellite-6
ATSOCC	ATS Operations Control Center
ATS-R	ATS ranging
ATSSIM	ATS simulator
Atten	attenuator (attenuation)
Aux	auxiliary

B

B&E	Broadcast and Engineering
BAM	building attenuation measurement
BB	baseband
BER	bit error rate
bps	bits per second
BRC	Balcones Research Center
BSA	bit synchronization acquisition
BTC	binary time code
BTE	bench test equipment
Btu	British thermal unit
BW	bandwidth

C

C	Celsius
Cap Com	Capsule Communicator
CCIR	International Radio Consultative Committee
CDD	command/decoder distributor
CEE	designator for "career education course for elementary-grade teachers"
CES	designator for "career education course for secondary-grade teachers"
CESP	computer executive system program
CFSS	coarse/fine Sun sensors

CIC	command interface control
CIE	cesium ion engine
C/L	capacitance-to-inductance
cm	centimeter
CM	communications module
C/M	carrier-to-multipath
CMD	command
CMOS	complimentary metal oxide semiconductor
C/N_o	carrier power to spectral noise density ratio
CNR, C/N	carrier-to-noise ratio
cntr	center
Comsat	Communications Satellite Corporation
ConUS, CONUS	Continental United States
CONV	converter
COSMOS	complimentary symmetry metal oxide semiconductor
CPI	cross polarization isolation
CPR	cross polarization ratio
CPU	central processing unit
CRT	cathode-ray tube
CSM	command-service module
CSP	command service program
CSS	coarse Sun sensor
CTNE	Companie Telephonica Nacional de Espana
CW	carrier wave, continuous wave

D

DA	design adequacy
D/A	digital to analog
DACU	data acquisition and control unit
DAF	Data Acquisition Facility
dB	decibel
dBi	decibel isotropic (gain relative to an isotropic antenna)
dB/K	decibel per degree Kelvin
dBm	decibels referred to 1 milliwatt
dBW	decibel (reference level 1 watt)
DC	downconverter
d.c.	direct current
DCP	data collection platforms
DDDF	duplex digital data formatter
DDS	digital Sun sensor
DECPSK	differentially encoded coherent phase shift key (modulated)
DEG, deg	degree

DEM	digital evaluation mode
Depl	deployment
DES	Delhi Earth Station
DESA	double electrostatic analyzer
DIB	data input buffer
div	division
DIX	data interface transmitter
DJS	Dzhusaly (designator)
DLO	dual local oscillator
DM	docking module
DOC	digital operational controller
DOD	depth-of-discharge
DOT	Department of Transportation
DOT/FAA	The Department of Transportation/Federal Aviation Administration
DOT/TSC	The Department of Transportation/Transportation Systems Center
DPRI	diagnostic and prescriptive reading instruction
DR	Copenhagen (designator)
DRR	data recorder/reproducer
DRS	direct reception system
DSS	digital Sun sensor
DSU	data switching unit
DTS	data transmission system
DUT	Denver Uplink Terminal

E

EBU	European Broadcast Union
ECH	Earth-coverage horn
ECI	Earth centered inertial
e.d.t., EDT	eastern daylight time
e.i.r.p.	effective isotropic radiated power
EME	Environmental Measurements Experiments
emi, EMI	electromagnetic interference
EML	equivalent monomolecular layer
enc	encoder
Eng.	engineering
EOL	end-of-life
EPIRB	Emergency Position Indicating Radio Beacon
EPS	electrical power subsystem
ERP	effective radiated power
ES	Earth sensor
ESA	Earth sensor assembly, European Space Agency
ESA/PSA	Earth sensor assembly/Polaris sensor assembly
e.s.t., EST	eastern standard time

ETR	Eastern Test Range
eV	electronvolt
EVM	Earth-viewing module
EVT	Eupatoria (designator)

F

f	frequency
F	Fahrenheit
FAA	Federal Aviation Administration
FCC	Federal Communications Commission
FCHP	feedback-controlled variable conductance heat pipe
FCP	flight computer program
FCT	fixed calibration terminal
f/d	ratio of focal distance to diameter
FDM	frequency diversity modulation; frequency division multiplexer
fm, FM	frequency modulated
FOV	field-of-view
FOWG	Flight Operations Working Group
Freq.	frequency
FRMS	Federation of Rocky Mountain States
fsk	frequency shift keying
FSS	fine Sun sensor
ft	foot, feet
FT	frequency translation
ft-lb	foot-pound
FTO	functional test objective
FTS	Federal Telecommunications System

G

g	grams, gravity
G	gain
GAC	ground attitude control
GEOS-3	Geodetic Earth-Orbiting Satellite-3
GFRP	graphite fiber reinforced plastic
GHz	gigahertz
gm	gram
G.m.t., GMT	Greenwich mean time
GRD	ground
GRP	group
GSFC	Goddard Space Flight Center
G/T	dB/K antenna gain over system noise temperature
GTT	ground transmit terminal
GVHRR	Geosynchronous Very High Resolution Radiometer

H

HAC	Hughes Aircraft Company
HDRSS	high data rate storage system
HET	Health, Education, Telecommunications (experiment)
HEW	Department of Health, Education, and Welfare
hf	high frequency
HGA	high gain antenna
HI	Honeywell International
HPBW	half power bandwidth
HR	hour
HSE	high-speed execute
HTR	heater; high-time resolution
Hz	hertz

I

IBM	International Business Machines
IDT	image dissector tube
IEB	interface electronics box
i.f.	intermediate frequency
IFC	in-flight calibration
IHS	Indian Health Service (Alaska)
IHSDL	interferometer high speed data link
IM	intermodulation
IMF	interplanetary magnetic field
IMP	Interplanetary Monitoring Platform
in.	inch
in.-oz	inch-ounce
Intelsat	International Telecommunications Satellite
INTF	interferometer
I/O	input/output
IPD	Information Processing Division
IR	infrared
IRAC	Interdepartment Radio Advisory Committee
ISRO	Indian Space Research Organization
IT	intensive terminal
ITS	Institute of Telecommunications Sciences
ITU	International Telecommunications Union
I-V	current voltage
IW	inertia wheel
IZMIRAN	Institute of Terrestrial Magnetism, Ionosphere and Radio Wave Propagation

J

JAM	jet-assist mode
Joburg	Johannesburg (designator)
JSC	Johnson Space Center

K

K	Kelvin
kbps	kilobits per second
keV	kiloelectronvolt
kg	kilogram
kHz	kilohertz
km	kilometer
KSC	Kennedy Space Center
kW	kilowatt

L

lb	pound
LC	inductive-capacitance
LD	linear detector
LFT	long form test
LIC	load interface circuit
LLD	lower level discriminator
LO	local oscillator
LOS	line-of-sight
LRIR	limb radiance inversion radiometer
LSB	least significant bit
LT	local time
LV	local vertical
L.V.	latch valve

M

m	meter
m^2	square meter
mA	milliamperes
Mad	Madrid
MAD-HYB	Madrid Hybrid
Mage	U.S./U.S.S.R. Magnetometer Experiment
Marad	Maritime Administration
MASEP	main sequential program
Max.	maximum

MCC-H	Mission Control Center, Houston
MCC-M	Mission Control Center, Moscow
MDAC	McDonnell-Douglas Aircraft Corporation
MDHS	meteorological data handling system
MESC	magnetoelectrostatic plasma containment
MeV	megnelectronvolts
MHz	megahertz
μf	microfarad
μm	micrometer (micron)
μs, μsec	microsecond
MILA	Merritt Island Launch Annex
min, MIN	minute
mlb	millipound
MMW	Millimeter Wave Experiment
mN	millinewton
MOCC	Multisatellite Operations Control Center
MOCR	Mission Operations Control Room
MONO	monopulse
MOR	Mission Operations Room
MOS	metal oxide semiconductor
MSB	most significant bit
ms, msec	millisecond
m/s	meters per second
MT	multitone
mV	millivolts
mW	milliwatt
MWE	Millimeter Wave Experiment
MW XMTR	microwave transmitter

N

N	Newton
NAFEC*	National Aviation Facilities Experiment Center
NASA	National Aeronautics and Space Administration
Nascom	NASA Communications Network
NBFM	narrowband frequency modulation
NCC	Network Coordination Center
NCE	normal command encoder
NDR	Hamburg (designator)
nm	nanometer
NMRC	National Maritime Research Center
NOAA	National Oceanic and Atmospheric Administration
N/P	negative/positive
NRL	Naval Research Laboratories

ns	nanosecond
NTSC	National Television System Committee color (U.S.)

O

O&M	operations and maintenance
OC	orbit control
OCJ	orbit control jet
OCP	operational control program
o.d.	outside diameter
OD	Operations and Distribution (Center)
omni	omnidirectional
OSR	optical solar reflectors
OSU	Ohio State University
OYA	Helsinki (designator)

P

PA	power amplifier, preamplifier
PAL	phase alternation live color (Europe)
PAM	pulse amplitude modulated
PAO	Public Affairs Office
PARAMP	parametric amplifier
PB	phonetically balanced
PBS	Public Broadcasting Service
P_c	course phase measurement
pcm, PCM	pulse code modulation
pcm/fsk/am	pulse code modulation/frequency shift keying/amplitude modulation
PCT	portable calibration terminal
PCU	power control unit
PDM	pulse duration modulation
pf	picofarad
PFD	power flux density
PFF	prime-focus feed
PGE	PLACE ground equipment
PIC	power interface circuit
PLACE	Position Location and Aircraft Communications Experiment
PLU	Project Look-Up
PM	phase-modulated
PN	pseudo-noise
POCC	Project Operations Control Center
p-p	peak-to-peak
PPK	Petropavlovsk-Kamchatski (designator)
ppm	parts per million

P_R	reference (phase) signal
P_{rgi}	power received at ground into an isotropic antenna
P_{rsi}	power received at spacecraft into an isotropic antenna
PRU	power regulation unit
PSA	Polaris sensor assembly
P_{SE}	probability function
PSK	phase shift keyed
Pv	vernier phase measurement
pW	picowatt
PWR	power

Q

QCM	Quartz-crystal microbalance contamination monitor
Q-M	quadrature phase modulation

R

Radsta	U.S. Coast Guard Radio Station
R&RR	range and range rate
RBE	Radio Beacon Expriment
RCA	Radio Corporation of America
RCC	Resource Coordinating Center
RCV	receive
RDA	rotating detector assembly
REC	receive
Ref., REF	reference
Rel	release
RESA	Regional Education Service Agency
rf	radio frequency
RFC	radio-frequency compatibility
rfi	radio frequency interference
RFIME	Radio Fequency Interference Measurement Experiment
RGA	rate-gyro assembly
RME	Rocky Mountain East
RMPBN	Rocky Mountain Public Broadcast Network
rms	root mean square
RMW	Rocky Mountain West
ROT	receive-only terminal
rpm	revolutions per minute
RR	rain rate

S

S/A	solar array
SAPPSAC	Spacecraft Attitude Precision Pointing and Slewing Adaptive Control (Experiment)
SAR	search and rescue
S&R	surveillance and ranging
Satcom	Satellite Communications
SC	sudden commencement
S/C	spacecraft
SCAMA	switching, conferencing, and monitoring arrangement
SCAMP	small command antenna medium power
SE	system effectiveness
sec, s	second
SECAM	Sequential Couleurs a Memoire (III) color (U.S.S.R.)
SEL	Space Environment Laboratory
SENS	sensor
S.G.	signal generator
SITE	Satellite Instructional Television Experiment
SITEC	sudden increase in total electron content
SIU	squib interface unit
S-IVB	Saturn IB second stage
SMSD	spin motor sync detector
SNR, S/N	signal-to-noise ratio
Spec	specification
SPS	spacecraft propulsion subsystem
SPU	signal processing unit
sr	steradian
SR	Stockholm (designator)
SRT	SAPPSAC remote terminal
SSC	sudden storm commencement
SSEA	Sun sensor electronics assembly
SSR	Staff Support Room
STA	station
STADAN	Space Tracking and Data Acquisition Network
STDN	Spaceflight Tracking and Data Network
STRUCT	structural
SWBT	Southwestern Bell Telephone Company
SYN	synthesizer
SYNC	synchronous
SYSSIM	system simulator

T

TACH	tachometer
T&CS	telemetry and command subsystem
T&DRE	Tracking and Data Relay Experiment
TART	transmit and receive terminal
TASO	Television Allocation Study Organization
TBC	time base corrector
TCD	transponder command decoder
TCS	telemetry and command subsystem, thermal control subsystem
TDA	tunnel diode amplifier
TDRE	Tracking and Data Relay Experiment
TEMP	temperature
THIR	temperature-humidity infrared radiometer
TID	traveling ionospheric disturbances
TLM, TM	telemetry
TORQ	torquer
TRUST	Television Relay Using Small Terminals
TSM	thermal structural model
TSP	telemetry service program
TSU	temperature (control) and signal (conditioning) unit
TT/N	test-tone signal-to-noise ratio
TTY	teletype
TV	television
TVOC	Television Operational Control Centers
TWT	traveling wave tube
TWTA	traveling wave tube amplifier

U

UC	upconverter
UCLA	University of California at Los Angeles
UCSD	University of California at San Diego
uhf	ultrahigh frequency
UK	United Kingdom
UKTV	University of Kentucky Television
ulf	ultralow frequency
UNH	University of New Hampshire
U.S.	United States
USA	ubiquitous spectrum analyzer
USAF	United States Air Force
USCG	United States Coast Guard
USK	Ussuruisk (designator)

U.S.S.R.	Union of Soviet Socialist Republics
UT	universal time
UV	ultraviolet

V

v	velocity
V	volt
VA	Veterans Administration
VCA	voltage controlled amplifier
VCHP	passive "cold-reservoir" variable conductance heat pipe
VCXO	voltage controlled crystal oscillator
Vdc	volts direct current
V/deg	volts per degree
Vert.	vertical
vhf, VHF	very high frequency
VHRR	very high resolution radiometer
VIP	versatile information processor
VIRS	vertical interval reference signal
VITS	vertical interval test signals
VPI	Virginia Polytechnic Institute
vs.	versus
VSWR	voltage standing-wave ratio
V/T	voltage/temperature
VTR	video-tape recorder
VU MTR	VU meter

W

W	watt
WAMI	Washington, Alaska, Montana, Idaho (medical education)
WBDU	Wideband Data Unit
WBVCO	wideband voltage-controlled oscillator
WHL, WH	wheel

X

XMIT	transmit
XMTR	transmitter
XTAL	crystal
XTAL DET.	crystal detector

Y

YIRU	yaw inertial reference unit

Z

ZAZ	Z-axis azimuth
Zcoel	Z-coelevation

BIBLIOGRAPHY

1. Afifi, M., and B. Keiser, "ATS-6 EMI Field Measurements Techniques and Results," *Proceedings of IEEE EASCON*, 1974.

2. Alexander, J., R. Luzier, and T. Swales, "ATS-F Notching Criteria as Determined by Analysis and Test," 20th Annual Meeting of Institute of Environmental Sciences, Washington, D.C., April 1974.

3. "Applications Technology Satellite-6," *IEEE Transactions on Aerospace and Electronics Systems*, Vol. AES-11, Number 6, November 1975.

4. Bartlett, R. O. and D. K. Purvis, "Active Control of Spacecraft Charging in Space Systems and Their Interaction with the Earth's Space Environment," *Progress in Astronautics and Aeronautics*, 71, pp. 299-317, AIAA, 1980.

5. Bartlett, R. O., et al., "Spacecraft Charging Control Demonstration at Geosynchronous Altitude," AIAA Paper 75-359, AIAA 11th Electric Propulsion Conference, New Orleans, Louisiania, (1975).

6. Bentilla, E. W., et al., "Research and Development Study on Thermal Control by Use of Fusible Materials," Northrop Space Laboratories, NASA N66-26691, April 1966.

7. Bienert, W. and P. J. Brennan, "Transient Performance of Electrical Feedback Controlled Variable Conductance Heat Pipes," ASME Paper 71-Av-27, July 1971.

8. Bienert, W., P. J. Brennan, and J. P. Kirkpatrick, "Feedback Controlled Variable Conductance Heat Pipes," AIAA Paper 71-421, 1971 (also in *AIAA Progress in Astronautics and Aeronautics: Fundamentals of Spacecraft Thermal Design*, Vol 29).

9. Brennan, P. J., "Summary Report for Thermal Analysis of ATFE Flight Data," prepared for NASA/ARC under P.O. A 15055 B(KT), December 1975.

10. Brennan, P. J., "Advanced Thermal Control Flight Experiment," (ATFE) Final Report, July 1979.

11. Cohen, H. A., et al., "Design Development and Flight of a Spacecraft Charging Sounding Rocket Payload," USAF/NASA Spacecraft Charging Technology Conference, Colorado Springs, Colorado, 1978.

BIBLIOGRAPHY (continued)

12. Corrigan, J. P., "ATS-6 Experiment Summary," *IEEE Transactions on Aerospace and Electronic Systems*, Vol. AES-11, No. 6, November 1975, pp. 1004-1014.

13. Depew, C. A., et al., "Construction and Testing of a Gas-Loaded Passive-Control Variable Conductance Heat Pipe," NASA CR-114597, June 1973.

14. Eby, R., "Performance Verification of ATS-6 Heat Pipes," 2nd Aerospace Testing Seminar, Institute of Environmental Sciences, March 1975.

15. Hale, D. V., et al., "Phase Change Material Handbook," NASA CR-73475, September 1970.

16. Hall, R., and W. Redisch, "ATS-6 Spacecraft Design/Performance," *Proceedings of IEEE EASCON*, 1974.

17. Isley, W. C. and D. L. Endres, "ATS-6 Spacecraft Attitude Precision Pointing and Slewing Adaptive Control Experiment," *IEEE Transactions on Aerospace and Electronics Systems*, Vol. AES-11, Number 6, November 1975.

18. Isley, W. C. and D. L. Endres, "ATS-6 Interferometer," *IEEE Transactions on Aerospace and Electronic Systems*, Vol. AES-11, No. 6, November 1975.

19. James, E., et al., "A North-South Stationkeeping Ion Thruster System for ATS-F," AIAA 10th Electric Propulsion Conference, November 1973.

20. James, E., et al., "A One Millipound Cesium Ion Thruster System," AIAA 8th Electric Propulsion Conference, August 1970.

21. Johnston, Jr., W., "ATS-6 Experimental Communications Satellite—A Report on Early Orbital Results," AIAA 11th Annual Meeting, February 1975, published as reprint in *AIAA Journal of Spacecraft and Rockets*, Vol. 13, No. 2, February 1976.

22. Johnston, Jr., W., and A. Whalen, "ATS-6—A Satellite for Human Needs," AIAA Communication Satellite Conference, July 1975.

23. Kampinsky, A., B. Keiser, and P. Mondin, "ATS-F Spacecraft: An EMC Challange," *IEEE 1974 Symposium on EMC*, Publication No. IEEE 1974 CH0803-7 EMC.

24. Keiser, B., "ATS-6 Spacecraft Surface Treatment for Control of Electronic Discharges," *IEEE Transactions on Electromagnetic Compatibility*, Vol. EMC-17, No. 4, November 1975.

25. Kirkpatrick, J. P. and P. J. Brennan, "The Advanced Thermal Control Flight Experiment," AIAA Paper 73-757, 1973.

BIBLIOGRAPHY (continued)

26. Kirkpatrick, J. P. and P. J. Brennan, "Performance Analysis of the Advanced Thermal Control Flight Experiment," AIAA Paper 75-727, March 1975.

27. Kirkpatrick, J. P. and P. J. Brennan, "ATS-6: Flight Performance of the Advanced Thermal Control Flight Experiment," *IEEE Transactions on Aerospace and Electronic Systems*, Vol. AES-11, No. 6, November 1975.

28. LaVigna, T., "The ATS-6 Power System—An Optimized Design for Maximum Power Source Utilization," *Tenth Intersociety Energy Conversion Engineering Conference Proceedings*, 759157, August 18-22, 1975, p. 1048.

29. LaVigna, T., and F. Hornbuckle, "The ATS-6 Power System: Hardware Implementation and Orbital Performance," presented at Intersociety Energy Conversion Conference, 1976.

30. LaVigna, T., and F. Hornbuckle, "The ATS-6 Power System: Hardware Implementation and Orbital Performance," NASA Technical Paper 1023, September 1977.

31. Lyon, W. C., "Monopropellant Thruster Exhaust Effects Upon Spacecraft," *Journal of Spacecraft and Rockets*, Vol. 8, No. 7, July 1971, pp. 689-701.

32. Marcus, B. D., "Theory and Design of Variable Conductance Heat Pipes," NASA CR-2018, April 1972.

33. Marsten, R. B., "ATS-6 Significance," *IEEE Transactions on Aerospace and Electronic Systems*, Vol. AES-11, No. 6, November 1975, pp. 984-993.

34. Moore, R., "Magneto-Electrostatically Contained Plasma Ion Thruster," AIAA 7th Electric Propulsion Conference, March 1969.

35. NASA, "Study to Evaluate the Feasibility of a Feedback Controlled Vehicle Conductance Heat Pipe," Technical Summary Report NASA CR-73475, September 1970.

36. Patterson, G., "ATS-6 Television Camera Reflector Monitor," *IEEE Transactions on Aerospace and Electronics Systems*, Vol. AES-11, No. 6, November 1975, pp. 1202-1205.

37. Rogers, John F., "ATS-6 Quartz-Crystal Microbalance," *IEEE Transactions on Aerospace and Electronic Systems*, Vol. AES-11, No. 6, November 1975, pp. 1185-1186.

38. Schreib, R., "ATS-6 Propulsion: Two Years in Orbit," AIAA Paper 76-629, *Proceedings of AIAA/SAE 12th Propulsion Conference*, Palo Alto, California, July 26-29, 1976.

BIBLIOGRAPHY (continued)

39. Schreib, R., "ATS-6 Propulsion Performance: Four Years in Orbit," AIAA Paper 78-1062, *Proceedings of AIAA/SAE 14th Joint Propulsion Conference*, Las Vegas, July 25-27, 1978.

40. Schreib, R., "Flow Anomalies in Small Hydrazine Thruster," AIAA Paper 79-1303, *Proceedings of AIAA/SAE/ASME 15th Joint Propulsion Conference*, Las Vegas, Nevada, June 18-20, 1979.

41. Smith, A., T. LaVigna, and L. Pessin, "Design Impact of a Unique Solar Array Configuration for the ATS-F Electrical Power Subsystem," *Proceedings of Eighth IECEC*, August 1973.

42. Smith, A., F. Hornbuckle, and F. Betz, "Evaluation of Flight Acceptance Thermal Testing for the ATS-6 Solar Array," presented at the 11th IEEE Photovoltaic Specialist Conference, 1975.

43. Suelau, H. J. and P. J. Brennan, "Advanced Thermal Control Flight Experiment Thermal Analysis–First Progress Report," prepared for NASA/ARC under P.O. 8380 B(KT), March 1975.

44. Swerdling, B. and R. Kosson, "Design, Fabrication and Testing of a Thermal Diode," NASA CR-114526, November 1972.

45. Swerdling, B., et al., "Development of a Thermal Diode Heat Pipe for the Advanced Thermal Control Flight Experiment (ATFE)," AIAA Paper 72-260, 1972 (also in *AIAA Progress in Astronautics and Aeronautics: Thermal Control and Radiation*, Vol. 31).

46. Worlock, R., et al., "The Cesium Bombardment Engine N-S Stationkeeping Experiment ATS-6," AIAA 75-363, New Orleans, Louisiana, March 19-21, 1975.

47. Worlock, R., et al., "ATS-6 Cesium Bombardment Engine North-South Stationkeeping Experiment," *IEEE Trans. Aerospace and Electronic Systems*, Vol. AES-11, No. 6, November 1975, pp. 1176-1183.

48. Worlock, R., et al., "Measurement of Ion Thruster Exhaust Characteristics and Interaction with Simulated ATS-F Spacecraft," AIAA 10th Electric Propulsion Conference, November 1973.

49. Worlock, R., et al., "An Advanced Contact Ion Microthruster System," *Journal of Spacecraft and Rockets*, Vol. 6, No. 4, April 1969, pp. 424-429.

BIBLIOGRAPHIC DATA SHEET

1. Report No.	2. Government Accession No.	3. Recipient's Catalog No.
NASA RP-1080		

4. Title and Subtitle	5. Report Date
ATS-6 Final Engineering Performance Report Volume II - Orbit and Attitude Controls	November 1981
	6. Performing Organization Code 415
7. Author(s) Robert O. Wales, Editor	8. Performing Organization Report No. 81F0034
9. Performing Organization Name and Address Goddard Space Flight Center Greenbelt, Maryland 20771	10. Work Unit No.
	11. Contract or Grant No. NAS 5-25464
12. Sponsoring Agency Name and Address National Aeronautics and Space Administration Washington, D.C. 20546	13. Type of Report and Period Covered Reference Publication
	14. Sponsoring Agency Code

15. Supplementary Notes

16. Abstract

The Applications Technology Satellite 6, an experimental communications spacecraft, operated for five years in a geosynchronous orbit. The six volumes of this report provide an engineering evaluation of the design, operation, and performance of the system and subsystems of ATS-6 and the effect of their design parameters on the various scientific and technological experiments conducted.

This volume (II) describes the orbit and attitude control design details and performance; the hydrazine jets, reaction wheels, onboard computer; the ion engine; and ground control experiments.

17. Key Words (Selected by Author(s))	18. Distribution Statement
Spacecraft Communication, Evaluation, Spacecraft Performance, Communications Technology Satellite, Command and Control, Satellite Attitude Control	Unclassified - Unlimited Subject Category 18

19. Security Classif. (of this report)	20. Security Classif. (of this page)	21. No. of Pages	22. Price*
Unclassified	Unclassified	289	A13

*For sale by the National Technical Information Service, Springfield, Virginia 22161.

GSFC 25-44 (10/77)

*U.S. GOVERNMENT PRINTING OFFICE: 1981 539-007/18 1-3